University of Glasgow

Graham, Lesley A. (2013) *Characterisation of Uromodulin as a candidate gene for human essential hypertension.* PhD thesis.

http://theses.gla.ac.uk/5215/

Characterisation of Uromodulin as a Candidate Gene for Human Essential Hypertension.

Lesley Anne Graham, MRes

This being a thesis submitted for the degree of Doctor of Philosophy
(Ph.D.) in the Faculty of Medicine, University of Glasgow, November 2013

BHF Glasgow Cardiovascular Research Centre
Institute of Cardiovascular and Medical Sciences
College of Medical, Veterinary, and Life Sciences
University of Glasgow

Author's Declaration

I declare that this thesis has been written by myself and is a record of research performed myself with exception of electrolyte analysis assays which were performed by Dr James Harvie at the University of Glasgow Veterinary Medicine School. Microarray technology was performed by Mrs Wendy Beattie at the University of Glasgow. RNA extraction and cDNA synthesis of human renal tissue and Taqman gene expression results were performed and analysed by Matthew Deniff of the University of Leicester. Any contribution from others has been clearly referenced and reproduced with permission. This work has not been submitted previously for a higher degree and was supervised by Dr Martin W. McBride and Professor Anna F. Dominiczak.

Acknowledgement

Table of Contents

List of Figures

List of Tables

List of Abbreviations, Acronyms & Symbols

µg	Micrograms
µl	Microlitres
µM	Micromolar
µM/g	Micromoles per gram
ACE	Angiotensin converting enzyme
ACTH	Adrenocorticotrophic hormone
ADH	Anti-diurectic hormone
AME	Apparent Mineralocorticoid excess
Ang I	Angiotensin I
AQP2	Aquaporin 2
BMI	Body mass index
bp	Base pairs
BP	Blood pressure
BRIGHT	British genetics of hypertension
CA	Carbonic anhydrase
Ca^+	Calcium ion
CaCl	Calcium chloride ion
CDH13	Cadherin 13 protein
cDNA	Complimentary DNA
ChIP	Chromatin Immunoprecipitation
CKD	Chronic kidney disease
Cl^-	Chloride ion
CO_2	Carbon dioxide
COX	Cyclooxygenase
COX-2	Cyclooxygenase-2
CrCl	Creatinine clearance
CVD	Cardiovascular disease
DBP	Diastolic blood pressure
DCT	Distal convoluted tubule
DNA	Deoxyribonucleic acid
ECF	Extracellular fluid volume
EGF	Epidermal growth factor
eGFR	Estimated Glomerular filtration rate
ELISA	Enzyme linked Immunosorbent assay
ENaC	Epithelial sodium channel
ENCODE	Encyclopaedia of DNA elements funded by the National Human Genome Research Institute
ER	Endoplasmic reticulum
FJHN	Familial juvenile hyperuricemic nephropathy
g	Gram
GCKD	Glomerular cystic kidney disease
GPI	Glycosylphosphatidylinositol
GRECO	Groningen Renal Hemodynamic Cohort Study Group
GWAS	Genome wide association study
h	Hour
H^+	Hydrogen
H_2CO_3	Carbonic acid
H_2O	Water
HCO_3^-	Bicarbonate
HERCULES	Hypertension Evaluation by Remler and CalciUria Level

HR	Heart rate
IgG	Immunoglobulin G
IL	Interleukin
INF-γ	Interferon gamma
IP	Immunoprecipitate
IPA	Ingenuity pathway analysis
K^+	Potassium ion
Kb	Kilobase
kDa	Kilodalton
KO	Knockout
LD	Linkage disequilibrium
LPS	Lipopolysaccharide
m	Meters
m^2	Meters squared
MAP	Mean arterial pressure
MCKD2	Medullary cystic kidney disease type 2
Mg^+	Magnesium ion
min	Minutes
ml	Millilitres
mmHg	Millimetres of mercury
mmol/d	Millimole per day
mmol/l	Millimole per litre
MR	Mineralocorticoid
MRC	Medical research council
mTAL	Medullary thick ascending limb of the loop of Henle
Na^+- K^+/ATPase	Na^+ pump
Na^+	Sodium ion
NaCl	Sodium chloride ion
ng	Nanograms
NHE	Sodium hydrogen exchanger
NHE3	Sodium hydrogen exchanger 3
NICE	National Institute for Health and Care Excellence
NKCC2	Sodium potassium chloride co-transporter
OH^-	Hydroxide
PBS	Phosphate buffered saline
PGE_2	Prostaglandin E_2
PHA I	Pseudohyoaldosteronism type I
PHA II	Pseudohyoaldosteronism type II
PP	Pulse pressure
PPXY	Proline, proline, proline, any amino acid, tyrosine
PRA	Plasma renin activity
QTL	Quantitative trait loci
RAAS	Renin angiotensin aldosterone system
RNA	Ribonucleic acid
ROMK	Renal outer medulla potassium channel
RPF	Renal plasma flow
SBP	Systolic blood pressure
SDS	Sodium dodecyl sulfate
SGK1	Serum and glucocorticoid regulated kinase 1
SHS	Silesian Hypertension Study
SNP	Single nucleotide polymorphism
SRTB	Silesian Renal Tissue bank

TAL	Thick ascending limb of the loop of Henle
TESS	Transcriptional element software search analysis
TF	Transcription factor
THP	Tamm Horsfall protein
TLR4	Toll like receptor 4
TNF-α	Tumour necrosis factor alpha
UAKD	Uromodulin associated kidney disease
UMOD	Uromodulin gene
UMOD	Uromodulin protein
UTI's	Urinary tract infections
v/v	Volume/volume
w/v	Weight/volume
WHO	World Health Organisation
WNK	With no kinase
WPKP	Western Poland Kidney Project
WT	Wild type
WTCCC	The Wellcome Trust Case Control Consortium
ɣ	Gamma
α	Alpha
β	Beta

Oral presentations, publications, and awards

Abstract: Oral Presentation

Graham, L.A., Graham. D., Kumar, S., Bates, J., Raffi, H.S., Padmanabhan, S., Fraser, N.J., Dominiczak, A.F., Mcbride, M.W. European meeting on Hypertension and cardiovascular protection, Milan, Italy (Jun 14-17) 2013. *Functional consequences of UMOD variation on blood pressure.*

Anderson, **L. A.,** Graham. D., Kumar, S., Bates, J., Raffi, H.S., Padmanabhan, S., Fraser, N.J., Dominiczak, A.F., Mcbride, M.W. British heart foundation 4 year program students meeting, Edinburgh, UK (Jan 2013). *Functional role of UMOD in blood pressure regulation.*

Anderson, **L. A.,** Graham. D., Kumar, S., Bates, J., Raffi, H.S., Padmanabhan, S., Fraser, N.J., Dominiczak, A.F., Mcbride, M.W. European meeting on Hypertension and cardiovascular protection, London, UK (Apr 26-27) 2012. *Functional characterisation of UMOD in hypertension.*

Anderson, **L. A.,** Graham. D., Kumar, S., Bates, J., Raffi, H.S., Padmanabhan, S., Fraser, N.J., Dominiczak, A.F., Mcbride, M.W. Integrative Mammalian Biology (BBSRC), Glasgow, UK (March) 2012. *Characterisation of the UMOD knockout mouse.*

Anderson, **L. A.,** Graham. D., Kumar, S., Bates, J., Raffi, H.S., Padmanabhan, S., Fraser, N.J., Dominiczak, A.F., Mcbride, M.W. Scottish Cardiovascular forum, Dundee, UK (Feb) 2012. *UMOD a candidate gene for human hypertension.*

Anderson, **L. A.,** Graham. D., Kumar, S., Bates, J., Raffi, H.S., Padmanabhan, S., Fraser, N.J., Dominiczak, A.F., Mcbride, M.W. Scottish society of Experimental Medicine, Glasgow, UK (Nov) 2011.

Delles, C., Carty,D.M., **Anderson,L.A**., Dominiczak, A. Sept 21-24; 2011, Orlando, FL. American Heart Association HBPR 2011 Scientific Sessions. *Peripheral Arterial Tonometry (PAT): A Tool for Endothelial Function in Pregnancy.*

Abstract: Poster Presentation

Carty, D.M., **Anderson, L.A**., Mcculloch, J., Dominiczak, A., and Delles, C. Apr 11-14; 2011, Birmingham, UK. Society of Endocrinology BES 2011. *Plasma Biomarkers for early prediction of preeclampsia.*

Journal Articles

Graham, L.A., Padamanabhan, S. *et al* Validation of Uromodulin as a candidate gene for human essential hypertension. *Hypertension.* 2014 March: 63 (3);551-8

Carty DM, **Anderson LA**, *et al*. Early pregnancy soluble E-selectin concentrations and pre-eclampsia. **J Hypertens**. 2012 May: 30 (5):954-9

Carty DM, **Anderson LA**, *et al*. Peripheral arterial tone: assessment of microcirculatory function in pregnancy. **J Hypertens**; 2012 Jan: 30 (1):117-23..

Miller, A.M., Asquith, A.L., Hunter, A.J., **Anderson, L.A.**, et al. 2010; 107 (5): 650-658. *Circulation Research*. Interleukin-33 Induces Protective Effects in Adipose Tissue Inflammation During Obesity in Mice.

Awards

Graham Wilson Travel award £750 - May 2011

Summary

Essential hypertension is a highly hereditable trait of complex aetiology, where multiple environmental and life style factors contribute to blood pressure variation. Family health studies of blood pressure suggest that heritability accounts for 30 – 50 % of variation. Consequently the study of genetic architecture has proven useful to detect a small number of genes, loci, and single nucleotide polymorphisms (SNPs) that have appreciable effects on blood pressure. Genetic linkage and association methods have long provided the foundation of gene identification in humans. Although linkage studies have proven to be highly successful in identifying genes of monogenic (or Mendelian) disorders, this analysis has minimal or limited power to detect gene of complex traits and disease. Furthermore, candidate gene approaches have not yet reported any reproducible associations with hypertension. Accordingly, gene identification efforts have become increasingly reliant on association approaches.

A recent genome wide association study (GWAS) identified a locus upstream of the Uromodulin (*UMOD*) gene transcriptional start site, which was associated with hypertension. This group used an extreme case - control design in a discovery sample of 1,621 hypertension cases and 1,699 hypercontrols, representing the top 2% and bottom 20% of the BP distribution. The minor G allele of rs13333226 when adjusted for estimated glomerular filtration rate (eGFR) was associated with a 7 % lower risk of developing hypertension. *UMOD* encodes the protein uromodulin which is interchangeably known as Tamm Horsfall protein (THP). It is a kidney specific protein and is exclusively synthesised at the level of the thick ascending limb of the loop of Henle (TAL) and is the most abundant protein in human urine. The biological role of uromodulin still remains unclear; however other *UMOD* variants have been associated with chronic kidney disease. Due to UMODs exclusive expression at the kidney it may have a role in regulating blood pressure via sodium homeostasis mechanisms. As hypertension is characterised by a disturbance of renal function that subsequently leads to an augmented Na^+ reabsorption, the present study aimed to follow up the GWAS signal to assess whether altered

UMOD expression and/or function impacts on sodium homeostasis and influence blood pressure phenotypes.

Promoter activity assays here demonstrate that the index SNP (rs13333226) is not a functional variant causing altered transcription, however the minor G allele of rs13333226 is associated with reduced promoter activity. These findings are consistent with the original GWAS study that this allele is associated with lower risk of hypertension. In this study we reported a SNP in LD with rs13333226 within the 2 Kb promoter region (rs4997081) that may be a causal variant altering transcriptional activity of *UMOD*. Furthermore, with computational and experimental evidence we show that binding of rs4997081 to *TFAP2A* in a genotype dependent manner leads to transcriptional changes of *UMOD* which were associated with altered sodium reabsorption via downstream signalling of Tumor necrosis factor alpha (TNF-α).

Cardiovascular characterisation of *UMOD* knockout mice (KO) revealed significantly lower systolic blood pressure (SBP) in comparison to the wild type (WT) counterparts. The reported novel blood pressure phenotypes in the KO mice were not sensitive to change by salt loading (2% NaCl) over a six week period. KO mice displayed increased concentrations of sodium in the urine upon salt loading, to greater levels than the WT mice (± 2% NaCl). Urinary electrolyte analysis corrected to creatinine levels revealed augmented sodium loss in the KO mice during the high salt diet. Chronic renal function curves demonstrate that the reduced SBP is attained by increased natriuresis via augmented GFR in the KO mice. Histological examination illustrated cellular swelling and papillary oedema in the KO mice before and after salt loading which may be triggered by the pro-inflammatory cytokines TNF-α and Interleukin 1 (IL-1) according to metabolomic analysis. These inflammatory signals may affect Na$^+$ homeostasis at the TAL in the KO mice by reducing NKCC2 expression. Expression analysis studied in outer medulla tissue illustrated down regulation of the major NaCl transporters in the absence of *UMOD* which were further attenuated upon salt loading conditions possibly by increased levels of TNF-α at the TAL. KO mice displayed increased levels of urinary TNF-α in addition to augmented mRNA abundance in the outer medulla tissue. In addition, immunohistochemical analysis revealed reduced NKCC2 staining with increased TNF-α staining in renal tissue of the KO mice during normal and high salt diets. These results were

confirmed *in vitro* and suggest *UMOD* acts as a negative regulator of TNF-α production by the TAL to maintain NaCl/volume homeostasis.

We have confirmed with a small pilot study using human renal tissue samples from normotensive and hypertensive individuals, that in times of altered *UMOD* expression there are changes in *NKCC2* and *NHE3* expression levels, but not *TNF-a*. More interestingly we have demonstrated that *UMOD*, *NKCC2*, and *NHE3* expression levels are altered in a genotype dependant manner, in that the minor G allele of rs13333226 appears to be associated with blood pressure via altered sodium homeostasis.

In summary we are the first to functionally follow up a hypertension signal from a GWAS. Our post GWAS follow up demonstrates novel biological evidence that *UMOD* plays a functional regulatory role in blood pressure regulation by means of fluid volume control and sodium homeostasis.

1 Introduction

1.1 Cardiovascular disease

Cardiovascular disease (CVD) is a common complex disease of major public health importance with high prevalence throughout the world. CVD refers to disorders of the heart and circulatory system, and includes hypertension, coronary heart disease, angina, myocardial infarctions, stroke, metabolic syndromes, and renal disease. According to the World Health Organisation (WHO), an estimated 17.5 million, or approximately 30% of total global deaths resulted from CVD, and hypertension is the leading cause of mortality globally (www.WHO.int, 2012). The 2012 WHO statistical report revealed that one in three adults worldwide have raised blood pressure which causes around half of all deaths from stroke or heart disease and end stage organ damage (www.WHO.int, 2012). Consequently the identification and characterisation of molecular mechanisms contributing to the pathogenesis of hypertension is fundamental for future treatment and prevention of the disease.

1.2 Human essential hypertension

Hypertension is a chronic medical condition of elevated BP, defined as clinically significant when systolic blood pressure (SBP) ≥ 140 mmHg and diastolic blood pressure (DBP) ≥ 90 mmHg. This cut off is used for patient diagnosis and treatment, however these reference cut offs are somewhat arbitrary, and it has long been debated the best way to define hypertension. In the 1940's and 1950's Sir Robert Platt and Sir George Pickering debated whether hypertension was a qualitative Mendelian trait that follows a bimodal distribution, with one peak at the level of normotension and another at hypertension where curves would likely overlap as blood pressure is affected by environmental factors. Whereas, Pickering believed that essential hypertension is a quantitative non-Mendelian trait with unimodal distribution. According to this concept hypertension represents the extreme far end of the overall blood pressure distribution, and does not exist separately (Platt, 1959, Oldham et al., 1960).

Hypertension is known as either essential (primary) or secondary hypertension. In approximately 5 – 10 % of hypertensive individuals, increased blood pressure is secondary to renal disease, constrictive vessel disease, or monogenic disease, the remaining 90 - 95 % have essential hypertension (Carretero and Oparil, 2000b). Human essential hypertension affects at least 10 million people in the

UK and is a major contributor to death from stroke, myocardial infarction, end stage renal disease, and congestive heart failure (Carretero and Oparil, 2000b). The condition is characterised by a disturbance of renal function that subsequently leads to an increase in Na^+ reabsorption (Coleman et al., 1977, Cowley, 1992, Guyton, 1991). Thus, there is an accumulation of Na^+ in the body, promoting a marked expansion of extracellular volume and therefore cardiac output. As cardiac output increases, it raises blood flow to virtually all body tissues. In response, an autoregulatory mechanism for local control of blood flow causes an immediate adjustment in the blood vessel diameter, re-establishing adequate tissue perfusion. Inadequate autoregulation therefore increases peripheral vascular resistance and blood pressure. The price for this biological adaptation is hypertension.

1.3 Blood pressure control – An overview

Blood pressure (BP) refers to the pressure exerted by circulating blood on the walls of blood vessels, and is chiefly determined by cardiac output and total peripheral resistance. It is a quantitative trait that is highly variable between and within individuals (Wright et al., 2003). Cardiac output and total peripheral resistance are controlled by a complex network of interacting physiological pathways involving vascular, neural, endocrine, and renal mechanisms to maintain continuous BP control. Through these networks, BP is maintained by a number of homeostatic systems that work together to interact and feedback in response to changes in BP caused by diet, activity, stress, and environmental factors, the main regulatory systems are outline in **Figure 1-1**.

Natriuretic peptides

Released in response to increased BP resulting in cardiac and vascular vasodilatation. Acts to inhibit vascular and renal effects of Ang II

Capillary fluid shift

Exchange of fluid across the capillary membranes between blood and interstitial fluid. Reduced capillary pressure increase osmosis, increasing blood volume and BP, reduced capillary pressure has the opposite effect

Renin Angiotensin system – Vasoconstriction (short term effect) of Ang II causing increased peripheral resistance and BP. Ang II can stimulate aldosterone production from the adrenal cortex resulting in increased tubule Na+ and water reabsorption ,increasing blood volume and BP

Blood pressure control

Kidney Kinin Kallikrein system

Controls renal blood flow. Stimulates increase Na+ and water excretion in times of increased BP to reduced ECF

Renin Angiotensin system

Baroreceptor reflexes

Carotid and aortic Chemoreceptors

Endothelium derived vasoactive substances

A renal body fluid regulatory system where hormones that regulates long term blood pressure via water and salt homeostasis

Nitric oxide (vasodilatory) and endothelin (vasoconstrictive) to alter vascular tone

Negative feedback loop where increased BP stimulates baroreceptors in the aortic arch and carotid sinus; inhibiting the vasoconstrictor center, exciting the vagal centre in the brain, causing vasodilatation, decreased HR, and reducing force of contraction. Converse response to reduced BP

Detect low O_2 levels and increase CO_2 and H_2 to excite the vasomotor centre to increase HR causing vasoconstriction

Figure 1-1 Physiological systems controlling blood pressure

1.4 The kidney and blood pressure control

The kidney is the principle organ responsible for long term BP management by regulating body fluid volume and osmolality via regulation of electrolyte balance. The main mechanism of the kidney to control blood pressure is by the renin angiotensin aldosterone system (RAAS). However, long term regulation of blood pressure relies on the synchronised regulation of Na^+ (sodium), K^+ (potassium), and Cl^- (chloride) movement in the kidney to maintain blood volume and water balance.

1.4.1 Renin Angiotensin Aldosterone System (RAAS)

The classical RAAS pathway is activated upon times of low extracellular fluid volume, low renal perfusion, and high sodium (Na^+) content in the distal tubules. The first response is the release of renin from the juxtaglomerular apparatus in the kidney into the circulation. Once in the blood, renin catalyses the liver derived angiotensinogen to form Angiotensin I (Ang I), which is physiologically inactive. Ang I is rapidly converted into active Ang II by hydrolysis in the lungs by angiotensin converting enzyme (ACE). This peptide plays important roles in blood pressure homeostasis via effects on the kidneys to conserve Na^+ and stimulate aldosterone release. Ang II is a potent vasoconstrictor and causes rises in blood pressure by activating the sympathetic nervous system to initiate increased heart rate and blood vessel constriction. In addition Ang II stimulates aldosterone secretion from the adrenal gland, leading to kidney tubular Na^+ and Cl^- reabsorption and water retention, resulting in further increases in blood pressure. Finally, Ang II also stimulates the pituitary gland to secrete anti-diurectic hormone (ADH), resulting in increased water reabsorption in the kidney collecting ducts. A negative feedback loop exists whereby increased juxtaglomerular perfusion caused by the above effects reduces renin release, thus regulating volume homeostasis via Na^+ balance (Clarke et al., 2013, Ng and Vane, 1967) (Cushman et al., 1971, Bruneval et al., 1986, Mehta and Griendling, 2007).

1.4.2 Sodium transport in the kidney

Na^+ is the predominant extra cellular cation and is of critical importance to maintain extra cellular fluid volume (ECF) and hence BP. The ability of the kidneys to absorb large quantities of Na^+ relies on sequential actions at various segments along the nephron, each with highly specialised transport capacities. A schematic of the nephron segments is outlined in **Figure 1-2** (adapted from **www.biomedsearch.com**).

The nephron consists of a renal corpuscle, a proximal tubule, a loop of Henle, a distal tubule, and a collecting duct system. The renal corpuscle consists of glomerular capillaries and Bowman's capsule. The proximal tubule initially forms several coils followed by a straight segment that descends into the medulla. The next segment is the loop of Henle, which consists of a straight section of the proximal tubule, the descending thin limb (which ends in a hair pin turn), the thin ascending limb, and the thick ascending limb. Near the end of the thick ascending limb, the nephron passes between its afferent and efferent arterioles. The short segment of the thick ascending limb is called the macula densa. The distal tubule begins a short distance beyond the macula densa and extends to the point in the cortex where two or more nephrons join to form the cortical collecting duct. The collecting ducts enter the medulla and become the outer medulla collecting ducts, and then the inner medullary collecting ducts.

Proximal tubule cells have an extensively amplified apical membrane (urine side of the cell) called the brush border. The basolateral membrane (blood side of the cell) of the proximal tubule is highly invaginated and these invaginations contain mitochondria. In contrast, the cells of the descending thin limb and ascending thin limb of the loop of Henle have poorly developed apical and basolateral surfaces. The cells of the thick ascending limb and the distal tubule have highly developed apical and basolateral membranes with extensive folding of the basolateral surfaces.

The collecting duct is composed of two cell types; the principle cell and the intercalated cell. Principle cells have a moderate basolateral membrane, whereas, intercalated cells have a high density of mitochondria thus a developed basolateral membrane. The final segment of the nephron is the inner medullary

collecting duct, where apical and basolateral surfaces are poorly developed. In terms of ion transport the proximal tubule is responsible for 60 – 70 % of the filtered Na^+, whereas 15 – 25 % is absorbed by the loop of Henle. The distal tubule reabsorbs 5 – 10 % and the collecting ducts only 1 -2 % (Sahay et al., 2007).
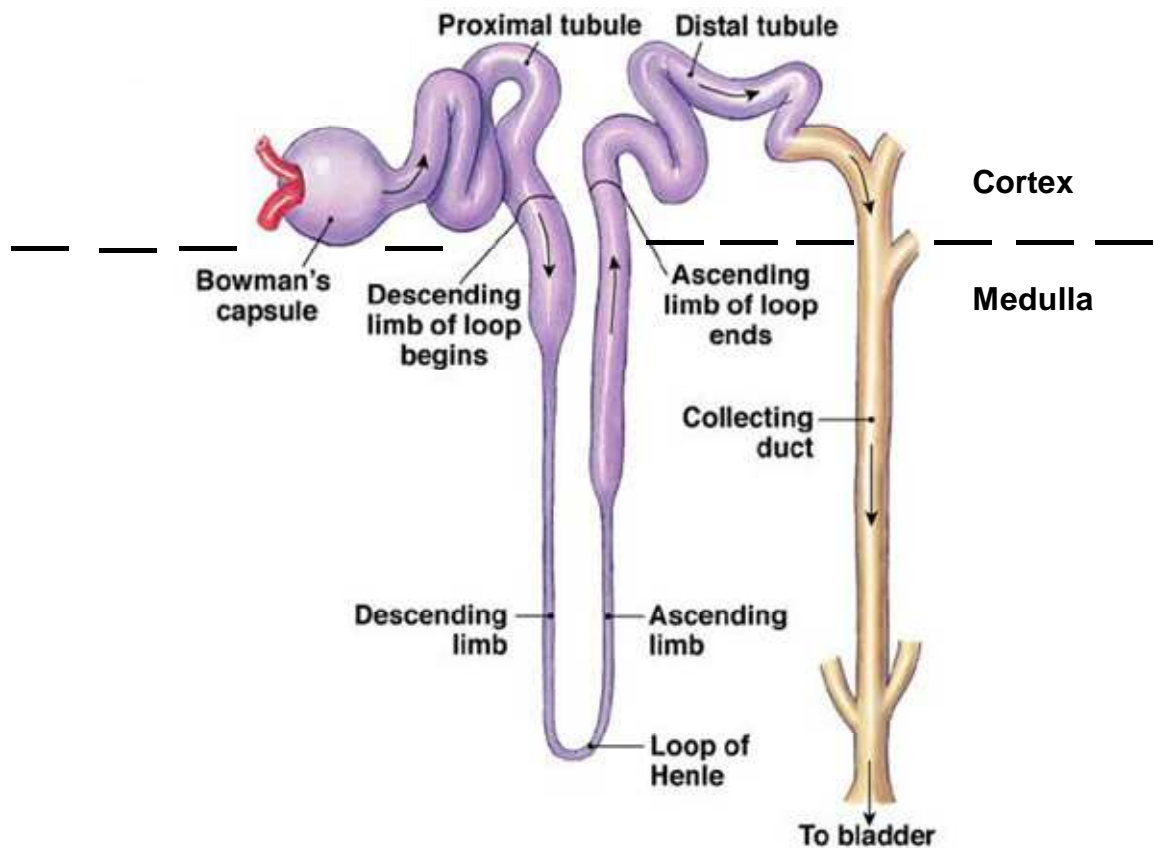
Figure 1-2 Schematic of a nephron segment (adapted from www.biomedsearch.com)

A variety of ion channels, pumps, and transporters are found along the nephron to accomplish the fundamental functions of the kidney in regulating Na^+ homeostasis. The following transporters comprise the main proteins involved in renal Na^+ handling: NHE (Sodium Hydrogen exchanger), NKCC2 (Sodium potassium chloride co-transporter), ROMK (renal outer medulla potassium channel) and ENaC (epithelial sodium channel), and the Na^+ pump (Na^+- K^+ /ATPase). **Figure 1-3**.

Tubules are lined with epithelial cells that contain Na^+- K^+ /ATPase in their basolateral cell membrane. Cells routinely expel Na^+ ions via the Na^+- K^+ /ATPase pump to create and maintain a lower concentration of Na^+ in the cytosol than in the surrounding ECF, which generates the electrochemical gradient that drives most Na^+ coupled transport processes (Fujimoto et al., 1980).

The Na^+ /H^+ exchangers (NHEs) are typical Na^+ coupled transporters that mediate the counter transport of one extracellular Na^+ for one cytolsolic proton (H^+) at the luminal apical membrane in the proximal convoluted tubule and the TAL. NHE3 is confined mainly to the apical membrane of renal cells (Amemiya et al., 1995), and functions by direct reabsorption of filtered Na^+ along with indirect reabsorption of bicarbonate and chloride and secretion of ammonium. The transporter is responsible for 10 - 20 % of total Na^+ reabsorption. NHE3 actions are outlined in **(Figure 1-4)**.

NKCC2 is localised at the apical membrane of the TAL. The function of this co-transporter is to reabsorb Na^+ without reabsorbing water. Na^+, K^+, and Cl- are transported into the cell over the apical membrane at a stoichiometry of 1:1:2 via the electrochemical gradient of the sodium pump. Na^+ and Cl^- are transported into the peritubular fluid while K^+ re-cycles back into the tubular lumen via ROMK (Ares et al., 2011). NKCC2 mediates approximately 90-100 % of Cl^- reabsorption, and 30- 50 % of all Na^+ transport, furthermore its function is linked with paracellular Na^+, Ca^+, and Mg^+ flux (Hebert and Andreoli, 1986). Inhibition of NKCC2 results in decreased K^+ exit through ROMK halting NaCl reabsorption and paracellular transport of Ca^+ and Mg^+ (Hebert and Andreoli, 1984, Herrera et al., 2009). Additionally, Na^+ and Cl^- reabsorption by the TAL maintains high interstitial osmolality, necessary for countercurrent multiplication and water reabsorption by the collecting duct system. Thus NKCC2 activity is essential for

salt conservation and for acute and chronic regulation of water. ROMK channels supply a sufficient amount of K^+ to the NKCC2 co-transporter to maintain reabsorptive transport of NaCl. As Na^+ transport of NKCC2 is rate limited by the availability of luminal K^+ in the TAL, changes in activity of ROMK has detrimental effects of NaCl reabsorption (Fang et al., 2010). **Figure 1-5** outlines the actions of NKCC2 and ROMK.

The collecting duct is responsible for the final adjustment in urine concentration, K^+ homeostasis, acid base balance, and Na^+ reabsorption which is accomplished by ENaC. This channel is a heteromultimeric channel consisting of three subunits; α, β, and ɣ and is found at the apical membrane, where the α-subunit is necessary for proper channel function and insertion onto the apical membrane (Loffing et al., 2000). When active, this channel accounts for electrogenic Na^+ reabsorption by active transport powered by the sodium pump. While mediating electrogenic Na^+ absorption, transepithelial Cl^- absorption is thought to be both paracellular (via tight junctions) and transcellular (across intercalated cells) (Pech et al., 2013). ENaC mediates Na^+ absorption across the apical membrane of principal cells, which provides the driving force for K^+ secretion through K^+ channels and plays a role in H^+ or HCO_3^- secretion (Garty and Palmer, 1997). The lumen-negative potential generated by ENaC also provides a driving force for Cl^- absorption across tight junctions and lateral intercellular spaces (Warden et al., 1988). ENaC inhibitors, such as amiloride or benzamil, eliminate the lumen-negative transepithelial voltage, which is thought to reduce Cl^- absorption by eliminating the driving force for paracellular Cl^- absorption (Sansom et al., 1984). **Figure 1-6** outlines the actions of ENaC.
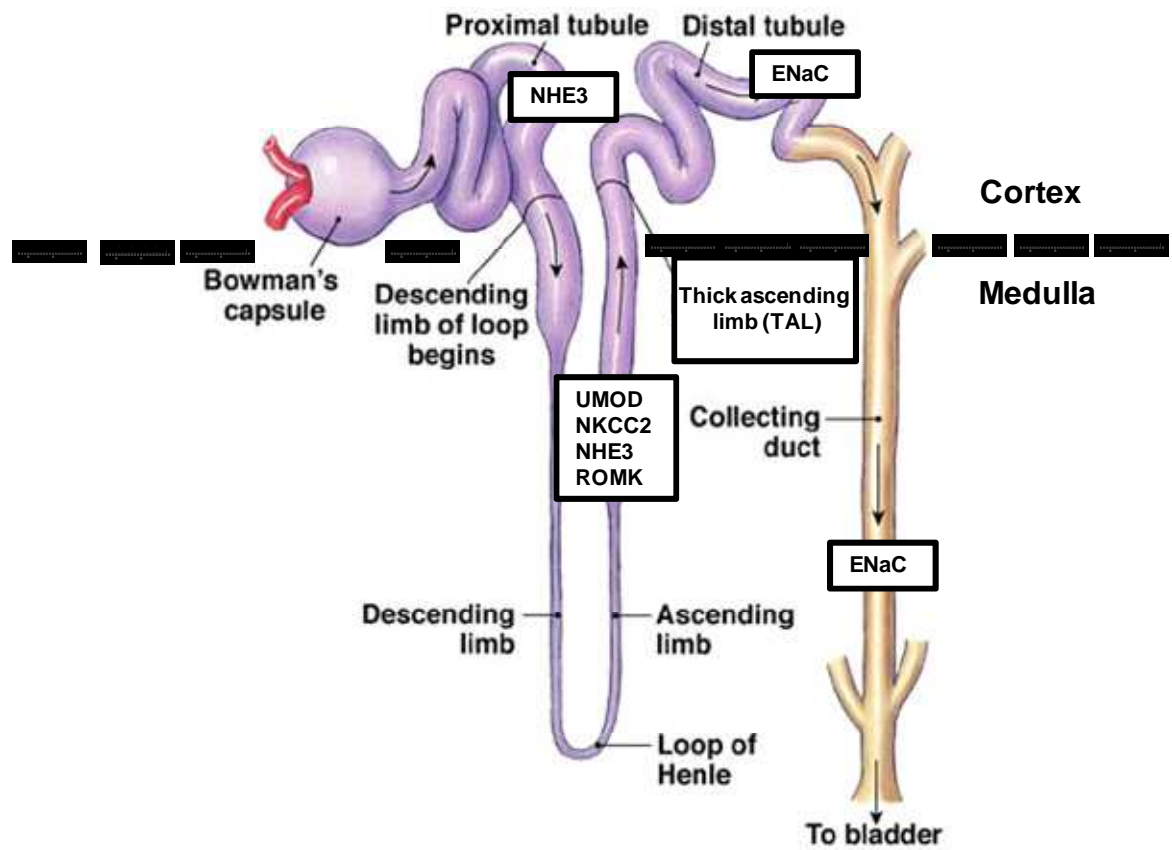
Figure 1-3 Indication of transporter position in the nephron.
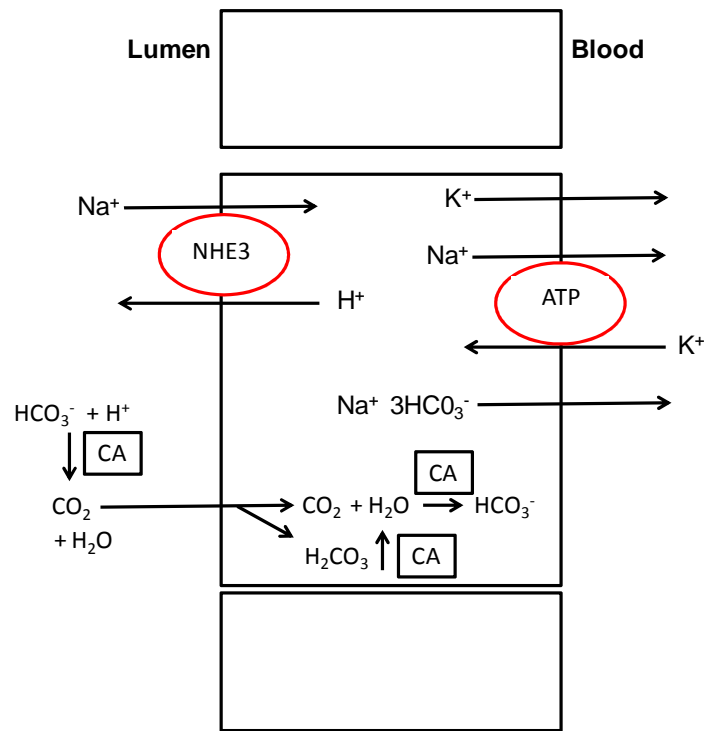
Figure 1-3 Na$^+$ transport actions of NHE3
The NHE3 anti-porters are positioned at the luminal apical membrane in the proximal convoluted tubule and the thick ascending limb (TAL) of the loop of Henle. NHE3 transports Na$^+$ into the cell in exchange for H$^+$ into the tubular lumen by the electrochemical gradient produced by Na+ -K+ /ATPase. The secreted H+ combines with HCO$_3^-$ to form H$_2$O and CO$_2$ and the latter diffuses into cells. Carbonic anhydrase (CA) allows rapid conversion of H$_2$CO$_3$ into H$_2$O and CO$_2$. Secreted H$^+$ generates OH$^-$ inside the cell which is then converted into HCO$_3^-$ by combining with CO$_2$. The HCO$_3^-$ leaves the cell via the basolateral Na$^+$ -3HCO$_3^-$ co-transporter (adapted from (Sahay et al., 2007)).
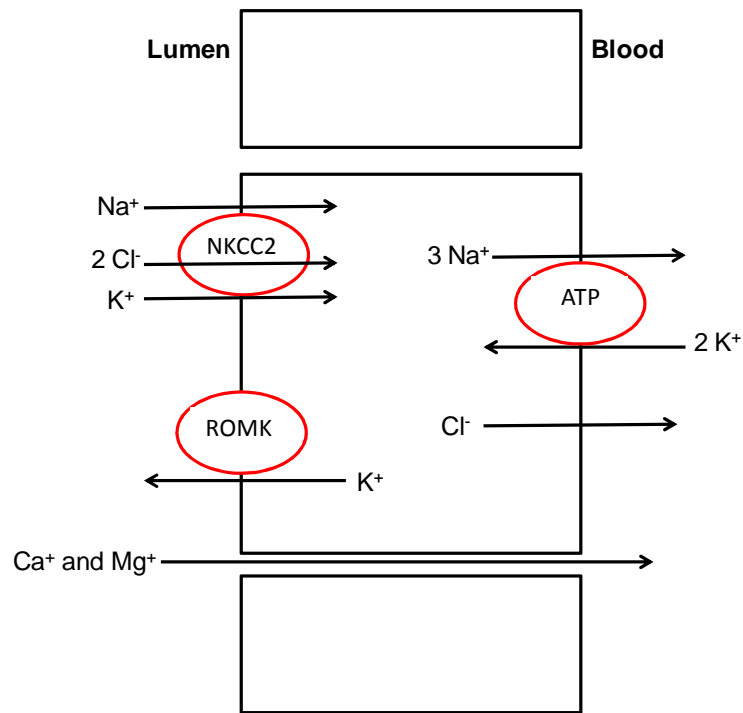
Figure 1-4 Na⁺ transport actions of NKCC2 and ROMK

NKCC2 and ROMK symporters are co-localised at the position of the luminal apical membrane at the TAL. NKCC2 transports 1 Na^+, 1 K^+, and 2 Cl^- into the cell via electrochemical gradient produced by Na^+ - K^+ /ATPase. Na+ and Cl- are transported to the peritubular fluid whilst K^+ is re-cycled back to the tubular lumen via ROMK. For each Na^+ ion transported into the cell by NKCC2, 1 Na^+ ion is absorbed via paracellular pathways. The absorption of Na^+ and Cl^- by NKCC2 is an example of secondary active transport (adapted from (Sahay et al., 2007)).
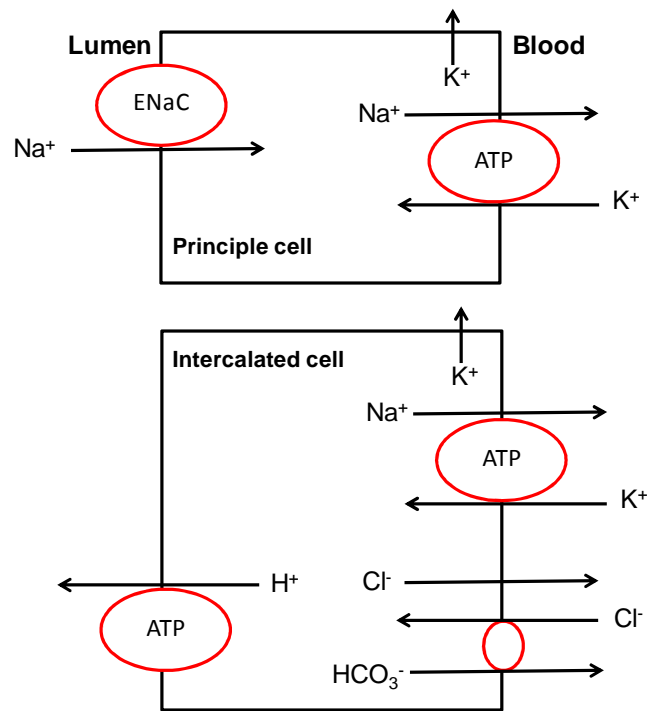
Figure 1-5 Na$^+$ transport actions of ENaC
ENaC sodium transporters are positioned on the apical membranes of the distal convoluted tubule and predominantly along the collecting duct. ENaC at the collecting duct is responsible for the electrogenic Na$^+$ reabsorption by the Na$^+$ -K$^+$ /ATPase pump across the apical membrane of principal cells. Providing the driving force for K+ secretion through K+ channels and plays a role in H$^+$ or HCO$_3^-$ secretion. The lumen-negative potential generated by ENaC also provides a driving force for Cl- absorption across tight junctions and lateral intercellular spaces (adapted from (Sahay et al., 2007)).

1.4.3 Pressure diuresis and natriuresis

A central component of the feedback system for long-term control of arterial pressure is the pressure-diuresis/natriuresis mechanism, whereby increases in renal perfusion pressure lead to decreases in sodium reabsorption with increases in urine output and sodium excretion. Guyton and colleagues were the first to demonstrate these mechanisms were capable of determining and maintaining long term arterial pressure (Guyton, 1967, Guyton et al., 1964, Guyton et al., 1980). The concept posed that when arterial pressure rises (regardless of stimulus or cause); the kidneys excrete excess quantities of salt and water, thus decreasing blood volume. The contraction of blood flow reduces as does BP. Conversely, when arterial pressure falls below normal levels, the incoming fluid is greater than the excreted fluid causing increased BP. They reported that if daily water intake and salt intake remained constant, then arterial pressure would be normal i.e. the rate of fluid loss is equal to the rate of fluid gained. The theory implicated that in times of increased peripheral resistance would result in increased urine output (with increased Na^+ and water excretion) to reduce ECF and blood volume. This kidney fluid system constituting a pressure feedback control mechanism was defined as "infinite gain" (Cowley, 1992). When a control system corrects a perturbation minimally, its feedback gain is near zero. When it corrects it completely, its gain is infinite, and the infinite gain function ultimately dominates.

The use of renal function curves demonstrates the normal effect of differing arterial pressures on fluid excretion by the kidneys (Guyton, 1991), in that arterial pressures below 40 to 60 mmHg in normal kidneys results in no urine output. However above this basal level, kidney excretion increases rapidly with pressure. Therefore, intake and excretion must be equal and to calculate pressure natriuresis and this is known as "equilibrium pressure". The kidney fluid system does not act rapidly as effects on pressure may not be apparent until 2 – 4 days pass before the pressure is within 1 mmHg of the equilibrium level (Guyton et al., 1980). The pressure diuresis/natriuresis mechanism is the only known control system of these capabilities. Hypertension provides the error signal for re-establishing extracellular fluid volume by turning on pressure natriuresis.

1.4.4 Glomerular filtration rate

Glomerular filtration rate (GFR) describes the flow rate of filtered fluid through the kidney, and is the accepted standard method to assess kidney function. Normal values in humans, related to age, sex, and body mass, are approximately 130 ml / m / 1.73 m^2 in healthy males and 120 ml / m / 1.73 m^2 in healthy females (Stevens et al., 2006). GFR is measured as urinary and plasma creatinine level as an estimated filtration maker. Creatinine is freely filtered by the glomerulus and studies support the similarity of creatinine clearance (CrCl) to GFR and its reciprocal relationship with serum creatinine levels (Stevens and Levey, 2005, Levey, 1990). An estimated GFR below 60 ml / m / 1.73 m^2 is associated with decreased kidney function and risk of essential hypertension as CVD is between 5 and 30 times higher in patients undergoing dialysis than in subjects of the same age, race, and gender from the general population (Sarnak et al., 2003, Go et al., 2004). This reflects a high prevalence, incidence, and fatality of CVD in subjects with compromised kidney function measured as GFR. Manjunath *et al* compared the risk relationship between GFR and CVD among middle aged and elderly subjects. Both cohorts displayed increased risk of CVD with lower GFR however the absolute risk was higher in the older cohort (Manjunath et al., 2003a, Manjunath et al., 2003b). Additionally, McQuarrie and colleagues reported that patients with essential hypertension and chronic kidney disease had a lower mean eGFR (38.6 ml / m / 1.73 m^2) in comparison to the control group of hypertensive subjects (90.4 ml / m / 1.73 m^2). These findings support the importance of GFR as a predictor or renal function and risk for hypertension.

1.5 Salt sensitivity in Hypertension

In a subset of the human population, BP rises as a result of habitual increased salt consumption (Weinberger, 1996); individuals who manifest this trait are salt sensitive. If the kidney fluid system for pressure control and the RAAS function normally, humans can consume extremely small or extremely high levels of salt without major alterations in arterial pressure (salt resistance) (Guyton, 1991). What distinguishes salt sensitive from salt resistance subjects is that in the face of high salt intake salt sensitive subjects raise their BP and can only maintain sodium balance by resorting to pressure natriuresis. An association between salt

sensitivity and a greater propensity to develop essential hypertension and renal failure has been described in some populations such as elderly people and black people (Luft et al., 1991, Aviv et al., 2004b). In elderly patients with hypertension, Shimamoto and colleagues demonstrated that the hemodynamic response to NaCl load changed with time. Initially the increased BP was sustained by increased cardiac output; however, after two weeks hypertension was sustained by peripheral resistance (Shimamoto and Shimamoto, 1990). Another study investigated effects of low and high NaCl diet on cardiac output and peripheral vascular resistance in salt sensitive and non salt sensitive subjects and found increments of cardiac output in the high and low NaCl diets in the salt sensitive subjects, whereas peripheral resistance did not differ between the groups on either diet (Fujita et al., 1980). Hemodynamic responses to high NaCl is easier to determine in rodent models in salt sensitive stains. During high NaCl intake cardiac output was similar between the strains but peripheral resistance reduced in Dahl resistant rats but increased in Dahl sensitive rats. Simchon *et al* confirmed that 4 weeks of 8% NaCl caused sustained hypertension in Dahl sensitive rats due to increased blood volume and cardiac output (Simchon et al., 1991). These studies are consistent with Guyton's hypothesis.

Other groups have described a model of salt sensitivity in differing ethnicities, and reported in comparison to white people; black people have lower plasma renin activity (PRA) (Kilcoyne et al., 1974, Berenson et al., 1979, Channick et al., 1969, El-Gharbawy et al., 2001, Lasker et al., 1985). With high sodium intake, black people have a higher GFR and a lower renal plasma flow (RPF) (Campese et al., 1991). With low sodium intake, the GFR/RPF ratio is not different between black people and white people (Price et al., 2002), however, interestingly, ACE inhibition is more effective than antihypertensive agents in attenuating the progression of decline in kidney function of black people who manifest kidney disease with essential hypertension (Sica and Douglas, 2001, Wright et al., 2002). It has been suggested that the lower PRA and sodium sensitivity in black people could arise from either; a primary increase in proximal tubule sodium reabsorption resulting in expansion of the ECF volume or a primary reduction in sodium reabsorption by the proximal tubules leading to tubular hyperfusion of the macula densa and suppression of the RAAS (reviewed

in (Aviv et al., 2004a)). Urinary excretion of K^+ is lower in black populations than white populations, Luft *et al* reported that black people consistently excreted less urinary K^+ than white people when maintained on a 80 mmol/d K^+ diet with differing regimes of NaCl, reaching as high as 1500 mmol/d. At the end of the study white subjects had a net K^+ deficit of -334 mmol, whereas black subjects had a net deficit of only -45 mmol (Luft et al., 1979b). Potassium transport is highly linked to sodium reabsorption; therefore sodium transport mechanisms described in section 1.4.2 may explain salt sensitivity in black people. Studies have suggested that NKCC2 activity is higher in black people as furosemide treatment increased urinary K^+ excretion in this demographic, thus increasing Na^+ reabsorption and ECF volume, reducing PRA, and urinary K^+ excretion (Luft et al., 1979a). In addition to the clinical evidence, animal models have illustrated that an increase of NKCC2 is associated with salt sensitive hypertension. In Dahl salt sensitive and Milan hypertensive rats NKCC2 Na^+ transport was elevated (Alvarez-Guerra and Garay, 2002, Ferrandi et al., 1990).

Although physiological examination of BP control has helped dissect the basic relationships between rapid, intermediate, and long term control systems of arterial pressure the causation of essential hypertension remains an important factor for investigation.

1.6 Causation and Epidemiology of essential Hypertension

The etiology of elevated blood pressure has not been determined in the vast majority of individuals with essential hypertension as there is no known singular cause of the complex heterogeneous and multifactoral disorder. Studies have focused on the dissection of environmental and genetic causality of essential hypertension in the search of understanding the molecular pathogenesis of the condition.

1.6.1 Environmental factors

There is growing evidence that complex interactions among multiple environmental factors play an important role in determining an individual's risk of various common diseases including hypertension (KUNEŠ J, 2006). This

evidence supports that gene-gene interactions and gene-environmental interactions must be ubiquitous given the complexities of intermolecular interactions that are necessary to regulate gene expression and the hierarchical complexity of quantitative traits. A number of environmental factors increase BP these include; obesity, high dietary sodium intake, excess alcohol consumption, smoking, stress, aging, sedentary life style, low K^+ intake, and low calcium intake (1988, Sever and Poulter, 1989). It has been documented that 50 -70 % of the variance in SBP is attributed to environmental factors (Cui et al., 2002, Annest et al., 1979), for example; populations who have inherited optimal BP will have SBP ≤120 and DBP ≤80 mmHg, whereas if one or more environmental factors were added to this population SBP would increase to the range of ≤135 mmHg and DBP ≤85 mmHg. If subjects who have inherited BP in the normal range (≤130 / ≤85 mmHg) were to have one or more environmental risk factors BP would increase to the high normal range (139/85 mmHg) or stage one of the hypertensive category (140 - 159/85 - 89 mmHg). If one or more environmental factors were added to populations of inherited hypertension (≥140/90 mmHg) these subjects would display severe high BP (Campese, 1994).

Therefore, it can be said that environmental factors also have an important link with genetic components. The relationship between the two can influence intermediary phenotypes such as sympathetic nerve activity, the Renin Angiotensin Aldosterone System (RAAS), the renal kallikrein system, vascular reactivity, Na^+ excretion, and cardiac contractility contributing to blood pressure phenotypes. Increased sodium intake is most relevant to studies of this thesis as this is linked with augmented extracellular fluid volume and BP.

The International Study of Salt and Blood Pressure (INTERSALT) project was a large, prospective epidemiological study involving 52 centres from 32 countries. Results from 10,079 individuals identified a strong link between sodium excretion and systolic blood pressure that was independent of any other risk factors for hypertension (Elliott et al., 1989). Additional intervention studies reduced salt intake in either normotensive or hypertensive individuals and showed that blood pressure levels were reduced on low sodium diets. This was the case for both acute (less than 4 weeks) and prolonged salt restricted diets, which reduced salt intake from 10 g/day to 5g/day (MacGregor et al., 1982, Meneton et al., 2005). Moreover, a recent meta analysis of 19 separate cohorts

demonstrated that high sodium intake (average increase in salt intake of 5 g/day) increased the risk of total incidence of CVD (Strazzullo et al., 2009).

1.6.2 Genetic factors

Epidemiology and family aggregation studies have established multiple lines of evidence demonstrating that genetic factors contribute 30-50 % of blood pressure variation (Levy et al., 2000). Individuals who have one or two parents with hypertension are approximately twice as likely to develop increased blood pressure phenotypes, furthermore, blood pressure is increasingly correlated in identical twins (monozygotic) than non identical twins (dizygotic) (Luft, 2001). The Victorian family Heart study investigated the correlation between SBP with family member pairs, reporting a decreased correlation of SBP with decreasing genetic similarity (Harrap et al., 2000). Adoption studies show correlations in blood pressure are more significant between biological parent and child than parent and adopted child (Biron et al., 1976, Mongeau et al., 1986). Similar to other complex diseases, the identification of genetic mechanisms in prevalent hypertension is difficult due to lack of identifying specific genes involved, and the extent to which particular genes contributes to the phenotypes, populations and environments. However, the study of genetic variation implicates common and rare mutations that are involved in the genetic architecture of essential hypertension.

1.6.2.1 Monogenic forms

Monogenic (single gene mutation) or Mendelian disorders have identified rare variants responsible for large effects on blood pressure. Work primarily performed by Lifton and colleagues (Lifton et al., 2001) identified rare mutations affecting at least 10 genes that altered BP predominantly through changed renal salt homeostasis and water handling, reinforcing the importance of renal involvement in long term blood pressure control. The Mendelian mutations can be characterised into groups that contribute to a common mechanism of altered tubular reabsorption of sodium, potassium, and chloride, volume expansion, hypertension, or hypotension. Each are discussed in turn below.

1.6.2.2 Glucorticoid Remediable Aldosteronism (GRA)

This is an autosomal dominant form of monogenic hypertension where aldosterone secretion is regulated by adrenocorticotrophic hormone. There are variable associated findings of the condition including: normal or elevated aldosterone levels despite lower or suppressed renin activity (Sutherland et al., 1966), low serum potassium levels (Hypokalemia), and metabolic alkalosis caused by elevated blood pH (Rich et al., 1992). The genetic mutation arises due to a chimeric gene fusing nucleotide sequence between two closely related aldosterone steroid biosynthesis genes. These genes encode aldosterone synthase and steroid 11ß- hydroxylase. The chimeric gene results from a mismatch crossing over to produce a gene containing the promoter region of 11ß- hydroxylase with the structural portion of aldosterone synthase (Lifton et al., 1992a, Lifton et al., 1992b). This encodes a protein with aldosterone synthase enzymatic activity whose expression is regulated by adrenocorticotrophic hormone (ACTH). As a consequence, aldosterone secretion becomes linked to cortisol secretion leading to increased volume expansion, metabolic alkalosis with hypokalemia, low plasma renin, high aldosterone, and hypertension.

1.6.2.3 Apparent Mineralocorticoid excess (AME)

AME is an autosomal recessive form of monogenic juvenile hypertension with hypokalemia, and metabolic alkalosis with suppressed plasma renin activity due to a virtual absence of aldosterone ((Carretero and Oparil, 2000b). The mutation is found in the renal specific isoform of 11ß- hydroxysteriod dehydrogenase (Mune et al., 1995). The normal functions of this enzyme converts cortisol into the inactive metabolite cortisone, which is of importance as cortisol and aldosterone have similar capacity to bind to the mineralocorticoid receptor (MR). This enzymatic discrepancy allows MR in the nephron to be occupied and activated by cortisol resulting in Na^+ and water retention, volume expansion, low renin, low aldosterone, and salt sensitive hypertension mediated by increased ENaC activity (Mune et al., 1995).

1.6.2.4 Liddle's syndrome

This syndrome is a dominant form of monogenic hypertension resulting from mutations of ENaC β or γ subunits. The condition results in the deletion or missense mutations of the cytoplasmic C terminal, PPXY (proline, proline, proline, any amino acid, tyrosine) of the ENaC subunits. The PPXY domain of the ENaC subunits interacts with Nedd4-1 and Nedd4-2 proteins as a first step in the ubiquitination and clearance of ENaC (Staub et al., 1996, Kamynina et al., 2001). Disruption of the PPPXY domain therefore causes reduced clearance of ENaC from the tubule membrane, resulting in increased ENaC numbers and activity, leading to salt retention and hypertension. This condition is associated with early onset of hypertension, hypokalemia alkalosis, suppressed plasma renin activity, and low plasma aldosterone levels (reviewed in (Lifton et al., 2001). The severity of the hypertension and hypokalemia vary between individuals raising the possibility that some sufferers have salt sensitive hypertension and some have Liddle's syndrome (Hansson et al., 1995).

1.6.2.5 Pseudohyoaldosteronism type I (PHA I)

This condition features severe neonatal hypotension with salt wasting despite marked elevations in aldosterone levels. There are two forms, autosomal recessive and autosomal dominant (Huang et al., 1995). Patients with the dominant form arise from a heterozygous loss of function mutation of the MR. This partial loss of function impairs salt reabsorption as ENaCs action to establish the electrical driving force for K^+ and H^+ secretion in the distal tubule is abolished accounting for the hyperkalemia and metabolic acidosis (Geller et al., 1998), indicating that two normal copies of MR are required for normal salt reabsorption. The autosomal recessive form arises from loss of function mutation in any of the ENaC subunits (Chang et al., 1996). Akin to the dominant form of PHA I, the recessive form features salt wasting and hypotension in neonates. Unlike the dominant form these sufferers do not improve with age. Expression studies have confirmed this mutation impairs ENaC function in the same way as dominant PHA I, however in addition to these affects on renal sodium handling these sufferers can display respiratory failure due to impaired clearance of water in the lung (Barker et al., 1998, Hummler et al., 1996).

1.6.2.6 Pseudohypoaldosteronism type II (PHA II)

Pseudohypoaldosteronism type II (PHAII), is also referred to as Gordon's Syndrome, with sufferers displaying hypertension, hyperkalemia, hyperchloraemia, and metabolic acidosis rather than volume depletion. It is an autosomal dominant condition caused by mutations in serine-threonine kinase genes, *WNK1* and *WNK4* (Mansfield et al., 1997, Wilson et al., 2001). WNK stands for "With No Kinase" and are named so as they lack lysine in the ATP-binding cassette of the catalytic region. Patients with WNK1 mutations have intronic mutations that increase the abundance of WNK1 and patients with WNK4 mutations have missense mutations that localise at the short region in a highly conserved WNK residue. PHA II mutant WNK4 mutations decrease cell surface expression of ROMK, inhibiting K^+ and Cl^- transport (Kahle et al., 2003). PHA II patients have increased distal chloride reabsorption resulting in reduced electronegativity of the lumen, thereby decreasing the electrochemical gradient for K^+ excretion. Yang *et al* developed a mouse model to replicate human PHA II; mice were generated with one normal copy of WNK4 and one mutant WKN4 (D561A) (Yang et al., 2003). The rodent model confirmed phenotypes of the human disease; hypertension and hyperkalemia. There are no *in vivo* studies so far dissecting the role of WNK1 mutations and ion transport, however *in vitro* assays have shown WNK1 mutations inhibits ROMK activity by stimulating endocytosis of ROMK (Wade et al., 2006). Serum and glucocorticoid regulated kinase 1 (SGK1) is induced and activates ENaC and ROMK by phosphorylation of effector molecules such as Nedd 4-2. The serine residues S1169 of SGK1 phosphorylate WNK4. Once phosphorylated at this site, WNK4 is no longer able to inhibit ENaC and ROMK (Ring et al., 2007).

1.6.2.7 Brachydactyly

Brachydactyly is an inherited condition which is defined by shortened fingers and toes due to unusually short bones. Hypertension and Brachydactyly are always inherited together (100 % co-segregation) (Luft, 1998) and map to the short arm of chromosome 12. In this monogenic condition, BP is not affected by volume expansion as the responses to renin, aldosterone, and norepinephrine appear to be normal, and individuals with the condition do not display salt sensitivity (Schuster et al., 1996). Studies on the autonomic nervous system have revealed

decreased baroreflex sensitivity with significantly impaired blood pressure buffering, which suggests that hypertension in the patients may be related to an abnormality in the baroreceptor reflex function (Jordan et al., 2000).Thus identification of the gene responsible may provide useful in the dissection of genetic alterations in essential hypertension.

1.6.2.8 Bartter and Gitelman syndromes

Gitelman syndrome presents as a form of hypotension and renal sodium wasting caused by monogenic mutations. This condition is genetically homogeneous and is caused by loss of function mutations of the NCC transporter (Na-Cl co-transporter in the distal convoluted tubule (DCT)) (Simon et al., 1996b). Patients usually present in adulthood with lower BP than the general population and display neuromuscular symptoms. These individuals have low serum magnesium (Mg^+) and low urinary calcium (Ca^+) (Bettinelli et al., 1992). The sodium wasting at the DCT activates the RAAS, however in this condition activation of the MR is able to augment ENaC activity, protecting sodium homeostasis at the expense of increased H^+ and K^+ secretion.

Bartter syndrome is distinguished from Gitelman syndrome by hypercalciuria (increased urinary calcium) with normal or only mildly reduced Mg^+ levels. Neonates usually present with life threatening hypotension where the mutation occurs from three genes that are necessary for normal sodium reabsorption in the TAL. Mutations result from loss of function of NKCC2 impairing sodium reabsorption across the apical membrane (refer to **Figure 1-5**), resulting in salt wasting phenotypes with consequent activation of the RAAS. ROMK and CLCNKB gene mutations cause similar phenotypes of low BP, sodium wasting and hypokalemia. ROMK usually directs K^+ across the apical membrane of the TAL (refer to **Figure 1-5**). The mutations results in salt wasting as: fluid entering the TAL has increased concentrations of Na^+ and Cl^- with low K^+ thus the stochiometric flux of Na^+ and K^+ via NKCC2 rapidly depletes K^+ in the luminal fluid which prevents efficient reabsorption of Na^+ and Cl^- (Simon et al., 1996a). This chain of events can be avoided by K^+ entering back into the luminal fluid, implicating ROMK as the necessary channel for the recycling of K^+ to maintain Na^+ and Cl^- reabsorption. Bartter's syndrome type 3 is caused by mutations of the Cl^- channel CLCNKB (Simon et al., 1997). NaCl entering the cell via NKCC2 at

the apical membrane must exit the cell via the Na^+ -K^+ /ATPase at the basolateral membrane; however this mutation prevents normal Cl^- exit due to inhibition of membrane localisation. Demonstrating the importance of synchronised actions of these channels in blood pressure regulation.

1.7 Antihypertensive Treatment

The goal of antihypertensive treatment is to reduce CVD risk and its morbidity and mortality rates. Life style modifications such as: weight reduction, increased physical activity, moderation of alcohol intake, dietary modification, sodium intake reductions, potassium repletion, calcium repletion, macronutrient alteration, and smoking cessation will benefit BP management (Carretero and Oparil, 2000a). In spite of this, pharmacological intervention is the required treatment to control BP in most cases. **Table 1-1** outlines the antihypertensive treatments for patients with comorbid conditions. Patients are commonly treated with one or more of the following antihypertensive therapies, angiotensin converting enzyme (ACE) inhibitors, angiotensin II receptor antagonists, calcium channel blockers, diuretics and beta-blockers. ACE inhibitors reduce the formation of angiotensin II and aldosterone, which leads to reduced vascular tone and extracellular fluid volume and thus reduce BP. Angiotensin II receptor antagonists and calcium-channel blockers act as vasodilators to widen resistance arteries, reducing peripheral resistance. Diuretics increase water and salt excretion, thereby reducing extracellular fluid, blood volume and BP. Beta-blockers reduce cardiac output and hence reduce BP. The National Institute for Health and Care Excellence (NICE) quality standard guidelines defined in March 2013 (**http://guidance.nice.org.uk/QS28**), recommend the management and treatment of primary hypertension in adults should be followed by clinicians as per **Figure 1-6** and **Figure 1-7**.

Condition	Drug Therapy (hypertension)
Heart Failure	ACE inhibitors, Diuretics, or B-blockers
Diabetes mellitus (type 1)	ACE inhibitors
Isolated systolic hypertension	Diuretics or calcium channel blockers
Myocardial Infarction	B-blockers or ACE inhibitors
Angina	B-blockers or calcium channel blockers
Atrial tachycardia and fibrillation	B-blockers or calcium channel blockers
Cyclosporine induced hypertension	Calcium channel blocker
Diabetes Mellitus (type 1 and 2)	ACE inhibitors or calcium channel blockers
Dyslipidemia	B-blocker (nonintrinsic sympathomimetic activity), diuretics, or α-blockers
Hyperthyroidism	B-blocker
Renal insufficiency (excluding renal hypertension)	ACE inhibitor
Peripheral vascular disease	B-Blocker
Pre-eclampsia	ACE inhibitor or angiotensin II receptor blockers
Renovascular disease	ACE inhibitor or angiotensin II receptor blockers

Table 1-1 Antihypertensive drug therapy for patients with comorbid conditions (adapted from (Carretero and Oparil, 2000a)
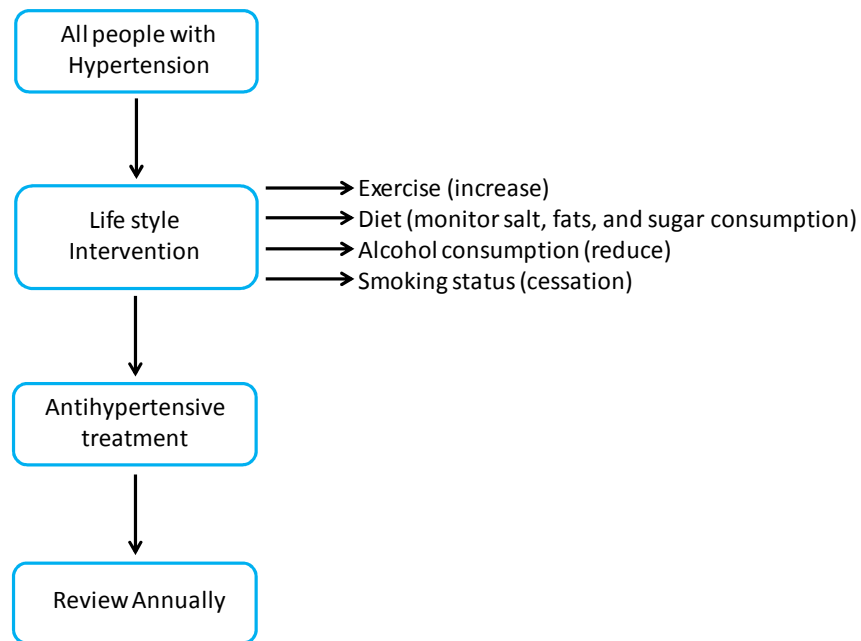
Figure 1-6 NICE guidelines to clinicians for management of hypertension.
Adapted from (**http://pathways.nice.org.uk/pathways/hypertension/management-of-hypertension**).

```
┌─────────────────────────────┐
│ Starting antihypertensive drug │
│         treatment            │
└─────────────────────────────┘
              │
              ▼
┌─────────────────────────────┐        ● Prescribe non-propietary drugs if appropriate
│    General treatment        │        ● People with isolated systolic hypertension ≥160
│      principles             │          mmHg should be treated the same as people with
└─────────────────────────────┘          raised SBP and DBP
              │                         ● Do not combine ACE inhibitors with
              │                           Angiotensin II receptor blocker
              ▼                         ● Take into account any co-morbidities
┌─────────────────────────────┐
│ Blood pressure targets: Daytime average of │ ──▶ ● Age ≤ 80 years BP should
│ ambulatory blood pressure or home blood    │       be ≤ 135/85 mmHg
│ pressure monitoring                        │
└─────────────────────────────┘ ──▶ ● Age ≥ 80 years BP
              │                        should be ≤ 145/85
              ▼                        mmHg
┌─────────────────────────────┐
│         Treatment           │
└─────────────────────────────┘
         │              │
         ▼              ▼
┌──────────────┐  ┌─────────────────────────┐
│  ≤ 55 years  │  │ ≥ 55 years or Black (African or │
└──────────────┘  │ Caribbean origin of any age)    │
         │         └─────────────────────────┘
         ▼                    │
┌──────────────┐              ▼
│ Step 1: ACE inhibitor │  ┌─────────────────────┐
│ or Ang II blocker     │  │ Step 1: Calcium     │
└──────────────┘         │ channel blocker     │
                          └─────────────────────┘
```

Step 2: Combine treatment of ACE inhibitor or Ang II blocker with Calcium channel blocker

Step 3: Combine step 2 with Thiazide like diuretic

Step 4: Resistant hypertension, follow step 3 and consider the addition of other diuretics and α and/or β blockers

Monitor treatment and review annually

Figure 1-7 NICE guidelines to clinicians for antihypertensive treatment
Adapted from (**http://pathways.nice.org.uk/pathways/hypertension/antihypertensive-drug-treatment**).

1.7.1 Hypertensive treatment with Diuretics

As the kidney is the principle organ responsible for long term blood pressure control via mechanisms regulating Na^+ homeostasis, fluid volume balance, and acid base balance defects in ion transport or regulators of ion transport can lead to the development of essential hypertension. In essential hypertension, pharmacological intervention targets kidney ion transporters. Diuretics are used as a common treatment (in combination with other pharmacological intervention) to produce natriuresis and diuresis by acting upon and blocking the activities of various Na^+ transporters along the nephron. There are many types of diuretics that fall into the following categories: high ceiling loop diuretics, Thiazides, carbonic anhydrase inhibitors, potassium and calcium sparing diuretics, osmotic diuretics, and low ceiling diuretics.

Carbonic anhydrase inhibitors act on the proximal tubule to inhibit, as the name implies, carbonic anhydrase and NHE3 function in hypertension. These are mild diuretics that promote natriuresis. However, these drugs can cause metabolic acidosis and hypokalemia. Loop diuretics are the most potent class of diuretic therapeutics, and they are effective even if GFR is compromised (Sahay et al., 2007). They reach the tubular lumen by secretion in the proximal tubule at the prime site of action; the thick ascending limb of the loop of Henle. This class of loop diuretics acts to block NKCC2 actions in hypertension, but can cause increased acid excretion and metabolic alkalosis (Reeves and Molony, 1988), akin to Barrter syndrome which share homology to the actions of loop diuretics. Thiazides are a type of diuretics that target the distal convoluted tubule, where they block 40 % of coupled reabsorption of Na^+ and Cl^-. The action of thiazides mimics the characteristics of Gitleman syndrome (Hoover et al., 2003). Potassium sparing diuretics comprise of two different classes; amiloride/triamterene and spironolactone. The former are epithelial Na^+ channel blockers and the latter are competitive aldosterone antagonists. Distal K^+ sparing agents act on the principle cells in the late distal convoluted tubule, initial connecting tubule, and cortical collecting duct where they inhibit luminal sodium entry. These drugs only allow short term natriuresis. One caveat of these drugs is the progressive diuretic tolerance in patients, this is due to diuretics blocking Na^+ reabsorption in one segment of the nephron which leads to hypertrophy of other nephron segments and consequent increase Na^+

reabsorption in these segments. Thus combining different classes of diuretics acting on differing segments of the nephron may minimise these effects. These diuretics and their actions are outlined in **Table 1-2**.

Drug name	Site of action	Mechanism
Acetazolamide	Proximal tubule	NHE3
Frusemide	Loop of Henle	NKCC2
Bumetanide	Loop of Henle	NKCC2 / Na^+ -K^+ /ATPase
Thiazides	Early distal convoluted tubule	NCC
Amiloride	Late distal convoluted tubule and collecting duct	ENaC
Spironolactone	Late distal convoluted tubule and collecting duct	Mineralocorticoid antagonist

Table 1-2 Common diuretics and their site of action (adapted from (Sahay et al., 2007))

1.8 The study of Genetic architecture to identify genes of essential hypertension

The most common type of human genetic variation is the single nucleotide polymorphism (SNP), a position at which two alternative bases occur at appreciable frequency (> 1 %) in the human population. These heritable variations lead to susceptibility to hypertension. Furthermore, detailed studies of genes involved in renal salt handling have identified rare variants (minor allele frequency < 0.1%) that influence blood pressure (Lifton et al., 2001, Ji et al., 2008). Low frequency variants may have substantial effects without demonstrating Mendelian segregation and could contribute to missing heritability (McCarthy et al., 2008). Strategies to identify variants involved in complex traits of essential hypertension can be divided in two broad categories; linkage and association studies. These can be further subdivided into candidate gene analysis and genome wide scans. Candidate gene analysis is where the study of physiologically relevant genes are tested for co-inheritance with phenotype (i.e. hypertension), while genome-wide scans, no assumptions are made and markers throughout the genome are analysed. In recent years, genetic markers studied in linkage and association studies have advanced in the cataloguing of SNPs throughout the genome improving high throughput genetic screening.

1.8.1 Candidate gene studies of hypertension

Candidate gene studies examine polymorphisms in a subset of genes based on prior biological evidence (i.e. test known physiological pathways that affect the phenotype of interest). This type of analysis allows detection of small effects using moderate sample size by limiting the number of SNPs tested allowing favourable multiple correction analysis. However, the use of moderate sample size precludes the study of rare variants as very few participants in the sample have rare genotypes. Furthermore, in candidate gene studies the number of genotyped polymorphisms limit the investigation of possible epistasis and discount variants that lack an obvious phenotype/physiological relationship to complex disease (Charchar et al., 2008). Candidate gene studies of over 15 Mendelian hypertensive or hypotensive syndromes have identified genes involved in renal sodium handling ion channels (*SLC12A3, SLC12A1, KCNJ1, SCNN1A, SCNN1B, SCNN1G, CLCNKB*), aldosterone signalling (*REN, AGT, ACE, AGTR1*), and ion channel regulation (*WNK1, WNK4, SGK1*). The implicated variants explain less than 1% of the observed population variance in BP and these studies are mainly assimilating physiological assumptions that reduce the significance threshold by an order of magnitude.

As these types of studies often ignore epistasis, gene environment interaction, and rare variants there are often inconsistencies between studies in essential hypertension (Pascoe et al., 1992, Wang et al., 2006, Williams et al., 2004, Ji et al., 2008). To date there are no reproducible candidate gene studies of essential hypertension (Padmanabhan et al., 2008), this is potentially due to some of the drawbacks of this type of assessment; the wrong genes may have been initially identified, causative genes may lie upstream or downstream of the investigated gene, and as candidate gene studies rely on previously reported disease mechanisms, limits the discovery of genetic variants in novel pathways.

1.8.2 Linkage analysis studies of hypertension

Linkage studies test the co-segregation of genomic loci and traits in related individuals (Bailey-Wilson and Wilson, 2011) to identify low frequency, rare variants with large effects. This type of analysis is performed in family cohorts where affected and unaffected family members are phenotyped and genotyped. The genetic relationship between family members are statistically analysed to find genetic markers in linkage disequilibrium (when two loci (genetic markers) are inherited together from parent to child more often than expected as a consequence of independent inheritance, they are considered to be linked) with the loci being responsible for the phenotype. When two loci are close together on the same chromosome they segregate more often, and are less likely to be separated by a recombination event at meiosis. Most linkage studies analyse affected sibling pairs, since siblings have on average 50% genetic identity, they should share markers near loci responsible for hypertension more often than would be expected by chance. The number of phenotypes studied, the family structure, the number of families, the number of genetic markers and the linkage between the markers and the loci all dictate the statistical power of linkage analysis.

Linkage analysis has identified BP loci on every chromosome (Binder, 2007). Only approximately half of these studies reported a genome wide significant QTL (quantitative trait loci), and these studies lacked replication. However, the MRC British Genetics of Hypertension (BRIGHT) study was successful in identifying susceptibility loci that modestly increase risk of hypertension by non-parametric linkage (Caulfield et al., 2003). This study initially recruited 2010 affected sibling pairs from 1599 families with severe hypertension (top 5% of blood pressure distribution) and included 3599 individuals in the genome-wide scan; it is the largest homogenous linkage study in hypertension genetics. The study identified a locus on chromosome 6q that achieved genome-wide significance, and three further loci with suggestive significance on chromosomes 2q, 5q and 9q (Caulfield et al., 2003). It has been reported that variants located near the telomere of the chromosome should be viewed with caution (Harrap, 2003) as linkage evidence can be difficult to interpret, as was the case of the locus at 6q in the BRIGHT study. Therefore, a follow-up study included additional polymorphic markers in the regions of interest, and increased the study cohort

to 2142 affected sibling pairs was performed (Munroe et al., 2006). Support for the loci at 2q, 6q and 9q were weakened with this analysis, however, there was increased support for linkage to the locus at 5q. A further two regions at 1q and 11q achieved suggestive significance. A second linkage study was performed using a cohort of families comprising an affected individual, and either two parents or siblings and single parent. The results confirmed the locus at 5q (Munroe et al., 2006).

Although useful, linkage studies have low power for variants with modest effects and fail to produce robust validated loci for hypertension. The field of complex disease genetics has recently progressed from linkage to association study design as association analysis has far greater power to detect variants of modest effect and of lower frequency. Therefore, association studies involving genotype and phenotype of unrelated individuals who are effected and unaffected by phenotype are studied to find disease causing variants. **Table 1-3** outlines the wide spread clustering of hypertension quantitative trait loci (QTLs).

Study	Phenotype	Subject (n)	Chromosome	Population
(Caulfield et al., 2003)	Hypertension	3599	2,5,6,9	White
(Munroe et al., 2006)	Hypertension	3863	5	White
(Rao et al., 2003)	Hypertension	1300	2	African American
(Chang et al., 2007)	Hypertension	1726	1	African American & European American
(Perola et al., 2000)	Hypertension (DBP)	113	1,2,3,22	White
(Hunt et al., 2002)	Hypertension (SBP)	2959	1,7,12,15,6	White
(James et al., 2003)	SBP	1671	1,3,8,17	White
(Puppala et al., 2011)	SBP	1089	6	Mexican-American
(Rice et al., 2002)	SBP	519	3,11	White
(Hamet et al., 2005)	DBP, Mean BP	500	DBP: 1,3,16. Mean BP: 16	French Canadian
(Atwood et al., 2001)	SBP	495	2,8,18,21	Mexican
(Kristjansson et al., 2002)	Hypertension	490	2,11,17,18	White
(Benjafield et al., 2005)	SBP	427	2,5,6,9,15,16,18,20,21	White
(Zhu et al., 2001)	Hypertension	393	2,3,8,15	Chinese
(Ciullo et al., 2006)	Hypertension	173	1,4,8	White
(Gong et al., 2003)	Hypertension	158	12	Chinese

Table 1-3 Linkage analysis studies

Study	Phenotype	Subject (n)	Chromosome	Population
(Yang et al., 2009)	Hypertension	1008	20	Chinese
(Simino et al., 2011)	Hypertension	4266,2154, 4299,2435	6,8,20,21	African American, Asian, White, Mexican American
(Bell et al., 2006)	Hypertension	3863	5,9,11,15,16,19	White
(Levy et al., 2000)	SBP	1585	17,18	White
(Xu et al., 1999)	BP	1450	3,11,15,16,17	Chinese
(Cooper et al., 2002)	DBP	792	2,3,5,7,10,19	Nigerian
(Rice et al., 2000)	SBP	679	1,2,5,7,8,19	White
(Pankow et al., 2000)	SBP	636	6,18	White
(Pausova et al., 2005)	Hypertension	389	1,8,11,13	White
(Allayee et al., 2001)	SBP	388	4,6,8,19	White
(Hamet et al., 2005)	DBP, Mean BP	500	DBP: 1,3,16. Mean BP: 16	French Canadian
(Krushkal et al., 1999)	SBP	427	2,5,6,9,15,16,1 8,20,21	White
(Angius et al., 2002)	Hypertension	77	1,2,13,15,17,19	White
(Barbalic et al., 2009)	SBP	1389	20	White

Table 1-3
Continued

1.8.3 Genome wide association studies of hypertension

The lack of convincing evidence from linkage studies has shifted attention to association studies to identify causative variants in hypertension. Genome wide association studies (GWAS) can uncover common variants with small effect sizes that are often not identified via candidate gene and linkage analysis studies (Ehret, 2010), they are hypothesis generating tests with the aim of identifying common variants not previously implicated in the disease process. There are no assumptions made regarding the location or function of the causal SNP, presuming that common diseases are attributed in part to allelic variants present in 1 – 5 % of the population (Reich and Lander, 2001). Typically, association studies are carried out in unrelated populations and the same allele(s) associated with the trait are assessed throughout the tested population. Differing from linkage studies where traits are associated with differing alleles in differing families. When considering qualitative traits of BP, association analysis measures statistical associations between hypertension (phenotype) and genetic marker (genotype) directly by comparing allele frequencies between cases and controls to establish if a particular allele(s) occurs more frequently in cases vs. controls and vice versa. Whereas, quantitative traits e.g. blood pressure values are assessed for association by means of linear regression. The tested association of both qualitative and quantitative traits operate over shorter genomic distances than that of linkage analysis, but requires more markers. Most association studies rely on large scale, indirect association, to detect causal variants (Palmer and Cardon, 2005). Indirect association measures the relationship between a phenotype and a genetic marker i.e. SNPs, which are correlated with the true causal allele due to linkage disequilibrium (LD). In general SNPs in LD with causal variants are more likely to be inherited together because they are physically close to one another on the genome. However, sometimes this is not the case; studies have shown that levels of local LD vary, with some adjacent SNPs being independent despite their proximity and others of ≥ 100 Kb apart being in useful LD (Weiss and Clark, 2002).

Technological advances now permit the genotyping of hundreds of thousands to more than one million SNPs on a single microarray at a reasonable cost (Fan et al., 2000, Oliphant et al., 2002), allowing investigation of a large proportion of

the variants in the genome. Association study of SNPs against hypertension and BP traits allows unbiased investigation of genetic causes of the traits, which can be considered one of the first direct applications of the Human Genome Project (Lander et al., 2001) and the HapMap project (Frazer et al., 2007).

To date there have been few GWAS studies on hypertension, that have had success in identifying genetic variants that are associated with increased BP, SBP, or DBP (Sabatti et al., 2009, Wang et al., 2009, Kato et al., 2008, Levy et al., 2007). The Wellcome Trust Case Control Consortium (WTCCC) was the first published GWAS in hypertension (2007). This study failed to identify significant variants of hypertension due to poor tagging by genotyping chips, misclassification bias in control groups, confounding by age, and insufficient power. Quantitative phenotypes (SBP and DBP) assessed by GWAS also failed to produce any significant genome wide hits, and implicated genes only an effect size of 2 mmHg for SBP and 1 mmHg for DBP (Levy et al., 2007). An intronic SNP to Cadherin 13 protein (CDH13) was suggestively associated with dichotomous hypertension is a GWAS meta-analysis in three European cohorts (Org et al., 2009). Consequent analysis revealed that even with large sample sizes, power was limited to < 1 % for the replicated variants (Altshuler and Daly, 2007).

Two influential GWAS were examined in two large meta-analyses of subjects of European descent, CHARGE (n = 29, 136) and GlobalBPgen (n = 34,433) (Newton-Cheh et al., 2009, Levy et al., 2009). Fourteen BP loci were discovered in or near genes encoding six enzymes, two ion channels, two transcription factors, a structural protein, and a hypothetical gene (Ehret, 2010). To date GWAS investigation has implicated more than 50 genes in essential hypertension and BP regulation (reviewed in (Simino et al., 2012)). These variants generally only have small effects on BP (< 1 mmHg) and collectively only explain approximately 2.5 % of BP variation within populations. The vast majority (> 80 %) of associated variants fall outside of the coding regions, emphasising the importance of including coding and non coding regions of the genome in search for disease associated variants (Hindorff et al., 2009).

SNPs in the promoter region of *UMOD* have been linked with kidney disease, the minor T allele at position -3,653 (rs12917707) was associated with a 20 % reduction in chronic kidney disease incidence (Kottgen et al., 2009). The minor C

allele at position -1,550 (rs4293393) was associated with enhanced renal function in both controls and subjects with chronic kidney disease (Kottgen et al., 2010), whereas the dominant T allele at this site was associated with increased risk of chronic kidney disease (Gudbjartsson et al., 2010).

One particular GWAS identified a promoter region variant (rs13333226) in the Uromodulin (*UMOD*) gene was associated with BP (Padmanabhan et al., 2010). Padmanabhan and colleagues carried out a GWAS in 1,621 hypertensive cases and 1,699 controls with follow up validation analysis in 19,845 cases and 16,541 controls using an extreme case control design. They identified a locus on chromosome 16 in the 5' region of *UMOD*. It was reported that the minor G allele was associated with a lower risk of developing hypertension, reduced urinary uromodulin excretion, improved renal function; and each copy of the G allele was associated with a 7.7% reduction in risk of CVD events after adjusting for age, sex, BMI, and smoking status. Suggesting that the expression of uromodulin in the TAL may play a putative role of this variant in hypertension via altered sodium homeostasis.

1.9 Discovery of Uromodulin

Tamm Horsfall Protein was discovered in 1950 by Igor Tamm and Frank Horsfall (Tamm and Horsfall, 1950). They used a salt precipitation procedure to isolate a potent inhibitor of viral hemoagglutination from urine. Subsequently, the group went on to characterise the mucoprotein by investigating its putative enzymatic inhibitory properties, and reported neuraminidase treatment abolished the inhibitory effects in hemoagglutination (Tamm and Horsfall, 1952). In 1964, Bayer *et al* confirmed by electron microscopy the binding of influenza to the urinary mucoprotien (Bayer, 1964). Urinary THP was visualised as a network of filaments made up of a collection of smaller fibrils (4 – 24 nm in diameter), however the length could not the detected due to the tendency of end to end aggregates forming. Albert Neuberger and co workers in the 1970's demonstrated that THP: migrates in SDS polyacrylamide gels at an apparent weight of 80 – 90 kDa, 20 – 30 % of which is derived from high sialic acid content and N-linked glycans; is the most abundant protein in the urine, excreted at approximately 50 mg/d; and is present in most mammalian urine (Fletcher et al., 1970a, Fletcher et al., 1970b).

Muchmore and Decker in 1985, used lectin based affinity chromatography to isolate a glycoprotein with *in vitro* immunosuppressive properties from urine of pregnant women, and called the protein uromodulin (Muchmore and Decker, 1985). In 1987, Pennica *et al* confirmed by complementary DNA (cDNA) analysis, that Uromodulin (UMOD) and THP were identical proteins (Pennica et al., 1987).

1.9.1 Protein Structure

Based on the cDNA sequence, the UMOD precursor is composed of 640 amino acid residues and motifs include signal sequence residues 1 – 24, 1 epidermal growth factor like and 2 calcium binding epidermal growth factor like domains (residues 31 – 64, 65 – 107, and 108 – 149), 1 zona pellucid domain at residues 334 - 585 (this is essential for polymerisation), 8 potential N-glycosylation sites, and 1 stretch of hydrophobic amino acids similar that acquire glycosylphosphatidylinositol (GPI) attachment site (residue 614). There are 48 cysteine residues involved in disulphide bond formation (Hamlin and Fish, 1977). It was proposed an additional epidermal growth factor like domain spanning residues 281 – 336 was present in the region between the 2nd calcium binding epidermal growth factor domain and zona pellucida domain. However, a new domain D8C (residues 199-287), common to families of proteins including liver specific zona pellucida, glycoprotein 2, UMOD and several other uncharacterised proteins was described by Yang *et al* (Yang et al., 2004).

UMOD is GPI anchored to the apical plasma membrane, thus its biosynthesis and intracellular trafficking must proceed through a secretory pathway. During biosynthesis, the UMOD precursor is translocated to the ER (endoplasmic reticulum). The signal peptide is then cleaved and the protein glycosylated on 7 of the 8 potential N-glycosylation sites. Disulphide bridges are formed and glypiation on its C terminus occurs, the Golgi apparatus further modifies the N-glycan moieties. The mature glycan moieties and the GPI modifications act to route the protein to the apical membrane of epithelial cells in the TAL, this is when UMOD is finally GPI anchored and facing the tubular lumen, here it is said to form supramolecular structures to ensure its proposed physiological properties are performed (Hoyer et al., 1979). The protein is released for the lumen side of the membrane by specific but currently unidentified protease(s). Proteolytic cleavage was originally thought to occur after residue F548 (Fukuoka and

Kobayashi, 2001), but later thought F587 (Santambrogio et al., 2008). Proteolytic cleavage of the GPI anchor still remains to be determined. The structure and suggested maturation of UMOD is outlined in **Figure 1-8** below**.**
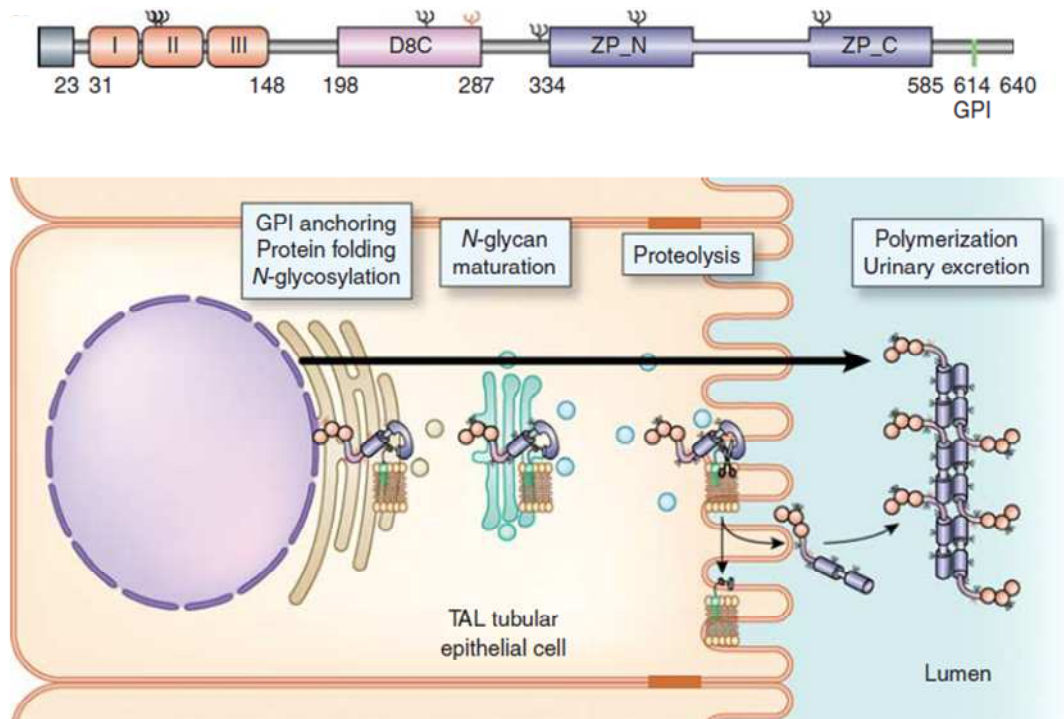
Figure 1-8 Structure and Maturation of Uromodulin
The top panel represents the structure of Uromodulin containing a "leader peptide" (where it is predicted to be cleaved at residue 23), 3 EGF-like binging domains, the unknown central domain of 8 conserved cysteine residues (D8C), a ZP domain, and the GPI anchoring site (predicted at position 614). The 7 N-glycosylation sites are indicated and the high mannose chain on residue Asn 274 is highlighted in red. The bottom panel represents the predicted model of Uromodulin maturation, excretion, and polymerisation. The site of the TAL is where Uromodulin is exclusively synthesised, and is co-translationally inserted in the ER where the GPI anchoring, formation of intramolecular disulphide bonds and N-glycosylation occurs. At the golgi, glycans chains are modified with the exception of the one at Asn 274, which retains high mannose moiety. Uromodulin then reaches the apical membrane in a polymerisation incompetent conformation established by the interaction of two hydrophobic motifs, one within the ZP domain, and one localised between the ZP domain and the GPI anchor. The protease that cleaves the hydrophobic components of Uromodulin into a polymerisation competent monomer from the membrane is yet to be defined. This image was reproduced with permission from (Rampoldi et al., 2011).

1.9.2 Gene

UMOD is located on the reverse strand of chromosome 16 (16p12.3) at the position between 20,344,374 – 20,364,037 bp. The gene is encoded on the reverse strand into 15 splice variants differing in their 5' untranslated region. According to Ensembl databases, 4 of the 15 transcripts have an alternative upstream exon, however further analysis is needed to verify the function of this additional exon in terms of gene expression. In spite of this, many studies have shown that *UMOD* is exclusively transcribed in the kidney, RNA isolated from 150 different tissues were hybridized using a probe for human THP revealed only RNA from human kidney gave positive signals (Pennica et al., 1987). Further immunofluorescence and immunochemical analysis indicated that UMOD resides in the kidney cells exclusively at the TAL (Sikri et al., 1981). Bachmann *et al* utilised protein gold immunocytochemistry to report that rat UMOD was localised in vesicles of Golgi cisternae, fused to the apical membrane of TAL cells (Bachmann et al., 1985). Recombinant UMOD in HeLa cells shows that UMOD accumulates intracellulary as a precursor of approximately 86 kDa, which is converted into a mature molecule of 97 kDa (Rindler et al., 1990)

The transcription specificity of UMOD in the kidney is determined by the *cis*-acting promoter sequence. It has been shown that 3, 3.9, and 1.5 Kb of mouse, bovine, and goat genomic sequences, respectively, locate upstream of the first *UMOD* exon (Zhu et al., 2002, Kim et al., 2003, Huang et al., 2005). The same was shown for the 5.6 Kb of the human genomic sequence, consisting of 3.7 Kb promoter, exon 1, intron 1, and the untranslated part of exon 2 (Zbikowska et al., 2002). Deletions in the Bovine *UMOD* promoter revealed *cis* elements critical for transcription specificity are located within the first 600 bp adjacent to the transcript start site (Kim et al., 2003). Zhu *et al* reported that the first 589 bp of the *UMOD* promoter as highly conserved across species (human, rat, mouse, and cow) and that the 3 Kb promoter region drives kidney specific function of the gene (Zhu et al., 2002).

1.10 Physiological and pathological roles of UMOD

Due to UMODs structure it has one peculiar feature; it has a tendency to aggregate with gel like properties in solution when NaCl concentrations are close to 100 mmol/l or CaCl (calcium chloride) is 1 mmol/l (Brown and Rose, 1992, Benting et al., 1999) which may be responsible for the binding properties of the protein. This along with the GPI anchoring and multidomain structure on the luminal side of the apical membrane, in conjunction with rich and highly variable post translational protein modification, and a large presence of polymerised protein in the urine suggests that UMOD may play multiple roles with site specific physiological functions. However, over 60 years of research has not elucidated the biological role of UMOD, the following sections below recapitulate some of the proposed functions.

1.10.1.1   Role of UMOD at the apical membrane

Sorting of the apical membrane proteins requires GPI anchors, N-glycosylation, and polymerisation, with the large turnover of UMOD and its half life of 16 hours it is assumed that the biosynthesis plays either a direct or indirect role in the formation of the apical membrane targeted cargo vesicles and vesicle trafficking. GPI anchored proteins associate with lipid raft domains that play a role in organising the apical membrane and signalling transduction pathways (Rajendran and Simons, 2005). When the apical membrane is highly ordered it allows for close packing of GPI anchored proteins on the surface of cell membranes, in the case of UMOD this may promote formation of the complex gel like structures providing a water barrier at the luminal membrane of the TAL cells, serving as a physical barrier to water permeability. Such a barrier may play a role in ion transport to maintain countercurrent gradients in the interstitium (Hoyer and Seiler, 1979).

1.10.1.2   Urolithiasis and bacterial infections

In the absence of UMOD there is susceptibility to calcium oxalate stones due to the lack of gel like properties of the protein, thus altered salt concentration at the apical membrane is apparent (Stevenson et al., 1971). Mo *et al* showed that *UMOD* knockout mice spontaneously formed intra-renal crystals predominantly in the interstitial space and in the collecting duct of the deep medulla and papilla

(Mo et al., 2004). They reported that the stones were consisted primarily of calcium phosphate in the form of hydroxyapatite and strongly resemble the stones found in humans caused by idiopathic calcium oxalate stones. The inhibitory affect of UMOD in stone aggregation had been described in cases of calcium oxalate (Bates et al., 2004, Diamond and Paolino, 1973). There is consensus that inhibition of stone formation in normal urine is caused mainly by urinary macromolecules rather than low molecular weight components, and this property has been associated with polyanionic structures (Fellstrom et al., 1986). UMOD is said to be a polyanionic macromolecule due to the large extent of sialylation and presence of sulphate groups bound to the N-linked glycans thus playing a crucial role in regulating stone formation (van Rooijen et al., 1998).

Urinary tract infections (UTI's) are mainly caused by *E Coli*, and critically depends on filamentous appendages on the bacterial surface called fimbriae (Bates et al., 2004). Colonization is mediated by binding of lectin like adhesins present on *E coli* fimbriae to carbohydrate structures carried by glycoprotiens exposed at the cell surface. *E coli* fimbriae are classified according to their sugar specificity: type 1, type P, and type S, Pak *et al* illustrated that UMOD binds with type 1 *E coli* fimbriae *in vitro*, and Raffi *et al* described UMOD as a general host defence mechanism against urinary tract infections (Pak et al., 2001, Raffi et al., 2005) *in vivo* with a UMOD knockout mouse model, supporting the notion that urinary UMOD represents a protective mechanism against UTI's.

1.10.1.3   Urinary excretion

In adults, there appears to be considerable variation in daytime excretion values, but does correlate with urinary volumes brought about with diuresis in those drinking in response to thirst (Lynn et al., 1982). A positive correlation between urinary UMOD and dietry salt intake revealed that in subjects with high salt sensitivity i.e. exaggerated BP response to high salt intake, there is a greater excretion of UMOD in the urine compared low salt intake (Torffvit et al., 2004). UMOD excretion seems to increase gradually from birth to adulthood, where it remains stable until a decline after the sixth decade of life (Ollier-Hartmann et al., 1984, Sobel and Kaye, 1985), with urinary UMOD/creatinine ratio also remains stable from the age of 4 until the age of 70. Reduced urinary excretion of UMOD has also been correlated with GFR and corresponds to

declining kidney function in virtually all chronic kidney diseases (Prajczer et al., 2010). In an attempt to elucidate why urinary UMOD excretion is altered in disease Ma *et al* studied potential mechanisms using human *UMOD* mutations in polarised Madin Darby canine kidney cells (MDCK). They found that a cysteine altering mutation in the evolutionary conserved cysteine rich domain had more sever deficits in ER exit and surface translocation, triggering increased apoptosis than a cysteine altering mutation outside of the domain. Both mutants were able to specifically bind and trap UMOD preventing it from exiting the ER and translocating to the cell surface, explaining partly in some diseases the marked reductions in urinary UMOD (Ma et al., 2012).

1.10.1.4   Inflammation

Identification of GPI anchored enriched endocytic compartments have lead to the hypothesis that UMOD exerts its immunosuppressive affects by binding with high affinity to tumour necrosis factor alpha (TNF-α) and interleukin one (IL-1) (Sabharanjak et al., 2002, Kirkham et al., 2005). Although the exact ligands responsible are yet to be defined, this gives rise to the hypothesis that UMOD may play a role in modulating cell surface events, receptor engagement, and signal transduction at the TAL. Older studies reported that UMOD induced pro-inflammatory effects, one group demonstrated that specific glycans of UMOD isolated from healthy adults interacts with IL-1ß, and glycans contain either N-acetylgalactosamine or sulphate residues for inhibition of lymphocyte proliferation (Tandai-Hiruma et al., 1999). Consequently, several reports have shown that urinary UMOD binds to and activates leukocytes, including neutrophils, lymphocytes, and monocytes (Toma et al., 1994, Horton et al., 1990). According to Yu *et al*, UMOD from pregnant women increases the phagocytic activity of neutrophils by prostaglandin E_2 release, suggesting that UMOD has specific interactions with the membranes of neutrophils (Yu et al., 1992). Similarly, blood mononuclear cells were activated by UMOD in pregnant women, in this case increased levels of IL-1, IL-6, and TNF-α were released from monocytes leading to the proliferation of both B and T lymphocytes (Yu et al., 1993). Another group observed that in non pregnant women UMOD induced secretion of TNF-α from monocytes but several fold lower than that of pregnant women (Su and Yeh, 1999). Human monocytes isolated form peripheral blood, deprived of lymphocytes are able to phagocytise a particle form of UMOD and

generate reactive oxygen metabolites as well as other lysosomal enzymes (Thomas et al., 1993).

Conversely, a more recent study has shown that UMOD binds with high affinity to human TNF-α and IL-8, and low affinity to IL-6 and INF-γ and UMOD is enzymatically digested by carbohydrate specific degrading enzymes reducing protein binding to pro-inflammatory cytokines, mononuclear cell proliferation, and neutrophil phagocytosis enhancing activities (Wu et al., 2008). Advances from the previous study have shown that in UMOD knockout mice there is a marked elevation of circulating TNF-α and IL-1 and enlarged spleens with prominent white pulp macrophage infiltration. They reported that lipopolysaccharide (LPS) exasperated the increase of circulating cytokines without an increase in urinary excretion in *UMOD* knockout mice. This along with a reduced CrCl suggests that diminished kidney function may contribute to reduced cytokine clearance in the *UMOD* knockout mice (Wu et al., 2008). In 2008 it was reported that *UMOD* protects the kidney from ischemic injury by decreasing inflammation and altering Toll like receptor 4 (TLR4). This group performed renal perfusion injury in *UMOD* wild type and knockout mice demonstrating that in the presence of *UMOD* there was less injury and increased expression of *UMOD*, whereas knockout mice displayed renal damage, tubular fibrosis, and increased inflammation. Furthermore, the outer medulla of the knockout mice had associated necrosis with significant interstitium neutrophil infiltration and basolateral location of TLR4 allowing greater affinity for pro-inflammatory cytokines (El-Achkar et al., 2008). Collectively, this suggests UMOD may have dual immunomodulating effects through regulating pro-inflammatory and anti-inflammatory cytokines.

The physiological role of UMOD remains to be fully determined; however there is mounting evidence and research reporting the consequences associated with changes in UMOD primary structure, transcription, expression, post translational modification, localisation, and urinary excretion have identified a number of pathological conditions that implicate potential biological roles of UMOD as a regulatory protein in health and disease.

1.10.1.5   Uromodulin and kidney disease

Renal cystic diseases are a major group of inherited renal conditions, representing the leading cause of end stage renal disease. Cystic kidney disease (CKD), in both the dominant and recessive variants, accounts for the clinical conditions. Hart *et al* and Rampoldi *et al* discovered autosomal dominant mutations in *UMOD* lead to medullary cystic kidney disease type 2 (MCKD2), familial juvenile hyperuricemic nephropathy (FJHN), and glomerular cystic kidney disease (GCKD) (Hart et al., 2002, Rampoldi et al., 2003). These conditions are characterised by urinary concentration deficits, urinary salt wasting, hyperuricemia, gout, medullary cysts, interstitial nephritis, glomerular cysts, hypertension, and end stage renal failure. MCKD2 is autosomal dominant disorder is mainly characterised by hypertension and end stage renal failure, in the fourth decade of life, with a triad of renal complications; tubular membrane disintegration, tubular atrophy, with cyst development at the corticomedullary border and interstitial cell infiltration associated with fibrosis. The condition share clinical and morphological similarities with the autosomal dominant FJHN. GCKD is characterised by a cystic dilatation of Bowmen's capsule and collapse of the glomerulus (Zaucke et al., 2010). All three disorders have significant clinical overlap and arise from *UMOD* mutations and are often referred to as Uromodulin associated kidney diseases (UAKD) and are said to cause the so called "uromodulin storage disease" (Vylet'al et al., 2006, Wolf et al., 2007).

To date there have been more than 58 UMOD mutations reported, that mainly localise to exon 3 and 4 of the *UMOD* gene, with the majority being missense mutations or small inframe deletions (Lhotta, 2010). Early genome wide linkage mapping in Italian, Czech, and Belgian families revealed loci for MCKD and FJHN on chromosome 16 in the regions of 16p11.2 and 16p12 (Dahan et al., 2001, Stiburkova et al., 2000) in close proximity to the *UMOD* gene. These conditions are associated with mutations that lead to amino acid changes at cysteine sites causing defective protein folding and immature UMOD being retained at the ER and not released at the apical membrane and remains intracellular (Bernascone et al., 2006, Rampoldi et al., 2003). Accumulation of misfolded UMOD in the ER causes ER stress causing ER degradation by increased synthesis of chaperones and foldases in order to activate elimination of the misfolded protein (Kitamura, 2008). This unfolded protein response may trigger apoptosis and autophagy or

alternatively lead to cell activation via MAP kinases and NF-$_k$B leading to the eventual progressive renal failure seen in MCKD2, FJHN, and GCKD (Lhotta et al., 1998).

It is known that the transcription factor hepatic nuclear factor 1-ß (HNFIß) positively regulates UMOD expression and binds to the promoter elements of the gene. Inactivation of HNFIß in vivo is associated with decreased *UMOD* transcription (Liu et al., 2012). Interestingly mutations of HNFIß are associated with features of MCKD2, FJHN, and GCKD (Smagula et al., 1990). This transcription factor is also known to regulate nephrocystins which prompted work by Zaucke *et al* in 2010 to investigate if UMOD is linked to cillary cystogenesis (Zaucke et al., 2010). They reported 7 novel *UMOD* mutations (missense or deletion mutations) between exon 4 - 5 and that UMOD is expressed in primary cilia of renal tubules and the number of UMOD positive tubules declines in UAKD. The mutations caused localisation of UMOD in the mitotic spindle poles co-localised with nephrocystin-1, suggesting a novel cause of cystic kidney disease pathologies of MCKD2, FJHN, and GCKD.

1.10.1.6   Deficits in urine concentration in UMOD associated kidney disease

The TAL are nephron segments characterised by high electrolyte and water impermeability and it was proposed that UMOD plays a role in salt transports and acts as a water barrier at this level, a process crucial for urine concentration. Bleyer *et al* reported low urine osmolality was consistent in subjects with *UMOD* mutations (Bleyer et al., 2003). A transgenic mouse model for UAKD confirmed urinary concentrating deficit (Bernascone et al., 2006). Water reabsorption by the tubule is regulated by transmembrane systems of aquaporin and ion channels (Agre and Kozono, 2003), Bachmann and colleagues studied the renal effects of UMOD deficiency in *UMOD* knockout mice and reported the inability of these mice to concentrate urine possibly due to a decrease in cyclooxygenase-2 (COX-2) expression (Bachmann et al., 2005). COX-2 inhibition prevents regulation of key renal water and sodium transport proteins including aquaporin 2 (AQP2), NHE3, and NKCC2 (Norregaard et al., 2005). Confirming the role of UMOD in urine osmolality.

1.11 Uromodulin and blood pressure

This far, it is clear that *UMOD* variants play a role in the pathogenesis of renal disease and plays an important role in the regulation of sodium homeostasis. Padmanabhan and colleagues successfully identified and verified the polymorphism rs13333226 with lower risk of hypertension (p= 1.14 x 10^{-7}) using an extreme case - control strategy. This group reported that each copy of the G allele was associated with a 0.49mmHg lower SBP and 0.30mmHg lower DBP in the Global BPGen cohort. The association plot of the genomic region around rs13333226 in the initial discovery sample is outlined in **Figure 1-9** (Padmanabhan et al., 2010).
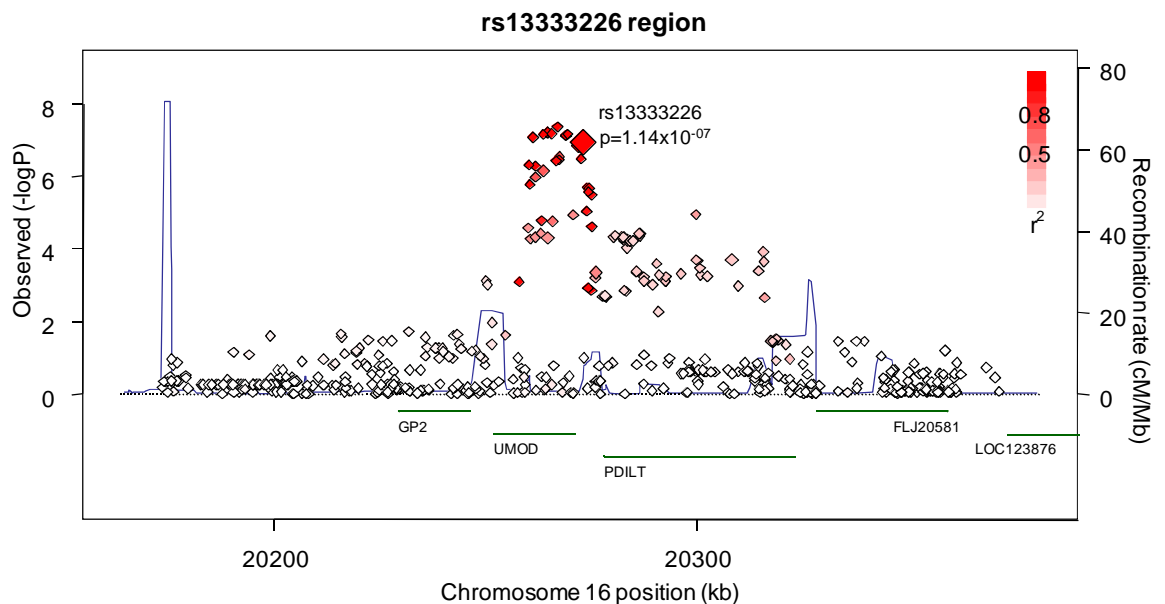
Figure 1-9 The association plot of the genomic region around rs13333226
Observed (-logP) is the –log10 transformed P values for association with hypertension status in the discovery sample. Recombination rate, is represented by the blue line. The level of LD between rs13333226 and the surrounding SNPs, measured by r^2, is indicated with red demonstrating high LD. GP2 = glycoprotein 2 (zymogen granule membrane). UMOD = uromodulin. PDILT = protein disulfide isomerase-like, testis expressed. FLJ20581 = acyl-CoA synthetase medium-chain family member 5. LOC123876 = acyl-CoA synthetase medium-chain family member 2A. Image reproduced from (Padmanabhan et al., 2010).

The genome wide association study further reported that the minor G allele of rs13333226 was associated with lower urinary UMOD excretion, and the association was independent of kidney function as the hypertensive subjects displayed a higher eGFR in association with the G allele. Whereas, in the normotensive participants this association did not reach statisitcal significance. Ultimatley suggesting that *UMOD*s association with hypertension is independent of renal function. In order to further examine the relationship of the G allele and changes in renal function, levels of urinary excretion were examined in hypertensive and normotensive individuals. The minor G allele at rs13333226 was shown to be associated with lower urinary uromodulin levels in both groups of participants. The hypertensive subjects who carried the GG genotype had lower urinary uromodulin levels as well as lower fractional urinary sodium excretion, therefore suggesting higher sodium reabsorption at the TAL. However, this was not replicated in the normotensive participants who appeared to have increased sodium excretion with increased uromodulin excretion. This relationship of lower uromodulin excretion and increased sodium reabsorption in the GG carriers, yet a lower risk of hypertension seem contradictory. Although lower sodium excretion could be the results of increased sodium reabsorption as a result of increased sodium load possibly corresponding to a decreased distal reabsorption. The dietary information for hypertensive and normotensive cohorts was not available therefore it cannot be proven that lower sodium excretion was simply attributed to low sodium levels in the diet (Padmanabhan et al., 2010).

In support of this hypothesis, analysis with the Hypertension Evaluation by Remler and CalciUria Level (HERCULES) study participants reported an inverse relationship between urinary UMOD levels and proximal tubule sodium reabsorption (Bochud et al., 2009). Additionally, G allele subjects from the Groningen Renal Hemodynamic Cohort Study Group (GRECO) study (Visser et al., 2008) show a larger increase in GFR in response to an increased sodium intake, whereas the fractional excretion of sodium was less **(Figure 1-10)**. Suggesting that subjects carrying the G allele restore sodium excretion by a rise in filtered load i.e. at a level that matches higher intake than in non carriers. This is associated with a larger rise in ECF volume in response to high salt, that maybe responsible for the larger rise in GFR. These data make a link between genetic variants in the *UMOD* gene and blood pressure through interactions, fluid volume

control, and sodium reabsorption. This is a critical point as rs13333226 is located in close proximity to the *UMOD* gene start site, and as already introduced *UMOD* mutations are associated with chronic renal failure and autosomal dominant renal diseases that lead to altered sodium transport and blood pressure phenotypes (Turner et al., 2003, Rampoldi et al., 2003, Hart et al., 2002).
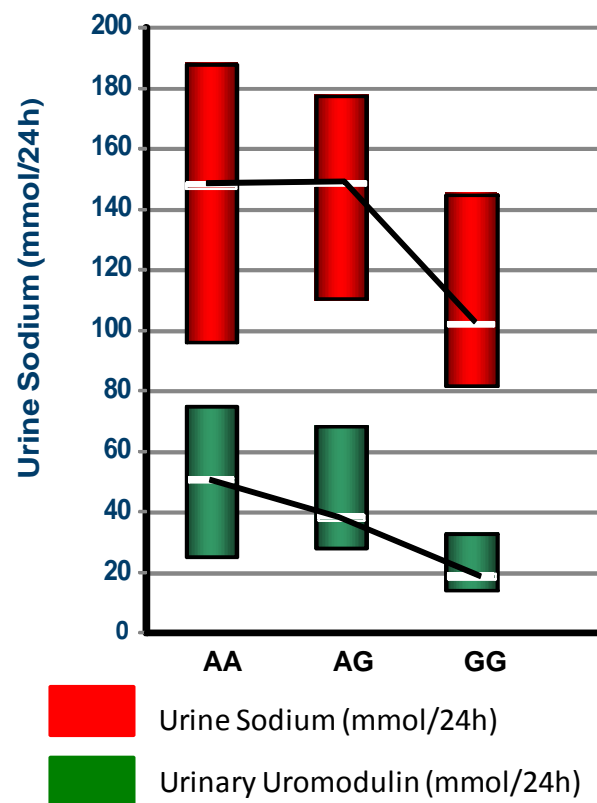
Figure 1-10 Genotype dependant urinary Uromodulin and sodium excretion
Padmanabhan and colleagues (Padmanabhan et al., 2010) measured urinary Uromodulin and sodium excretion in healthy 64 male individuals from the GRECO study (Groningen Renal Hemodynamic Cohort Study Group) (Visser et al., 2008) who took part in a 7 day low sodium diet (50 mmol Na+/day) followed by a 7 day high sodium diet (200 mmol Na+/day). Urine was collected over a 24 hour period and commercial ELISAs were used to assess urinary UMOD levels. The minor G allele was associated with reduced urinary UMOD levels and sodium exaction. Image produced by (Padmanabhan et al., 2010).

As a clinical follow up, the association of rs13333226 with lower risk of hypertension was evaluated by examining subjects from the Malma diet and cancer study, a ten year follow up cohort (Berglund et al., 1993). The G allele was examined in this cohort to assess if it prevents the occurrence of cardiovascular disease over long-term, revealing a 7% reduction in the risk of CVD. Although these studies did not reveal a definitive functional explanation

for the effect of UMOD on blood pressure the finding of an association between hypertension and the genetic *UMOD* variant rs13333226 is biologically plausible.

The original GWAS performed by Padmanabhan *et al* reported that a high salt diet in healthy individuals, the minor G allele was associated with a larger increase in measured GFR and hence filtered sodium load with smaller increases in tubular sodium excretion. Taken together with reported findings from the literature suggests that *UMOD* variants may alter gene expression and contribute to qualitative traits of blood pressure via regulation of sodium homeostasis, providing a new window of opportunity to study the physiological role of UMOD as a regulator of blood pressure. We hypothesis that altered *UMOD* expression and/or function impacts on sodium homeostasis and influence blood pressure phenotypes.

1.12 Aims

The specific aims of this thesis are:

- To investigate human *UMOD* promoter sequences to identify the potential functional promoter polymorphisms that maybe a causal SNPs in blood pressure regulation

- To investigate the physiological role of UMOD in blood pressure regulation and sodium homeostasis utilising a *UMOD* knockout rodent model

- To investigate expression levels of ion transporters at the thick ascending limb of the loop of Henle by UMOD

- To perform a small pilot study in human kidney samples from normotensive and hypertensive cohorts to translate the findings from *in vivo* and *in vitro studies* of this thesis

2 General Methods

This chapter outlines laboratory practices and laboratory methods common to more than one chapter. Each subsequent results chapter has specific Materials and Methods section.

2.1 General laboratory practice

Laboratory equipment and reagents were of the highest commercially available grades. Hazardous reagents were handled as described in the Control of Substances Hazardous to Health regulations. A laboratory coat and non-latex powder-free gloves were worn during all procedures.

Laboratory glassware was cleaned in Decon 75 detergent (Decon Laboratories Ltd, East Sussex, UK), rinsed with distilled water and dried at 37°C. Otherwise, sterile disposable plastic ware were used, including 0.5 ml, 1.5 ml and 2 ml microcentrifuge tubes (Greiner Bio-one, Stonehouse, UK), 15 ml and 50 ml centrifuge tubes (Corning, Birmingham, UK), and also 5 ml and 20 ml 'Universal' containers (Sterilin, Newport, UK). Laboratory-ware and liquids requiring sterilisation were autoclaved in a Priorclave Tactrol 2.

Reagents were weighed using an Ohaus Portable Advanced balance (sensitive to 0.01 g), or a Mettler HK160 balance (sensitive to 0.0001 g). Solutions were pH'd using a Mettler Toledo digital pH meter calibrated with pH 4.0, 7.0 and 10.0 prepared from buffer tablets (Sigma, Dorset, UK). Volumes from 0.1 μl to 1,000 μl were dispensed with Gilson Medical Instruments pipettes. Volumes from 1 ml to 25 ml were measured with sterile disposable pipettes (Corning, Birmingham, UK) and a Gilson battery-powered pippetting aid (Gilson Medical Instruments). Autoclaved distilled water (dH$_2$O) was used to prepare aqueous solutions unless otherwise indicated, and a Jenway 1000 hotplate/stirrer was used to aid dissolving and mixing.

Vortexing was carried out using an FSA Laboratory Supplies WhirliMixer. Centrifugation for samples up to 2 ml was performed at 4-20°C in a table top Eppendorf 4515 microcentrifuge, while larger sample volumes were centrifuged in a Sigma 4K15, compatible with 15 ml and 50 ml centrifuge tubes, 20 ml 'Universal' tubes and with carriers for standard reaction plates. A Julabo TW8

water bath was used for experiments requiring incubations from 37°C to 90°C, and a Grant SBB14 boiling water bath was used for temperatures up to 100°C.

Experiments involving ribonucleic acid (RNA), certified nuclease-free reagents and plastic ware used, including RNase-free microcentrifuge tubes, RAININ nuclease-free filtered pipette tips and Ambion nuclease-free H_2O. Pipettes and benches were wiped with Ambion RNaseZap reagent before all RNA experiments.

2.2 General Techniques

2.2.1 Nucleic acid extraction

Total genomic DNA was extracted from animal tissues and cell lysates using the DNeasy Blood and Tissue kit (QIAGEN, Manchester, UK) following manufacturer's instructions for the spin-column protocol. In brief, appropriate volumes of ATL buffer and proteinase K were added to animal tissue samples or cell lysate suspension and vortexed to begin the lysis process. Samples were then incubated at 56°C until completely lysed. Appropriate volumes of AL buffer were added to each sample and mixed thoroughly by vortexing. Buffer AL contain chaotrophic salts which allows nucleic acid to be absorbed onto the silica gel membrane of the Spin Columns by removing water from the hydrated molecules in solution. Polysaccharides and proteins are not absorbed and are removed. 100% ethanol was added to the sample, mixed, and transferred on to the Spin Column. Samples were centrifuged at 6000 x g for 1 minute at room temperature to allow DNA to bind to the silica gel membrane of the Spin Column. The Spin Column was then washed with buffer AW1 and centrifuged at 6000 x g for 1 minute, followed by a second wash step with AW2 buffer and centrifuged at 16000 x g for 3 minutes at room temperature. Finally, the DNA was eluted with 50µl nuclease free water by centrifugation at 6000 x g for 1 minute.

2.2.2 Polymerase Chain Reaction (PCR)
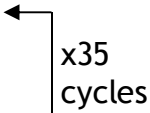
All thermal cycling for standard PCRs was performed on an MJ Research PTC Gradient Cycler in 96-well plates (Thermo Fischer Scientific, Loughborough, UK). PCR primers were designed using the Ensembl online resource database and purchased from MWG Biotech. *KOD HotStart* (Novagen, Darmstadt, Germany) a commercial 'Hotstart' Taq polymerase PCR system, was used for standard PCRs in

this project. For amplifying from genomic DNA templates, 100 ng of genomic DNA was used, while 5-10 ng of template was used for amplifying plasmid templates. All primers sequences are listed in specific results chapters. The standard reaction mixes and temperature cycling parameters follow:

KOD HotStart:

Reaction mix	Volume (µl)	Final concentration
10X Buffer	5	1X
25mM MgSO$_4$[a]	3	1.5mM
dNTPs (2mM) each	5	0.2mM each
Sense (5') Primer (10µM)	1.5	0.3µM
Anti-Sense (3') Primer (10µM)	1.5	0.3µM
Template	X	100ng
PCR Grade Water	up to 25µl	
KOD Hot Start DNA Polymerase	1	0.02U/µl
Total reaction volume	50	

Temperature cycling:

Heat cycling	Time	
95°C	2 min	
95°C	20 sec	
58°C – 64°C	10 sec	x35 cycles
70°C	10 – 20 sec/kb	

KOD Hot Start was used in this project to ensure absolute fidelity of DNA replication, as it employs proofreading capability. This is of benefit as other commercially available *Taq* polymerases can incorporate incorrect nucleotides. *KOD DNA* polymerase is derived from *Thermococcus kodakaraensis* thermophilic bacteria and possesses 3'-5' exonuclease activity that excises mis-incorporated bases during PCR.

2.2.3 Agarose Gel Electrophoresis

Throughout, 0.8-1.5% agarose (Eurogentec, London, UK) gels were used, dissolved and electrophoresed in 1 X Tris-Borate EDTA (TBE) buffer (Fisher Bioreagents, Loughborough, UK). Gels were electrophoresed at 6 V per cm of gel. BIO-RAD Power Pac 300 and BIO-RAD electrophoresis tanks were used, 1 ng /

100 ml ethidium bromide (Sigma, Dorset, UK) was added to molten agarose before pouring gels. Gels were visualised by UV transillumination on a BIO-RAD Fluor-S MultiImager. Promega 1kb and 100bp DNA ladders were used for sizing products. Samples were loaded with 6 X loading dye (50% glycerol, 0.05% bromophenol blue).

2.2.4 Agarose DNA extraction and purification

Unless stated otherwise agarose gel extraction of PCR products or restriction-digested DNA was performed with the Qiagen QIAquick Gel Extraction kit following the manufacturer's instructions, using a bench microcentrifuge at full speed. Bands in agarose gels were visualised on a UV transiluminator (UVP) and carefully excised with a scalpel blade. The bands were weighed and 300 µl of buffer QG was added per 100 µg of agarose before heating the agarose/buffer QG mixture to 50°C for 10 minutes. After centrifugation to absorb the DNA to the membrane, the membrane was washed with 500 µl of buffer QG followed by 750 µl buffer PE (which contains 70% ethanol) with centrifugation. All traces of ethanol were removed by a final centrifugation for 1 minute; DNA was eluted in nuclease-free water. Fragments were then ready for cloning in preparation for promoter activity assays *in Vitro*.

2.2.5 Plasmid purification

2.2.5.1 Transformation of competent bacteria (PCR vector)

StrataClone PCR-Script vectors containing PCR "inserts" were transformed in JM109 competent *Escherichia coli* (*E.coli*) bacteria (Promega, Southampton, UK) as hosts for eukaryotic expression vectors. For transformation, competent cells were thawed on ice and separated into 50µl aliquots in chilled 1.5ml centrifuge tubes. For transformation of an intact plasmid, 2ng plasmid DNA was added to the bacteria, for transformation of ligated plasmid/insert mixes 2-5µl of the ligation reaction was added to JM109s. Tubes were flicked gently to mix and returned to ice for 10 minutes, then 'heat shocked' at 42°C for 45 seconds before returning to ice for a further 2 minutes. Chilled SOC medium (Sigma, Dorset, UK) (900 µl) was added to the cells and they were placed in a shaking incubator (New Brunswick Scientific Inova 44) at 37°C, 225 rates per minute, for one hour. Unless otherwise stated all plasmids used in this project encoded ampicillin

resistance for selection of transformed cells. Transformation mixtures were spread onto 90 mm culture plates (Sterilin, Newport, UK) of Luria agar (Sigma) containing 100 μg/ml ampicillin (Sigma). For transformations of intact plasmids 100 μl of neat, 1 in 10 and 1 in 100 dilutions in SOC media were spread, for transformations of ligation reactions; the entire transformation culture was spread onto 5 plates. Culture plates were inverted and placed in a 37°C incubator (Heraeus) overnight. Plates were checked for bacterial colonies the next morning and if necessary screened for positive clones as detailed in section 2.3.3.

2.2.5.2 Small scale DNA purification

The QIAprep Spin Miniprep Kit (QIAGEN, Manchester, UK) was used to purify plasmid DNA from overnight starter cultures. One ml of the incubation was transferred into a 1.5 ml tube, and centrifuged at 10,000 x g for 10 minutes to pellet the cells. The supernatant was discarded and the cell pellet lysed by resuspending them in 250 μl of Buffer P1. The DNA was denatured by adding 250 μl Buffer P2 and inverted to mix thoroughly. The reaction was then neutralised by adding 350 μl of Buffer N3 and immediately mixed by inversion. Samples were then centrifuged for 10 minutes at 13, 000 x g in a table top centrifuge. The supernatants were transferred into a QIAprep spin column, which was centrifuged at 13,000 x g for 1 minute to bind DNA on to the silica membrane. The flow through was discarded and the column washed with 500 μl of Buffer PB. The sample was then centrifuging at 13,000 x g for 1 minute. Another wash with 750 μl of Buffer PE was performed, after which the column was centrifuged at top speed for 1 minute to ensure there was no residual buffer remaining. The column was transferred to a new 1.5 ml tube and the DNA eluted by adding 50 μl of nuclease-free water, standing at room temperature for 1 minute then centrifuging at 13, 000 x g for 1 minute. Plasmid DNA was quantified by Nanodrop (2.3.11) and stored at -20°C until required.

2.2.5.3 Large scale DNA purification

Large scale plasmid DNA was extracted from bacteria using the filter column based Qiagen Plasmid Maxi kit (QIAGEN, Manchester, UK). Bacterial cultures were streaked and grown overnight at 37°C on ampicillin Luria agar plates.

Single colonies were picked and used as a 'starter' culture grown over a 12 hour period in 5 ml Luria broth (Sigma, Dorset, UK) containing 100 μg/ml ampicillin in a shaking incubator at 37°C. One ml of this culture was used to inoculate 100-500 ml 100 μg/ml ampicillin Luria broth to produce an overnight culture from which the plasmid was extracted (100 ml was sufficient for most plasmids, however when low yields were obtained, the extraction was repeated with 500 ml culture). Bacteria were harvested by centrifugation at 6,000 g for 15 minutes at 4°C in a Beckman Coulter Avanti J-26XP. Culture media was removed and the bacteria were resuspended in 10 ml buffer P1 (50mM 2-amino-2-hydroxymethyl-1,3-propanediol, pH8; 10 mM EDTA, 100 μg/ml RNase A). Ten ml of buffer P2 (200 mM NaOH; 1% sodium dodecyl sulphate (SDS)) was added and the solutions were kept on ice for exactly five minutes. Ten ml of chilled buffer P3 (3 M potassium acetate at pH5.5) was added to neutralise the lysate. The precipitated lysates were centrifuged at 20000 x g at 4°C for 30 minutes, the supernatant was retained. Columns were equilibrated with 10ml of buffer QBT (750 mM NaCl; 50 mM 3-morpholinopropanesulfonic acid pH7 (MOPS); 15% isopropanol; 0.15% Triton-X 100). The supernatant was then applied and the columns were allowed to empty by gravity flow, the columns were washed twice with 30 ml buffer QC (1 M NaCl; 50 mM MOPS pH7; 15% isopropanol), and the plasmid DNA was eluted with 15 ml buffer QF (1.25 M NaCl; 50 mM Tris pH8.5; 15% isopropanol) into polypropylene centrifuge tubes. Plasmid DNA was precipitated with 10.5 ml isopropanol and centrifuged at 15000 x g for 30 minutes at 4°C. The supernatant was carefully removed. The DNA pellets were washed with 5 ml 70% ethanol, and aliquoted into five 1.5 ml microfuge tubes. The samples were centrifuged at maximum speed for 10 minutes at 4°C on a table top centrifuge. The ethanol was carefully pipetted off and the pellets were thoroughly air-dried (10-20 minutes) before resuspending the DNA in 50 μl H_2O per tube. Finally, the contents of the five tubes were pooled together and DNA yields measured.

2.2.6 Glycerol stocks

Successfully transformed bacteria were preserved for long-term storage by preparing glycerol stocks. One ml of overnight broth cultures was mixed with 1 ml sterile 40% glycerol solution and frozen at -80°C. Bacteria were recovered from glycerol stocks by streaking for single colonies on selective agar.

2.3 *UMOD* Promoter Sequence cloning

2.3.1 Promoter Sequence PCR

To amplify the 2kb *UMOD* promoter region, primers were designed and PCR run using KOD polymerase as per section 2.2.2. **Table 2-1** below outlines the primer sequences used to amplify the 1 and 2Kb *UMOD* promoter regions from genomic DNA from each cell type. Each primer pair contained *SacI* and *Hind III* restriction sites at the 5' end of the forward or reverse primers respectively and preceded by 3xC residues:

Primer	Sequence (5'-3')
Human *UMOD* Pr 2000 FWD	CCCGAGCTCGGTGATTACACTTATGAATAGATTC
Human *UMOD* Pr 1000 FWD	CCCGAGCTCTTTCCTGCTCAGCCCAAGTTCACAC
Human *UMOD* Pr REV	ATAAGTATGAGGCACATCATGACCAAGCTTCCC

Table 2-1 Amplification of the 1 and 2 Kb *UMOD* promoter region.

Primers used to amplify the 1 and 2Kb *UMOD* promoter sequences from genomic DNA were designed to contain the sequences for incorporating restriction endonucleases (marked in blue) in preparation for cloning and sub-cloning.

2.3.2 DNA blunt cloning of the 2Kb *UMOD* promoter region into PCR vectors

PCR products were 'blunt cloned' into PCR amplification vectors (Stratagene PCR-Script Amp SK(+) (PCR-Script)) using the Stratagene blunt PCR cloning kit following the manufacturer's instructions (Agilent Technologies, California, USA). The PCR-Script plasmid is supplied linearised by digestion with *SrfI* restriction enzyme. This cloning platform also allowed blue/white selection based on *lacZ* gene disruption; IPTG (isopropyl-beta-D-thiogalactopyranoside) (20 mM) and X-gal (8 µg/ml) were added to ampicillin (100 µg/ml) selective LB agar, white colonies were screened for the insert. All cloning in this chapter utilised plasmids expressing the ampicillin resistance gene, selective Luria agar and broth were used with 100 µg/ml ampicilin (Sigma, Dorset, UK).

In this project, promoter sequence PCR reactions were electrophoresed as described in section 2.2.3, bands were excised from the agarose gel and purified as per section 2.2.4. PCR products (5 µl) were used in ligation reactions with 10 ng Staratgene PCR vector, the precise molar ratio of plasmid:insert was not calculated but the insert was vastly in excess, as is necessary in PCR-cloning. The ligation reactions constituted of:

Reaction Mix	Volume (µl)
PCR vector (10 ng/µl)	1
10 X Stratagene PCR buffer	1
rATP (10 mM)	0.5
PCR product	5
Srfl (5 U/µl)	1
T4 DNA ligase	1
Nuclease free water	0.5
Total Reaction Volume	10

Ligation reactions were incubated at room temperature for an hour, and then de-activated by heating to 65°C for 5 minutes.

Forty µl of XL-10 Gold cells were thawed on ice and 1.6 µl ß-mercaptoethanol was added. Cells were incubated on ice for 10 minutes, 4 µl of ligation reaction was added and cells were incubated on ice for 30 minutes, then heat-shocked at 42°C for 30 seconds before returning to ice for 2 minutes. SOC media was heated to 42°C and 450 µl was added and transformation cultures were incubated in a shaking incubator at 37°C for an hour. Transformation cultures were spread over IPTG/X-Gal/ampicillin (IPTG (isopropyl-beta-D-thiogalactopyranoside) (20 mM) and X-gal (5-bromo-4-chloro-3-indolyl b-D-galactopyranoside) (8 µg/ml) selective LB agar plates, where white colonies were selected and screened for the insert by PCR.

2.3.3 Selecting positive clones

Individual colonies were picked with a sterile pipette tip, streaked onto a numbered 0.8 cm grid on a selective agar plate. The pipette tips were then washed in a numbered well of a 96-well plate containing 10 µl H$_2$O. KOD *HotStart* polymerase PCR reaction master mixes were added to each well to make a 20 µl PCR reaction. Following PCR, products were electrophoresed to screen the for the expected size. Positive PCR results were later confirmed by DNA sequencing. Positive white colonies were screened by PCR across the cloning site in the PCR-Script cloning vectors with T7 (5' TAATACGACTCACTATAGGG3') and T3 (5' ATTAACCCTCACTAAAGGGA 3') primers. PCR products were then sequenced using 8 overlapping primer pairs (1R+1F, 2R+2F, 3R+3F, 4R+4F, 5R+5F, 6F+6R, 7F+7R, 8F+8R) to confirm the *UMOD* promoter. The primer sequences and region covered are listed in **Table 2-2.** Single positive colonies identified in the StrataClone PCR-Script vectors, were picked and used as a 'starter' culture grown over a 12 hour period in 5 ml Luria broth (Sigma, Dorset, UK) containing 100 µg/ml ampicillin in a shaking incubator at 37˚C. This culture was then used for DNA purification (section 2.2.5). The PCR product was then digested out in preparation for sub-cloning into luciferase vectors to investigate promoter activity.

Primer	Sequence	Coverage (bp)	Position
UMOD 1F	GACACCCATAATAAGGTTTAGACA		20366046-20366022
UMOD 1R	CCACTGGCACTGGTGTTGTCATCT	357	20365712-20365688
UMOD 2F	CCACTTATCCTTTTGGCAAAGATG		20365899-20365875
UMOD 2R	ATTCCACGGTGTATATGTGCCACA	350	20365573-20365549
UMOD 3F	GTCCATCAATGATAGACTGGATTA		20365603-20365579
UMOD 3R	TCGAGGTTTGTTACATATGTATAC	358	20365152-20365128
UMOD 4R	GAATTGAACAATGAGAGCACTTG		20364977-20364953
UMOD 4F	CAGACCCAGTTCAACATACATGA	349	20365303-20365278
UMOD 5F	TGATATTTTCCTGCTCAGCCCAA		20365066-20365043
UMOD 5R	TCACTGGACCTGACCCACTCTGTA	470	20364620-20364596
UMOD 6F	CATGAATATAATCATTACTATGA		20364878-20364854
UMOD 6R	TGAAACACCCATTCTCATGAGATC	362	20364518-20364494
UMOD 7F	AAGGTTAAGAAATGAGCCCACTG		20364759-20364735
UMOD 7R	CCAGGCAGAAGCCAGTATCTGAA	364	20364417-20364394
UMOD 8F	GAATATCCCTTTTGTCCTTATGCA		20364448-20364424
UMOD 8R	GGTCATGATGTGCCTCATACTTAT	412	20364147-20364123

Table 2-2 Colony screening by PCR and sequencing.

Primer pairs used to confirm the 1Kb (denoted in red) and 2 Kb (denoted in black) *UMOD* promoter regions by PCR and sequencing reactions.

2.3.4 Restriction endonuclease digest

To enable the targeted ligation of the *UMOD* promoter sequences into plasmid backbones, appropriate restriction enzymes were used to digest inserts from PCR plasmids to generate compatible ends for ligation. Restriction endonucleases were purchased from New England Biolabs (Herts, UK) and used for digestions according to the manufacturer's protocols. Restriction endonucleases and reaction mixes used in this project are:

Reaction Mix	Volume (µl)
Template DNA	X (1-2 µg)
10 X Restriction buffer	2.5
Bovine serum albumin (BSA)	0.25
Restriction enzymes	1
Nuclease free water	X
Total Reaction Volume	25

One unit of restriction enzyme is defined as the amount required to digest 1 µg of template in one hour. Reaction mixtures were mixed gently and briefly pulsed in a bench microcentrifuge, then incubated at 37°C for between 1 and 4 hours. Cloning in this project was performed using 'double digests', wherein the insert and backbone were digested with two restriction enzymes, resulting in different overhanging ends, allowing directional cloning and minimising the likelihood of self-ligation of the plasmid backbone. The restriction enzymes used throughout this project are listed as follows:

Enzyme	Sequence	Buffer
Sac I	5'...G A G C T C...3' 3'...C T C G A G...5'	Buffer 2
Hind III	5'...A A G C T T...3' 3'...T T C G A A...5'	Buffer 2

Restriction digested PCR reactions were then electrophoresed as described in section 2.2.3, and bands excised from the agarose gel (2.2.4).

2.3.5 DNA sub-cloning

Promoter sequences were digested out of the PCR-Script vectors with *SacI* and *Hind III* restriction enzymes prior to sub-cloning into similarly double-digested pGL4.70 Basic luciferase plasmids. Digested Stratagene PCR plasmids, pGL4.70 Basic vectors, and "dropped" promoter sequences (inserts) were electrophoresed and gel purified. Prior to ligation of the insert into the pGL4.70 luciferase vector, the backbone was de-phosphorylated using New England Bio

labs Antarctic Phosphatase (Herts, UK). The reaction catalyzes the removal of the 5' phosphate of DNA, thus the phosphatase treated fragment cannot self ligate due to the lack of the 5′ phosphoryl termini required by ligases. The reaction protocol is listed below:

Reaction Mix	Volume (µl)
Template DNA	X (1-5 µg)
10 X Antarctic phosphatase buffer	1
Phosphatase enzyme	1
Nuclease free water	X
Total Reaction Volume	10

The reaction mix was incubated at 37°C for 1 hour, then heat inactivated for 5 minutes at 65°C. Unless stated otherwise, digested plasmid fragments or digested PCR products were ligated into digested plasmid backbones using the New England Biolabs Quick Ligation Kit. The kit includes a 2X reaction buffer (1332mM Tris pH7.6; 20mM $MgCl_2$; 2mM dithiothreitol; 2mM ATP; 15% polyethylene glycol) and 'Quick' T4 DNA ligase (supplied in 50 mM KCl, 10 mM Tris (pH7.4), 0.1 mM EDTA, 1 mM dithiothreitol, 200 µg/ml BSA and 50% glycerol). Ligation reactions constituted are as follows:

Reaction Mix	Volume (µl)
pGL4.70 backbone	X (50–100 ng)
Insert (1 or 2Kb *UMOD* promoter)	X (molar ratio of 3:1)
2 X quick ligation buffer buffer	10
T4 DNA ligase	1
Nuclease free water	X
Total Reaction Volume	20

Reactions were mixed by gentle pipetting, pulsed in a microcentrifuge and incubated at room temperature for five minutes, and then put on ice. Ligations were transformed immediately or stored at -20˚C before transformation. The amount of insert DNA to add to the ligation reaction for a given Insert:backbone

ratio and given amount of backbone DNA was calculated according to the following formula:

$$\text{ng insert DNA} = \frac{\text{Molar ratio insert:backbone)} \times \text{(ng backbone)} \times \text{(insert length,bp)}}{\text{(backbone length, bp)}}$$

2.3.6 Transformation of competent bacteria (Luciferase vector)

One Shot® TOP10 competent *Escherichia coli* (*E.coli*) bacteria (Invitrogen, Paisley, UK) were used as hosts for luciferase expression vectors. Transformation protocols were carried out according to the manufacturer's instructions. In brief, competent cells were thawed on ice and separated into 50µl aliquots per reaction, 2ng plasmid DNA was added to the bacteria, and mixed gently. Tubes were returned to ice for 10 minutes, then 'heat shocked' at 42°C for 45 seconds before returning to ice for a further 2 minutes to cool. Chilled SOC medium (900 µl) (Sigma, Dorset. UK) was added to the cells and they were placed in a shaking incubator (New Brunswick Scientific Inova 44) at 37°C, 225 rates per minute (RPM), for one hour. Unless otherwise stated, all plasmids used in this project encoded ampicillin resistance for selection of transformed cells. Transformation mixtures (approximately 200µl) were spread onto 90 mm culture plates (Sterilin, Newport, UK) of Luria agar (Sigma, Dorset, UK) containing 100 µg/ml ampicillin (Sigma). Culture plates were inverted and placed in a 37°C incubator (Heraeus) overnight. Plates were checked for bacterial colonies the next morning and screened for positive clones as detailed in section 2.3.3 with the addition of pGL4.70 vector primers that anneal either side of the pGL4.70 Basic multiple cloning site (MCS), pGL4.70 forward primer 5' CTAGCAAAATAGGCTGTCC 3' and pGL4.70 reverse primer 5' GTCTTCGAGTGGGTAGAATGG 3'. Positive clones were definitively confirmed by DNA sequencing and Maxi-preps were prepared for each pGL4.70 Basic plasmid. The six pGL4.70 Basic plasmids were named according to the promoter sequences they encoded: ACHN 1KB, 786-0 1Kb, TK10 1Kb, ACHN 2Kb, 786-0 2Kb, and TK10 2Kb.

2.3.7 Reporter construct transient transfection

Prior to promoter activity assays, transfection efficiency protocols were conducted with GFP plasmid with >90% transfection efficiency in HeLa, NRK, HEK293 and HK-2 cells. Invitrogen Lipofectamine® 2000 lipofection reagent was used for all experiments involving transfection of cultured cells (Invitrogen, Paisley, UK). Lipofectamine® 2000 is a proprietary mix of lipids in 80% ethanol; it binds to and packages plasmid DNA into a lipid complex that allows the plasmids to cross cell membranes. Transfection protocols were optimised individually for each cell type used in experiments following suggested methods in the product literature. This involved ascertaining the optimal ratio of Lipofectamine® 2000:DNA for maximal gene expression and minimal cytotoxicity. Ratios of 1:1, 2:1 and 3:1 Lipofectamine® 2000:DNA (µl:µg) were used, with a total amount of DNA per well of 200 ng, 500 ng and 1 µg. Transfections were optimised and performed in 24-well culture plates. Regardless of the final conditions used, the same transfection protocol was followed: Cells were seeded the day before to be at 70-80% confluence at transfection. Lipofectamine® 2000/DNA mixtures were made in additive-free media in 5 ml universal tubes, Lipofectamine® 2000 was added to the media and mixed gently, plasmid DNA was added after five minutes, mixed, and once more then left for 30 minutes to allow Lipofectamine® 2000/DNA complex formation. Transfection mixtures were then applied to cells, and assayed 24 hours later.

2.3.8 RNA extraction

Total RNA was extracted from animal tissue and cell lysates using Qiagen column based miRNeasy Mini kits (QIAGEN, Manchester, UK). Whole tissues or cells were homogenised in buffer RLT lysis solution, containing 0.01% (v/v) β-mercaptoethanol or Qiazol homogenisation reagent included in the kit. Cultured cells were pelleted, supernatant removed, and rinsed with PBS and homogenised by pipetting. Unless otherwise stated tissues were homogenised with a Polytron 2100 rotor homogeniser at full speed, then centrifuged at 5000 g to collect lysates. An equal volume of 70% ethanol was added to the sample lysates before being applied to the RNeasy columns, followed by centrifugation (15 seconds at 8000 g) to wash cellular debris through the column. The flow through was discarded and 700µl of buffer RW1 was added to the Spin Columns, samples were

spun as before and the flow though discarded. An optional on column DNA digest was carried out (refer to section 2.3.10). Spin Columns were then transferred to fresh collection tubes and 500µl of buffer RPE added, and centrifugations repeated as before. The flow through was discarded prior to another 500µl of buffer RPE. The Spin Column was then centrifuged for 2 minutes, at 8000 x g, at room temperature to dry the RNeasy silica gel membrane. RNA was eluted in 30-50 µl RNase-free H$_2$O. Samples were then centrifuged for 1 minute at 8,000 x g and room temperature. RNA samples were stored at -80°C until time of analysis.

2.3.9 RNA Validation (Agilent tested)

Total RNA isolated was quality tested for degradation prior to cDNA synthesis via electrophoresis on the Agilent Bioanalyser 2100 and a Eukaryote Total RNA Nano Series II chip. The analysis was run at the Molecular Biology Support Unit at the University of Glasgow. Electrograms produced indicate defined bands for 18S and 28S ribosomal RNA (rRNA) species and a RNA integrity number (RIN) (**Figure 2-1**).
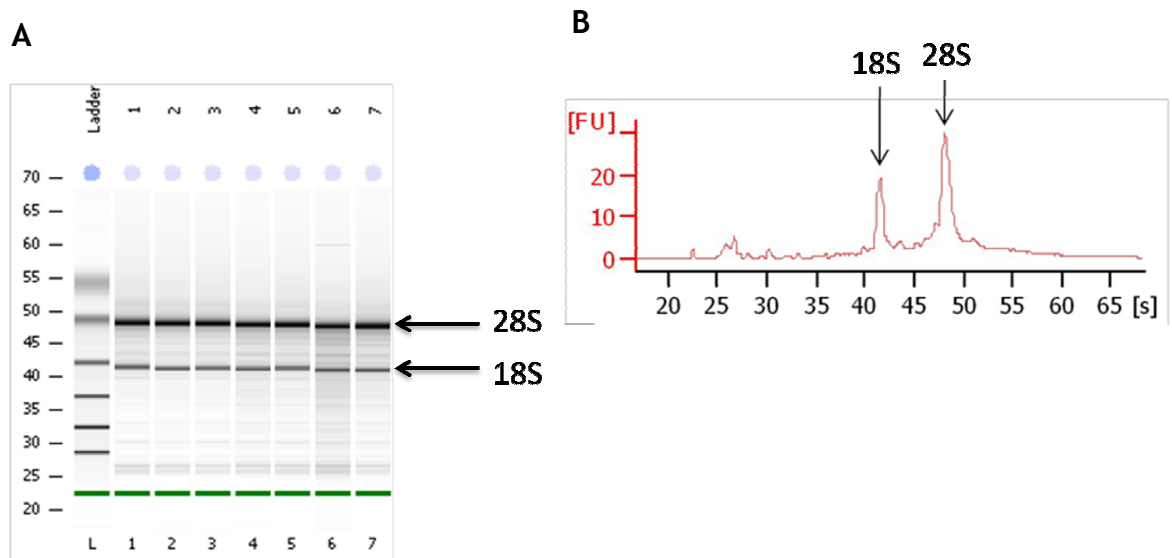
Figure 2-1 Agilent Bioanalyser 2100 assessment of mRNA quality.

(A) Electrophoresis of mRNA samples showing bands for 28S and 18S rRNA. The lower band in each lane is a 200 bp size marker to align samples and controls. **(B)** Representative individual electropherogram, with sharp peaks for 28S and 18S rRNA and no RNA species smaller than 41S rRNA.

2.3.10   DNase treatment of extracted RNA

In order to remove any contaminating DNA, extracted total RNA was treated with DNase using the reagents provide in the QIAGEN miRNeasy mini kit (QIAGEN, UK) and according to the manufacturer's instructions. The on column digestion of DNA during the RNA purification is as follows; 350µl of buffer RWT was added to the spin column and centrifuged for 15 seconds at 8000 x g, 10µl of DNase I stock was solution was added to 70µl of buffer RDD, this was then added to the spin column and left to incubate for 15 minutes at room temperature, finally 350µl of buffer RWT was added to the column and centrifuged for 15 seconds. All flow through was discarded and spin column carried over for completion of RNA purification (2.3.8).

2.3.11   Measuring Nucleic acid concentration

A Nanodrop$^{®}$ ND-1000 spectrophotometer (Thermo Scientific, Loughborough, UK), was used to measure DNA and RNA concentrations. This method is sensitive at measuring concentrations between 2-37000 ng/µl of double-stranded DNA. Absorbance ratios (260 nm/280 nm) of approximately 1.8 for DNA and 2.0 for RNA indicated that the nucleic acid preparations were sufficiently free from protein contamination for downstream experiments. Additionally, the ratio of absorption at 260 nm and 230 nm was used as an indicator of RNA purity; pure RNA has a ratio of 2.0 - 2.2, (a common contaminant is phenol, which absorbs at 230 nm and is used in Total RNA extraction). The concentration of the sample is calculated using the Beer-Lambert Law of absorption;

Concentration of DNA (µg/ml) = (A260 reading – A320 reading) x 50
Concentration of RNA (µg/ml) = (A260 reading – A320 reading) x 40

2.4 Quantitative Real-Time PCR

An Applied Biosystems 7900HT Sequence Detection System (Taqman$^{®}$) was used for all quantitative real-time PCR in this project. The system encompasses a heating block for thermal cycling and detectors to measure fluorescence in each well of a 384-well optical plate. Fluorescence is measured after every amplification cycle to quantify the accumulation of PCR product; during the

exponential phase of PCR cycling the rate of product accumulation is proportional to template concentration, relative template abundance can therefore be quantified by monitoring increasing fluorescence in each well during temperature cycling. This is explained in more detail in subsequent sections below with specific protocols for cDNA template preparation and reaction set up.

2.4.1 Preparation of cDNA

cDNA preparations for quantitative real-time PCR (qRT-PCR) were prepared by reverse transcription from RNA templates. Applied Biosystems 'TaqMan Reverse Transcription Reagents' were used for cDNA synthesis using random hexamer or oligo dT primers. 1 µg of RNA template was used unless RNA concentrations were low; the same amount of RNA template was always used in all reactions in the same experiment, dictated by the lowest RNA concentration. Reverse transcription reactions were performed in 96-well plates to allow multichannel pipettes to be used for PCR reaction set up, the reaction constituents and temperature programs follow:

Applied Biosystems TaqMan Reverse Transcription Reagents:

RNA Up to 1µg

H2O Adjust to 7.7µl

Then add the following to each tube from a master mix:

	Vol.(µl)
10X Reaction Buffer	2.0
MgCl2 (25mM)	4.4
dNTPs (2.5mM ea.)	4.0
Primers (50µM)	1.0
RNase Inhibitor (20U/µl)	0.4
MultiScribe RT (50U/µl)	0.5

Heat to 25°C for 10 minutes, 48°C for 30 minutes then 95°C for 5 minutes.

2.4.2 Taqman® qRT-PCR

Applied Biosystems Gene Expression Assays were used for all qRT-PCRs in this project. The assays consisted of a 20 X reaction mix containing template-specific forward and reverse primers (18 mM each) and a probe that anneals between the two primers (5 mM). The probe DNA is fluorescently tagged at its 3' end, but fluorescence from intact probes is prevented by a quencher molecule that is bound to its 5' end. During PCR amplification, the 5'-3' nucleolytic activity of the DNA polymerase cleaves the quencher from the probe, resulting in fluorescence levels proportional to the amount of PCR product present. All Gene Expression Assays used in this project were designed to anneal across two exons in cDNA, guaranteeing that non-specific amplification did not occur from residual genomic DNA. Expression of the gene of interest was always measured relative to the housekeeping control gene (ß-actin). The gene of interest and ß-actin were amplified in duplex PCR reactions, probes for the gene of interest were tagged to 'FAM' labelled fluorescent dyes, while ß-actin probes were labelled with 'VIC' dye, they fluoresce at different wavelengths, allowing them to be measured in the same reaction. All reactions were performed in 5 µl volumes in 384-well plates. The pre-designed RT-PCR gene expression assays are listed in specific results chapters. The reaction constituents and temperature cycling parameters follows:

Reaction mix	Volume (µl)
2X PCR Master Mix	2.5
20X Gene Expression Assay	0.25
20X ß-actin Expression Assay	0.25
cDNA	2.0
Nuclease-free H_2O	-
Total Volume	5 µl

Temperature cycling:

Heat Cycle	Time	
50oC	2 min	
95oC	10 min	
95oC	15 sec	x35
60oC	1 min	

All samples were amplified in technical replicates of duplicate or triplicate, with at least three biological replicates. Fluorescence of FAM and VIC dyes were measured for all reactions during temperature cycling, data was analysed using a combination of Applied Biosystems SDS (Sequence Detection Software) and Microsoft Excel (2007) software.

2.4.3 Analysis of qRT-PCR

SDS plotted the amplification curves as cycle number vs. fluorescence for both dyes in every well. FAM and VIC fluorescence were analysed as separate data sets, a fluorescence threshold was identified for each data set where amplification curves were in their exponential phase. The extension phase of PCR releases fluorescence from the respective qRT-PCR probe, and a threshold of fluorescence is set during the exponential phase of amplification. The cycle number at which the threshold crosses this set threshold is termed the cycle threshold (Ct). qRT-PCR results in this project were analysed using the relative quantification method of comparative Ct. The 'cycle threshold value' (Ct value) for each amplification curve was interpolated by finding the precise fractional cycle number (to 5 decimal places) at which the curve crossed the fluorescence threshold. Ct values for FAM and VIC data were exported from SDS as text files and converted to Excel documents for data analysis. This method assumes that assay efficiencies are equal. Efficiencies were calculated using serial dilutions of cDNA product and the following equation:

Efficiency (%) = $(10^{-1}/\text{slope})$ x 100

The housekeeper (ß-actin) acts as a normalising control for RNA concentrations and small pipetting discrepancies. This house keeper was tested for consistent expression and reproducibility in appropriate samples. Housekeeping gene expression was used to calculate the ΔCt for the given gene of interested and the equation to calculate ΔCt is as follows:

$\Delta Ct = Ct_{(sample)} - Ct_{(Housekeeper)}$

All experiments were compared to a reference control to calculate the ΔΔCt as follows:

$$\Delta\Delta Ct = \Delta Ct_{(sample)} - \Delta Ct_{(reference)}$$

Fold change (Relative quantification) was calculated as follows:

Relative Quantification (RQ) = $2^{-\Delta\Delta Ct}$

This method calculates gene expression normalised to the endogenous control relative to a calibrator from within the experiment (i.e. a sample or sample group designated to have relative gene expression level of 1.0), it is advantageous because it does not require the inclusion of a standard curve from a serial dilution of template in each experiment.

2.5 DNA Sequencing

DNA sequencing was performed by purifying end point PCR products, to remove un-incorporated dNTPs, primers and salts, followed by dideoxy sequencing reactions, and a second purification step before capillary electrophoresis to separate sequencing products by size. The steps of DNA sequencing are outlined below:

2.5.1 PCR Clean up

PCR products were purified for sequencing using the Agencourt AMPure kit. This relies on binding of DNA products over 100bp in length to magnetic beads in the kit solution. Ninety µl of AMPure was added to each 50µl PCR reaction, the plates were sealed, briefly vortexed, and centrifuged to 1000 rpm for 1 second. They were left to stand for 5 minutes and then placed onto a SPRIPlate (solid phase reversible immobilisation plate) magnetic plate holder (Agencourt) for 10 minutes allowing the separation of beads/PCR products from the liquid phase. Keeping the PCR plate on the SPRIPlate, the PCR reaction constituents were removed by inverting the plates upside-down. The beads were then washed with 200µl of freshly prepared 70% ethanol for 30 seconds before inverting the plate (still on the magnet) and centrifuging upside-down to 600rpm for 1 second to remove as much ethanol as possible. PCR Plates were removed from the SPRIPlate and left to air-dry for 20 minutes.

The PCR product was eluted from the beads by the addition of 40 µl of nuclease free water. The PCR plates were sealed and vortexed to resuspend the AMPure beads, then returned to SPRIPlates plates, 10µl was carefully pipetted out per sequencing reaction. This cleaned PCR product was either stored at -20°C or taken forward to the next step.

2.5.2 Dideoxy Sequencing

Applied Biosystems BigDye Terminator v3.1 Cycle Sequencing kits were used for all sequencing reactions in this project, reactions were performed in 96-well plates as follows:

Reaction mix	Volume (µl)
5X Sequencing Buffer	3.5
Ready Reaction Mix	0.5
Template	10 (variable for plasmid DNA)
Primer (1pmol/µl)	3.2
Nuclease Free water	2.8 (variable for plasmid DNA)
Total Reaction Volume	20 µl

Temperature cycling:

Heat Cycle Time
96°C   45 sec
50°C   25 sec   X25
60°C   4 min

2.5.3 Sequencing Reaction Purification

Sequencing reactions were purified to remove reaction constituents and unincorporated nucleotides and primers prior to electrophoresis using Agencourt CleanSEQ reagent. 10µl of CleanSEQ reagent was added to each sequencing reaction, followed by 62µl of freshly prepared 85% ethanol. Plates were briefly vortexed and centrifuged to 1000 rpm for 1 second to collect the liquid to the bottom of the wells, then placed on a SPRIPlate for 3 minutes. Wells were emptied by inverting the plates upside-down, the CleanSEQ beads were washed twice with 100 µl 85% ethanol for 30 seconds each, emptying the wells between washes. Plates were inverted and centrifugation at 600 rpm for one second. Plates were removed from the SPRIPlates and air dried for 20 minutes, 40 µl of

H_2O was added to each well and CleanSEQ beads were resuspended by vortexing. Plates were briefly centrifuged to 1000 rpm for 1 second and returned to SPRIPlates. 20 µl of sequencing products were loaded into optically clear barcoded 96 well plates ready for capillary electrophoresis.

2.5.4 Capillary Electrophoresis

Sequencing capillary electrophoresis was performed on a 48-capillary Applied Biosystems 3730 Genetic Analyser with 36 cm capillaries. Electrophoresis was preceded by filling the capillaries with fresh POP-7 polymer (Applied Biosystems) and warming the capillaries to 60°C. Sequencing products were separated by size by electrophoresis at 8500 volts for 50 minutes.

2.5.5 Sequencing Analysis

Sequencing was analysed offline using CLC genomics workbench 5. Experimental sequences were aligned with known sequences derived from the bioinformatic database ENSEMBL genome browser.

2.6 Cell culture

Eukaryotic cell lines were handled under sterile conditions using class II biological safety cabinets (Holten Safe 2010). Cells were grown in a monolayer and maintained in tissue culture flasks with vented caps (Corning, Birmingham, UK) in inCusafe 37°C, 5% carbon dioxide (CO_2) incubators.

HeLa cells (an immortalised human cell line derived from cervical cancer), NRK52E cells (an immortalised rat kidney epithelial cell line), and HEK293 cells (an immortalised cell line derived from human embryonic kidney cells) were obtained from The European Collection of Animal Cell Cultures (ECACC). HeLa cells were maintained in Dulbecco's modified Eagles medium supplemented with 10% (v/v) fetal calf serum (FCS), 2mM L-Glutamine, and 100 U/ml Penicillin, and 100 µg/ml streptomycin (Invitrogen, Paisley, UK). NRK52E and HEK293 cells were maintained in Dulbecco's Modified Eagle Medium containing 4.5g/L D-glucose; 10% (v/v) FCS; 2mM GlutaMAX; 1mM sodium pyruvate; 100 U/ml Penicillin; 100 µg/ml streptomycin (Invitrogen, Paisley, UK). HK-2 cells (an immortalised Human proximal tubule cell line derived from human kidney) obtained from

Lonza, UK. The cells were maintained with Keratinocyte serum free media (K-SFM, Gibco, Invitrogen, Paisley, UK) supplemented with epidermal growth factor (5ng/ml) and bovine pituitary extract (40μg/ml).

2.6.1 Cell Passage (sub culturing) and Cryopreservation

Cell were passaged regularly and when approximately 80-90% confluence to prevent overcrowding in culture flasks. All experiments were performed with cells of lowest possible passage number and experiments were completed in as few passages as possible. Fresh cell culture stocks were recovered from storage in liquid nitrogen after approximately 25 passages.

Passaging was performed by removing culture media and rinsing cells gently with sterile phosphate buffered saline (PBS), (Lonza, Slough, UK) before detaching them from the flask with 2ml 1X TE (0.05% trypsin; 0.2% ethylenediamine tetraacetic acid (EDTA). Cells were collected in 10 ml foetal bovine-serum (FBS)-containing medium, which inactivates the trypsin, and centrifuged at 1500 rpm for 5 minutes. As HK-2 cells are maintained in serum free media, soyabean trypsin inhibitor (Sigma, Dorset, UK) was used to neutralise and inactivate the trypsin. Following centrifugation, the media/TE mix was poured off and the cell pellets were resuspended in cell culture media for sub culturing at ratios 1 in 3. For cyrostorage cells, were resuspended in growth media with 10% (v/v) dimethylsulfoxide (DMSO) to prevent ice particle forming during the freezing process then aliquotted into cryopreservation viles. The cryoviles were placed in an isopropanol freezing container (Nalgene) in a -80°C freezer overnight, ensuring freezing no faster than 1°C per minute.

2.6.2 Cell Revival

To revive cells from cryopreservation they were quickly defrosted at 37°C and the cell suspension immediately transferred into a 10ml universal containing 5mls of complete growth media. The suspension was then centrifuged at 1500 rpm for 5 minutes. The supernatant was poured off leaving the cell pellet behind, this removes the DMSO. The cell pellet was then resuspended in complete growth media and seeded accordingly.

2.6.3 Cell counting

Cells were counted with a Bright Line Haemocytometer (Sigma, Dorset, UK). 10 µl of a cell suspension was pipetted under a cover slip onto the grid, using a light microscope; the number of viable cells in each 1 mm corner square was counted and averaged. Cells crossing the bottom or right-hand edge of any square were not counted. The average number of cells in each 1 mm square was derived, and then multiplied by 10^4 to give the number of cells per ml in the suspension. The subsequent concentration of cells per ml can be determined using the following calculation:

Cell number / ml = average cell count per square x 10^4 x original volume

The calculated cell concentration (cells/ml) was then used at seeding cells at the desired density.

2.7 Extraction and Quantification of Protein

Protein was routinely extracted from animal tissues and cell cultures in this project via the following methods detailed below.

2.7.1 Extraction from tissues and cells

Protein samples were prepared from cultured cells by rinsing with PBS and scraping with a pipette tip in 1X RIPA buffer (50mM Tris HCl, pH8, 150mM NaCl, 1% Triton X-100, 0.5% Sodium deoxycholate, 0.1% Sodium dodecyl sulphate (SDS), and 100Mm Ethylenediaminetetraacetic acid (EDTA), final pH 7.4. Protease (complete, mini EDTA free) (Roche, Hertfordshire, UK) and phosphatase inhibitors (x100 stock solution) (Sigma) were added on the day of use as they do not remain stable in H_2O. Samples were thawed to -80°C and passed through a hypodermic needle 10 times, then wheeled at 4°C for 30 minutes, before briefly centrifuging to remove cell debris. The protein rich supernatant was collected and concentration determined (2.7.2). Animal tissues were homogenised with a Polytron 2100 rotor homogeniser at full speed in 1X RIPA buffer containing protease and phosphatase inhibitors as above, then centrifuged at 5000 g at 4°C for 5 minutes. The protein rich supernatants were transferred to fresh tubes and

protein concentration determined (2.7.2). All protein samples were stored at -80°C.

2.7.2 Determination of protein concentration

Protein concentrations were determined using a Pierce BCA (bicinchoninic acid) Protein Assay Kit (Thermo Scientific, Loughborough, UK) according to the manufacturer's instructions. Assays were performed in flat bottom 96 well plates and dilutions of an albumin protein standard (provided) ranging from 25ng/μl - 2 μg/μl were reconstituted in PBS and used to generate a standard curve for each assay. Reagents A and B included in the kit were mixed at a ratio of 50:1 respectively, before being added to either protein samples or standards at a ratio of 8:1 (25 μl of sample:200 μl BCA reagent mixture). Plates were protected from light and incubated at 37°C for 30 minutes. Absorbance at 560nm was determined for all wells using a Wallac Victor^2 plate reader. Both standards and samples were measured in duplicate and the average calculated. The concentration of the protein was then interpolated from the standard curve by Work Out software.

2.8 Western Blotting

Western blotting was used in this project to determine expression levels of proteins in animal tissues and cell lysates. Each results chapter details specific antibodies used to investigate expression levels of varying proteins. Each step of the Western blotting protocol used in this study follows:

2.8.1 SDS polyacrylamide electrophoresis

Protein samples were prepared in a total volume of 20 μl at a concentration of 20 μg, incorporating the appropriate volume of 6 X Laemmli reducing loading dye (constituting 50% glycerol; 9% SDS; 0.375 M Tris pH6.8; 10% β-mercaptoethanol; 0.05% bromophenol blue dye). Samples were denatured for 10 minutes at a temperature greater than 90°C to ensure proteins were denatured before adding to resolving gels. Proteins were then resolved using sodium dodecyl sulphate polyacrylamide gel electrophoresis (SDS/PAGE). 12% polyacrylamide gels (containing 40% (v/v) polyacrylamide (30%), 11.25 mM Tris pH 8.8, 0.1% (v/v) SDS, 300 μl ammonium persulphate (APS) and 30 μl TEMED) were used. A 5%

stacking gel (13.3% (v/v) polyacrylamide (30%), 3.75 mM Tris pH 6.8, 0.1% SDS, 300 µl APS and 30 µl TEMED) was used with each gel.

Also added was 15 µl of Amersham 'Rainbow markers' a protein molecular weight marker (full range 10 kDa - 250 kDa) linked to coloured dyes for easy identification on the blotting membrane. Empty wells were loaded with 20µl 6X Laemmli loading dye to help provide a constant resistance across the gel.

The mix for each resolving gel constituted:

Reagent	Volume
30% acrylamide	12 ml
1.5 M Tris (pH8.8)	7.5 ml
10% SDS	300 µl
H_2O	10.2 ml
TEMED	30 µl
10% APS	300 µl

Stacking gel consisted of:

Reagent	Volume
30% acrylamide	2 ml
0.5 M Tris (pH6.8)	3.75 ml
10% SDS	159 µl
H_2O	9.1 ml
TEMED	15 µl
10% APS	150 µl

2.8.2 Protein blotting

Following electrophoresis the stacking gel was removed and lanes not including protein were cut from the resolving gel. Six pieces of Whatman 3 mm chromatography blotting paper and a piece of Amersham Hybond-P membrane were cut to the same size of the gel. Filter paper and transfer sponges were equilibrated in transfer buffer and membranes were activated with methanol. Transfer buffer consisted of 0.025 M Tris pH10.5; 0.2 M Glycine; 0.1% SDS; 20% methanol. Transfer apparatus was prepared as follows (cathode to anode): 2 X transfer sponge, 3 x Whatman sheets, gel, membrane, 3 x Whatman sheets, and 2 x transfer sponge. Blots were transferred overnight at 88 mAmps, 7 volts overnight in a Hoefer TE 50X transfer tank.

2.8.3 Antibody probing and washing

Once the membranes had been transferred the membrane was blocked overnight at 4°C in Tris-buffered saline Tween buffer (TBST) (0.025 M Tris pH7.4; 0.14 M NaCl; 0.0027 M KCl; 0.1% Tween (Sigma, Dorset, UK)), 5% (w/v, g/ml) dried skimmed milk (Marvel) or 5% Bovine Albumin Serum (BSA) (Sigma, Dorset, UK) depending on the antibody specifications. All blocking was carried out on a lab shaker (Luckham R100) at 50 oscillations per minute with the membranes heat sealed into plastic bags using a Russell Hobbs heat sealer with minimal airspace to enhance contact of the antibody preparations with the membrane. Primary antibody exposure was performed in a total volume of 10-20 ml TBST, 1% milk or BSA. Membranes were again heat-sealed. The bags were taped to a lab shaker and left overnight at 4°C at 180 oscillations per minute. Primary antibody dilutions are detailed in specific methods sections.

The membranes were washed with 100ml TBST in 5 x 10 minute washes. Horse-radish peroxidase (HRP) conjugated secondary antibodies targeting the species in which the primary antibody was raised (DAKO, Norfolk, UK). Membranes were incubated in a total volume of 50 ml with 5% milk or BSA. Membranes were incubated for one hour at room temperature; details of specific antibodies used and dilutions are given in relevant chapters. Membranes were then washed for 5 further 10 minutes washes with 100 ml TBST.

2.8.4 Enhanced chemiluminescence and detection

Proteins were visualised using Amersham enhanced chemiluminescence (ECL) Western blotting detection reagents per the manufacturer's instructions. ECL detects binding of the HRP-conjugated secondary antibodies. Kodak general purpose blue medical X-ray film was used to develop the membrane to visualise present proteins. Films were exposed for varying lengths of time ranging from 1 second to 15 minutes. A Kodak X-Omat 1000 was used to develop the X-ray films. The developed film, with sufficient protein banding, was placed on top of the membrane to mark on the rainbow size markers, allowing accurate sizing of protein bands.

2.8.5 Membrane stripping and re-probing

The level of a particular protein in a sample was always measured relative to the level of a 'housekeeping' protein, such as glyceraldehyde-3-phosphate dehydrogenase (GAPdh) or beta-actin (ß-actin). Membranes were stripped to remove conjugated antibodies and re-probed with antibodies specific to the housekeeper. The membrane were stripped in 100ml of a mild stripping buffer (0.2M Glycine, 1%SDS, and 1%Tween20$^{®}$, pH 2.2) for 30 minutes at room temperature on a shaker at 50 oscillations per minute, then washed 3 X for 5 minutes in TBST. Membranes were then re-blocked overnight at 4°C in TBST, 5% milk or BSA and probed, washed and analysed for the housekeeping protein exactly as described above.

2.8.6 Densitometry

Immuno-detected protein bands on photographic films were measured to compare protein levels between samples using the BIORAD Fluor-S MultiImager and 'Quantity One' software (BIORAD). This allows the scanning of X-ray films to generate a digital image. Individual bands were labelled and demarked by boxes using a drawing tool in the Quantity One software. The intensity of the bands was then measured by the software and expressed in units of optical density per mm^2 (ODU/mm^2). The intensity of the protein band of interest was divided by the intensity of the band for the housekeeping gene to find the relative level of the protein of interest in each sample.

Two methods of background subtraction were used for densitometry analysis. A 'global' background subtraction method was used for blots with clean and constant background intensities, this involved drawing a box in an area of the image that represented the background, the software then calculated the average intensity of all pixels in this box and subtracted it from all pixels in boxes containing bands. Alternatively, 'local' background subtraction was used for blots where the background intensity level was variable or high across the blot; the software calculated average background intensity for each box by measuring the average intensity of all pixels in a one-pixel border around each box and subtracted this from each pixel in the box to find the band intensity.

The applicable densitometry method used for individual western blots is described in each results chapter.

2.9 Experimental animals

A *UMOD* KO (UMOD-/-) mouse model that was generated by Bates *et al* (Oklahoma University, USA) along with the WT (UMOD+/+) strain (129/sv), have been utilised in this project (Bates et al., 2004). All experiments in this thesis have been performed using litter mates of KO or WT mice, unless stated otherwise. Generation of the KO mice follows; in brief, human cDNA *UMOD* probes were used to isolate mouse cDNA *UMOD* which was then used to probe a mouse 129/sv liver λ Fix II genomic library to obtain full length mouse *UMOD*. Restriction analysis, sequencing, and comparison with human and rat gene restriction maps were used to characterise the *UMOD* gene. The KO mice were generated with an omega type replacement targeting vector incorporating a 2kb segment 5' of the cap site of the *UMOD* gene and the first four exons plus the intervening introns. The linearised vector was introduced to the embryonic stem cells of a 129/sv strain mouse via electroporation. Successfully transfected embryonic stem cells were then injected into developing blastocysts of C57Bl/6 mice, thus producing chimeric pups. The chimeric pups were then bred with black Swiss female mice to obtain hetergozygous mice for *UMOD* deficiency. These mice were then inbred for 10 generations to produce WT mice and KO. The genotype of the WT and KO mice was verified using end point PCR of tail genomic DNA with specific primers (forward: 5' AGGGCTTTACAGGGGATGGTTG-3' and reverse: 5' GATTGCACTCAGGGGGCTCTGT 3') **Figure 2-2**. Throughout this thesis *UMOD*-/- mice will be referred to as KO and *UMOD*+/+ mice will be referred to as WT.
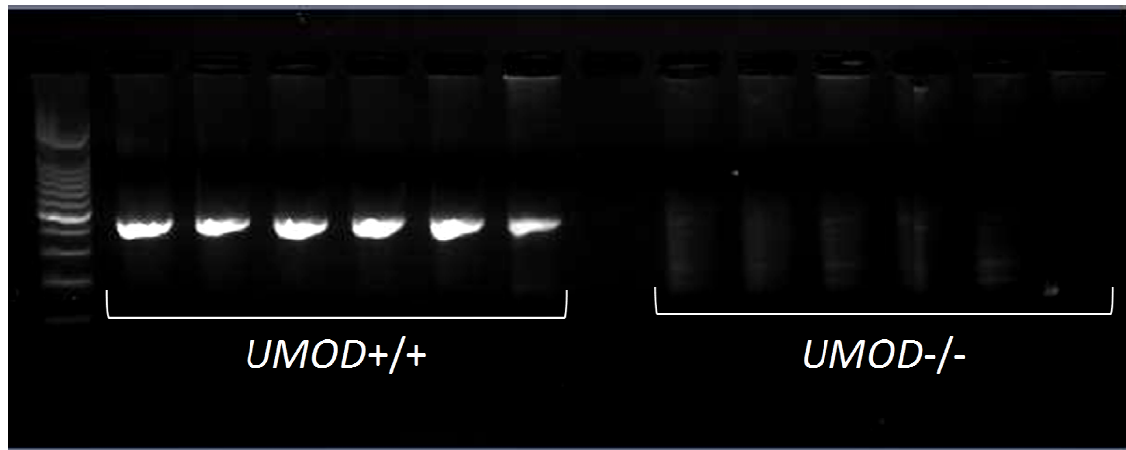
Figure 2-2 Confirmation of the *UMOD* knockout strain.

End point PCR verified the *UMOD*-/- (KO) strain with the absence of a PCR product band at exon three of the *UMOD* gene.

2.10 Hemodynamic parameters

2.10.1 Tail cuff plethysmography

Blood pressure was assessed indirectly in conscious mice using the Harvard mouse tail cuff plethysmography pressure equipment (Panlab Harvard apparatus, Edenbridge, UK). The plethysmography equipment utilizes volume pressure recording (VPR) technology and operates by placing a tail cuff over the mouse tail and occluding the tail blood flow by an internal pressure transducer. Upon deflation the tail blood volume is measured as a change in pressure. Precise details of the procedure and animals used are outlined in specific results chapters.

2.10.2 Radiotelemetry

Hemodynamic parameters were then measured directly using the Radio-Telemetry Monitoring of Blood Pressure and Heart Rate Dataquest IV Telemetry System (Data Sciences International, New Brighton, USA). Radiotelemetry provides scheduled sampling every 5 minutes of systolic, diastolic, mean arterial pressure, heart rate, pulse pressure, and activity levels throughout 24 hour periods as previously described (Huetteman and Bogie, 2009). Before the implantation of the transmitter (radio frequency transducer PA-C10), calibration was performed to verify accuracy to within 3 mmHg.

The mouse carotid artery cannulation with subcutaneous device placement procedure was as follows: mice of 12 week old were anesthetized with Isoflurane

(inhalant) and monitored throughout the surgical procedure. Hair was removed from the upper back and the neck area by shaving and the incision areas were cleaned with ethanol. The first incision was made on the back between the right shoulder blade and the mid scapula, where a small subcutaneous pocket was formed by blunt dissection for the telemetry probe to nest in (PA-C10, Data Sciences International, Virginia, USA). The mouse was then placed in a supine position to expose the neck. A vertical 1.5 cm midline incision through the skin overlaying the trachea was made and a Luer-Lock needle (Henleys Medical supplies Ltd, London, UK) was used to tunnel the catheter of the telemetry probe through to the open incision. The mandibular glands were carefully separated and the common carotid artery was isolated with blunt dissection. The cleaned up vessel was then ligated permanently with a suture (4-0 silk, Ethicon, Edinburgh, UK) at the site of bifurcation of internal and external branches of the carotid artery. The suture was then secured and retracted towards the head of the mouse. Another suture was placed approximately 8-10mm below the first suture, and retracted towards the tail of the mouse, to prevent blood flow through the artery. A third and final suture was placed in the middle of the two retracted sutures and tied loosely, this suture acts as an anchor to hold in place the telemetry pressure sensing catheter during advancement on cannulation. A 26 gauge hypodermic needle (BD Biosciences, New Jersey, USA) was bent to 90 degrees (bevel side up) and used to puncture the carotid lumen. Right angled forceps (Fine Science Tools, Heidelberg, Germany) were used to open the puncture site to allow entry and advancement of the telemetry catheter. The catheter was advanced until reaching the retracted occlusion suture towards the tail end. The middle suture was then tied with one knot to secure the catheter whilst the occlusion suture was released; this allows further advancement of the catheter without it being forced out by the consequent blood flow back into the vessel. Once in place, the sutures were secured and all retracted suture were released. The open incision at the neck was sutured with 4-0 vicryl silk (Ethicon, Edinburgh, UK). The back pocket containing the telemetry probe was sutured securely (4-0 Vicryl silk). Mice where then allowed to recover in a hot box (32°C). Following surgery intraperitoneal injection of carprofen analgesia was administered. Once the mice had regained consciousness, they were returned to their cages and allowed one week recovery period before initiation of recording and/or cardiovascular stimulation. At the end of the recording period mice of

18 weeks of age were placed in metabolic cages for a 24 hour period (described below) then sacrificed by exsanguination.

2.11 Renal function

2.11.1 Metabolic cage measurements

Mice were placed in the metabolic cages (Techniplast, model number 3700M022, Buguggiate, Italy) at week 6 of the ± 2% NaCl for a 24 hour period. Urine output and fluid intake was monitored and recorded at the end of the 24 hours. Urine samples collected within the 24 hour period were used for further analysis.

2.11.2 Creatinine clearance

Estimated glomerular filtration rate (eGFR) was measured indirectly by quantitative determination of creatinine clearance (CrCl) by measuring creatinine, glucose, and urea in WT and KO mice (± 2% NaCl) plasma and urine samples. CrCl was measured using Roche/Hitachi cobas c systems kits (Roche Diagnostics, Burgess Hill, UK). The following kits were used; CREP2 (for creatinine measurements), GLUC3 (for glucose measurements), and UREAL (for urea measurements). The protocol included in the kits was a standardised method using 150 µl of sample (urine or plasma). Urine was collected as per section 2.11.1 and blood was collected by cardiac puncture into heparinised tubes. Whole blood was spun down by centrifugation at 1000 g for 15 minutes at 4^oC. Plasma was carefully removed and stored at $-80\,^oC$ until required.

The test principle to measure creatinine is an enzymatic method based on the conversion of creatinine with the creatininases, creatinase, and sarcosine oxidase to glycine, formaldehyde, and hydrogen peroxide. Catalyzed by peroxidase, the released hydrogen peroxide reacts with 4-aminophenazone and HTIB to form a quinone imine chromogen. This chromogen formation causes a colour change of the solution and the intensity of the colour change is directly proportional to the creatinine concentration of the sample and is measured photometrically at 700/540 nm. Creatinine of the sample is destroyed by creatinase, SOD, and catalase during incubation with TAPS buffer (N-

Tris(hydroxymethyl)methyl-3-aminopropanessulfionic acid), 30 mmol/l, pH8.1)).
The enzymatic processes are as follows:

$$\text{Creatinine} + H_2O \longrightarrow \text{Creatine}$$

$$\text{Creatine} + H_2O \longrightarrow \text{Sacrosine} + \text{Urea}$$

$$\text{Sarcosine} + O_2 + H_2O \longrightarrow \text{Gylcine} + \text{HCHO} + H_2O_2$$

$$H_2O_2 + 4\text{-aminophenazone} + \text{HTIB} \longrightarrow \text{Quinone imine chromagen} + H_2O + HI$$
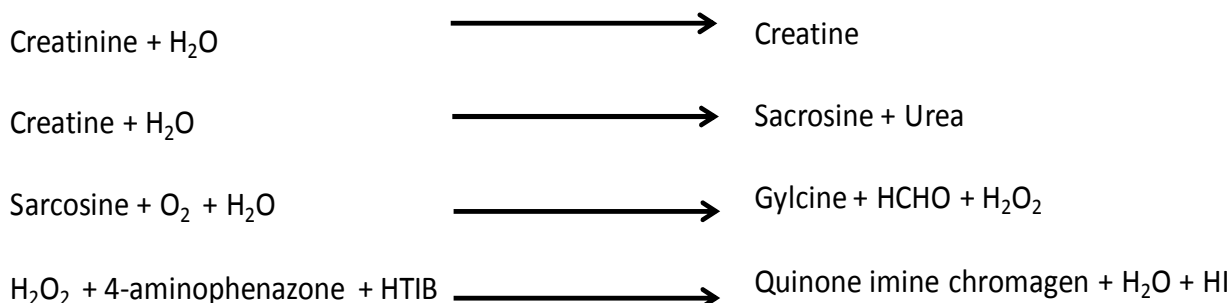
Glucose was also measured using an enzymatic reference method with hexokinase which catalyzes the phosphorylation of glucose to glucose-6-phosphate by ATP. Glucose-6-phosphate dehydrogenase oxidises glucose-6-phosphate in the presence of NADP (Nicotinamide adenine dinucleotide) to gluconate-6-phosphate. The rate of NADPH (Nicotinamide adenine dinucleotide phosphate) formation during the reaction is directly proportional to the glucose concentration and is measured photometrically.

Finally Urea was measured as a kinetic test with urease and glutamate dehydrogenase (GLDH). Urea is hydrolyzed by urease to form ammonium and carbonate. In the second phase of the reaction 2-oxoglutarate reacts with ammonium in the presence of GLDH and the coenzyme NADH to produce L-glutamate. In this reaction 2 moles of NADH are oxidised to NAD^+ for each mole of urea hydrolyzed. The rate of decrease in the NADH concentration was directly proportional to the urea concentration of the sample, and is measured photometrically at 700/340 nm.

The assays were ran on a clinically validated automated analyser (c311, Roche diagnostics, Burgess Hill, UK), using the manufacturers calibrators and quality controls. Values were then normalised to kidney weight and urine flow per minute. The following calucaltions was used to dervie CrCl (ml/min):

Urinary creatinine concentration x urine rate flow

_____

         plasma creatinine concentration

The values were then corrected to kidney weight (ml/min/mg).

2.11.3   Electrolyte analysis

Urine samples collected from the 24 hour metabolic cage study were taken forward to investigate electrolyte analysis. The measurements were carried out by Dr James Harvie at the University of Glasgow Veterinary Medicine School. The assays were run on the Olympus AU640 clinical chemistry analyzer (Beckman Coulter Ltd, London, UK) using the indirect ISE (ion selective electrode) method known as potentiometry. The ISE coverts the activity of a specific ion dissolved in a solution into an electrical potential which is then measured as voltage. The voltage sensing electrode is an ion specific membrane and works alongside a reference electrode of a stable and known electric potential (acting as the assay control). The concentration of Na^+, K^+, and Cl^- were measured in the 150 µl mouse urine samples as µmol/l and normalised to the voltage reading from the stable electrode. Values were then normalised to kidney weight.

2.12 Histology

2.12.1   Ex vivo analysis

Mice were sacrificed by cervical dislocation, upon termination tissues were removed, cleaned of any connective tissue, and prepared for histological analysis. Body weight, kidney weight, and tibia length were recorded. All tissue weights were normalised to tibia length.

2.12.2   Fixation and sectioning

Left and right kidneys from WT and KO mice (± 2% NaCl) were dissected, cleaned of any connective tissue, and fixed in 10 % (v/v) neutral buffered formalin (10 % formalin: 90 % H_2O, 33 mM NaH_2PO_4, 45 mM Na_2HPO_4) overnight. Tissues were processed through a gradient of alcohol solutions to Histoclear (a xylene substitute, Thermo Scientific, Loughborough, UK), with the terminal step into paraffin wax. The fixation of tissue was performed in a Citadel 1000 processor (Thermo Scientific, Loughborough, UK) in the following sequence:

Solution	Length of incubation (min)
70 % ethanol	15
85 % ethanol	15
90 % ethanol	25
95 % ethanol	25
100 % ethanol	15
100 % ethanol	15
100 % ethanol	15
Histoclear	30
Histoclear	30
Paraffin wax	30
Paraffin wax	30

Glass histology slides were coated with aminoalkylsilanes by placing in 2% 3-aminopropyltriethoxysaline (APES) and acetone for 30 seconds. Sections were washed twice with acetone for 10 seconds followed by two washed with dH_2O for 5 minutes each. Slides were then dried at $37^{o}C$ overnight. Kidney tissues were cut transversely along the corticopapillary axis and embedded in this orientation in paraffin wax in preparation for sectioning using a Shandon Histocentre 3 embedding centre (Fisher Scientific, Loughborough, UK). Paraffin blocks were sectioned at 3 µm slices to expose the transverse section of embedded kidney tissue using a Leica Finese 325 Microtome (Fisher Scientific. Loughborough, UK). Tissue sections were mounted onto the prepared slides and baked for 3 hours at $65^{o}C$ and then at $40^{o}C$ overnight. Paraffin was removed from the tissue sample by 2 x 7 minute washes in Histoclear. Samples were then rehydrated by passing through a decreasing ethanol concentration gradient of 100 %, 90 %, and 75 % ethanol for 7 minutes each, followed by a final wash in dH_2O for 7 minutes.

2.12.3 Haematoxylin and eosin staining (H & E)

Haematoxylin and eosin (H & E) stain is a standard method used to stain the nucleus and cytoplasm respectively. H & E was used in this project to investigate the morphology of kidney tissue from WT and KO before and after 2% NaCl stimulation. Deparaffinised sections were stained in haematoxylin for 4 minutes and washed in dH_2O for 10 minutes, followed by one 30 second wash in acid alcohol (1 % (v/v) HCI in ethanol) to remove the excess haematoxylin. Nuclei were counter stained in eosin for 2 minutes followed by a further 5 minute wash in dH_2O. Sections were dehydrated through increasing concentrations of ethanol

(75 %, 95 %, and 100 %) for 7 minutes each. Sections were then cleared by 2 ten minute washes in Histoclear and cover slips were fixed using DPX mounting medium (non-aqueous xylene based, Sigma, Dorset, UK). The nuclei appear blue/purple whereas cytoplasm appeared pink.

2.12.4   Periodic acid-Schiff (PAS)

This method was employed to localize total insoluble polysaccharides. Periodic acid is an oxidative reagent which acts upon the 1, 2 glycol linkage within the sugar molecule of carbohydrate, resulting into production of two free aldehyde groups. The produced aldehydes then react with leucobasic fuschin of Schiff's reagent to produce visible magenta red colour. This method is commonly employed for polysaccharides as it does not breakdown polysaccharide chains and provides a clear basis for reaction which is specific to polysaccharides allowing investigation of tissue structures.

WT and KO mice kidney sections (3 μm) ± 2% NaCl were stained as follows: Sections were deparaffinised and hydrated in an ethanol gradient (100 %, 95 %, and 70 % for 7 minutes each), and incubated in 0.5% Periodic acid (Sigma, Dorest, UK) for 15 minutes. Sections were rinsed for 5 minutes in running tap water followed by incubation in Schiff's reagent (Sigma, Dorest, UK) for 15 minutes. The sections were rinsed again in running tap water for 5 minutes prior to being counterstained with haematoxylin for 2 minutes. A final 5 minute wash step was performed in running tap water, followed by dehydration in ethanol (70 %, 95 %, and 100 %) and cleared in Histoclear for 7 minutes each. The sections were then mounted using DPX mounting medium. The nuclei appear blue, whilst PAS positive structures appear magenta red. Sections were visualized using the EnVision detection system for mouse primary antibodies (K5007, DAKO, Glostrup, Denmark). All slides were imaged using an Aperio scanner XT at 20X magnification producing a resolution of 0.495 μm/pixel and investigated using the ImageScope software (Aperio v12.0.0.5039).

Preparations of reagents are listed:

<u>**Schiff's reagent**</u>

1gm of basic fuschin was dissolved in 0.15N HCl; agitated for three hours and then 1gm of sodium metabisulphate added and kept for overnight. Then decolorizing charcoal was added and kept shaking and filtered.

0.5% Periodic acid

0.5gm of periodic acid was dissolved in 100ml distilled water.

2.12.5   Immunohistochemistry

Paraffin was removed from the cut kidney sections using Histoclear and then hydrated thorough an ethanol gradient of 100 %, 90 %, and 70 % for 7 minutes each and washed in dH_2O for 7 minutes. Heat induced antigen retrieval was then performed with the sections incubated in 10 mM citric acid (pH 6.0) at 95 -100°C for 15 minutes and allowed to cool at room temperature. The slides were then washed twice in dH_2O for 10 minutes. The endogenous peroxide was quenched from the tissue sections by incubating the slides for 15 minutes in 3 % hydrogen peroxide (H_2O_2) (v/v in methanol)), followed by 2 washes in dH_2O. Sections were then incubated for 60 minutes with 2.5 % normal horse serum in a humidified chamber, to block all non specific binding. The kidney sections were then incubated overnight at room temperature with the primary antibody diluted in 1 % (w/v) BSA in PBS (Sigma Aldrich, Poole, UK) in a humidified chamber. Each experiment included a blank and a negative control using 1 % BSA in PBS (no antibody and rabbit IgG antibody diluted in 1 % BSA in PBS respectively. The following day sections were washed 3 times in PBS for 5 minutes each. The sections were incubated for 30 minutes with Vectastain universal biotinylated secondary antibody (Vector Laboratories, ABC kit, Peterborough, UK), followed by two 5 minutes washed in PBS. DAB chromagen solution (3,3- diaminobenzidine and hydrogen peroxide solution) (Vector Laboratories, Peterborough, UK) was utilised for immunoperoxidase staining by incubating the sections for 5 minutes or until stain turns dark brown, at room temperature in a humidified chamber. The reaction was stopped by adding the sections to dH_2O. Sections were then counterstained with Haematoxylin for 2 minutes, this enabled visualisation of the nuclei. Sections were washed in running tap water for 5 minutes then dehydrated in an ethanol gradient as follows; 70 % , 95 %, and 100 % for 7 minutes each with a final incubation in Histoclear for 7 minutes also. Cover slips were then fixed using DPX. Antibodies, concentrations, and dilutions used are detailed in specific results chapters.

2.13 Enzyme Linked ImmunoSorbent Assay (ELISA)

TNF-α levels were measured in urine from KO and WT mice (±2% NaCl) by enzyme linked immunosorbent assay (ELISA), using a commercially available mouse TNF-α ELISA kit (BD Sciences, Oxford, UK) following the manufacturer's instructions.

The assay was performed as follows; 96 well flat bottom plates were coated with anti TNF-α detection antibodies (monoclonal anti-mouse TNF-α phage antibody with fetal bovine serum (FBS)) overnight at 4°C. The following day, plates were washed with PBS containing 0.1% Tween 20 and blocked with 2% milk/PBS (w/v) for 2 hrs at room temperature. 50 µl of ELISA diluent (buffered protein base containing 0.09 % sodium azide) was added to each well followed by 50 µl of standard or sample. All samples and standard reactions were performed in triplicate. Standards were prepared by serial dilutions from a 2000 pg/ml stock solution (made from reconstituting a lyophilized Standard with standard/sample diluent solution (bovine serum containing 0.09 % sodium azide)) to produce the following standard concentrations; 1000 pg/ml, 500 pg/ml, 250 pg/ml, 125 pg/ml, 62.5 pg/ml, and 31.3 pg/ml with the addition of a zero standard (0 pg/ml) which was standard/sample diluent only. A subsequent 2 hour incubation period was performed at room temperature.

Plates were then aspirated and washed with the provided wash buffer (300 µl per well), followed by decanting and aspirating until the wells were washed 4 times. 100 µl per well of a horseradish peroxidise conjugated secondary antibody to bind to the captured TNF-α (provided in the kit) was added and incubated for 30 minute at room temperature. Wash steps were repeated 5 times. TMB One-Step Substrate Reagent (3,3',5,5'-tetramethylbenzidine) was added to each well (100 µl) and incubated for 30 minutes at room temperature whilst protected from the light, to initiate peroxidase catalyzed colour change. Following the incubation step 50 µl of Stop solution (provided in the kit) was added to stop the reaction by acidification. Absorbance readings were measured at 450 nm. The mean absorbance for was calculated for each set of triplicate samples and standards. The mean zero standard absorbance was then subtracted from each mean sample value. The standard curve was plotted with absorbance on the x-axis and TNF-α concentration on the y-axis. Linear regression was used to apply the best fit line to the curve, applying a gradient. Each sample absorbance was

then normalised to the gradient. All samples were then corrected to urine volume.

2.14 Metabolomic analysis

Whole kidney tissue was extracted from WT and KO mice (± 2% NaCl) and prepared for metabolomic analysis as follows:

Tissue was homogenised using 1 ml of extraction buffer (20 % H_2O, 60 % methanol, and 20 % chloroform (v/v) using the Polytron 2100 method described in section 2.7.1. Tissue homogenates were then cold quenched to extract the metabolome. The extraction process involved rapidly cooling the tissue homogenate to 4 ^{o}C by submersion of the tube into a dry ice ethanol mix and incubating for 1 hour with agitation on a shaking platform. Debris was then pelleted by centrifugation at 13,000 g for 3 minutes and the supernatant retained for analysis by liquid chromatography tandem mass spectrometry (LC–MS) analysis. Metabolite extracts were analysed using an UltiMate 1 LC system (Dionex, Camberley, UK) coupled to an Orbitrap Exactive (Thermo, Hemel Hempstead, UK). A 4.6 × 150 mm ZIC-HILIC column was used for separation. Buffers consisted of: A) 2% acetonitrile, 97.9% H_2O, 0.1% formic acid and B) 97.92% acetonitrile, 2% H_2O, 0.08% formic acid. The gradient applied ran from 80% B to 5% B over 30 min, followed by a 10 min wash at 5% B and equilibration for 6 min at 80% B. Metabolites were detected in a mass range from 70 to 1400 amu, in both positive and negative ionisation modes at 50,000 resolution at m/z 100. RAW data was converted to MzXML files using READw.exe and further split into positive and negative modes using MzMatch. Peaks were detected and metabolites were identified using MzMine 1.97 (Pluskal et al., 2010). Statistical analysis was performed using SigmaStat software (Cosmol, Östringen, Germany). t-tests were used to analyse the data, unless the assumptions of normal distribution or equal variance in the data were not met, in which case the Mann–Whitney U test was used in its place as the alternative non-parametric test. Differentially expressed metabolites were uploaded and analysed with Ingenuity Pathway Analysis (IPA) software (386), where conical metabolic pathways of interest were investigated.

2.15 Renal Microarray mRNA expression analysis

RNA amplification for array analysis was prepared using the Illumina® TotalPrep RNA Amplification Kit (AMIL1791) (Life Technologies, Paisley, UK). RNA from WT and KO mice ± 2% NaCl was extracted from whole kidney as per section 2.3.8, and the integrity of the sample analysed and validated to ensure it was free of protein, DNA, phenol ethanol, and salts (section 2.3.9). RNA samples were diluted to 45.45 ng / µl, and concentrations were confirmed by nanodropping each sample in triplicate (section 2.3.11) in preparation for first and second strand cDNA synthesis.

2.15.1.1   First and second stand cDNA synthesis

A reverse transcription master mix was comprised containing the following reagents;

Reaction mix	Volume (µl)
T7 Oligo(dT) primer	1
10 X First strand buffer	2
dNTP Mix	4
RNase Inhibitor	1
Arrayscript	1
Diluted RNA	11
Total Volume	20

The reaction mix was incubated for 2 hours at 42°C, and then placed on ice to stop the reaction prior to the second strand cDNA synthesis. For second strand cDNA synthesis the following master mix was comprised;

Reaction mix	Volume (μl)
Nuclease free water	63
10 X Second strand buffer	10
dNTP mix	4
DNA Polymerase	2
RNase H	1
Total Volume	80

The reaction mix was added to the reverse transcription reaction and mixed fully; the combined mix was incubated at 16°C for 2 hours, and then placed on ice prior to the cDNA purification step. 250 μl of cDNA binding buffer (supplied in kit) was added to each sample and this mix was added to a cDNA filter cartridge (supplied with kit) and centrifuged at 10,000 *g* for 1 minute. The flow through was discarded and the filter cartridge was placed in a provided wash tube. A wash buffer was provided by the kit and was reconstituted with 100 % ethanol, once prepared 500 μl of the wash buffer was added to the cDNA filter cartridge and the previous centrifugation step repeated. The flow through was discarded and the cDNA filter cartridge was placed in a provided elution tube. Nuclease free water was heated to 55 °C, and 20 μl of it added to the cDNA filter cartridge and incubated at room temperature for 2 minutes, followed by centrifugation at 10,000 *g* for 1 minute. The elute was transferred to a 0.5 ml RNase free PCR tube in preparation for *In Vitro* Transcription (IVT) cRNA synthesis.

The following master mix was comprised for the IVT step (for each cDNA sample);

Reaction mix	Volume (μl)
T7 10 X reaction buffer	2.5
T7 enzyme mix	2.5
Biotin-NTP mix	2.5
Total Volume	7.5

Biotin-NTP biotinylates nucleic acid and binds with high affinity to Strepdavidin-Cy3, allowing detection of downstream hybridisation of cRNA. The IVT master mix was added to each cDNA sample and incubated for 14 hours at 37 ^{o}C. The reaction was quenched by the addition of 75 µl of nuclease free water and being placed on ice. The cRNA purification step immediately followed; 350 µl of cRNA binding buffer (supplied with kit) and 250 µl of 100 % ethanol were added to each sample and this mix was applied to the cRNA filter cartridge supplied. The filter was centrifuged for 1 minute at 10,000 g and the flow through discarded. 650 µl of provided wash buffer was added to the cRNA filter cartridge and the centrifugation step repeated. Nuclease free water was preheated to 55 ^{o}C and 200 µl was added to the cRNA filter cartridge then centrifuged for 1.5 minutes at 10,000 g. The cRNA samples were diluted to 150 ng / µl, and the concentration was confirmed by nanodropping the samples in triplicate.

2.15.1.2   Hybridization to the BeadChip

Hybridization buffer (HyB) and humidity control buffer (HCB) were prepared by heating to 58°C for 10 minutes to dissolve any salts, and cooled to room temperature before use. The BeadChip Hyb chamber apparatus was prepared by the addition of 200 µl of HyB and HCB to each well; the apparatus lid was applied and incubated at room temperature. The BeadChips were placed on the Hyb chamber insert. 5µl of the diluted cRNA was added to 10µl HYB buffer, and heated for 5 minutes at 65°C, vortexed, pulse centrifuged and allowed to cool to room temperature. The sample mixes were then applied to the inlet ports on the BeadChip.

The BeadChip was loaded into the Hyb chamber, and incubated for 16 hours at 58°C, on a rocking platform. A 1 X High-Temp wash buffer (provided with kit) was prepared, and placed in the hybex water bath insert within the hybex heating base, at 55°C overnight. The following day, BeadChips were removed from the Hyb chamber, and submerged face up in a pyrex beaker containing wash E1BC buffer (provided with kit). The cover seal was removed carefully, and placed in a slide rack in a wash chamber containing wash E1BC buffer. The slide rack was then placed in the hybex water bath, and the BeadChips were incubated for 10 minutes at 55°C. The slide rack was then placed in the wash chamber containing wash E1BC buffer used previously, and plunged in and out of the buffer 5 to 10 times, followed by agitation on an orbital shaker for 5 minutes

at room temperature. The rack was removed and placed in a staining chamber containing 250ml 100% ethanol and plunged in and out of the buffer 5 to 10 times. The rack was agitated again on an orbital shaker for 10 minutes at room temperature and subsequently placed in a staining chamber containing 250ml of fresh wash E1BC buffer and plunged in and out of the buffer 5 to 10 times, followed by further agitation on an orbital shaker for 2 minutes at room temperature. 4ml of Block E1 buffer (provided with kit) was added to individual wash trays, and the BeadChip was placed in face up. The wash tray was placed on an orbital shaker for a final 10 minutes at room temperature.

Streptavidin-Cy3 was diluted to 1:1000 with Block E1 buffer (provided with kit), and placed in a clean individual wash tray. Streptavidin-Cy3, acts as secondary agent to the biotinylated cRNA hybridized to the BeadChip, and is used to detect the intensity of this signal. The BeadChip was transferred to the wash tray and placed on an orbital shaker for 10 minutes at room temperature. The BeadChip was transferred to a slide rack and placed in a clean staining dish containing 250ml fresh wash E1BC buffer, and plunged in and out of the buffer 5 times, followed by agitation on an orbital shaker for 5 minutes at room temperature. The BeadChip was then dried by placing the slide rack on clean paper towels, and centrifuging at 275 g for 4 minutes at room temperature. The dried BeadChips are then transferred to the Illumina® BeadArray Reader to scan, and the output data visualised using Beadstudio software.

2.15.1.3   Microarray data analysis

Illumina® Gene Expression Beadchips employ internal control features to monitor sample independent and sample dependent data quality. Control data results and microarray results were visualised with BeadStudio software. Quantile normalisation was performed without background subtraction; the BeadChip represents each probe (gene) with an average of 30 beads, where each bead has a given normalised expression value. The values were averaged per probe with unpaired 2 sample t-tests performed using Illumina® custom error model (386). Differentially expressed probes (genes) were identified using a difference score cut off +/- 13.0103 equating to a P value < 0.05. Ingenuity Pathway Analysis (IPA) software (386) was used to analyse differentially expressed probes.

2.15.1.4   Metabolomics and Microarray IPA anlysis

Canonical pathways analysis identified link from the IPA library that were most significantly associated with the data set (differentially expressed gene/metabolites), and which from the data set that met the *P* value cut-off of 5%. From here any genes/metabolites that were associated with a canonical pathway in the Ingenuity Pathways Knowledge Base (IPKB) were considered for the analysis. The significance of the association was measured firstly, by calculating a ratio of the number of genes with differentially expressed probes that mapped to the canonical pathway divided by the total number of genes with probes in the actual data set that mapped to the pathway displayed. Secondly, Fisher's exact test was used to calculate a *P* value determining the probability that the association between the significant genes in the data set and the canonical pathway could be explained by chance alone.

2.16 Statistical Analysis

Values in this project are stated as Means ± standard error of the mean (SEM) unless otherwise indicated. The significance threshold (p value) for all analysis was set at 0.05. For comparisons of a continuous variable between 2 experimental groups, paired and unpaired Student's t-tests were applied as appropriate. For statistical comparisons in data sets with more than two groups, analysis of variance (ANOVA) was applied, followed by the Dunnett's or Tukey's post-tests, comparing all samples groups against a designated control group or for comparisons between the groups. Detailed statistical analyses for particular experiments are specified in the relevant results chapters.

3 Human 2 Kb *UMOD* promoter studies

3.1 Introduction

Genome-wide association studies of disease typically result in the identification of genomic susceptibility loci, in which several SNPs showing strong inter-marker linkage disequilibrium (LD) are equally associated with disease predisposition. To date, the search for rare and common variants affecting BP has identified thirteen loci from two large meta-analysis consortia, with each association revealing only a very small proportion of the total variation in systolic or diastolic blood pressure (Licht et al., 2009, Levy et al., 2009, Newton-Cheh et al., 2009). Moreover, the sum of rare and common genetic variants robustly identified so far through linkage and genome wide association studies explain only 1-2% of the population variation in BP and hypertension, suggesting the existence of more undiscovered blood pressure related variants.

SNPs that are commonly linked with disease are frequently found in non-coding regions where they were thought to have no obvious function. However, the ENCODE (encyclopaedia of DNA elements funded by the National Human Genome Research Institute) revealed that up to 80% of the components of the human genome have at least one biochemical association with function, identifying regions of transcription, transcription factor association, chromatin structure, and histone modification in the human genome sequence (**www.nature.com/encode/#/threads**).

Padmanabhan and colleagues identified and validated SNP rs13333226 at position -1,617 upstream of the *UMOD* transcriptional start site. When carried on the minor G allele rs13333226 was associated with a lower risk of hypertension (Padmanabhan et al., 2010). A previous candidate gene study of *UMOD* and hypertension revealed the minor allele of rs6497476 (located at -744 BP upstream of the transcriptional start site) was associated with lower risk of hypertension in a Japanese population, although did not reach significance (Iwai et al., 2006). Additional published GWAS have reported SNPs in the *UMOD* promoter region that help towards elucidating genetic risk of CVD – the minor T allele at position -3,653 (rs12917707) was associated with a 20% reduction in chronic kidney disease incidence (Kottgen et al., 2009), the minor C allele at position -1,550 (rs4293393) was associated with improved renal function in controls and sufferers of chronic kidney disease (Kottgen et al., 2010), whereas the major T allele at this site was associated with increased risk of chronic

kidney disease (Gudbjartsson et al., 2010). These genetic variations indicate that the *UMOD* locus is independently associated with hypertension as renal function was not compromised, thus, implicating *UMOD* functionally at altering blood pressure.

It has been reported that not all implicated causal SNPs are directly associated with changes in phenotype (Collins et al., 1999), therefore it should be investigated whether the implicated SNPs are in fact functional variants or are SNPs in LD leading to changes in BP. This association mapping relies on studying SNPs in LD with SNPs of interest to investigate multiple alleles in coding and non-coding regulatory regions to identify rare variants with large effect on phenotype and disease. Transcription is the initial step of gene expression requiring a multitude of actions involving transcription factors (TF), their corresponding *cis*-acting elements on DNA, additional co-factors, and chromatin structure. LD SNPs may alter expression of nearby genes via differential transcription factor (TF) binding. To date there are lacking examples of GWAS that have identified promoter SNPs linked with TF binding and altered transcription in essential hypertension. More recently, new strategies are being utilised to identify regulatory SNPs by combining computational and experimental approaches, for example *in silico* analysis with chromosomal immunoprecipitation (ChIP) technology (Kim et al., 2008, Ameur et al., 2009, Haring et al., 2007). Chromatin remodelling results in histone alterations which play a crucial role in post transcriptional modifications to gene expression.

The experimental work in this chapter explores the 2 Kb *UMOD* promoter region to compare transcriptional activities of *UMOD* promoter SNPs derived from contrasting genotypes for rs13333226. The rational for investigating the 2 Kb promoter region was prompted by the findings from the GWAS implicating rs13333226 with lower risk of hypertension where SNPs up to the 2 Kb region have high levels of LD (>94%), with a reduced number of haplotypes. If a substantial decreased risk is caused by a single SNP, there is more likely to be an association between that risk and SNPs in LD with the implicated causal SNP (Weiss and Clark, 2002). Moreover, the discovery of a *UMOD* TAL specific gene promoter (Zhu et al., 2002) opens new avenues for studying molecular mechanisms behind *UMOD* gene regulation of blood pressure regulation and hypertension.

3.2 Aims

- To identify human renal cell lines that are of contrasting genotype for SNP rs13333226 and sequence the 2Kb *UMOD* promoter.

- To investigate the transcriptional effects of *UMOD* promoter polymorphisms with luciferase expression constructs to implicate causative SNP(s) that alter promoter activity.

- To utilise the 'Transfac' transcription factor database to identify potential candidate transcription factor binding sites that may affect *UMOD* transcription.

- To utilise Chromatin ImmunoPrecipitation (ChIP) assays to assess predicted transcriptional genotype-dependent binding to the 2kb *UMOD* promoter region.

- To utilise small molecule transient transfection into cell cultures to validate transcription factor binding on *UMOD* promoter activity.

3.3 Methods

3.3.1 Identifying renal cell lines with contrasting genotype for SNP rs13333226

ACHN, 786-0 and TK10 are cell lines of the National Cancer Institutes' collection of 60 human cancerous cells (NCI-60 collection). The cell types were chosen from the panel as they were of renal lineage. They were purchased from the American Type Culture Collection (ATCC) and used throughout this project. The cells were maintained in Dulbecco's Modified Eagle Medium containing 4.5g/L D-glucose; 10% (v/v) FCS; 2mM GlutaMAX; 1mM sodium pyruvate; 100 U/ml Penicillin; 100 µg/ml streptomycin (Invitrogen, UK). Genomic DNA was extracted from the cell culture lysates as described in section 2.2.1 and genotyped for SNP rs13333226. Full experimental manipulations are detailed in the subsequent sections.

3.3.2 Genotyping

Before PCR amplification and sequencing of the 2Kb *UMOD* promoter region, the genomic DNA from ACHN, 786-0, and TK10 was genotyped for SNP rs13333226 using Applied Biosystems genotyping assay (C_31122293_10, context sequence: GTCAAAGAGGTAGCACAGCTGTAGG[A/G]ATATTGACTCCTCTTCCCAAACAGC). The genotyping assay utilises double labelling to determine between alleles. The A allele being VIC labelled and G allele being FAM labelled. The genotyping assay was carried out in a 384 well format with at least four negative controls (containing no DNA) and two positive controls (where the allelic state was known) using the reaction mix and cycling conditions listed below. The assay reaction was completed on a GeneAmp PCR System 9700 (Applied Biosystems, Paisley, UK).

Reaction Mix	Volume (µl)
2X Genotyping master mix	2.5
20X working stock SNP genotyping assay	0.5
Template	Xµl for 20µg genomic DNA
Nuclease Free water	0 (variable depending on DNA concentration)
Total Reaction Volume	5

Temperature cycling:

Heat Cycle	Time
95°C	10min
92°C	15 sec
60°C	1min
70°C	10 min
10°C	Hold

X40 cycles (applied to the 92°C 15 sec and 60°C 1min steps)

3.3.3 *UMOD* Promoter Sequence cloning

Following identification of human renal cell types of contrasting genotype for SNP rs13333226, PCR amplification of the 2Kb *UMOD* promoter region was performed followed by sequencing to confirm the promoter sequence and present polymorphisms in preparation for DNA cloning. All *UMOD* promoter construct cloning was performed as per sections 2.2 and 2.3 in the general methods.

3.3.4 Promoter Activity Analysis

Dual reporter Luciferase activity assays were performed to compare transcriptional activities of the 1 and 2 Kb *UMOD* promoters derived from all three renal cell lines of contrasting genotypes for SNP rs13333226. HeLa, NRK, HEK-293, and HK-2 cells were cultured as per section 2.6 for transient transfection experiments. Each pGL4.10 basic Luciferase expressing construct was transfected into triplicate wells of HeLa, NRK, HEK-293, and HK-2 cell cultures. Cells were seeded at 1×10^5 one day prior to transfection. When cells were approximately 80% confluent, the transfection reagent; Lipofectamine®2000 was used at a 3:1 ratio (Lipofectamine® 2000:plasmid DNA). A total of 1µg of plasmid DNA at a ratio of 1:50 (Renilla:plasmid DNA) was transfected. Optimem (Invitrogen, Paisley, UK), the necessary transfection media was used over the 24 hour transfection period. After transient transfection for 24 hours, the cells were harvested and the activity of the promoter constructs assayed using the Dual Luciferase Reporter Assay System (Promega, USA). Renilla and Firefly luciferase activity was measured in cell lysates, lysed in 1X passive lysis buffer, using the Dual Luciferase Reporter Assay System (Promega, Southampton, UK). All reagents were prepared following the

manufacturer's instructions. Light emission measurements were carried out using the Lumat LB 9507 tube luminometer (Berthold Technologies, Harpenden, UK). The lumat 9507 was set to inject 50µl of LAR II reagent, pause for 2 seconds to measure the luciferase present in the lysates. Immediately followed by an injection of 50 µl of the Stop and Glo reagent, a further 2 second time pause occurs to allow measurement of the renilla over a ten second period. To determine the promoter activity, firefly luciferase expression levels (relative light units) were normalised against Renilla luciferase levels. Duplicate ratios were averaged to indicate luciferase activity within the sample.

3.3.5 Site Directed Mutagenesis

To investigate the effect of polymorphic variation on *UMOD* promoter activity, SNPs of interest were mutated to the alternative allele using the QuikChange Site-Directed Mutagenesis kit (Agilent Technologies, Wokingham, UK). The pGL4.10 luciferase plasmid containing the 2Kb *UMOD* promoter fragment from the 786-0 cell type was used in the site directed mutagenesis assays in this project. Mutagenic primers utilised to alter each SNP of interest were designed using the online Quikchange Primer Design Program (**www.agilent.com/genomics/qcpd**) and ordered from Eurofins MWG Operon (Manchester, UK); primer sequences are listed below:

Oligo name	Sequence (5'-3')	Allele change
786-0 1F	TTTGGCAAAGATGAAAGCAAATTACCAATGCTCAG AACTGG	G to A
786-0 1R	CCAGTTCTGAGCATTGGTAATTTGCTTTCATCTTT GCCAAA	
786-0 2F	GGTGGGATTGTAAACCAATTTATAATAATTCTCGG GGTGCT	T to A
786-0 2R	CAGCACCCCAGAGAATTATTATAAATTGGTTTACA ATCCCA	
786-0 3F	CTATTGTGGGATGCGGGGAGCGGGGAG	G to C
786-0 3R	CTCCCCGCTCCCCGCATCCCACAATAG	

The Stratagene QuikChange Lightening Site Directed Mutagenesis assay allows mutagenesis at sites in a double stranded DNA plasmid, eliminating the need for subcloning. The principles of the assay can be outlined in three steps: step 1

uses an accelerated thermal cycling procedure to achieve multiple rounds of mutant strand synthesis. Components of the thermal cycling reaction include a supercoiled double stranded DNA template, two or more synthetic oligonucleotide primers containing the desired mutations, and the kit-provided enzyme blend featuring a *Pfu* Fusion DNA polymerase. First the mutagenic primers are annealed to denatured template DNA. The *Pfu*-based DNA polymerase then extends the mutagenic primers with high fidelity and without primer displacement, generating ds-DNA molecules with one strand bearing the mutations.
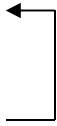
In Step 2 of the procedure, the thermal cycling reaction products are treated with the restriction endonuclease *Dpn* I. The *Dpn* I endonuclease (target sequence: 5´-Gm6ATC-3´) is specific for methylated and hemimethylated DNA5 and is used to digest the parental DNA template. DNA isolated from almost all *Escherichia coli* strains is dam methylated and therefore susceptible to digestion.

In Step 3, the reaction mixture, which is highly enriched for multiple mutated single stranded DNA, is transformed into XL10-Gold ultracompetent cells. Double stranded plasmid DNA was then prepared from the transformants and analyzed by sequencing to identify clones bearing each of the desired mutations.

Preparation of the mutant strand synthesis and control reactions with thermal cycling reactions was as follows:

Reaction mixture	Template DNA (≤5 Kb)	Control template (4.5Kb)
10 X QuikChange Multi reaction buffer	5 µl	5 µl
ds-DNA template	X µl (50 ng)	5 µl (25 ng)
Mutagenic primers (sense and anti-sense)	1.25 µl (125 ng)	1.25 µl (125 ng)
dNTP mix	1 µl	1 µl
QuikSolution reagent	1.5 µl	1.5 µl
Nuclease free water	X µl final volume of 50 µl	34 µl
QuikChange Lightening enzyme	1 µl	1 µl
Total reaction volume	50 µl	50 µl

Temperature cycling:

Heat Cycle	Time
95°C	2 min
95°C	20 sec
60°C	10 sec
68°C	30 sec/Kb of plasmid length
68°C	5 min

X 18 cycles

Following the temperature cycling, reactions were placed on ice for 2 minutes to reduce the temperature to ≤37°C. Once the reactions had cooled 10 U of *Dpn* I restriction enzyme was added directly to each amplification reaction. Reactions were then mixed, centrifuged for 1 minute at full speed, and incubated at 37°C for 1 hour to digest the parental (non mutated) ds-DNA.

The mutated DNA plasmid was then transformed as per section 2.2.5. Positive colonies were screened as per section 2.3.3.

3.3.6 TESS analysis and Ingenuity pathway analysis

Transfac Professional is a commercial transcription factor database curated by Biobase the bioinformatics company, it includes information on over 8,000 TFs and over 18,000 TF binding sequences found in vertebrate, bacteria, fungi, insect, nematode and plant genomic sequences (**www.cbil.upenn.edu/tess**). Biobase use experimental and bioinformatic evidence of TF binding to construct nucleotide positional weight matrices that can provide the relative likelihood that a TF binds to particular input sequences. Matrices are constructed by aligning multiple known TF binding sequences and recording the frequency that each nucleotide occurs at each position. This is collated into a consensus sequence for the matrix. The five most highly conserved consecutive bases are designated the 'core' binding sequence. Many matrices are constructed using the evidence of a single experimental study in a particular species, for example where libraries of random or mutated sequences were tested for TF binding. Thus a particular TF will have multiple matrices, relating to evidence from different studies and species. Other matrices are constructed by collating the evidence of several publications, often across several species. Here we examined potential putative transcription factor binding sites at position 16:20365234.

The Ingenuity Pathway Knowledge Base (**http://www.ingenuity.com**) is currently the largest annotated database of knowledge on biological networks. This project exploited the database to define the presence of functional associations of *TFAP2A* with the *UMOD* gene and to draw simplified network connections among other genes.

3.3.7 ChIP assay

Functional Transcription factor binding sites can be identified in the genome by computational approaches or experimentally by Chromatin ImmunoPrecipitation (ChIP). In brief, ChIP relies on antibodies to selectively enrich chromatin fragments to identify the presence of specific histone modification at precise regions of the genome. The chromatin fragment bound to the antibodies are captured using protein A/G beads, where DNA and protein can then be isolated from the precipitate and analysed to determine the abundance of a region of interest. In this project X-ChIP was utilised to explore the potential binding of transcription factor *TFAP2A* to SNPs in the *UMOD* promoter region. The assay contains multiple steps which are outlined in **Figure 3-1** and detailed as follows:
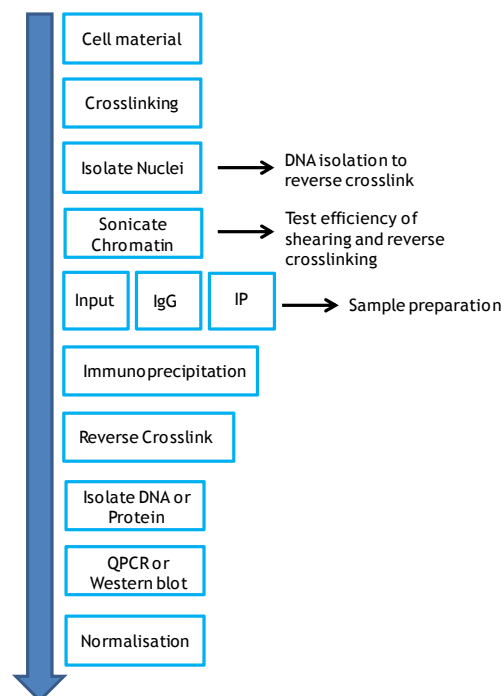
Figure 3-1 Outline of the ChIP procedure.

The flow chart outlines the ChIP experiment described in the subsequent sections. In this project samples were either used as Input (sonicated only), IgG treated, or immunoprecipitated for an antibody of interest (*TFAP2A*).

3.3.7.1 Isolation of chromatin

ACHN, 786-0 and TK10 cells were cultured and used for the extraction of total chromatin. Cells were seeded at 1 X 10^5 in 10cm cell culture dishes and were maintained as outlined in 2.6. Once cell cultures reached 80-90% confluence the culture media was removed and monolayers washed three times with ice cold PBS in preparation for crosslinking.

3.3.7.2 Cross linking

Cells were crosslinked with the addition of formaldehyde to a final concentration of 1% in culture media and incubated for 15 minutes at room temperature whilst shaking gently. Crosslinking the starting material with formaldehyde ensures that the chromatin structure is preserved during the isolation and ChIP procedure. Crosslinking was stopped by the addition of glycine to a final concentration of 0.125 M for 5 minutes at room temperature gently shaking. Media was then discarded and dishes PBS washed 3 times. Cells were then collected with the addition of lysis buffer (1 X PBS supplemented with complete protease inhibitor cocktail, Roche, West Sussex, UK) and 1 X phosphatase inhibitors (100 X cocktail Sigma, Poole, UK) and PMSF (phenylmethanesulfonylfluoride) at a final concentration of 50 μg/ml). Cell lysates were centrifuged at 200 g for 5 minutes at 4^oC. Cross linked cells were then re-suspended in a collection buffer constituted of a 1:1 ratio of mNLB:IPDB buffers including the above mentioned inhibitors (mNLB: 50 mM Tris; 10mM EDTA, 5mM EGTA , 0.1%SDS, final pH8.0 and IPDB: 20 mM Tris, 1 mM EDTA, 1 mM EGTA, 1% Triton X-100, 0.01% SDS, and 150 mM NaCl, final pH8.0). Cell sediments were incubated on ice for 10 minutes, following sequential re-suspension in the mNLB:IPDB buffer mix. The crosslinked chromatin was taken forward for shearing by sonication.

3.3.7.3 Sonication

Chromatin was fragmented to an average size of 100-500 bp using a temperature controlled ($\leq 10^o$C) bio- ruptor (Diagenode) water bath sonicator (hydrodynamic shearing) for 20 minutes (24 s on followed by 24 s off). The temperature must be maintained below 15^oC to prevent the reversal of crosslinking by heat. Debris was then removed by centrifugation for 10 minutes at 15,000 g at 4^oC and supernatants transferred to new tubes. To verify successful sonication 20 μl of

each sample was reverse crosslinked in elution buffer (10 mM Tris-HCl, 1 mM EDTA, and 1% SDS, final pH8.0) at 65°C overnight. Samples were diluted in equal volumes of TE (10 mM Tris and 1 mM EDTA, final pH 8.0), treated with proteinase K (10 mg/ml) for 2 hours at 55°C, and finally purified using Qiagen Qiaquick DNA extraction kit. Reverse crosslinked samples were electrophoresis on 1.2% agarose gels (2.2.3). All successfully sonicated samples were taken forward in the experiment.

Chromatin DNA concentrations were determined using the Qubit$^®$ dsDNA HS kit (Invitrogen, Paisley, UK) and chromatin preps were adjusted to the same concentration (μg/ml) using mNLB:IPDB buffer plus inhibitors (1:1 ratio). In preparation for ChIP, IP buffer (plus inhibitors) was added to the chromatin to a final concentration of 0.1% SDS, 0.1 Triton X-100, 10 mM Tris-HCl, and 1 mM EDTA, final pH8.0.

3.3.7.4 Chromatin immunoprecipitation

Dynabeads$^®$ Magnetic beads (Invitrogen, Paisley, UK) coated with ChIP grade *TFAP2A* primary antibody (Rabbit monoclonal to *TFAP2A*, Abcam, Cambridge, UK) or IgG Control beads (rabbit anti mouse, Sigma, Dorset, UK) were used for all ChIP experiments in this project. Beads were prepared as follows:100 μl of beads (per 500 μl of chromatin) were placed in 1.5 ml tubes and spun down briefly by centrifugation then placed on a magnetic rack (DynaMag^{TM} -2 Magnet, Invitrogen, Paisley, UK) for 5 minutes at room temperature. Beads were then washed twice with 0.5% BSA in PBS, following resuspension in 500 μl of 0.5% BSA in PBS and rotated for 1 hour at room tempareture to block non specific epitopes binding. Beads coated with ChIP grade *TFAP2A* and the IgG control beads were used at a 1:500 dilution for each chromatin sample. Beads were incubated with appropriate antibodies for 1 hour at room temperature whilst rotating. During the bead preparation phase chromatin samples were prepared for overnight incubation with the specific antibody coated beads. Samples were spun down by centrifugation at 2000 g for 5 minutes at 4°C. The chromatin rich supernatants were collected and the debris discarded. Protein concentrations of chromatin samples were measured and 500 μg used for each ChIP or input prep (untreated total chromatin from sonicated starting material). Beads were added to chromatin samples and incubated overnight at 4°C whilst rotating.

The next day ChIPs were washed twice with IPDB buffer, once with a high salt wash (20 mM Tris, 1 mM EDTA, 1% Triton X-100, 0.01% SDS, and 500 mM NaCl, final pH8.0, once with IPWB2 buffer (10 mM Tris, 1 mM EDTA, 1% Triton X-100, 1% NP40, 1% Na-DOC, and 250 mM LiCi, final pH8.0, and finally two TE washes (10 mM Tris and 1 mM EDTA, final pH 8.0). The second TE wash was not aspirated off as each ChIP was then split in to two new tubes and treated for either DNA purification or protein purification.

3.3.7.5 DNA purification (Chelex method)

All ChIP samples, IgG samples and Input (total, 1%, and 10%) were DNA purified using the chelex method: samples were placed on the magnetic column and the TE was carefully aspirated off from the beads. 50 µl of 10% Chelex-100 (BioRad, Hemel Hempstead, UK), was added and the sample vortexed then heated to 97°C for 15 minutes. Chelex-100 acts as a chelating reagent to purify the DNA via ion exchange; it protects the DNA during heating by binding to $Mg2+$ in the extract to release it from the chromatin complex without degradation. 450 µl of nuclease free water was added to the bead/Chelex-100 mixture and vortexed once more, and the tube returned to the magnet. The supernatant was collected and ready for QPCR.

3.3.7.6 Protein purification
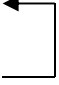
Protein purification was carried out on the other half of the sample for downstream analysis by western blot. This procedure required eluting the ChIP material from the beads and reversing crosslinked covalent bonds introduced by the formaldehyde treatment. Both aims were achieved by incubating the samples in 4 X SDS sample buffer to a 1 x final concentration: 40% glycerol, 240 mM Tris pH6.8, 8% SDS, 0.045 bromophenol blue, and 5% beta-mercarptoethanol and heating to 97°C for 5 miuntes. The sample buffer is added to solubilise the protein and heated to denature the protein. Tubes were placed on the magnetic rack and the supernatant collected. 5 µl of 1 M DTT (Dithiothreitol) was added and samples incubated for a further 5 minutes at 97°C. The sample was then ready for SDS-PAGE and western blot.

3.3.7.7 Analysis by QPCR

Quantitative PCR was carried out on ChIP-enriched DNA using Power SYBR® green master mix (Life Technologies, UK). The master mix contained: SYBR® green I DYE, AmpliTaq Gold® DNA polymerase, dNTPs, and ROX passive reference dye. The SYBR green dye binds to double stranded DNA providing a fluorescent signal that reflects the amount of double stranded DNA product generated during PCR in relationship to the internal reference dye ROX. Fluorescence was monitored on an Applied Biosystems 7900HT Sequence Detection System (Taqman®). The subsequent primer pairs were used for QPCR covering the region of interest; 5' CACTTGGACACAGGAAGGG 3' and 5' CAAGTTAATGGGTGCAGC 3' (*TFAP2A* sense and anti sense respectively). Reaction mixtures and cycling conditions are listed below:

Reaction Mix	Volume (µl)
2X Power SYBR® Green PCR master mix	25
Forward primer	Xµl (50 nM)
Reverse primer	Xµl (50 nM)
Template	Xµl (50 ng)
Nuclease Free water	variable depending on DNA concentration
Total Reaction Volume	50

Temperature cycling:

Heat Cycle	Time	
95°C	10 min (Hold)	
95°C	15 sec (denature)	X 40 cycles
60°C	1 min	

Melting curves were performed to assess the dissociation of the double stranded DNA and to detect non-specific amplification of QPCR runs. ChIP enrichment was determined for IP samples, IgG samples, Input samples (total, 1%, and 10%), and non template controls for the region of interest in triplicate from three independent biological replicates.

3.3.7.8 Analysis by Western blot

To validate successful immunoprecipitation protein extracts from ChIP samples, IgG samples, and input (1%) where immunoblotted as per section 2.8 using the ChIP grade *TFAP2A* primary antibody (Rabbit monoclonal to *TFAP2A*, Abcam, Cambridge, UK). It was not necessary to quantify protein band density here as blotting was to determine pull down *TFAP2A* within the chromatin.

3.3.7.9 Data normalisation

The ChIP and QPCR procedure consists of many steps that may influence the final results, therefore, before the data obtained can be interpreted the variation must be considered. The QPCR data were normalised for differences in the amount of input chromatin, precipitation efficiency, and recovery of DNA after ChIP. Normalization only served to correct for technical variation and not biological variation. There is no consensus on how to normalise ChIP-QPCR in the literature and as a result there are multiple methods being used (**Table 3-1**).

Table 3-1 Assay dependent ChIP normalisation strategies

Normalisation strategy	Normalisation method
No normalisation	ChIP data is not normalised, equal amount of input chromatin varies between experiment
Background subtraction	No-antibody signal is subtracted from ChIP signal
Fold enrichment	Normalised to background signal
% of Input	Normalised to the amount of input chromatin
Relative to control genes	Normalised to ChIP signal obtained at a control sequence
Relative to nucleosome density	Normalised to the ChIP signal obtained with an antibody for modified histone protein

In this project, % of input method was used, where the QPCR signals derived from the ChIP are divided by the QPCR signals derived from 1% input taken after sonication during the ChIP assay. With this method, the input samples represent the amount of total chromatin used in the ChIP. Typically 1% input of starting chromatin is used as input. To calculate percent input the following calculations are used:

Step 1: Adjust 1% input to 100%.

Raw Ct (Ct Input – 6.644)

The starting input fraction is 1%, which is a dilution factor of 100 which equates to 6.644 cycles. This is then subtracted from the Ct value of the diluted input.

Step 2: Percent Input.

Triplicate average Ct100*2^ (Adjusted input – Ct (IP)

The above calculation was also used to determine IgG ChIp samples.

3.3.8 Transient transfection of small molecules

To assess the effect of transcription factor (*TFAP2A*) binding on SNP rs4997081 and promoter activity, transient siRNAoligo-mediated gene silencing was performed in HeLa cells following transfection with the 2 Kb UMOD promoter constructs (ACHN, 786-0, and TK10). HeLa were cultured and transfected using Lipofectamine®2000 (Invitrogen, Paisley, UK) in 24 well plates, and all reactions were performed in triplicate. Cells were seeded at a density of 1×10^5 per well using normal growth media (2.6) and incubated at 37°C for 24 hours. The next day luciferase plasmids containing the contrasting genotype 2Kb *UMOD* promoter sequences were transfected into the HeLa cell cultures (2.3.7) and once again incubated at 37°C overnight. On day three siRNA was prepared for transfection by dilution in Optimem® (Invitrogen, Paisley, UK). Constituents of the transfection reaction per well on a 24 well plate are as follows: 500 µl Optimem®, 50 nM siRNA (*TFAP2A* siRNA, Cy™3 negative control, or *GAPDH* (Invitrogen, Paisley, UK)), and Lipofectamine®2000 at a 3:1 ratio

(Lipofectamine®2000: siRNA) and incubated over night at 37°C. Following the 24 hour silencing period normal growth media replaced the transfection mix on cell cultures for 4 hours. Cell lysates were then collected and promoter activity assays performed (3.3.4). Additional plates were set up in parallel to the above experiment to collect cell lysates for RNA (2.3.8) isolation.

The optimum conditions for transient delivery of *TFAP2A* siRNA into HeLa cells was assessed using siRNA that targeted *GAPDH* and Cy™3, as positive and negative controls respectively. Each siRNA were transfected separately into HeLa cell cultures as described above at the following concentrations: 5 nM, 10 nM, 15 nM, 20 nM, 30 nM, 50 nM, and 100 nM. RNA was isolated and *GAPDH* and *TFAP2A* measured by qRT-PCR (2.4.1) with Applied biosystems Taqman assay probes (NM_002046.3, NM_002046.3, and X03205.1; *GAPDH, TFAP2A,* and 18s respectively).

3.4 Results

3.4.1 Human *UMOD* promoter constructs

Successful sub-cloning of the promoter fragments are demonstrated by endonuclease restriction digest shown in **Figure 3-2** the "dropped" fragments represent the 1 and 2Kb promoter region fragments**.** The corresponding 1 Kb and 2 Kb sequencing chromatograms are shown in **Figure 3-3.** Alignments of polymorphisms in the human *UMOD* promoter (1 and 2 kb) from **Figures 3-2 and 3-3** have been outlined in **Table 3-2**. A schematic outline of the SNPs contained in the 1 and 2 Kb human promoter constructs are shown in **Figure 3-4 A**. The polymorphisms in red represent the SNPs in linkage disequilibrium (LD) with rs13333226 and the polymorphisms in blue represent the SNPs not in LD with rs13333226 **Figure 3-4 B.**

3.4.2 Transcriptional activity of the *UMOD* promoter

The transcriptional activity of the 1 and 2 Kb human *UMOD* promoter SNPs were assessed as per 3.3.4. Relative promoter activity of the 1 Kb constructs of contrasting genotype for rs13333226 did not show any significant differences in transcriptional activity when measured in HeLa **(Figure 3-5 A)**, NRK **(B)**, Hek293 **(C)**, or HK-2 **(D)** cells. However, relative promoter activity was consistently and significantly increased in the TK10 2Kb promoter construct in all cell types **(Figure 3-5)** (4.5, 18, 17, and 6 fold change in; HeLa, NRK, Hek293, and HK-2 cells respectively, ***$p < 0.0001$). This indicates that the TK10 construct (of AA genotype for the index SNP rs13333226) harbours the risk allele associated with altered *UMOD* promoter activity and/or expression (**Figure 3-6**). One SNP is in LD with rs13333226, the C allele at position 20325634 (rs4997081). The other SNPs are the A alleles at position 20365697 (rs12708631) and 20365843 (rs18444928) which are not in LD with rs13333226.
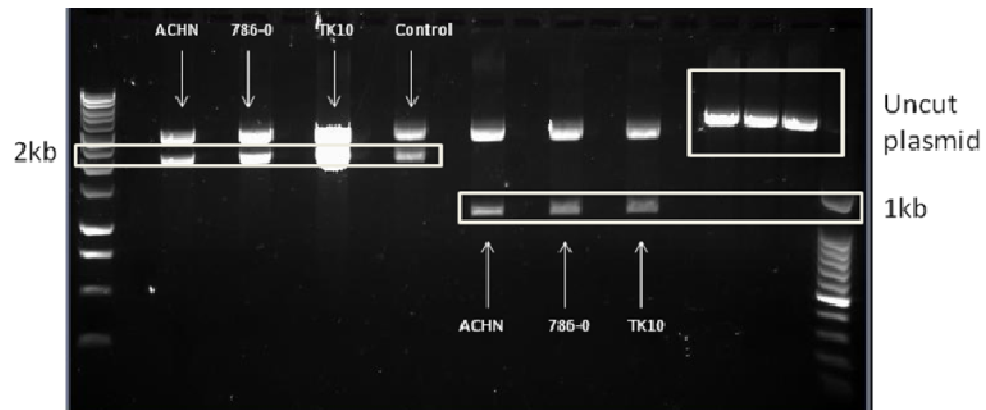
Figure 3-2 1% Agarose gel image of *UMOD* promoter sub-cloning into pLG4.10 luciferase vector.

Amplification of 1 Kb and 2 Kb promoter sequences from ACHN (GG), 786-0 (AA), and TK10 (AA) cell types, were double digested from the pGL4.10 basic luciferase plasmid with *SacI* and *HindIII* restriction enzymes. Undigested pGL4.10 basic luciferase plasmids are shown as uncut plasmid. The Control plasmid is pGL4.10 basic luciferase backbone containing an unrelated random 2 Kb insert. DNA was loaded at 1 µg per lane (plasmids were confirmed with sequencing).
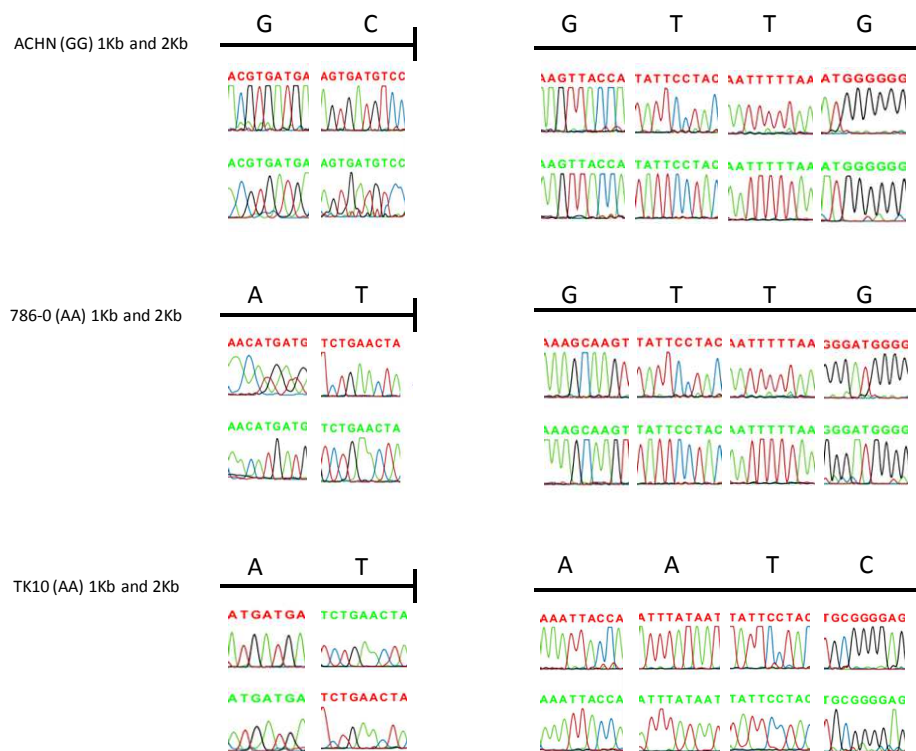
Figure 3-3 Chromatogram display of 1 Kb and 2 Kb SNPs in the *UMOD* promoter (sense strand).

Sequencing confirmed the presence of SNPs in the promoter region. The *UMOD* gene is present on the anti sense strand, thus the SNPs presented in this figure are designated from the reverse and complement strand.

Table 3-2 Promoter alignment and position of polymorphisms within the 1 and 2 Kb human *UMOD* promoter.

Promoter region	Polymorphism	Position	Ensembl ID	Allele
1Kb	C/T	16:20364588	rs4293393	G/A
1Kb	A/G	16:20365012	rs28362063	T/C
2Kb	G/C	16:20365234	rs4997081	G/C
2Kb	T/C	16:20365654	rs13333226	A/G
2Kb	T/A	16:20365697	rs12708631	T/A
2Kb	G/A	16:20365843	rs184444928	T/A

The exact location of the SNPs can be mapped to chromosome 16 upstream in the *UMOD* promoter using the Ensembl database.
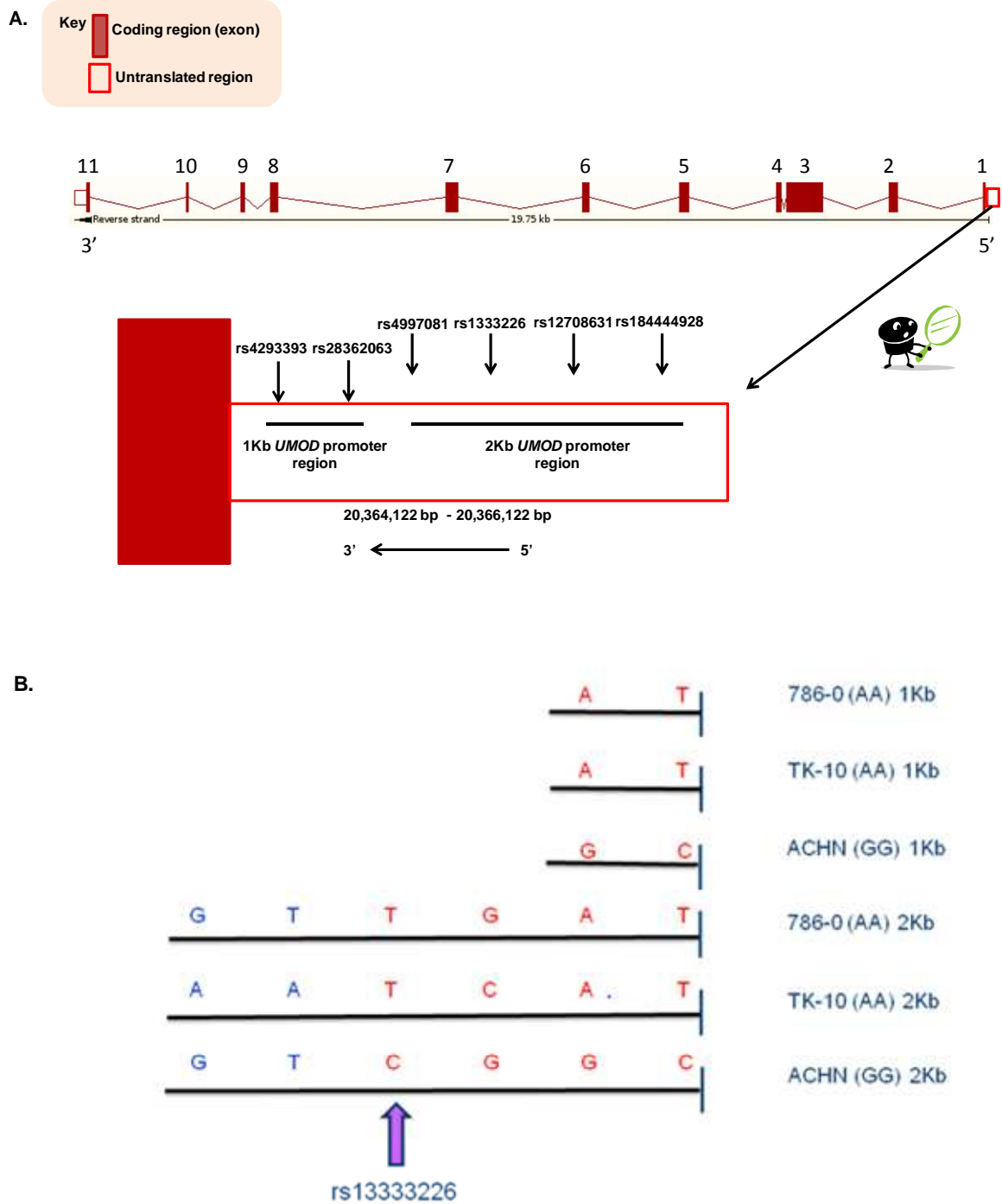
Figure 3-4 Schematic summary of SNPs within the 1 and 2 Kb *UMOD* promoter region.

(A) There are 6 currently known SNPs within the 2 Kb human *UMOD* promoter region. **(B)** Three human renal cell lines (786-0 (AA), TK-10 (AA), and ACHN (GG)) of contrasting genotype for the SNP of interest (rs13333226) were used in this project to represent the *UMOD* promoter regions for testing transcriptional activity of the incorporated SNPs. The *UMOD* gene is present on the anti sense strand, thus the SNPs presented in this figure are designated from the reverse and complement strand.
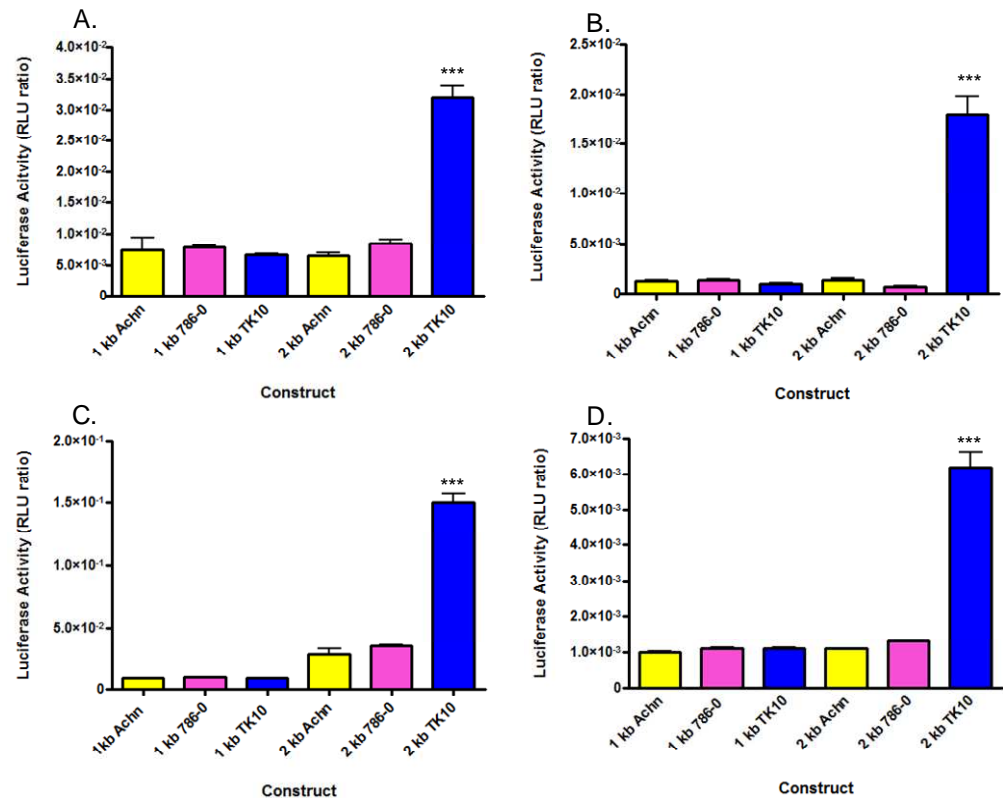
Figure 3-5 Transcriptional activity of the 1 and 2 Kb human *UMOD* promoter constructs.

Transcriptional activity of contrasting genotype of SNP rs13333226, was assessed in **(A)** HeLa, **(B)** NRK, **(C)** Hek293, and **(D)** HK-2 cells, using luciferase activity assays (representative graphs). An increase in luciferase levels implicates altered promoter activity. Cells were seeded at 1×10^5 on day one. Transient transfection was performed on day two (1µg total plasmid (1:50 ratio; renilla:DNA)). Luciferase activity assays were performed on day three. Mean ratio ± SEM (normalised to Renilla), one way ANOVA followed by Tukey's post hoc test, n=3 (independent technical replicates), ***p<0.0001.
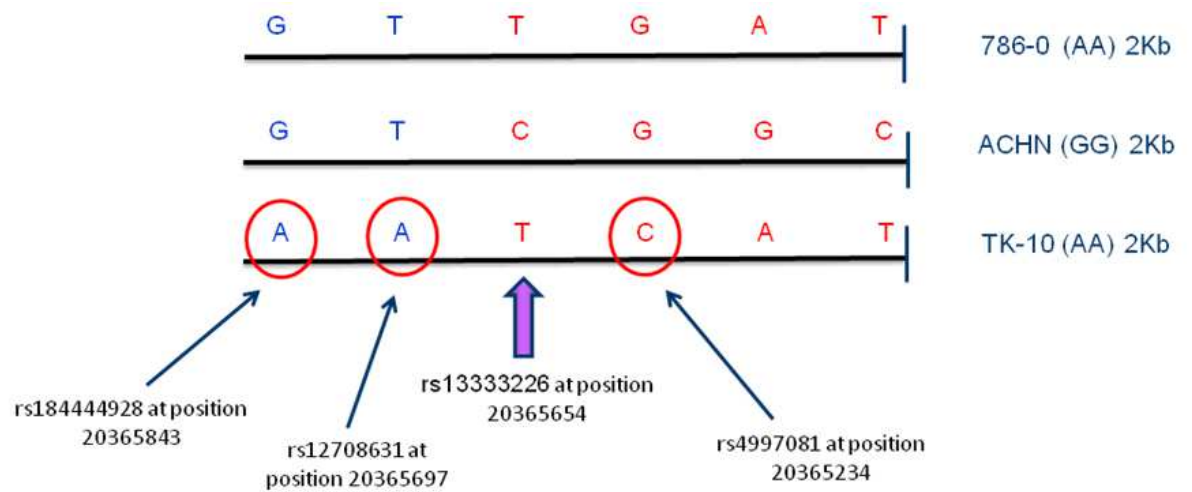
Figure 3-6 Three implicated functional SNPs in the 2 Kb *UMOD* promoter region.

rs4997081, rs12708631, and rs184444928 are implicated as risk alleles associated with altered *UMOD* promoter activity predicted to increase/alter *UMOD* expression levels. The *UMOD* gene is present on the anti sense strand, thus the SNPs presented in this figure are designated from the reverse and complement strand.

3.4.3 Site directed mutagenesis of the 2Kb *UMOD* promoter region

Site directed mutagenesis was performed (section 3.3.5) to assess transcriptional activity of each of the three implicated functional SNPs associated with enhanced *UMOD* promoter activity. The implicated SNPs from the promoter activity assays were introduced into pGL4.10 luciferase vectors by site directed mutagenesis creating three new novel promoter constructs (construct 1, 2, and 3) outlined in **Figure 3-7 (A and B)**. The 2Kb construct of AA genotype for SNP rs13333226 from the cell type 786-0 was used as the 'wild type' construct as this promoter region sequence did not have altered promoter activity during the luciferase assays between the 1 Kb and 2 Kb constructs. Luciferase promoter activities of the wild type (786-0), construct 1 (G to A allele change), construct 2 (T to A allele change), and construct 3 (G to C allele change) were compared by transfection into HeLa, NRK, Hek293, and HK-2 cells (**Figures 3-7 C-F**). Relative promoter activities were measured 24 hours after transfection. The luciferase assays reveal that SNP rs4997081 results in significantly increased promoter activity in HeLa (7.5, 15, and 3 fold change; construct 3 vs. WT, construct 1, and construct 2 respectively ***$p<0.0001$), NRK (20, 4.5, and 3 fold change; construct 3 vs. WT, construct 1, and construct 2 respectively, ***$p<0.0001$), Hek293 cells (10, 7.8, and 1.75 fold change; construct 3 vs. WT, construct 1, and construct 2 respectively, ***$p<0.0001$), and in HK-2 cells (14.4, 4.6, and 4.4 fold change; construct 3 vs. WT, construct 1, and construct 2, ***$p<0.0001$).
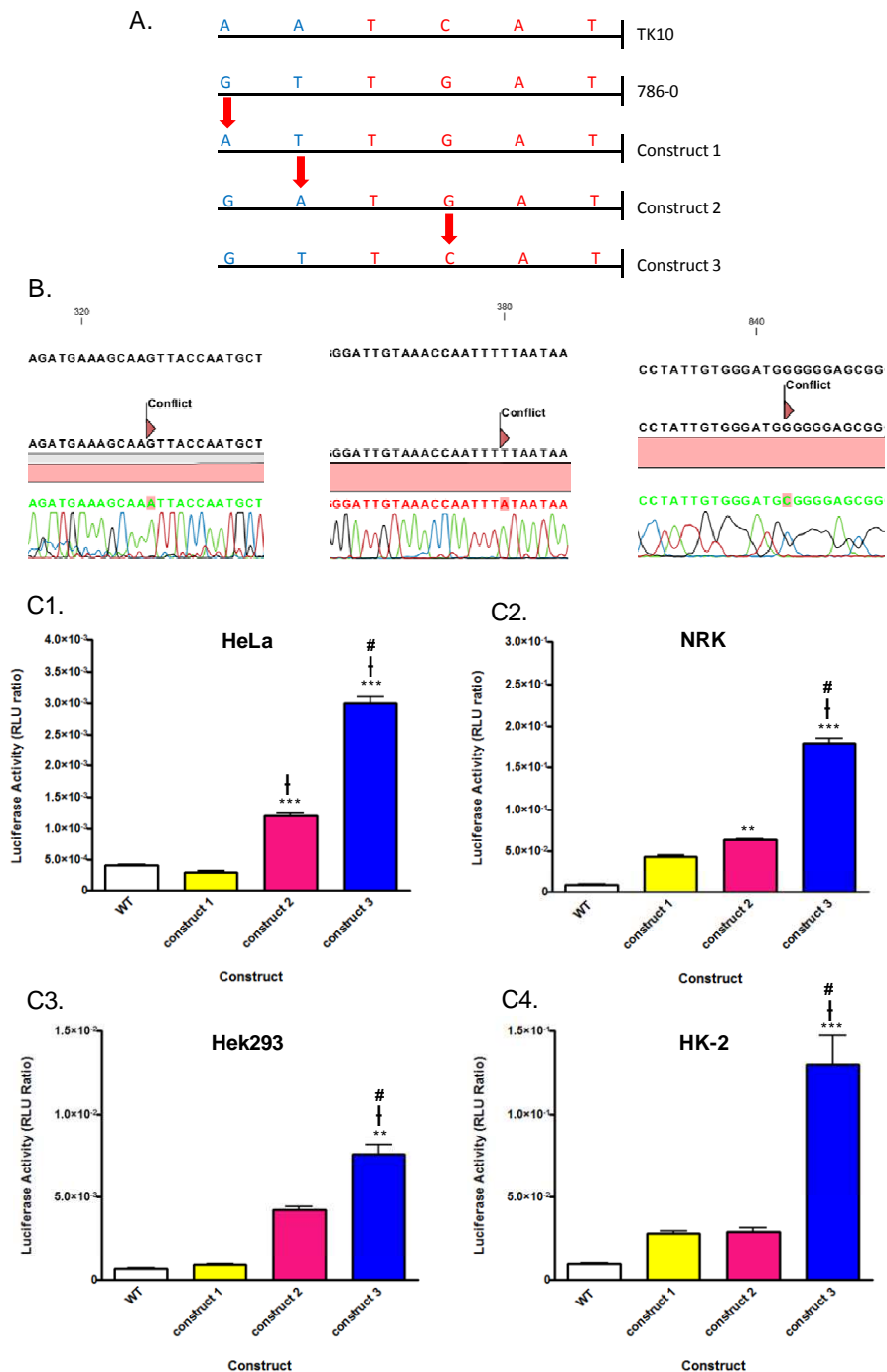
Figure 3-7 Assessment of SNPs rs184444928, rs12708631, and rs4497081 in the 2Kb *UMOD* promoter region.

(A) The schematic outline of the novel promoter constructs derived from site directed mutagenesis. **(B)** Corresponding chromatographs confirming successful site directed mutagenesis (construct 1, 2, and 3 respectively). Comparison of the three implicated SNPs in the 2 Kb promoter construct of TK-10 origin (AA genotype for SNP rs13333226) **(C1)** HeLa, **(C2)** NRK, **(C3)** Hek293, and **(C4)** HK-2 cells (representative graphs). Cells were seeded at 1×10^5 on day one. Transient transfection was performed on day two (1µg total plasmid (1:50 ratio; renilla:DNA)). Luciferase activity assays were performed on day three. Mean ratio ± SEM (normalised to Renilla), one way ANOVA followed by Tukey's post hoc test, n=3 (independent technical replicates), ***$p<0.0001$, **$p<0.001$ (all comparisons against WT construct), ‡$p<0.001$ (construct 2 and 3 vs. construct 1) #$p<0.001$ (construct 3 vs. construct 2). The *UMOD* gene is present on the anti strand the SNPs presented in this figure are designated from the reverse and complement strand.

3.4.4 Transcriptional Element Search Software (TESS) analysis

In Silico analysis of the 2 Kb promoter constructs with TESS software (section 3.3.6), predicted 9 putative transcriptional binding sites for the G allele on the 2 Kb ACHN and 786-0 constructs. Whereas, only 8 were identified for the contrasting C allele on the 2 Kb TK10 promoter construct. Moreover, all 8 predicted transcriptional binding sites were identical for the C and G alleles with one exception, *TFAP2A* (Transcriptional factor also known as AP-2 alpha) suggesting this transcription factor may interact with a specific SNP genotype in the *UMOD* promoter (**Table 3-3**). To date there are no known transcription factor binding sites on *UMOD* promoter SNPs therefore **Figure 3-8** outlines the predicted transcription factor binding sites of rs4997081 dependant on genotype.

3.4.5 Ingenuity pathway analysis (IPA) of *TFAP2A*.

We explored potential connections between *UMOD* and *TFAP2A* using IPA. The exploration for putative transcriptional factor binding elements harboured by the *UMOD* promoter polymorphism (rs4997081), revealed that *TFAP2A* may signal downstream of TNF-a altering *UMOD* expression (**Figure 3-9)**. IPA therefore generated the hypothesis that in the absence of binding of rs4997081 at the C allele to *TFAP2A* may result in altered *UMOD* expression via downstream signalling to TNF-α. **Figure 3-9** suggests a negative feedback loop that regulates *UMOD* expression levels that needs biological follow up.

Table 3-3 Differential putative transcriptional binding sites present in the *UMOD* promoter.

C allele transcription binding sites (TK10)	G allele transcription binding sites (ACHN/786-0)
	AP2-alpha (*TFAP2A*)
Sp1	Sp1
MAZ	MAZ
T-Ag	T-Ag
CTCF	CTCF
GAL4	GAL4
AML1c	AML1c
GCR1	GCR1
GAGA	GAGA

TFAP2A is an additional transcription factor of the G allele of rs4997081 that is absent on the haplotype of contrasting genotype (C allele of rs4997081)
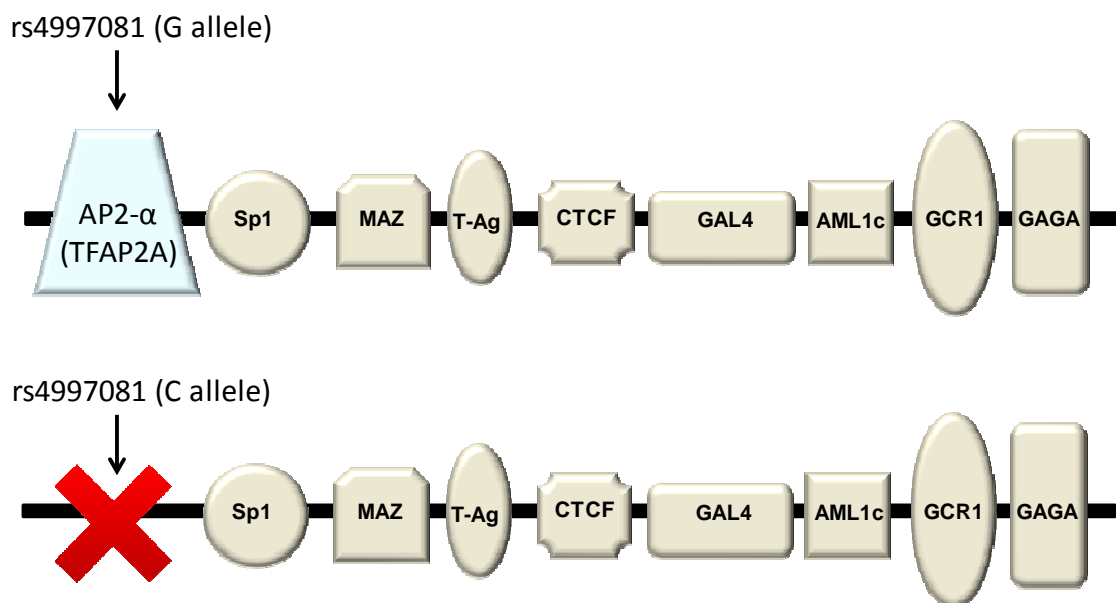
Figure 3-8 Genotype dependant binding of rs4997081 to *TFAP2A*
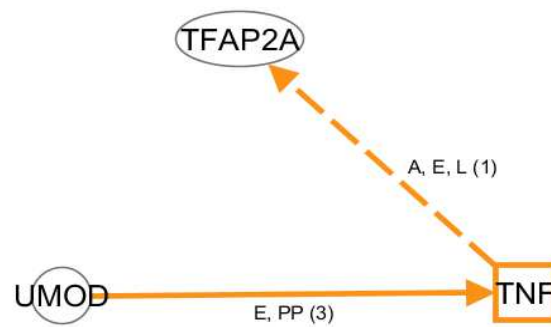
Figure 3-9 Connections of *UMOD* with *TFAP2A*

A simplified signalling network pathway, obtained using IPA systems, represents a suggested molecular association between *UMOD* promoter variation and *TFAP2A* signalling. The signalling network pathway demonstrates a biologically plausible negative feedback loop that alters *UMOD* expression and potential molecular pathways to functionally follow up. The continuous orange line represents direct connections between *UMOD* and TNF-α known in the literature. The dashed orange line represents potential mechanisms demonstrated in the literature. Abbreviations and numbers under the continuous or dashed line represent the relevant publications associated with the pathway.

3.4.6 ChIP assay

As TESS analysis predicted altered putative transcriptional binding to rs4997081 dependant on genotype, potential *TFAP2A* binding to SNP rs4997081 was assessed by ChIP in HeLa cells (positive control), ACHN, 786-0, and TK10 cell lines, all of which endogenously express the transcription factor. The resolution obtained by the ChIP procedure is determined by fragment size of the chromatin sample used as input material. Sonication was optimised and achieved as per section 3.3.7.3. The differences between genomic DNA (from control cells (HeLa) and cell lines of interest (ACHN, 786-0, and TK10), with and without sonication is detailed in **Figure 3-10**.

Following ChIP, no enrichment was observed at approximately 50 kDa in the pull down for TK10 cell types compared with HeLA, ACHN, and 786-0, confirming that the C allele on TK10 cell types is not a direct target for *TFAP2A* binding **(Figure 3-11)**.

ChIP analysis by QPCR confirmed *TFAP2A* binding to SNP rs4998071 on the G allele on HeLa, ACHN, and 786-0 cell types, all of which exhibited significant enrichment compared to an IgG control (% input of enriched chromatin samples are as follows; HeLa; 0.16% vs. 1.52%, $p < 0.001$, ACHN; 0.23% vs. 0.99%, $p < 0.001$, and 768-0; 0.075 vs. 0.53%, $p < 0.01$ (IgG vs. chromatin samples respectively). TK10 was not significantly different from the IgG control (0.29% vs. 0.39%, IgG vs. chromatin sample, $p = 0.5$). All ChIP samples were significantly different from the experimental positive control (HeLa chromatin) **(Figure 3-12)**.

Unsonicated
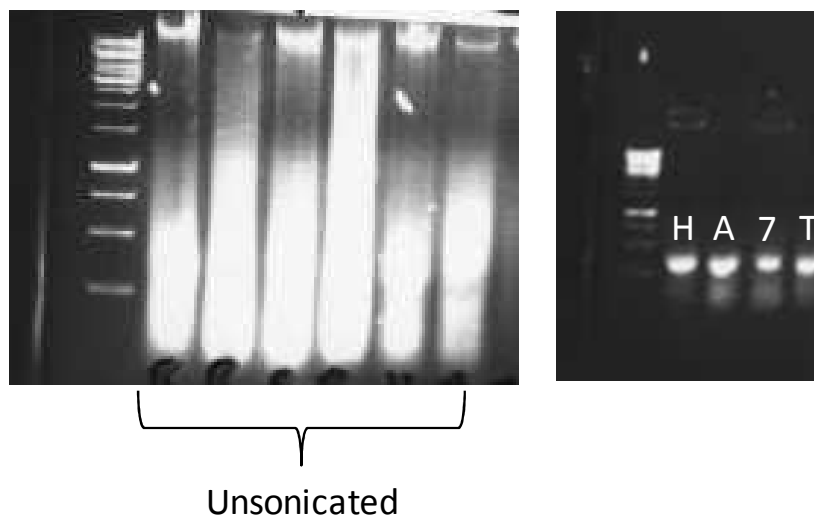
Figure 3-10 Hydrodynamic shearing of Input.

Electrophoresis demonstrates optimal fragmentation following sonication as the bulk of the chromatin has been sheared to a length between 500 and 250 bp (right hand panel, samples denoted as H; HeLa, A; ACHN, 7; 786-0, and T; TK10). To confirm optimum shearing conditions, some samples were not sonicated and whole chromatin electrophoresed (left hand panel), revealing larger chromatin fragment sizes.

A.
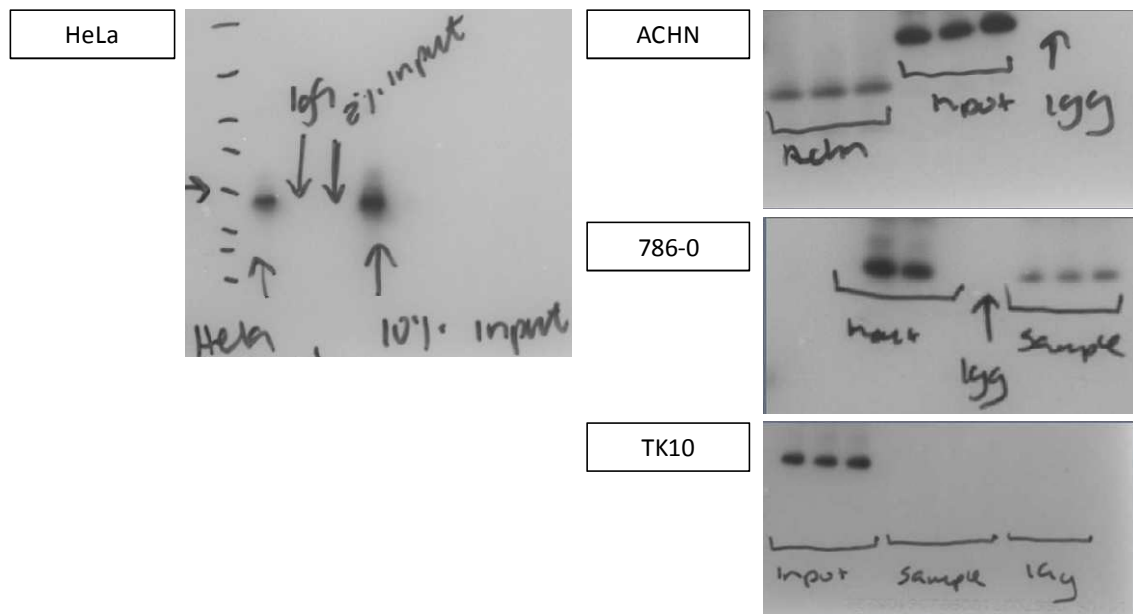
B.
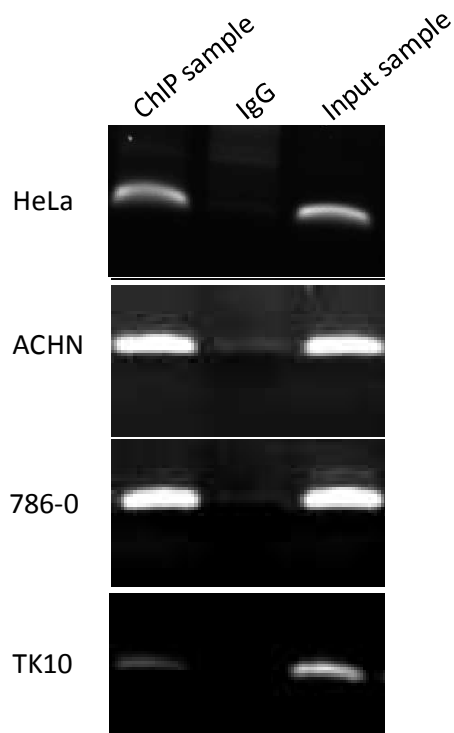
Figure 3-11 Chromatin ImmunoPrecipitation (ChIP) analysis for putative *TFAP2A* binding sites on the 2 Kb *UMOD* promoter SNP rs4997081.

Pre-cleared chromatin from HeLa, ACHN, 786-0, and TK10 cells were immunoprecipitated with either non-specific IgGs or anti-*TFAP2A*. **(A)** Immunoprecipitated DNA or non-immunoprecipitated chromatin samples (input) were tested for enrichment by western blot and **(B)** amplified by PCR using primers designed across the *TFAP2A* potential binding site at SNP rs4997081. Both methods confirm enrichment of *TFAP2A* in HeLa, ACHN, and 786-0 cell types. TK10 cells do not show enrichment for *TFAP2A* at position 16:20365234.
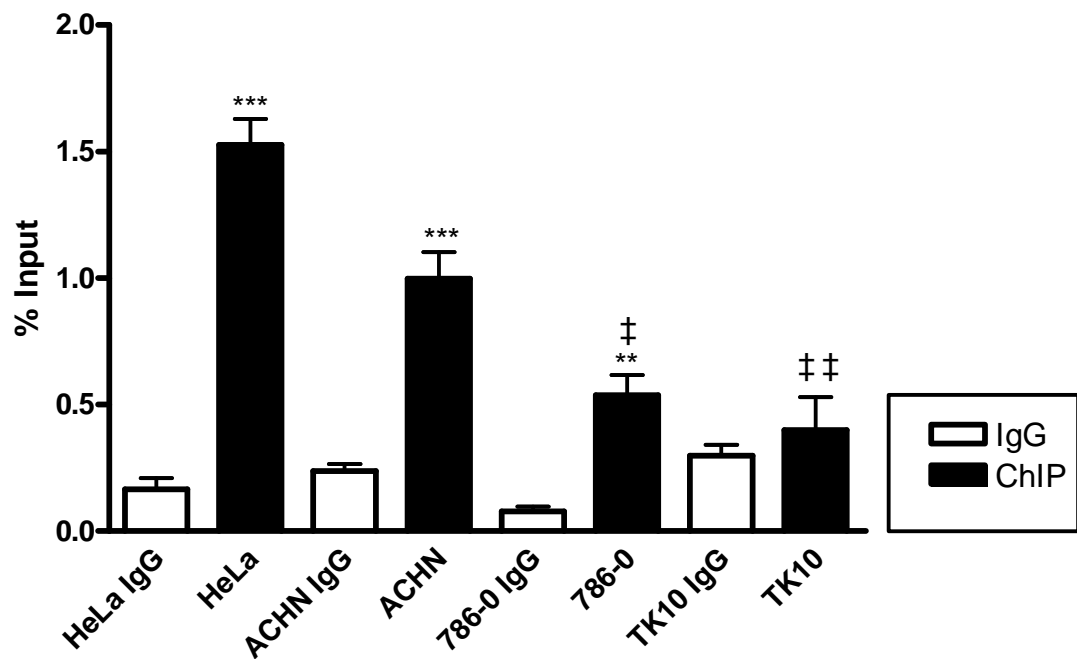
Figure 3-12 *In vitro* **validation of** *TFAP2A* **as a potential regulator of** *UMOD* **promoter activity.**

Immunoprecipitation of chromatin from HeLa, ACHN, 786-0, and TK10 revealed enrichment of *TFAP2A* on the *UMOD* promoter only at position 16:20365234 on the G allele, the C haplotype does not display binding to the transcription factor (Data represent the mean of three biological replicates expressed as % input ± SEM). ChIP chromatin vs. IgG ***p<0.001, **p<0.001. HeLa chromatin vs. ACHN, 786-0, and TK10 chromatin ‡p<0.05, ‡ ‡p<0.001.

3.4.7 Optimisation of siRNA Transfection in HeLa cells

Prior to assessing *TFAP2A* binding on promoter activity, optimisation of endogenous knock down of the transcription factor with siRNA was performed as per section 3.3.8. Suitability of the transfection conditions for siRNA delivery to ACHN, 786-0, and TK10 cells was assessed using a positive control siRNA targeted against *GAPDH* and a negative control of Cy3^{TM} labelled siRNA. Following transfection of the pGL4.10 luciferase plasmid and siRNA, RNA was isolated; and subsequent *TFAP2A* and *GAPDH* mRNA levels measured. Cy3^{TM} labelled siRNA transfection at a range of 0-100 nM concentrations had no effect on *TFAP2A* mRNA expression levels in ACHN (7.4%), 786-0 (7.7%), or TK10 (5.3%) cell types (average % change over the range of concentration doses compared to non treated cells) (**Figure 3-13**). GAPDH-specific siRNA transfection at a final concentration of 100 nM resulted in efficient (>60 %) knock down of *GAPDH* in all cell types compared with non treated cells (ACHN; 62 %, 786-0; 64 %, and TK10; 63.3 % knockdown) (**Figure 3-14**). Similarly, TFAP2A-specific siRNA transfection resulted in an efficient knock down of *TFAP2A* mRNA levels at a final concentration of 50 nM in all cell types compared to the non treated cells (ACHN; 61 %, 786-0; 59 %, and TK10; 59 % knockdown) (**Figure 3-15).**

(A) *TFAP2A* mRNA

(B) *TFAP2A* mRNA

(C) *TFAP2A* mRNA
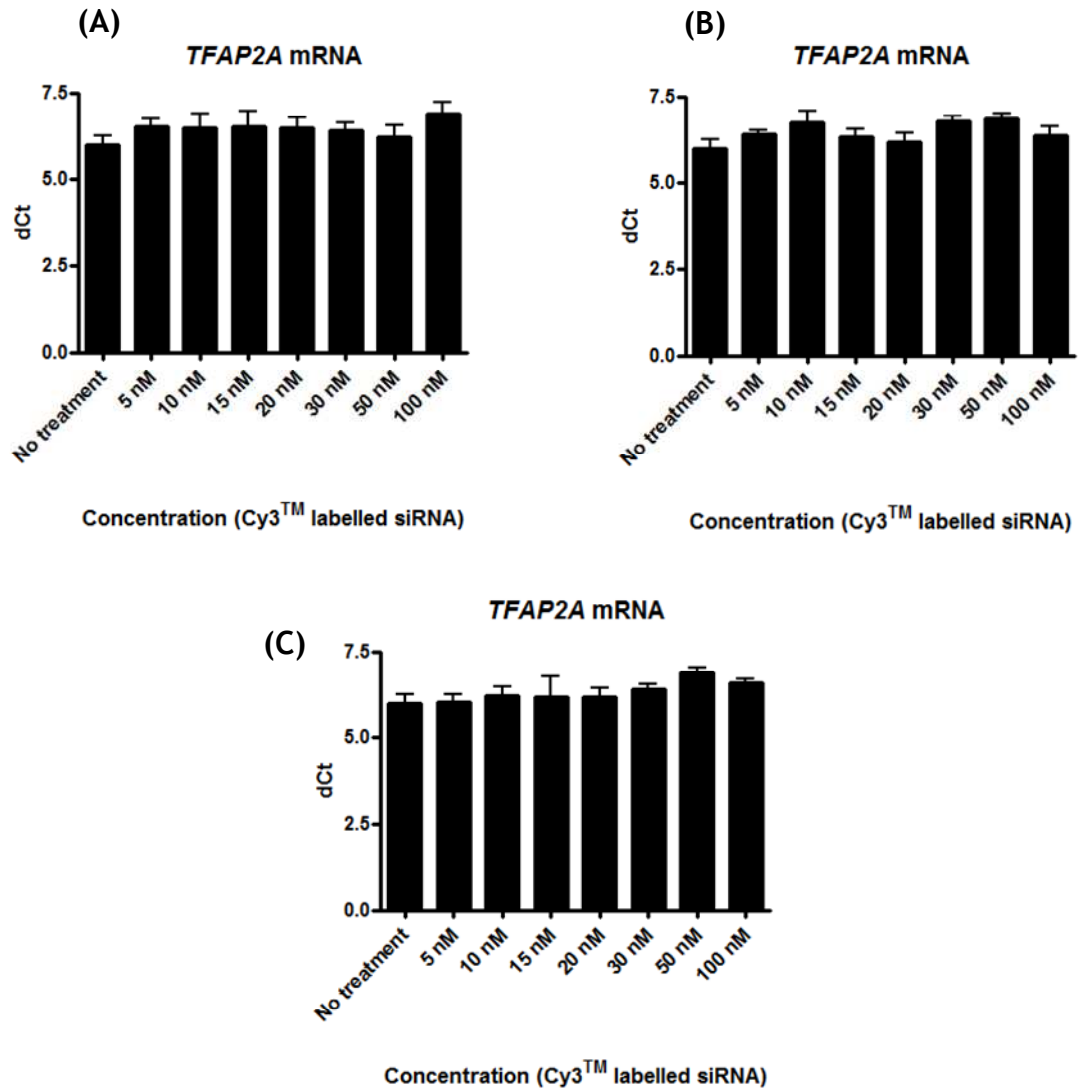
Figure 3-13 Cy3™ labelled transient transfection optimisation into HeLa cells containing human 2Kb *UMOD* promoter constructs.

(A) HeLa cells containing the 2 Kb ACHN plasmid, **(B)** HeLa cells containing the 2 Kb 786-0 plasmid, or **(C)** HeLa cells containing the 2 Kb TK10 plasmids were transfected with a scrambled negative control siRNA (Cy3™ labelled) (final concentration range of 0-100 nM). *TFAP2A* mRNA was analysed 24 hours post transfection by qRT-PCR. Cycle threshold values were normalised to the cycle threshold of β-actin mRNA giving rise to the delta cycle threshold (dCt) where increasing dCt represents reduced expression. The mean of three independent biological experiments performed in triplicate, error bars represent SEM. Each condition of increasing concentration of siRNA was analysed against the non treated cells using a Student's T-Test where $p < 0.05$ was considered significant.
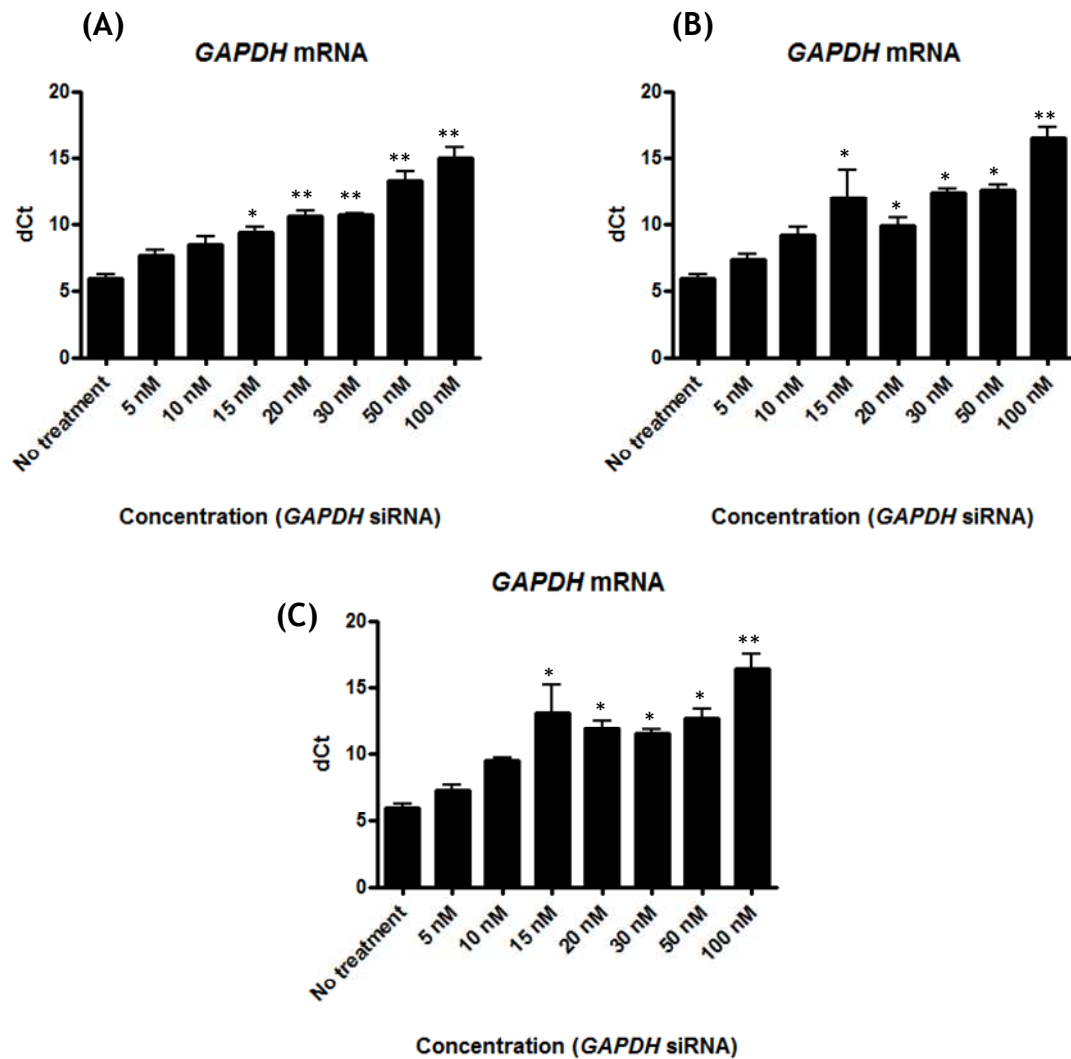
Figure 3-14 *GAPDH*-specific siRNA transient transfection optimisation into HeLa cells containing human 2Kb *UMOD* promoter constructs.

(A) HeLa cells containing the 2 Kb ACHN plasmid, **(B)** HeLa cells containing the 2 Kb 786-0 plasmid, or **(C)** HeLa cells containing the 2 Kb TK10 plasmid were transfected with a GAPDH-specific siRNA positive control siRNA (final concentration range of 0-100 nM). *TFAP2A* mRNA was analysed 24 hours post transfection by qRT-PCR. Cycle threshold values were normalised to the cycle threshold of β-actin mRNA giving rise to the delta cycle threshold (dCt) where increasing dCt represents reduced expression. The mean of three independent biological experiments performed in triplicate, error bars represent SEM. *p<0.01, **p<0.001 compared to non treated cells using a Student's T-Test where p<0.05 was considered significant.
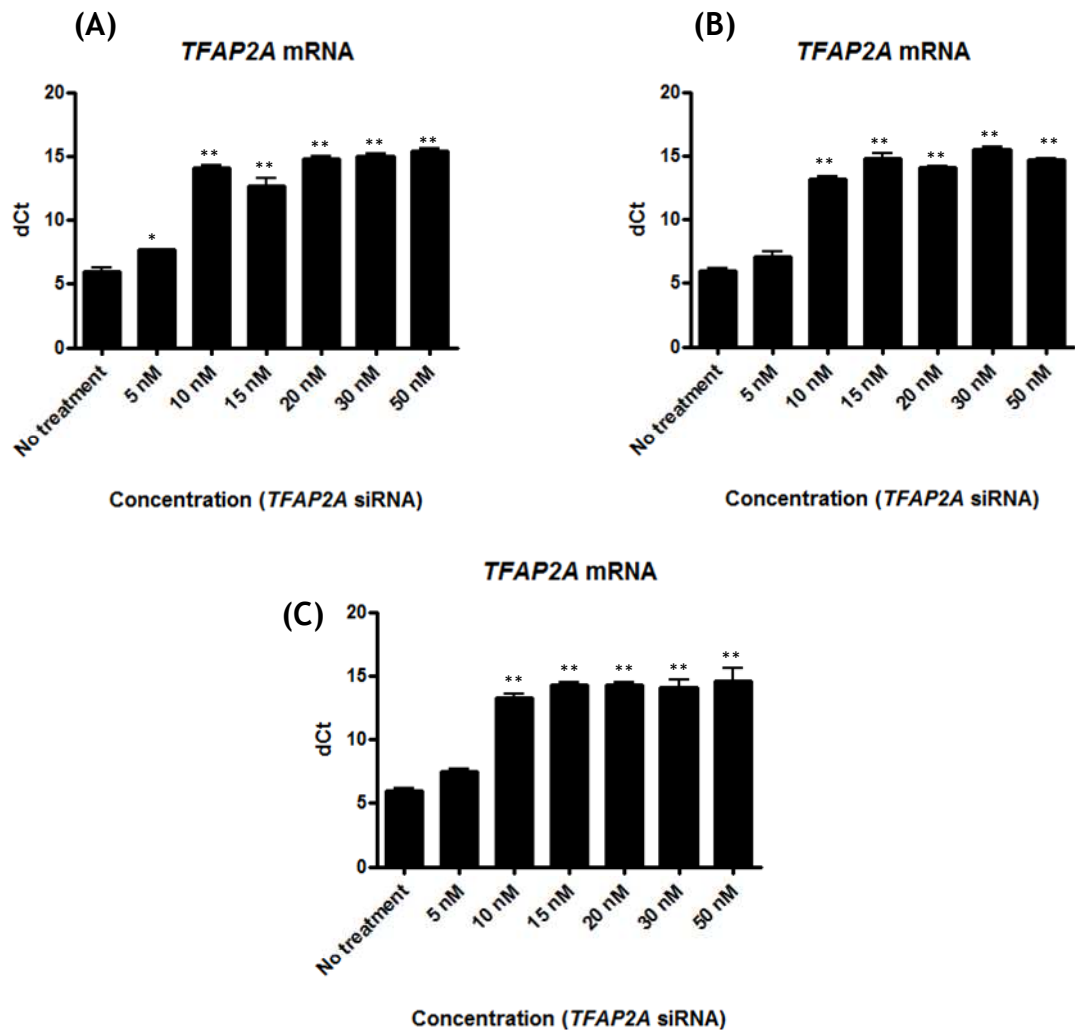
Figure 3-15 Transient transfection of *TFPA2A*-specific siRNA into HeLa cells containing human 2Kb *UMOD* promoter constructs.

(A) HeLa cells containing the 2 Kb ACHN plasmid, **(B)** HeLa cells containing the 2 Kb 786-0 plasmid, or **(C)** HeLa cells containing the 2 Kb TK10 plasmid were transfected with a *TFAP2A*-specific siRNA (final concentration range of 0-100 nM). *TFAP2A* mRNA was analysed 24 hours post transfection by qRT-PCR. Cycle threshold values were normalised to the cycle threshold of β-actin mRNA giving rise to the delta cycle threshold (dCt) where increasing dCt represents reduced expression. Transfection with 100 nM concentrations of TFAP2A-specific siRNA resulted in undetermined ct values by QRT-PCR. The mean of three independent biological experiments performed in triplicate, error bars represent SEM. *$p<0.01$, **$p<0.001$ compared to non treated cells using a Student's T-Test where $p<0.05$ was considered significant.

3.5 *UMOD* Promoter activity following knockdown of *TFAP2A*

Following transient *TFAP2A* silencing, functional validation of potential transcription factor binding to SNP rs4997081 was assessed. Transfection of Cy3^{TM} labelled siRNA had no effect on the increased promoter activity of the TK10 construct (14 and 12 fold increased compared to ACHN and 786-0 respectively, ***p<0.0001) **(Figure 3-16)**. Conversely, the increased reporter activity of the TK10 construct was repressed by 12 fold in the absence of *TFAP2A* **(Figure 3-16)**.
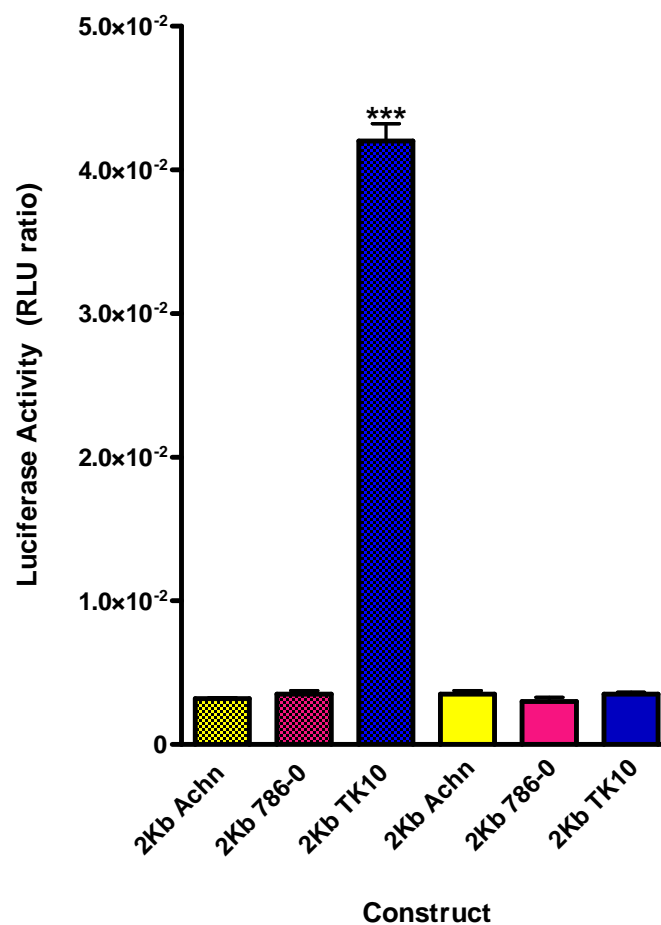
Figure 3-16 Promoter activity following knockdown of *TFAP2A*

Cy3 labelled transfection did not alter promoter activity of the 2 Kb TK10 construct (shaded bars). Silencing of *TFAP2A* in HeLa cells (transfection with the 2 Kb *UMOD* promoter sequences of contrasting genotype for rs13333226 (ACHN, 786-0, or TK10)), reduced reporter activity of the 2 Kb TK10 promoter construct, suggesting indirect effects of binding or inefficient binding to SNP rs4997081 on promoter activity. Three independent experiments were performed and the representative graphs are shown. Mean ratio ± SEM (normalised to Renilla), one way ANOVA followed by Tukey's post hoc, n=3 (independent technical replicates), ***p<0.0001.

3.6 Discussion

The experiments conducted in this chapter combined the use of experimental and computational analysis to determine causal variants within the 2 Kb promoter (*cis-acting*) region of the human *UMOD* gene. Sequencing the 2 Kb *UMOD* promoter confirmed 3 previously identified SNPs in LD with rs13333226 (rs4293393, rs28362063, and rs4997081) and 2 SNPs not in LD (rs12708631 and rs184444928). SNPs rs4293393 and rs28362063 have formerly been examined in association with kidney disease and hypertension (Gudbjartsson et al., 2010, Kottgen et al., 2010), but to date the SNPs rs4997081, rs12708631, and rs184444928 have not been investigated in relation to hypertension, prompting the investigation in this study of rs13333226 associated *UMOD* haplotypes.

Promoter studies herein demonstrate that the 2 Kb *UMOD* promoter locus around rs13333226 is associated with altered promoter activity. From the haplotypes studied, it is clear that rs13333226 is not a causative SNP directly affecting function and does not account for observed difference in promoter activity. Increased promoter activity was identified in the 2 Kb TK10 construct of AA genotype for rs13333226. The promoter activity assay results in this chapter demonstrate the minor G allele of rs13333226 is associated with reduced transcript activity, consistent with findings from the GWAS, BRIGHT and HERCULES cohorts where this haplotype is associated with lower UMOD excretion and lower risk of hypertension (Padmanabhan et al., 2010). It is not an unusual finding that functionally implicated SNPs are not the casual variants. Previous studies have re-sequenced candidate genes identified by GWAS to identify rare genetic variants of potentially stronger association with phenotype than trait-associated variants (Palmer and Cardon, 2005) and found that the increased GWAS signal was accounted for by SNPs in LD with the original implicated variants (Kottgen et al., 2012). Accordingly, this study required to consider whether rs13333226 is directly functional (i.e. could lead to the observed biology) or is it indirectly associated with other DNA sequence variants (LD SNPs) in the *UMOD* promoter.

Site directed mutagenesis was performed to test the hypothesis that SNPs in LD with rs13333226 may be the casual variants associated with changes in promoter activity. The results implicated the minor C allele of SNP rs4997081 as

responsible for increasing transcriptional activity since additional implicated SNPs not in LD with rs13333226 did not alter promoter activity. To investigate this finding further, Transfac matrices were generated to list potential TF binding sites lost, created or affected by the C allele polymorphism of rs4997081. The Transfac analysis protocol used here demonstrated that the C allele of rs4997081 (2 Kb TK10 construct) has one less predicted putative TF binding site to that of the contrasting G allele (2 Kb ACHN construct). Nine predicted TF sites were linked with the G allele whereas only 8 were predicted to bind with the C allele; furthermore, the predicted TF sites were identical between the genotypes with the exclusion of *TFAP2A* on the C allele.

TFAP2A is a transcription factor that can positively or negatively regulate the promoter activity of many genes involved in physiological and pathological processes such as development, cell growth, differentiation, proliferation, tumorigenesis, and apoptosis but is predominantly associated with pro-inflammatory genes (Hilger-Eversheim et al., 2000, Orso et al., 2010) and G protein coupled receptors (Salanga et al., 2009). In the kidney, inflammatory G protein coupled receptors such as prostaglandin E_2 (PGE_2) predominate in the TAL and are activated by cyclooxygenase (COX) causing reduced NaCl reabsorption, and promotes natriuresis and diuresis (Breyer and Breyer, 2001). Ferreri and colleagues (Battula et al., 2012) reported that the COX2 mediated PGE_2 synthesis in the TAL is constitutively produced by increased TNF-α expression which consequentially inhibits NKCC2 activity and Na^+ reabsorption. *In vivo*, TNF-α infusion causes decreased GFR with increased fractional excretion of sodium, supporting previous studies that suggest the pro-inflammatory cytokine has natriuretic and diuretic actions at the TAL (Shahid et al., 2008a). There is evidence in the literature to suggest TNF-α signals downstream of *TFAP2A* exerting inflammatory events. Immunohistochemical examination of invasive breast cancer tissue indicated that *TFAP2A* acted as a tumor suppressor gene by inhibiting TNF-α induced inflammation and apoptosis (Gee et al., 1999), whereas Nyormoi *et al* reported more recently that TNF-α downregulates *TFAP2A* post transcriptionally by cleavage degradation during TNF-α induced inflammation (Nyormoi et al., 2001). *TFAP2A* was also shown to be differentially expressed in blood samples from pregnant patients with pre-term delivery caused by mechanisms of COX2 and TNF-α signalling (Enquobahrie et al., 2009). Thus,

despite conflicting results from published work there is evidence of a functional link between *TFAP2A* and TNF-α in inflammatory pathways that may be linked with enhanced natriuresis.

The functional relationship of *TFAP2A* and TNF-α was also predicted in the current study by the pathway analysis software, where IPA revealed a possible negative feedback loop regulated by *UMOD* expression levels. As introduced in section 1.10.1.1 identification of GPI anchored enriched endocytic compartments have lead to the discovery that *UMOD* exerts its immunosuppressive affects by binding with high affinity to TNF-α. It is recognised that cytokine excretion is predominantly via the kidney and augmented levels of TNF-α at the TAL decrease Na^+ and Cl^- reabsorption (Escalante et al., 1994), suggesting the interaction between UMOD and cytokines may be critical in promoting clearance of TNF-α to maintain sodium regulation. There have been no direct links between Na^+ reabsorption and *TFAP2A* published to date, however, *TFAP2A* is found in kidney tissue acting as a tumour suppressor (Dalgin et al., 2008) where it could be hypothesised as having functional roles in ion regulation. This hypothesis suggests variants in the *UMOD* promoter may give rise to altered or inhibitory effects on inflammatory cytokines suggesting a feedback loop involving *TFAP2A* binding and TNF-α signalling, affecting sodium transport. To examine this hypothesis a number of future functional studies are required to be undertaken to investigate if in the absence of binding of *TFAP2A* to the C allele leads to loss of function of native UMOD; or does it lead to gain of harmful functions of UMOD ?

In the meantime and in attempt to address the functional consequences of *TFAP2A* binding on genetic control of transcription was assessed. Results illustrated by ChIP confirmed the absence of *TFAP2A* binding to the C allele, as lack of enrichment was evident in western blot analysis. This absence was consolidated further by experimental validation and quantification using QPCR, where enrichment was approximately 3.4 fold higher on the G allele of rs4998071 in ACHN cell types. To examine the enrichment functionally, transient transfection of siRNA to knock down expression of *TFAP2A* was performed and promoter activity re-assessed. It was expected that in the absence of *TFAP2A* binding to the C allele of rs4997081 (2 Kb TK10 construct) the knock down of the TF would have no effect on promoter activity of this haplotype and the

contrasting G allele haplotype (2 Kb ACHN and 786-0 constructs) would display increased promoter activity. Conversely, results here demonstrated reduced promoter activity of the C allele with no effect on the contrasting G allele.

There are a number of reasons that may explain this finding: *TFAP2A* may not in fact be causing transcriptional changes to *UMOD* gene expression resulting in altered promoter activity, there may be indirect binding or inefficient binding to rs4997081 at the C allele driving enhanced promoter activity. Furthermore, there are SNPs in LD with rs13333226 and rs4997081 that extend beyond the 2 Kb region of the *UMOD* promoter, as a result future work should focus on investigating additional variants in promoter region. In addition, the initial putative TF binding predictions were based on *in silico* methods, which have been known to result in false positives. Nonetheless, in this chapter the ChIP analysis was consistent with *in silico* analysis in that *TFAP2A* did not bind to the C allele of rs4997081. Future work should focus on the other putative predicted TF binding sites of rs4997081 starting with those implicated with TESS software, as should SNPs in LD with rs13333226 in the 3 Kb promoter region as this promoter region has been shown to drive kidney specific function of *UMOD* (Zhu et al., 2002).

Taken together the data demonstrates that the index SNP (rs13333226) is not a functional variant causing altered transcription, however the minor G allele of rs13333226 is associated with reduced promoter activity, consistent with the original GWAS study that this allele is associated with lower risk of hypertension. The evidence suggests that the C allele of rs4997081 leads to increased transcriptional activity and is a causal variant to follow up. *TFAP2A* was predicted and confirmed to be a putative TF binding site for the G allele of rs4497081. The increased promoter activity on the C allele of rs4997081 cannot be explained by the absence of *TFAP2A* binding as knockdown of the TF reduced promoter activity of the C allele and not the G allele as would have first been expected. However, this does not mean that the absent binding of *TFAP2A* to the C allele of rs4997081 is not involved in altered gene transcription because transient knockdown did result in reduced promoter activity of the C allele suggesting indirect effects of binding at the G allele on transcriptional activity. The subsequent chapters now consider the physiological role of UMOD in BP regulation and sodium homeostasis to elucidate the mechanisms of altered *UMOD* expression.

4 Cardiovascular Phenotype of the *UMOD+/+* and *UMOD-/-* mice

4.1 Introduction

The role of UMOD has remained elusive for many years, although recent studies are now reporting its intra and extra cellular functions. The former being related to urinary concentrating mechanisms which disturb transcellullar electrolyte transport (Bachmann et al., 2005, Malagolini et al., 1997) whereas; the latter have been linked with anti-inflammatory properties of the glycoprotein (Bates et al., 2004, Mo et al., 2004, Schroter et al., 1993, Dahan et al., 2003). Insight into the proposed physiological roles of *UMOD* has been evaluated using *UMOD-/-* (KO) mice models, established independently by two groups. Bates *et al* (Bates et al., 2004) obtained successful knockout of *UMOD* by deletion of the first four exons, intervening first intron, and the 3 Kb gene promoter region. Whereas, Mo *et al* (Mo et al., 2004) deleted the first four exons and the 650 bp of the promoter region, both KO methods resulted in ablation of the transcriptional activity of the gene. To date there are no reported phenotypic differences between the two independently generated *UMOD* KO strains.

Reports from these groups detail that *UMOD* deficiency predisposes knockout mice to frequent urinary tract infections and bladder colonization by type-1 fimbrated *E coli*, demonstrating that *UMOD* acts as a general host defence factor against infection (Raffi et al., 2005, Raffi et al., 2009). It has also been shown that the KO mice spontaneously formed calcium oxalate stones primarily in the collecting duct and papillary regions (Mo et al., 2004) and display kidney injury due to increased levels of the pro-inflammatory cytokine TNF-α. This injury was accompanied by altered tubular expression of Toll like receptor 4 (El-Achkar et al., 2008), reinforcing the findings of extracellular functions of UMOD.

In terms of intracellular roles of UMOD, steady state electrolyte handling in the KO mice is similar to the WT counterparts, however in terms of renal function; creatinine clearance has been shown to be significantly reduced in KO mice with urine concentration ability being impaired under water deprivation (Bachmann et al., 2005). The TAL is responsible for reabsorbing approximately 25% of filtered NaCl and plays an essential role in the generation of the medullary interstitial hyperosmolality. It has been suggested that UMOD could participate in the water impermeability at the TAL (Serafini-Cessi et al., 2003), accordingly a failure of this feature in KO mice would reduce NaCl reabsorption, decrease

the interstitial osmolality, and impair the urine concentrating ability potentially explaining manifestation of monogenic diseases that cause changes in BP. Intracellular examination of *UMOD* deficient mice did indeed show impaired urinary concentrating ability; with increased expression of the thiazide sensitive NaCl channel (NCC) in the distal convoluted tubule, suggesting a compensatory adaptation for putatively insufficient NaCl reabsorption in the TAL (Bachmann et al., 2005, Abdallah et al., 2001, Wagner et al., 2008). Biochemical and histological analysis has been used to assess changes in biosynthesis of proteins related to NaCl transport along the nephron in *UMOD* KO mice. Bachmann *et al* revealed upregulation of major distal transporters (Na^+/K^+ -ATPase, NKCC2, NHE3, ROMK, and ENaC) and downregulation of juxtaglomerular apparatus components (Bachmann et al., 2005). Further studies by this group, reported that the augmented total NKCC2 expression was in fact as a result of increased intracellular expression of NKCC2, where it remained unphosphorylated and inactive in *UMOD-/-* mice (Mutig et al., 2011b). This group also reported that in the absence of *UMOD* the reduced NKCC2 activity results in impaired NaCl reabsorption at the TAL, implying the permissive role of UMOD in the modulation of Na^+ transport.

Data collected thus far from *UMOD-/-* mice conclusively document the absence of any of the morphological defects observed in humans with UMOD associated kidney disease (UAKD). It seems a reasonable hypothesis that the physiological consequences of UAKD outlined in section 1.10.1.5, are a direct result of an altered in UMOD function at the TAL (Dahan et al., 2003, Rampoldi et al., 2003). Reports from the KO mice so far support the idea that absent or altered *UMOD* expression and function may be the pathological cause of altered ion transport contributing to hypertension. However, lack of cardiovascular characterisation and evidence of Na^+ handling and transport studies in the *UMOD -/-* mice, the functional role of UMOD in blood pressure control and sodium homeostasis still remains elusive. The potential impact UMOD has on the ability to reabsorb NaCl at the TAL and the important role of pressure natriuresis on blood pressure control is investigated in this chapter in WT and KO mice to follow up the hypertension signal identified in the GWAS study (Padmanabhan et al., 2010). It is hypothesised that cardiovascular characterisation studies in the *UMOD* KO mice will demonstrate an altered cardiovascular phenotype.

4.2 Aims

- To assess hemodynamic parameters in the WT and KO mice under basal conditions and following cardiovascular stimulation with 2% NaCl.

- Assessment of sodium balance and ion regulation in the WT and KO mice under basal and 2% NaCl loading.

- Assessment of renal function in the WT and KO mice under basal conditions and following stimulation with 2% NaCl.

4.3 Methods

4.3.1 Experimental Animals

Experimental animals used in this project were produced by Bates *et al* as per section 2.9 (Bates et al., 2004). The strains used here were WT and KO where the knock out was confirmed with end point PCR (section 2.9). Throughout this chapter male mice of 12 weeks of age of were used for all procedures with the exception of tail cuff plethysmography where animals of 11 weeks of age onwards were studied. All mice used for experimental procedure were housed in individual cages in a temperature controlled room (24 ± 1 ^{o}C) at a constant humidity of 60 % (± 5 %), with light cycles from 6 AM to 6 PM. All mice were allowed access ad libitum to standard rodent chow (rat and mouse No.1 maintenance diet, Special Diet Services) and normal tap water (normal salt). All procedures were performed in accordance with Animals (Scientific procedures) Act, 1986 and under the project licences held by Dr Delyth Graham (University of Glasgow, UK) (project license number 60/4286).

4.3.2 Salt Challenge

Male mice of both strains (WT and KO) were utilised at 12 weeks of age for salt loading studies. Mice were housed and maintained as above. Each strain was then grouped into either normal salt or high salt, giving rise to the following 4 groups: WT normal salt, WT +2% NaCl, KO normal salt, and KO +2% NaCl. Animals received (ad libitum) either normal tap water or 2% NaCl in the drinking water for a six week period. Normal tap water was used to prepare 2% NaCl (w/v).

4.3.3 Hemodynamic parameters

4.3.3.1 Tail cuff plethysmography

Tail cuff plethysmography technology is outlined in section 2.10.1. Male mice of 11 weeks were studied over a 7 week period, week zero was performed as a training period for the animals to become familiarised with the procedure. The training period was used to reduce stress limiting factors by familiarising the mice with handling and pre-warming for vasodilatation. Data obtained in this period was not used in any statistical analysis. During the training week animals

were exposed to the procedure on 5 consecutive days. At week one, the mice were 12 weeks of age and the pressure recordings from the plethysmography procedure were now included. Salt loading also began on week one. On the day of procedure mice were pre-warmed to 32-35°C and maintained at this temperature throughout with heat mats. Mice were wrapped in a muslin cloth to restrain them during pressure recordings. For each animal averages of 10 inflation/deflation cycles were conducted to obtain mean SBP. The procedure was performed over three consecutive days which represented one week of data and repeated the same days every week and at the same time of the day, until the study was completed.

4.3.3.2 Radiotelemetry

Male mice of 12 weeks of age (both WT and KO) were implanted with radiotelemetry probes to monitor hemodynamic parameters directly; the surgical procedure is outlined in section 2.10.2. Following the surgical procedure and once mice had regained consciousness, they were returned to individual cages and allowed one week recovery period before initiation of recording. The first BP study was termed "baseline" where hemodynamic parameters were monitored in WT and KO mice under normal salt conditions (n=6 per group). The baseline measurements were recorded over a 21 day period with cycles of scheduled sampling every 5 minutes over a 24 hour period. Averages of daytime (7:00 am – 7:00 pm) and night time (7:00 pm - 7:00 am) BP were recorded and data points displayed as daytime/night time averages. The second BP study was performed over a six week period where WT and KO (n= 8 per group) were subjected to cardiovascular stimulation with 2% NaCl in the drinking water and was termed "salt loaded". Data here were generated from three consecutive daytime and night time averages and data points were represented as weekly daytime and night time averages. As the battery life of the radiotelemetry probes do not extend beyond 26 days, it is not possible to carry out a longitudinal continuous (real time) study for six weeks; therefore, probes were switched on for 3 full 24 hour cycles then off for the remainder of the week. This is the accepted way of showing long- term data with mouse telemetry (Carlson and Wyss, 2000, Zhao et al., 2011). This method was consistent with the tail cuff studies as BP was measured in the mice on three consecutive days each

week. Statistical analysis of radiotelemetry was performed using repeated measures ANOVA.

4.3.4 Renal Function

Renal function was assessed in WT and KO mice ± 2% NaCl at the end of the 6 week study by means of metabolic cage measurements, creatinine clearance, and electrolyte analysis as outlined in sections 2.11.1, 2.11.2, and 2.11.3. Mice were placed in the metabolic cages for a 24 hour period, where fluid intake was monitored and urine was collected. Mice were individually placed in the metabolic cages for the 24 hour period.

4.3.5 Ex *vivo* analysis

At the end of the 6 week study all mice were of 18 weeks of age. The procedure was terminated as per section 2.12.1. Tissues were removed, cleaned of any connective tissue, and prepared for analysis. Body weight, kidney weight, and tibia length were recorded. All tissue weights were normalised to tibia length. *Ex vivo* investigation including; histological investigation, metabolic analysis, and microarray mRNA expression analysis which are detailed in section 2.12.

4.3.6 Generalised Estimation Equation regression analysis (GEE)

Generalised estimating equations (GEE) were used in this project to analyse longitudinal correlated response data in WT and KO mice following six weeks ± 2% NaCl loading. The variables used in this study were; the correlation of SBP (mmHg) with, fluid intake (µl/24h), urine output (µl/24h), and electrolyte analysis (Na^+, K^+, and Cl^- µmol/24h) in both mouse strains (± 2% NaCl). The main function of GEE analysis is to estimate the population averaged mean effect and the estimation of inferences of the regression coefficients in the model. In GEE models, the estimated regression coefficient represents the effect of the explanatory variables (SBP, fluid intake, urine output) on the population average effect of the response variables (electrolyte excretion). GEE describes the change in population mean given the changes in covariates after accounting for correlation between observations. The GEE regression co-efficient (β co-efficient) is interpreted as change in mean outcome for a unit change of the

exposure in the entire population derived from General Linear Model statistical analysis (GLM), where p<0.05 is considered significant.

4.4 Results

4.4.1 Cardiovascular phenotype (baseline blood pressure)

Hemodynamic parameters were firstly, investigated in WT (*UMOD+/+*) and KO (*UMOD-/-*) mice under basal conditions using radiotelemetry (as described in section 4.3.3.2). Baseline hemodynamic parameters were measured over a three week period as daytime and night time daily averages, in male mice of 12 weeks of age in WT and KO strains (**Figure 4-1**). KO mice have significantly lower daily averaged day and night time systolic blood pressure (SBP) than WT counterparts under normal salt conditions (116.6 ± 0.3 mmHg vs. 136.2 ± 0.4 mmHg; KO vs. WT respectively, n=6 per group, *** $p<0.0001$ **(Figure 4-1 A)**. However, daily averaged day and night time diastolic blood pressure (DBP) were not significantly different between the two strains (115 ± 1.4 mmHg vs. 113.7 ± 1.6 mmHg) (WT vs. KO) n=6 per group, $p=0.34$ **(Figure 4-1 B)**. KO mice had significantly lower daily averaged daytime and night time mean arterial pressure (MAP) compared to the WT counterpart (125.5 ± 5.2 mmHg vs. 115.1 ± 5.7 mmHg, KO vs. WT respectively), n=6 per group, **$p<0.001$ **(Figure 4-1 C)**. Daily averaged daytime and night time pulse pressure (21.9 ± 0.5 vs. 9.4 ± 0.2) (WT vs. KO) and heart rate (553.2 ± 5.2 bpm vs. 485.8 ± 2.5 bpm) (WT vs. KO) were also significantly different between the strains; n=6 per group, ***$p<0.0001$ **(Figure 4-1 D and E)**. Although, activity levels were not different between WT and KO mice (3.9 ± 0.2 vs. 3.7 ± 0.6, WT vs. KO respectively) n=6 per group, $p=0.49$ **(Figure 4-1 F)**. Week one is a recovery period from the surgical procedure and was not included in the statistical analysis.

4.4.2 Cardiovascular stimulation with 2% NaCl (Indirect blood pressure monitoring)

Hemodynamic parameters were then assessed in WT and KO mice that had undergone cardiovascular stimulation over a six week period with 2% NaCl in the drinking water. During the 6 week period with 2% NaCl, SBP was measured by tail cuff plethysmography (section 4.3.3.1) in both mouse strains following salt loading **(Figure 4-2)**. Salt loading significantly elevated SBP in WT mice from the third week onwards compared to non salt loaded controls, this elevation was distinctly increased at week 6 of the salt loading period; 136.2 ± 1.4 mmHg vs.

173.3 ± 2.9 mmHg (WT control vs. WT +2% NaCl, *** p<0.0001, n=10 per group) **(Figure 4-2 A)**. However, salt loading the KO strain, over a 6 week period, did not significantly affect SBP (119.4 ± 3.1 vs. 126.2 ± 3.1 mmHg; KO control vs. KO +2% NaCl; week 6, n=10 per group) **(Figure 4-2 B)**.

4.4.3 Cardiovascular stimulation with 2% NaCl (Direct blood pressure monitoring)

The difference in hemodynamic response to salt between WT and KO mice was confirmed by radiotelemetry **(Figure 4-3)**. Salt loading significantly increased weekly daytime and night time average SBP WT mice compared to the KO strain (WT: 144.4 ± 6.3 mmHg vs. KO: 122.2 ± 7.0 mmHg), **p<0.001, n=8 per group, **Figure 4-3 A**. Weekly averaged daytime and night time PP was also significantly different between WT mice and the KO mice; n=8 per group, ***p<0.0001, **Figure 4-3 D**. However, all other parameters measured including weekly averaged daytime and night time; DBP (p=0.88) **(Figure 4-3 B)**, MAP (p=0.10) **(Figure 4-3 C)**, HR (p=0.06) **(Figure 4-3 E)**, and Activity (p=0.25) **(Figure 4-3 F)**, were not significantly different between the strains under 2% NaCl loading, n=8 per group.
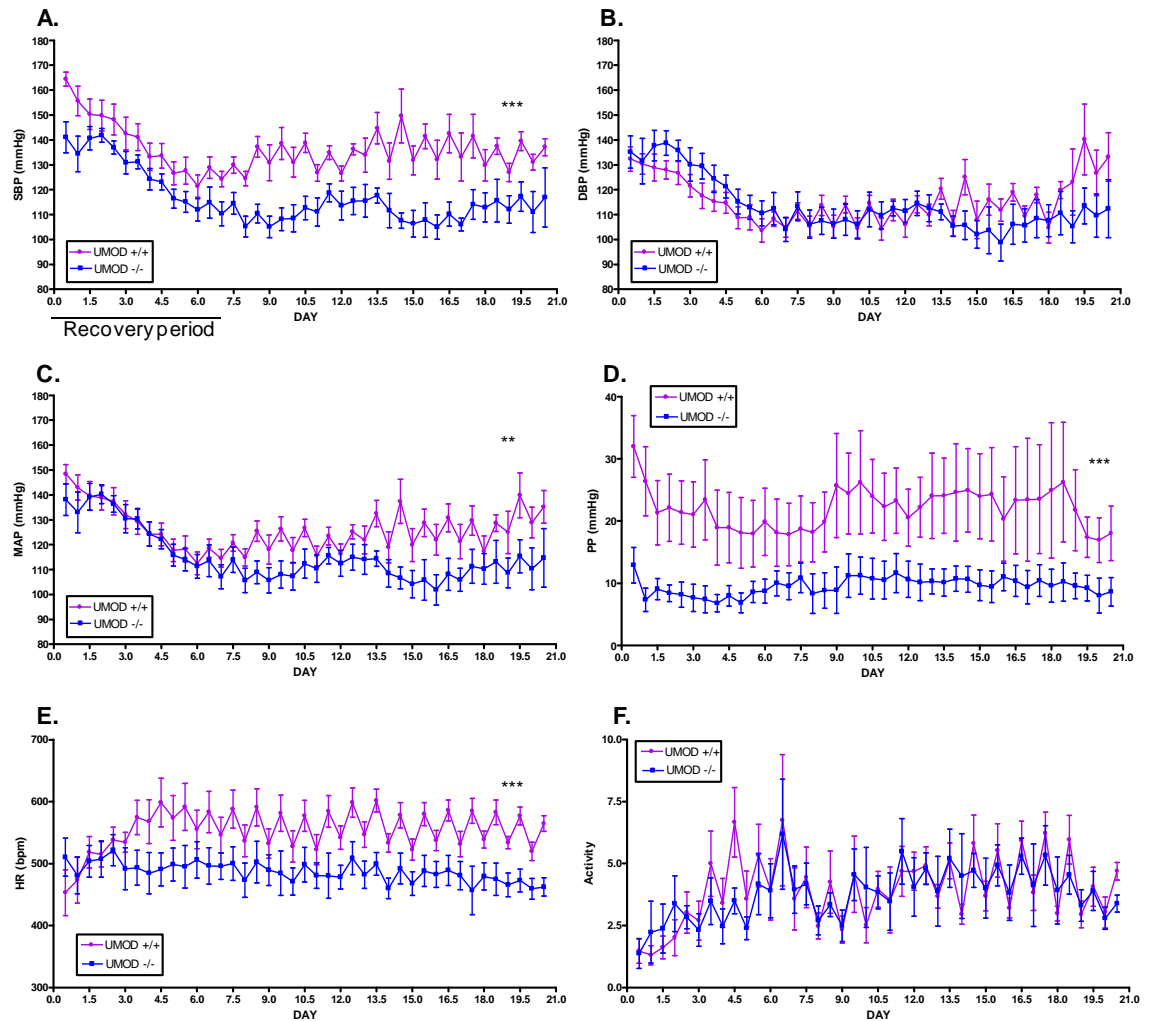
Figure 4-1 Summary of WT (UMOD$^{+/+}$) and KO (UMOD$^{-/-}$) baseline hemodynamic parameters using radiotelemetry.

Radiotelemetry probes were implanted in male WT and KO mice of 12 weeks of age to record baseline hemodynamic parameters over a three week period. Baseline hemodynamic parameters were measured as daytime and night time daily averages. **(A)** SBP, **(B)** DBP **(C)** MAP, **(D)** PP, **(E)** HR, and **(F)** activity recordings in WT and KO mice (***p<0.0001, **p<0.001), n=6 per group. Displayed as daily averaged daytime and night time Mean ± SEM. Week one was a recovery period following surgery and was not included in the analysis. Analysed with repeat measure ANOVA.
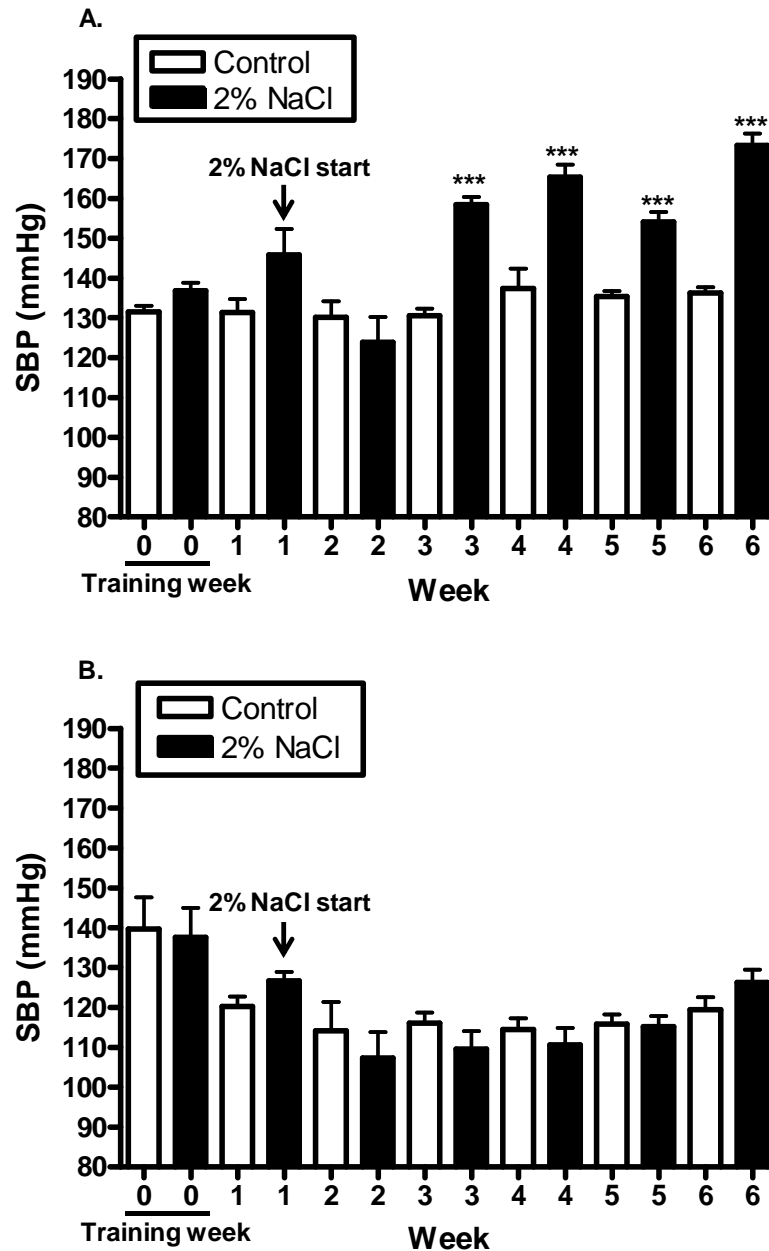
Figure 4-2 Summary of SBP from WT (UMOD$^{+/+}$) and KO (UMOD$^{-/-}$) mice by Tail cuff plethysmography.

Non invasive tail cuff plethysmography was utilised to asses SBP in male WT and KO mice (±2% NaCl). Week zero represents the training period where data obtained was not used in any statistical analysis. At week one, the mice were 12 weeks of age and the pressure recordings were included in the analysis. Salt loading also began on week one. For each animal averages of 10 inflation/deflation cycles were conducted to obtain mean SBP. The procedure was performed over three consecutive days which represented one week of data and repeated the same days every week and at the same time of the day, until the study was completed. **(A)** Comparison of SBP in WT mice and **(B)** KO mice, control (non salt loaded mice) vs. 2% NaCl loaded. WT mice have increased SBP upon stimulation with 2% NaCl from week three onwards, whereas SBP in the KO mice is not affected by NaCl loading. Results displayed as weekly Mean ± SEM, n=10 per group, ***p<0.0001. Analysed with Student's T test.
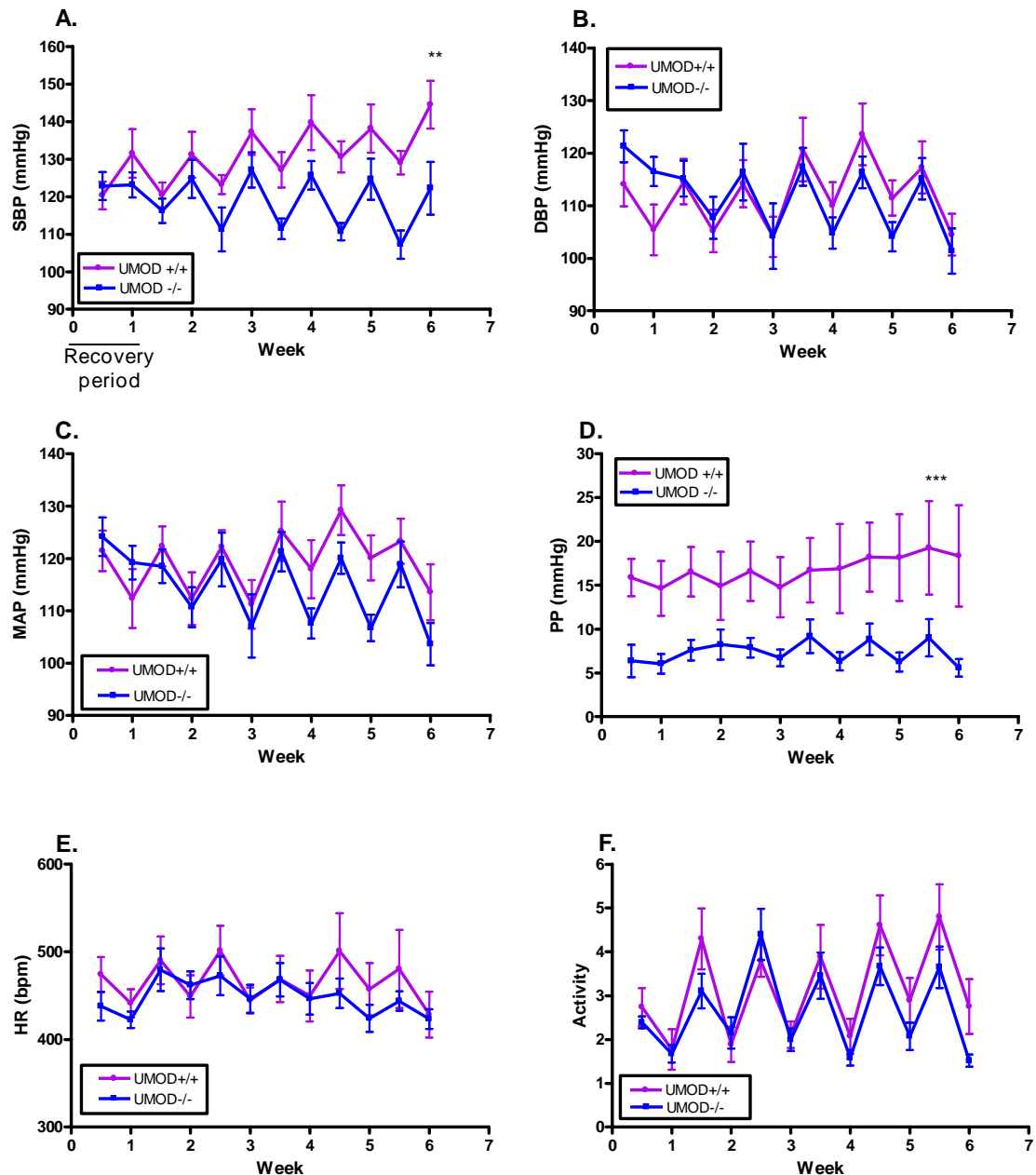
Figure 4-3 Summary of hemodynamic parameters following administration of 2% NaCl in WT and KO mice measured by radiotelemetry.

Radiotelemetry probes were implanted in male WT and KO mice of 12 weeks of age to record hemodynamic parameters in response to NaCl stimulation (2% NaCl in the drinking water). Hemodynamic parameters were measured over a six week period as daytime and night time weekly averages. **(A and D)** SBP and PP were significantly different between WT and KO mice (***$p<0.0001$, **$p<0.001$. **(C- F)** DBP, MAP, HR, and activity were not significantly different between the strains.   Displayed as weekly Mean ± SEM weekly daytime and night time averages, n= 8 per group. Hemodynamic parameters were recorded over a 6 week period where week one was a recovery period following surgery and was not included in the analysis. Analysed with repeated measure ANOVA.

4.4.4 Sodium Excretion

Detailed analysis of fluid intake, urine output, body weight and urine electrolytes were performed at week 6 of the ± 2% NaCl to assess sodium excretion between WT and KO mice. **(Figure 4-4).** Fluid intake was increased in WT mice at week one and six of the salt loading period (week one; 5.3 ± 0.6 ml vs. 7.8 ± 1.1 ml; and week six; 6.4 ± 0.7 ml vs. 9.1 ± 0.9 ml; normal NaCl vs. 2% NaCl respectively, *p=0.02, n=10 per group). The KO mice showed increased fluid intake at weeks one, three, and five when treated with 2% NaCl (week one; 5.0 ± 0.8 ml vs. 8.1 ± 1.1 ml; week three; 5.4 ± 0.7 ml vs. 8.1 ± 0.4 ml and week five; 5.8 ± 0.6 ml vs. 9.3 ± 0.9 ml; normal NaCl vs. 2% NaCl respectively, *p=0.03, **p=0.005 and **p=0.009, n=10 per group) **(Figure 4-4 A)**. Body weight was unchanged in WT mice on salt loading whereas KO mice + 2% NaCl had a lower body weight at weeks one (21.2 ± 0.5 g vs. 19.4 ± 0.2 g), two (21.6 ± 0.6 g vs. 19.3 ± 0.2 g), four (22.4 ± 0.9 g vs. 19.9 ± 0.3 g), five (22.0 ± 0.6 g vs. 20.1 ± 0.3 g) and six (23.3 ± 0.8 g vs. 20.7 ± 0.4 g) (*p<0.05, **p<0.01, KO normal salt vs. KO +2% NaCl respectively, n=10 per group) **(Figure 4-4 B)**.

Sodium homeostasis was assessed further at week six of the salt loading period, by measuring urine output and urinary sodium excretion **(Figure 4-5).** Twenty four hour urine output was significantly increased in KO mice before and after salt loading compared to the WT counterparts, (45.7 ± 4.1 µl/g vs. 25.1 ± 6.7; KO vs. WT normal salt and 59.8 ± 5.8 µl/g vs. 36.4 ± 7.1 µl/g; KO vs. WT following six weeks of salt loading, *p<0.05, n=5 per group) **(Figure 4-5 A)**. Urinary Na^+ excretion was increased in KO mice following six weeks of salt loading compared to the non salt loaded controls (3.2 ± 0.6 µmol/24h/g vs. 27.7 ± 4.8 µmol/24h/g, ***p<0.0001, n=5 per group). WT mice also had significantly increased urinary sodium compared to the non salt loaded controls (2.4 ± 0.8 µmol/24h/g vs. 10.1 ± 1.0 µmol/24h/g, **p<0.001, n=5 per group) however, KO salt loaded mice had a 2.7 fold increased Na^+ in the urine compared to the salt loaded WT mice (ɫp<0.0001, n=5 per group) **(Figure 4-5 B)**. These findings remained when urinary Na^+ (µmol/g) was corrected to urinary creatinine (µmol/g) (KO vs. all groups *p=0.01, n=5 per group and WT normal NaCl vs. WT +2% NaCl *p=0.02, n=5 per group) **(Figure 4-5 C)**. All data was normalised to urine volume collected over a 24 hour period and kidney weight upon animal

sacrifice. Displayed as Mean ± SEM analysed with one way ANOVA followed by Tukey's post hoc test.

When adjusted for the salt affect using GEE analysis (section 4.3.6), urinary Na^+ concentrations in the KO mice were consistently increased (516.8 μmol/d (95% CI 256.6; 776.9 ***$p<0.0001$)) when salt loaded (2% NaCl) over a 6 week period compared to the WT mice, n=5 per group) **(Table 4-2)**. In the GEE model, after adjusting for the salt effect, KO mice had an increased fluid intake of 1.1 ml/24 h compared to WT animals **(Table 4-3)**. The GEE analyses for urine volume and electrolytes at 6 weeks were adjusted for both salt and fluid volume intake to dissect strain specific effects. KO mice had significantly greater urine volume (548.3 ± 123.1 μl/24 h, **$p<0.001$, n=10 per group), as well as urine sodium, potassium and chloride excretion compared to WT mice **(Table 4-2)**. The urinary Na^+/K^+ ratio was similar in both strains. However, in week 6, after adjusting for salt-intake, the average 24 hour urinary sodium excretion in KO mice was appreciably greater than observed for the WT strain (**$p<0.001$).

The chronic renal function curves showed a left ward shift in SBP, MAP, and DBP KO mice compared to the WT strain **(Figure 4-6)**. A left-ward shift in the renal function curve demonstrates that sodium is being excreted at a lower arterial pressure in the KO mouse.
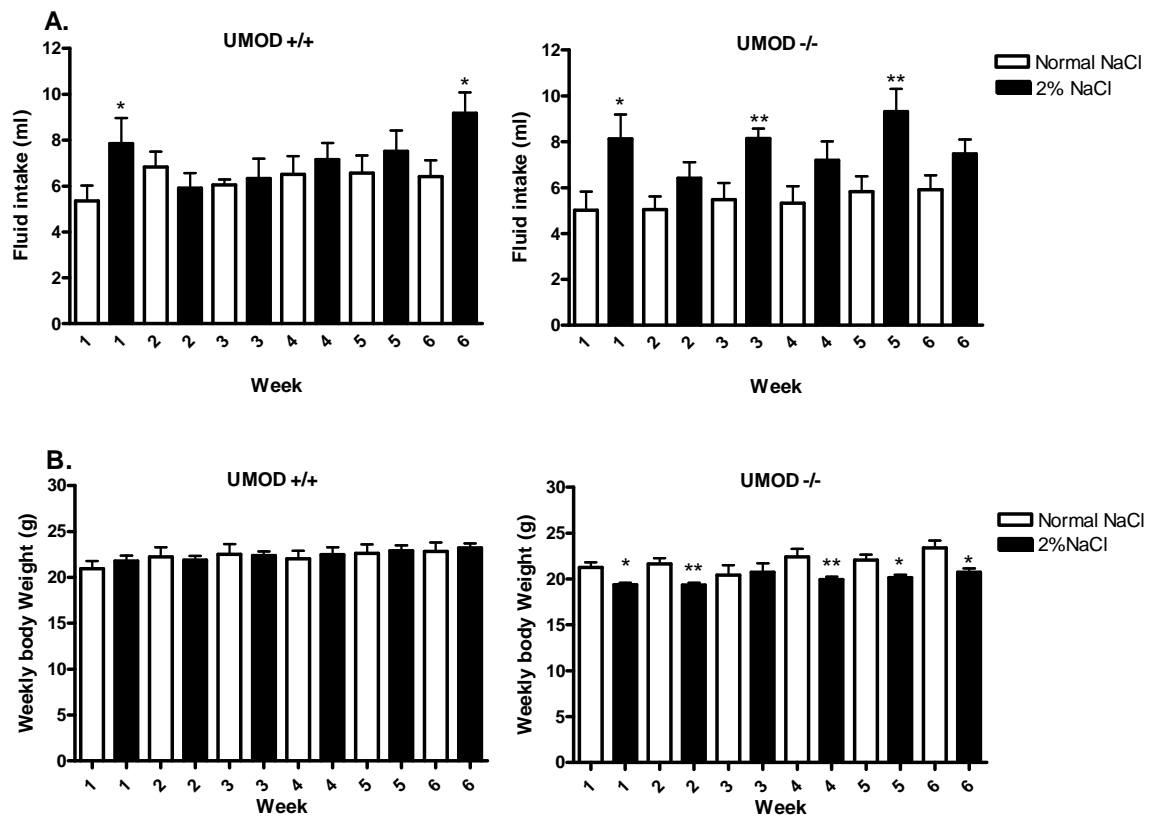
Figure 4-4 Water balance in WT and KO mice ± 2% NaCl.

Male WT and KO mice were housed in individual cages over a six week period where fluid intake and body weight was monitored on a daily basis. **(A)** Fluid intake was significantly increased at week 1 and 6 in WT mice when salt-loaded compared to the control WT animals (*p=0.02, n=10 per group). The salt loaded KO mice displayed increased fluid intake at weeks 1, 3 and 5 compared to the non salt-loaded control animals (*p=0.03, **p=0.005, and **p=0.009, n=10 per group). In addition to monitoring fluid intake, male WT and KO mice were weighed daily **(B)** Body weights were significantly reduced in KO mice at weeks 1, 2, 4, 5 and 6 of the salt loading period compared to the non salt loaded control (*p<0.05, **p<0.01). Body weights were unchanged in WT mice following salt loading. Results displayed as weekly Mean ± SEM analysed with unpaired Student's T test.
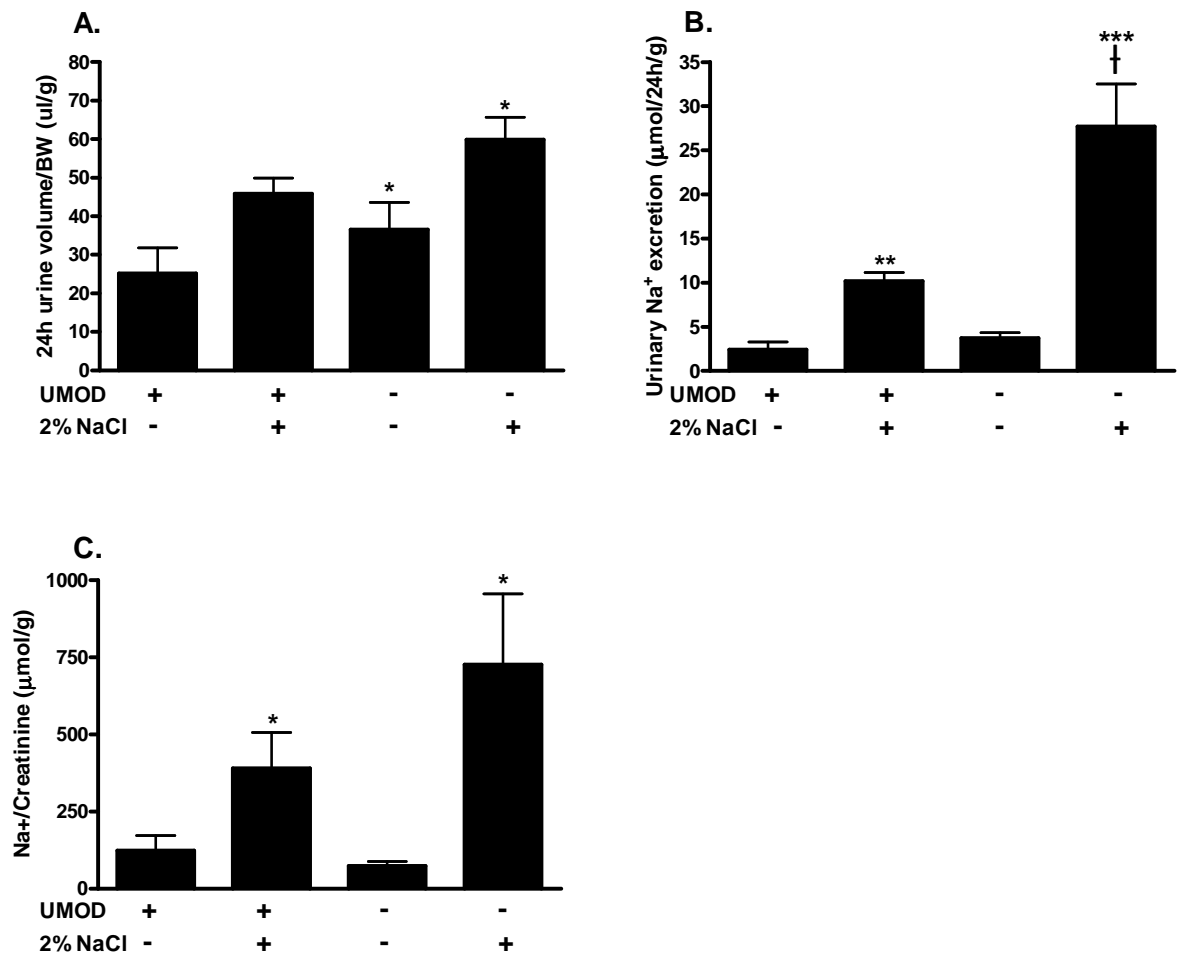
Figure 4-5 Micturition and natriuresis in WT and KO mice under salt loading conditions.

Male WT and KO mice were placed in metabolic cages at week six of the ±2% NaCl loading study for a 24 hour period. Urine was collected and measured. **(A)** Urine output was significantly increased in KO mice before and after salt loading compared to the WT mice (*p<0.05, n=5 per group). All data was normalised to body weight. Urine collected from the metabolic cages was then assessed for Na^+ content (μmol/24h/g) using the indirect ion selective electrode method; potentionmetry. **(B)** Urinary Na^+ was increased in WT and KO mice following six weeks of salt loading with 2% NaCl (** p<0.001 ***p<0.0001, n=5 per group) however the KO mice displayed a 2.7 fold increased natriuresis compared to the WT salt loaded mice (ǂ p<0.0001, n=5 per group). Urinary Na^+ concentrations were normalised to urinary creatinine concentrations (μmol/g). **(C)** Na^+/creatinine ratio was significantly increased in WT mice upon salt loading (*p=0.02, n=5 per group). KO mice also displayed an increase Na^+/creatinine ratio which was significantly higher than all other groups (*p=0.01, n=5 per group). All data was normalised to urine volume collected over a 24 hour period and kidney weight upon animal sacrifice. Both data sets are displayed as Mean ± SEM analysed with one way ANOVA followed by Tukey's post hoc test.
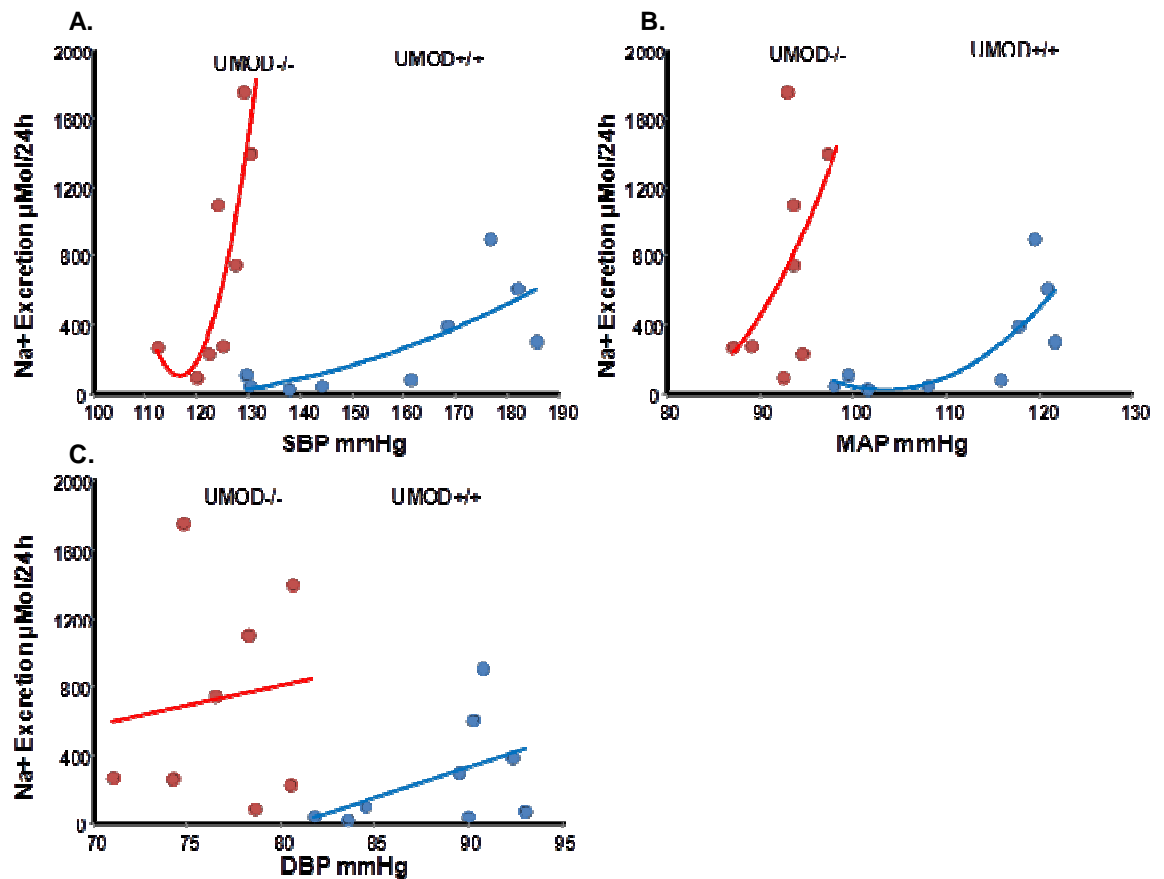
Figure 4-6 Chronic renal function curves in WT and KO mice ± 2% NaCl.

Chronic renal function curves for **(A)** SBP, **(B)** MAP, and **(C)** DBP. Curves were shifted to the left in KO mice compared to the WT strain. A leftward shift demonstrates an increased Na$^+$ excretion in the salt loaded KO animals with no change in arterial pressure. Data residuals are plotted as Mean SBP, MAP, or DBP (mmHg) against 24 hour urinary Na$^+$ excretion normalised to urine volume and kidney weight. Each data point represents one animal n=8 per group. No statistical analysis was performed.

Table 4-1 Cardiovascular parameters measured by radiotelemetry in WT and KO mice during the 6th week of 2% NaCl loading.

Period	Variables	UMOD^{+/+}		UMOD^{-/-}		GEE/GLM	
		Normal Salt	High Salt	Normal Salt	High Salt	Beta	P
Week 6	SBP (mmHg)	133.5(3.1)	153.5 (17.3)	116.7(2.6)	116 (8.5)	-27.2 (3.9)[*]	<0.001
	Water intake (µl/24h)	6412.7(1516)	9174.6 (2149.7)	5904.8 (1191)	7476.2 (944.9)	-1103.2 (487.6)[*]	0.024
	Urine Vol (µl/24h)	555.6 (316.7)	777.8 (370.1)	1044.4 (342.3)	1388.9 (422.6)	548.3 (123.1)[#]	<0.001
	Urine Na^+ (µmol/24h)	54.9 (35.7)	457.4 (314.2)	217 (85.1)	1258 (372.1)	460.9 (176.8)[#]	0.009
	Urine K^+ (µmol/24h)	64.4 (37.4)	177.5 (106.2)	310.7 (192.4)	425.1 (87.4)	195.8 (62.5)[#]	0.002
	Urine Cl^- (µmol/24h)	88.2 (50.7)	532.4 (358.7)	408.3 (217.2)	1407.4 (364.1)	540.7 (181.9)[#]	0.003
	Urine Na^+/K^+ Ratio	1.2 (0.91)	2.51 (0.27)	1.05 (0.76)	2.94 (0.55)	0.222 (0.37)[#]	0.545

GEE GLM beta co-efficients are presented as KO effect with respect to WT after adjustment for covariates.
Covariates for GEE GLM - *=strain, salt intake # =strain, salt intake, water intake (n=8 per group)

4.4.5 Renal function

Having shown that KO mice had increased sodium excretion renal function was assessed **(Figure 4-7)**. At baseline, KO mice had significantly decreased glomerular filtration rate, estimated by measurement of creatinine clearance (CrCl), compared to WT (15.6 ± 0.4 ml/min/g vs. 20.4 ± 0.1 ml/min/g; KO vs. WT respectively,**p<0.001, n=7 per group) **(Figure 4-7 A)**. Although, salt loading resulted in increased glomerular filtration rate in KO mice only, compared to all other groups (**p<0.001, n=7 per group). There was no difference in CrCl after treatment with 2% NaCl in the WT mice (p=0.07). Renal mass index (RMI) was similar between strains ±2% NaCl (p>0.5, n=10 per group) **(Figure 4-7 B)**. Furthermore, histological evaluation showed normal cortical and outer medullary structure without arterial lesions, glomerulosclerosis, adhesions, tubular atrophy or interstitial fibrosis, with no signs of necrosis or apoptosis. However, diffuse oedema with cellular and interstitial swelling was observed in the papillary tissue of KO animals, both before and after salt loading **(Figure 4-7 C)**.

4.4.6 Systems approach using Metabolomics and Microarray analysis to investigate WT and KO mouse kidney profiles

To further dissect the phenotypic differences in SBP and sodium handling between WT and KO mice, a systems approach was utilised for additional characterisation studies to provide insight into potential biological pathways to functionally follow up with mechanistic studies. Metabolic profiling in WT and KO mouse kidney (± 2% NaCl) identified 13 unique significant metabolite changes between KO and WT (normal salt), with 1 metabolite a common change in both strain comparisons **(Figure 4-8 A)**. When comparing metabolic profiles between KO and WT following 6 weeks of salt loading with 2% NaCl, there were 8 unique metabolic changes identified and only one being common between the two strains **(Figure 4-8 A)**. Salt loading the KO strain resulted in 14 significant unique metabolite changes, whereas there were 27 changes in the WT mice under salt loading conditions **(Figure 4-8 A)**. Using IPA software, a canonical pathway was created illustrating the changes in metabolites that were directly

associated with Na$^+$ and UMOD, demonstrating the metabolic changes may be directly associated with UMOD via TNF-α **(Figure 4-8 B)**.

The Illumina microarray and IPA analysis performed on kidney tissue from WT and KO mice (±2% NaCl) to identify and gain biological insights of genes differentially expressed between the strains and the effects of 2% NaCl. The data for each strain was filtered into the venn diagram illustrated in **Figure 4-9 A**. The area of intersect displays genes in common between the two strains (± 2% NaCl) equating 51 genes. There were 67 differentially expressed genes in the WT mice between the normal NaCl group and the 2% NaCl group, whereas the KO mice displayed 210 differentially expressed genes between normal NaCl and 2% NaCl groups B **(Figure 4-9 A)**. To narrow down the gene list IPA was used to analyse genes only associated with Na$^+$ transport, demonstrating 3 differentially expressed genes in the KO strain (± 2% NaCl) compared to the WT mice (± 2% NaCl) **(Figure4-9 B)**. The 3 identified genes were NKCC2 (SLC12a1), Sodium dependant neutral amino acid transporters (SLC38ac, also known as SNAT), and Peroxisome proliferator activated receptor gamma (PPARG). SLC12a1 was shown to be down regulated by 1.4 fold change, whereas SLC38ac and PPARG were up regulated by 1.4 fold change in KO mice upon salt loading **(Table 4-3)**. All differentially expressed genes, including those not related to sodium transport, identified via microarray technology are list in the appendix **(Table A1 and A2)**.
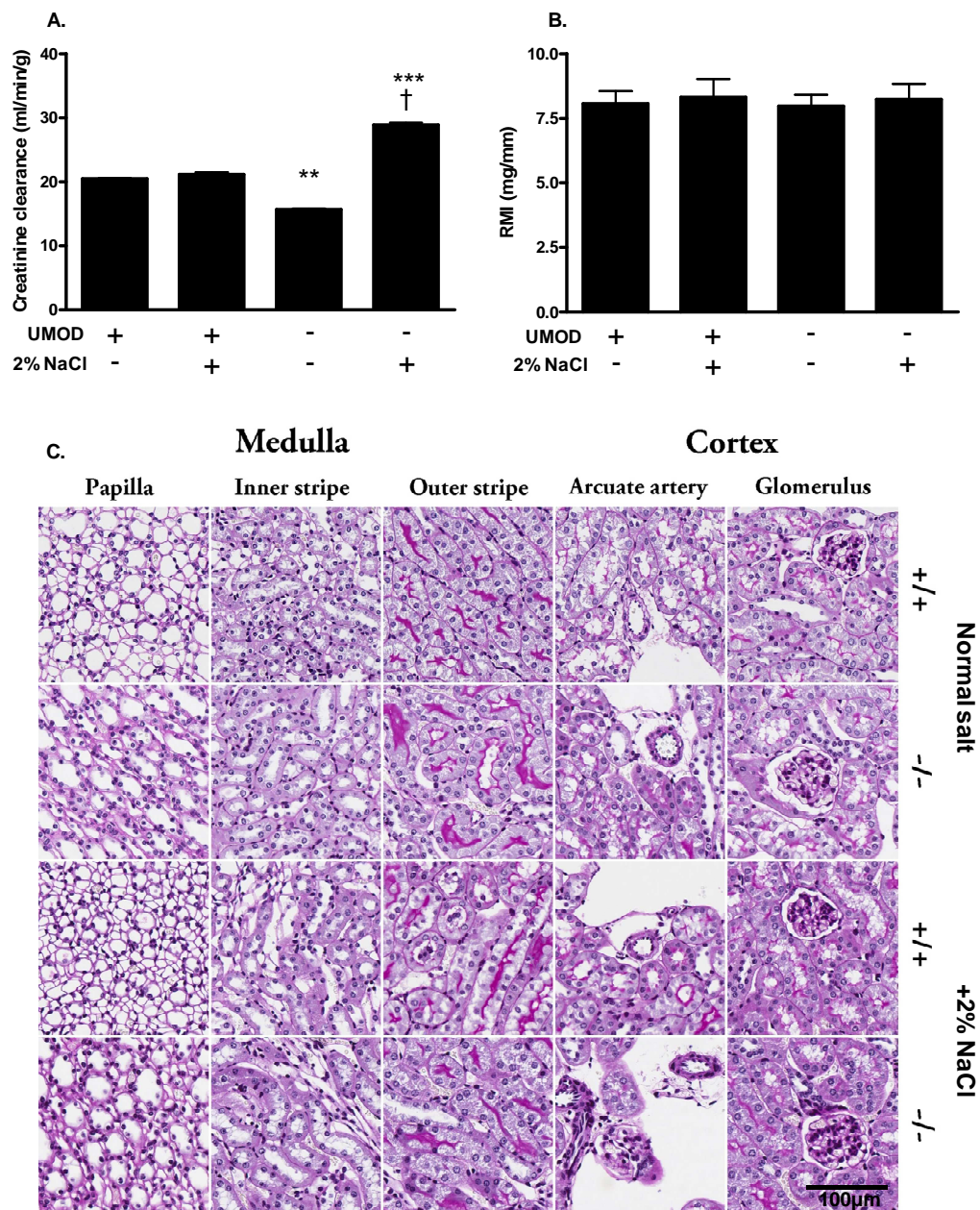
Figure 4-7 Creatinine clearance in WT and KO mice ± 2% NaCl.

Indirect creatinine clearance and renal mass index were assessed in male WT and KO mice (±2% NaCl**). (A)** Under basal conditions, KO mice had significantly reduced CrCl than WT mice, **p<0.001, n=7 per group. Salt loading (2%NaCl), resulted in a significant increase in renal function in KO mice compared to all other groups, (†p<0.001, n=7 per group) with significant, increased CrCl in KO mice following salt loading (***p<0.0001, n=7 per group). There was no increase in glomerular filtration rate in WT mice upon salt loading, p=0.07, n=7 per group. **(B)** There were no differences in renal mass index between strains under either condition**.** All values were displayed as Mean ± SEM. All data was normalised to urine volume collected over a 24 h period and kidney weight (renal mass index normalised to tibia length), analysed with one way ANOVA followed by Tukey's post hoc test. Periodic acid-Schiff assays were performed on sectioned (3µm) paraffin embedded whole kidney tissue from male WT and KO mice (±2%NaCl) **(C)** PAS in WT and KO mice ±2% NaCl show glomeruli and arcuate arteries with normal structure. Tubular structure was normal in the cortex, and the outer and inner stripe of the outer medulla in both strains. However, the papilla showed diffuse oedema with widened interstitium and cellular swelling in KO but not WT mice. Scale bar represents 100 µm.

A.
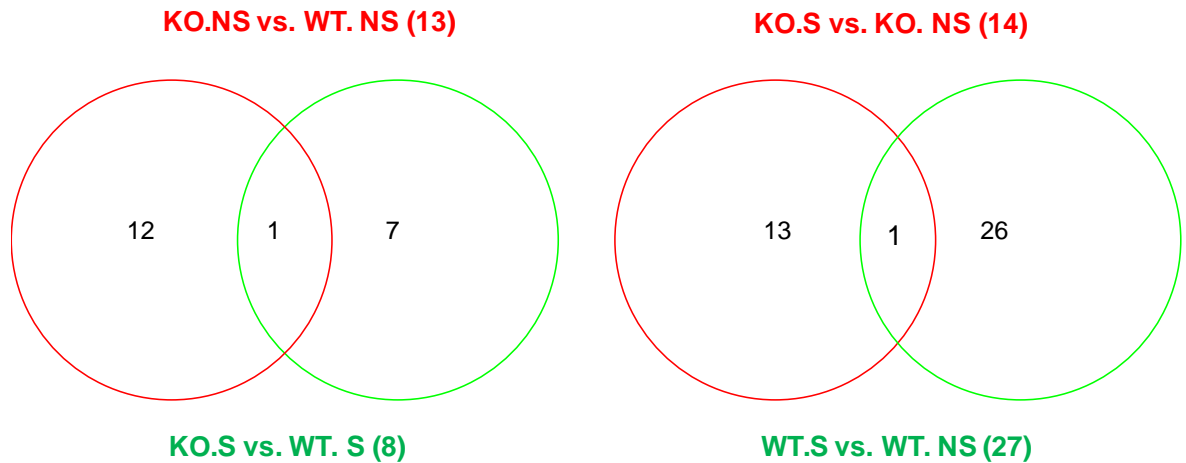
B.
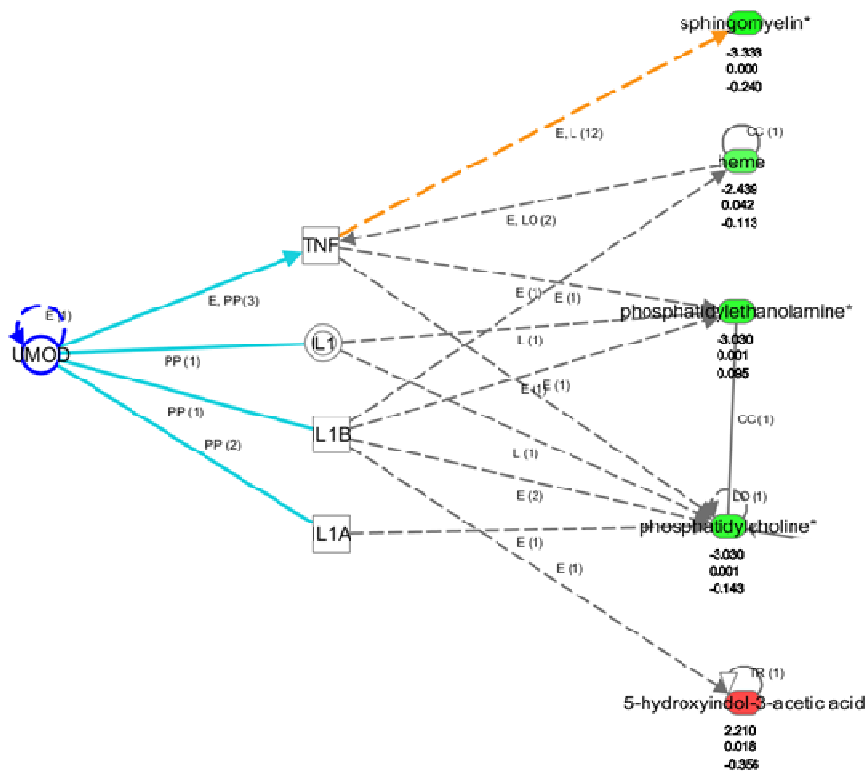
Figure 4-8 Metabolic analysis of kidney tissue from WT and KO mice (normal NaCl).

Pathway analysis demonstrates UMOD is linked to the identified metabolite changes via TNF-α, IL-1, IL-1B, and IL-1A. Dashed lines represent indirect interactions, whereas continuous lines represent direct interactions. Abbreviations and numbers under the continuous or dashed line represents the relevant publications associated with the pathway. The green coded shapes represent reduced expression and the red coded shapes represent increased expression.

A.

B.
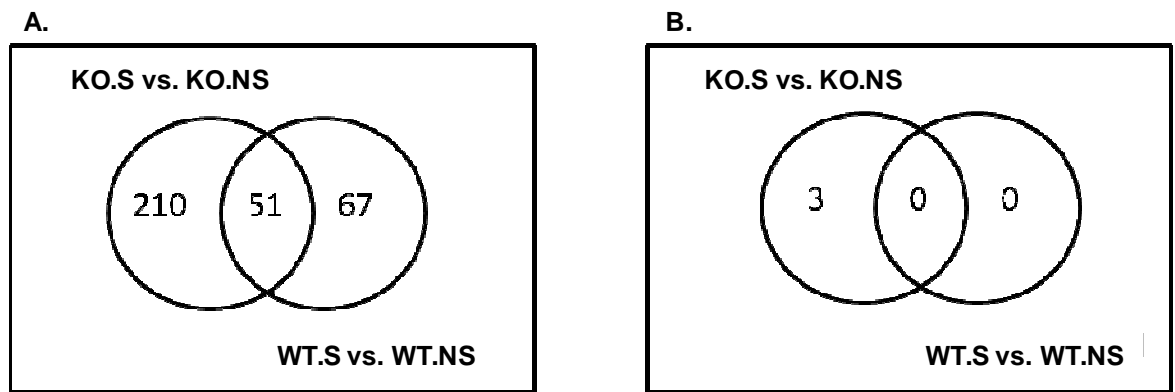
Figure 4-9 Microarray analysis of differentially expressed genes in WT and KO renal tissue (± 2% NaCl).

Venn diagrams illustrating gene expression profiles in kidney tissue of WT and KO mice (± 2% NaCl). The number of probes (genes) significantly differentially expressed for each strain and NaCl conditions are shown. The intersect displays genes in common between the strains. **(A)** Displays all genes identified, whereas **(B)** displays only genes associated with Na$^+$ transport. Normalisation using Illumina/differential expression analysis (determined FDR cut off of p<0.05)/ explored connections using IPA.

Table 4-2 Differentially expressed sodium transport genes.

Illumina ID	Symbol	False Discovery Rate (FDR<0.05)	Fold Change
ILMN_3048630	Slc12a1	0.04	-1.4
ILMN_2750089	Slc38a3	0.04	1.4
ILMN_1221060	PPARG	0.04	1.4

Conical pathway analysis of genes implicated in the microarray revealed 3 genes directly involved in Na$^+$ to be differentially expressed in the salt loaded KO mice. SLC12a1 was down regulated whereas SLC38ac and PPARG were upregulated.

4.5 Discussion

To investigate the role of UMOD in BP regulation, this chapter examined hemodynamic parameters, sodium excretion, and renal function under conditions of normal sodium and high sodium (2% NaCl) intake in WT and KO mice. There are clear blood pressure differences between the strains, in that the KO mice display a lower baseline SBP and are insensitive to salt induced changes in BP. Results here are the first to provide novel functional evidence that UMOD is involved in blood pressure regulation through altered sodium excretion. The results reported here are a major discovery confirming the role of UMOD in blood pressure regulation.

The BP findings in this chapter were confirmed by two independent methods; tail cuff plethysmography and radiotelemetry. The methodological approaches chosen here are in concordance with previous reports demonstrating that SBP pressure values monitored with, indirect tail cuff plethysmography and direct intra-arterial pressure recordings are similar, providing that potential artefacts caused by stress are not included in data collection (Bunag, 1983, Ikeda et al., 1991). Reports have suggested that errors in data collection maybe encountered with tail cuff plethysmography due to restraining and pre warming the animals causing stress artefact resulting in BP variability. This is apparent during the training week where the KO mice demonstrate increased SBP compared to the WT mice, consequently demonstrating the importance of this training period. However, beyond the training week tail cuff plethysmography demonstrated reduced error and defined BP differences between WT and KO mice (± 2% NaCl). Radiotelemetry is the most reliable method of BP pressure measurements in rodents, although it comes with increased costs and the surgical procedure is technically challenging. Here radiotelemetry confirmed the BP phenotypes (± 2% NaCl) demonstrated with tail cuff plethysmography, showing the KO mice have lower baseline SBP which is not increased upon salt loading, whereas the WT mice had significantly increased BP when salt loaded for six weeks with 2% NaCl. A recovery period post surgical procedure is necessary before data collection can occur with radiotelemetry as animals recover from surgery over a period of time; up to 7 days is optimally required for the animal to recover completely from surgery and before BP recordings, activity, and heart rate will to return to

normal (Meneton et al., 2000). BP values taken within this time display artefact and should not be included in any statistical analysis. Radiotelemetry results in this study display this pattern, with blood pressure values between the strains not separating until approximately day 8 post surgery, consequently data collected in the first week post surgery was not used in the analysis to demonstrate BP levels in KO or WT mice.

Chronic renal function curves can be used to predict the long-term level at which SBP will be regulated for any given level of salt intake (Guyton, 1987). The chronic renal function curves in this chapter demonstrate progressively increasing levels of SBP, DBP, and MAP with increased sodium excretion in the WT mice. Usually when sodium intake vs. sodium output are in balance, blood pressure is maintained and renal function curves remaining to the "left" which is the case for KO mice here. Multiple studies in animals have shown that chronic renal function curve are shifted to the "right" in every type of hypertension studied thus far; hypertension in spontaneously hypertensive rats (Bianchi et al., 1974), hypertension caused by aldosterone infusion (Lohmeier et al., 1980), hypertension caused by angiotensin II infusion (Declue et al., 1978) and hypertension caused by volume loading (Guyton, 1991). Therefore, the significantly lower BP phenotypes in KO mice can be explained by a leftward shift in the chronic renal function curves depicting the effect of urinary Na^+ output on arterial pressure in the absence of *UMOD*.

The KO mice in this study revealed increased fluid intake and urine output when salt loaded, suggesting the lower arterial pressure observed in KO mice may be explained in terms of increased Na^+ loss. Urinary Na^+ excretion was significantly increased in both mouse strains upon salt loading, but to a greater degree in the KO mice. The premise that KO mice do indeed have lower arterial pressure due to Na^+ loss is further supported by lower lean body mass in this strain when salt loaded, as augmented natriuresis is normally accompanied by reduced extracellular fluid volume and blood volume which, in turn, leads to lower body weight. Therefore, on a high-salt diet, the KO animals retained less Na^+ compared to the WT strain. Taste preference studies have shown that C57BL/6 mice have a strong aversion to sodium addition in drinking water at any concentration, whereas 129 s/v mice prefer salty water to pure tap water

(Beauchamp and Fisher, 1993), as the mice used here were of 129 s/v background it could be thought the effect of taste preference may be a factor causing the increased fluid intake and hence urine output in the KO mice. However, this is not the case as both strains are on the background of 129 s/v, and only the KO mice display increased fluid intake with 2% NaCl conditions. As a result the increased micturition with natriuresis in salt loaded KO mice reflects the inability of these mice to reabsorb Na^+ driving the lower BP phenotype in the absence of *UMOD*.

One limitation of this study is that the reported fluid intake did not compare with urine output under normal sodium conditions. The urine volumes reported in our study are well within the typical ranges reported for male adult mice of approximately 20-30g i.e. 0.5 – 2.5ml/24 hours so evaporation during collection was not an issue (Stechman et al., 2010), on the contrary fluid volumes were more than the normal reported daily averages for these mouse strains. Bachmann *et al* utilised the same mice strains and reported that drinking is on average 134 μl / g BW in the WT mice and 157 μl / g BW in the KO mice, results here show almost two fold these volumes (Bachmann et al., 2005, Beauchamp and Fisher, 1993). These reports do support the present results in that there is a trend towards an increased fluid intake in the KO mice, but they did not consider salt loading in these strains. One explanation for the over estimation of fluid intake is that water bottles used in metabolic cages studies have a tendency to leak, as water volumes were measured every 24 hours some residual water may have been lost. To overcome this, bottles should have been weighed rather than volume measured and the water that leaks in to the troughs should be accounted for. Future studies should consider this method alongside a gelatine diet to ensure all mice receive exactly 2% NaCl in the diet for the duration of the study. Since the potential imbalances between fluid in and urine out may have confounded the finding of increased natriuresis in the KO mice, hence urinary Na^+ excretion was corrected to creatinine levels.

Steady state electrolyte handling has been investigated previously in the KO mice and demonstrated no differences compared to the WT strain. These findings are consistent with results here; WT and KO mice displayed no differences in Na^+ excretion under normal salt conditions (Bachmann et al.,

2005). Although previous studies have not examined the effects of salt loading in these mouse strains, and this chapter is the first to demonstrate that under high salt conditions the KO mice have altered Na$^+$ handling. A defect in renal function related to renal damage does not appear to contribute to this effect as no differences in renal mass index or renal structures were observed between the strains. However, diffuse oedema with cellular and interstitial swelling was observed in the KO mice before and during salt loading suggesting increased inflammation that could impact Na$^+$ reabsorption. The KO mice show lower CrCl under normal salt conditions, consistent with previous reports (Starremans et al., 2003) and higher CrCl when salt loaded compared to WT mice. This increase in CrCl suggests that KO mice have a greater capacity to excrete Na$^+$ thereby maintaining body homeostasis despite increased Na$^+$ intake. The present study did not investigate urinary excretion levels of magnesium (Mg$^+$) and/or calcium (Ca2$^+$), and to date these parameters have not been fully investigated in *UMOD* WT and KO mice. There have been previous studies investigating urinary levels of Mg$^+$ and Ca2$^+$ in mice following high and low Mg+ diets and found *UMOD* to be involved in Mg$^+$ handling (de Baaij et al., 2013). This group reported that a high Mg$^+$ diet resulted in high urinary Mg+ and Ca2+ levels, with no associated change in urinary Na+, K+, and Cl- concentrations. *UMOD* gene expression levels were significantly reduced during times of high Mg+ apparently due to increased urinary flow rate, proposing that after cleavage of UMOD into the pro-urine, UMOD forms gel like structures that prevent the movement of positively charged ions and uptake of cations such as Mg$^+$ and Ca2$^+$ (Vyletal et al., 2010). Additional reports have demonstrated that urinary Ca2$^+$ loss in mutant *UMOD* mouse models exceeds the urinary sodium loss (Wolf et al., 2013). The dissociation of hypercalciuria from urinary sodium excretion in mutant *UMOD* mice suggests that UMOD may have a role in regulating transcellular Ca^{2+} reabsorption in the nephron. These urinary parameters, alongside Mg+ and Ca+ transporters should be investigated in the WT and KO mouse models in future studies.

The lower baseline CrCl in KO mice reported here is in contrast to previous human GWAS studies which showed alleles associated with low UMOD excretion are associated with high eGFR (Padmanabhan et al., 2012, Kottgen et al., 2009). As KO mice displayed high CrCl only in relation to high salt intake, it is possible that the associations found in the GWAS were confounded by high dietary salt

intake in the population cohorts used. As previously reported, the minor G allele of rs13333226 (allele frequency 0.18 in Europeans) was associated with a lower risk of hypertension, lower urinary UMOD excretion and increased proximal tubular sodium reabsorption (Padmanabhan et al., 2010). These findings illustrated that the lower urinary UMOD excretion associated with the G allele was present only on low salt diets, and that this association was lost when the sodium intake was high. In the human study, the observation of increased proximal tubular sodium reabsorption was observed in studies where salt intake was not strictly controlled, so it is difficult to ascertain whether this is a consequence of increased GFR, or a compensatory reaction to a primary decrease in distal reabsorption (Padmanabhan et al., 2010). To elucidate this further implicated functional pathways driving Na^+ loss in the KO mice were investigated via a systems approach.

Metabolite analysis between WT and KO mice revealed that UMOD attenuated expression of metabolites linked with apoptosis, oxidative stress, atherosclerosis, and diabetes. Sphingomyelin, heme, phosphatidylethanolamine, and phosphatidylcholine were all reduced in the presence of UMOD and these four metabolites were shown by IPA analysis to be linked to UMOD via effects on TNF-α, IL-1, IL-1A, or IL-B. Sphingomyelin is associated with lipid rafts involved with oxidative stress and apoptosis. Lipid rafts can accumulate proteins involved in the cascade of apoptosis (Green, 2000). Heme was also down regulated in WT mice suggesting in the presence of UMOD there are lower levels of cytotoxic free radicals reducing risk of programmed cell death caused by pro-inflammatory cytokines in the kidney (Pamplona et al., 2007). Phosphatidylethanolamine and phosphatidylcholine are metabolites associated with atherosclerosis and diabetes caused by oxidative stress (Eitsuka et al., 2012, Wang et al., 2011b) and were also found to be down regulated in the WT mice by actions of UMOD via regulation of pro-inflammatory cytokines. The only metabolite upregulated in WT mice was 5-hydroxyindole-3-acetic acid which is linked with increasing endothelial nitric oxide synthase availability (McDuffie et al., 2000) however, vascular tone experiments were not performed in the current study and should be considered for future studies.

The strong association identified here between UMOD and metabolites regulated via TNF-α and IL-1 further supports the concept that UMOD is an immunoregulatory molecule in the kidney. As introduced in section 1.10.1.5 UMOD exerts its immunosuppressive affects by binding with high affinity to TNF-α and IL-1 (Sabharanjak et al., 2002, Kirkham et al., 2005). This gives rise to the hypothesis that available UMOD at the apical membrane may play a role in modulating cell surface events, linked with Na$^+$ reabsorption. *In vivo* reports from Shahid and colleagues reported that TNF-α infusion in mice resulted in reduced renal blood flow and reduced GFR, along with increases in excretion of Na$^+$ (Shahid et al., 2008b). This suggests TNF-α induces renal vasoconstriction via enhancing activity of O_2^- which reduces the availability of nitric oxide. These reports coincide with metabolomics results discussed above. The natriuretic response described by Shahid *et al* of TNF-α is related to its direct effects on tubular sodium reabsorption. Ferreri *et al* demonstrated TNF-α inhibits ion fluxes, particularly Na$^+$ reabsorption and water movement at the TAL, thus in the absence of UMOD ion transport in the TAL may be modulated by TNF-α release or accumulation which infiltrates the kidney (Escalante et al., 1994). Furthermore, in damaged kidneys TNF-α accumulates in the interstitium and once there promotes inflammatory cell recruitment and activation via engagement with Toll like receptor 4, scavenger receptors, and cell surface lectins (El-Achkar et al., 2008). All of the above could lead to the reported consequence of increased interstitial swelling and cellular odema in the papillary regions of the kidney in KO mice.

To dissect the salt effect in KO mice further and in addition to metabolomic profiling, microarray technology was utilised. Microarray analysis identified three genes specifically linked with Na$^+$ transport that were differentially expressed in the salt loaded KO mice. Sodium dependent amino acid/proton anti porter (SLC38a3) and Peroxisome proliferator activated receptor gamma (PPARγ) expression were increased whereas, NKCC2 (SLC12a1) expression was decreased. SLC38a3 is not a TAL specific Na$^+$ transporter and to date there are limited implicated roles of this gene in hypertension. PPARγ is primarily involved in fatty acid storage and glucose metabolism, and is well documented to be linked with diabetes and related cardiovascular morbidities (Mollsten and Torffvit, 2010). UMOD has also been connected to diabetes with sufferers displaying altered

urinary UMOD excretion, low nitric oxide synthase levels, increased mean arterial pressure, and low metabolic control (Mollsten and Torffvit, 2010). The *UMOD* variant rs13333226 on the minor G allele was associated with lower risk of nephropathy in patients with diabetes after correction for BP and kidney function (Ahluwalia et al., 2011). The excretion rate of UMOD has been shown to be directly correlated with distal tubular reabsorption in patients with chronic diabetic nephropathy, suggesting that Na^+ may affect UMOD secretion (Torffvit et al., 1998). Therefore, increased PPARγ levels in salt loaded KO mice may be a consequence of increased Na^+ excretion. Recently PPARγ has been associated with sodium and water homeostasis related to cardiovascular disease (Wang et al., 2008).

The collecting ducts express PPARγ suggesting that ligands for this receptor modulate sodium and water homeostasis via ion transport regulation. ENaC is also expressed in this segment of the nephron and clinical data has already well established that stimulation of ENaC activity leads to an increase in Na^+ and water reabsorption, resulting in elevated BP. Previous *in vivo* studies in PPARγ null mice have shown these mice gain weight, display volume expansion, and consequently demonstrate raised BP (Zhang et al., 2005, Guan et al., 2005). *In vitro* studies in primary cells cultures derived from the collecting duct of these mice displayed increased ENaC activity (Nofziger and Blazer-Yost, 2009). Thus, there is a consensus that loss of PPARγ increases BP potentially via increased Na^+ reabsorption. This would postulate that increased PPARγ expression in the salt loaded KO mice may be a compensatory mechanism in the aim to regulate BP and Na^+ reabsorption in the absence of UMOD, however, further investigation is needed.

More interestingly the Na^+-K^+-$2Cl^-$ cotransporter (NKCC2) expression levels were reduced in the KO salt loaded mice according to microarray analysis. NKCC2, is selectively expressed in the TAL where it transports the vast majority of NaCl and is said to be modulated by co-localised UMOD (Mutig et al., 2011a). In humans inactivating mutations of the NKCC2 gene (*SLC12A1*) cause a significant reduction in BP, with severe natriuresis developing a severe salt wasting phenotype (Bartter syndrome) (Garcia et al., 1999, Acuna et al., 2010). In contrast to genetic inactivation of NKCC2, enhanced activities of NKCC2 have

been linked to salt sensitive hypertension (Ares et al., 2011). Indicating the important role NKCC2 plays in blood pressure regulation. Recent studies have implicated UMOD expression at the apical membrane in the TAL is responsible for modulating NKCC2 specific sodium reabsorption (Mutig et al., 2011b). As a result, the absence of UMOD may cause deficits in Na^+ reabsorption inhibiting NKCC2 expression and activity. Renal pro-inflammatory cytokines are documented as reducing ion transport. TNF-α is produced by the TAL and acts in an autocrine manner to down regulate NKCC2 expression (Battula et al., 2011), lowering NaCl reabsorption at this site (Bachmann et al., 2005, Sherblom et al., 1988, Mutig et al., 2011b, Hao et al., 2011). Collectively suggesting the absence of UMOD may increase TNF-α levels at the TAL, reducing Na^+ reabsorption and providing a potential link between the intracellular and extracellular roles of UMOD in blood pressure control.

In summary this results chapter has provided novel findings that *UMOD* KO mice have lower blood pressure than the WT counterparts, and do not display increases in BP when salt challenged. The KO mice display increased diuresis with substantial natriuresis, confirmed by a leftward shift in the chronic renal function curves. Urinary electrolyte analysis corrected to creatinine levels revealed augmented sodium loss in the KO mice during a high salt diet. Histological examination illustrated cellular swelling and papillary oedema in the KO mice before and after salt loading which may be triggered by the pro-inflammatory cytokines TNF-α and IL-1 according to metabolomic analysis. These inflammatory signals may affect Na^+ homeostasis at the TAL in the KO mice by reducing NKCC2 expression. All of the findings from this chapter suggest UMOD has a fundamental role in regulating Na^+ reabsorption and extracellular volume homeostasis regulating BP.

To assess potential mechanisms altering BP in the KO mice the next results chapter examines functionally the role UMOD plays in BP regulation by mediating the effects of TNF-α and NKCC2 on sodium homeostasis.

5 The role of *UMOD* in sodium regulation at the Thick Ascending Limb of the Loop of Henle.

5.1 Introduction

The thick ascending limb of the loop of Henle (TAL) is pivotal in the regulation of extracellular fluid volume and blood pressure control via sodium homeostasis. The reabsorption of NaCl at the TAL accounts for 25% of total renal salt retrieval, and it generates the energy for the urinary concentrating mechanism. NaCl uptake across the apical membrane of TAL cells is mediated to at least 80% by a co-transport process in which the influx of Na^+ drives the uptake of Cl^- and K^+. To achieve net salt absorption, apical electroneutral co-transport of Na^+, K^+, and Cl^- via NKCC2 is complemented by recycling of K^+ via ROMK, efflux of Cl^- via basolateral Cl^- channels (CLC- Kb/Barttin), coupled transport of Na^+ and H^+ via NHE3 transporters, basolateral extrusion of Na^+ by Na^+ /K^+ ATPase, and the final adjustment to urine concentration, K^+ homeostasis, acid base balance with Na^+ reabsorption is accomplished by ENaC.

The results from the KO mice in the previous chapter suggest a possible link between UMOD and ion transport in the TAL. In the absence of *UMOD* there is augmented sodium excretion in the KO mice, suggested to be a consequence of reduced expression of the sodium transporter NKCC2. This modulated Na^+ reabsorption by reduced NKCC2 leads to exaggerated natriuresis and lower arterial pressure in the KO mice and is consistent with findings in humans where salt wasting phenotypes and hypotension are characteristics of Bartter's syndrome (Pressler et al., 2006, Simon et al., 1996a, Vargas-Poussou et al., 1998). Ion channels, pumps, and transporters found along the nephron accomplish the fundamental functions of the kidney in regulating Na^+ homeostasis and blood pressure phenotypes. In times of altered activity, blood pressure, ECF volume, and sodium reabsorption can be impaired and in contrast to hypertension, leads to hypotension and salt wasting phenotypes as seen thus far in the KO mice.

Since the reabsorptive capacity of Na^+ in downstream portions of the nephron is limited, it is likely that inhibition or modulation of NKCC2 expression is largely responsible for marked natriuresis and micturition with consequent reductions in arterial pressure. Three NKCC2 variants (A, B, and F) are derived by differential splicing of exon 4 of the *SLC12A1* gene. These isoforms differ in their distribution

along the nephron and account for 20%, 10% and 70%, for A, B, and F respectively, of the total NKCC2 transcript abundance in mice (Castrop and Schnermann, 2008). Ferreri *et al* have previously reported that TNF-α is an endogenous inhibitor of NKCC2A in the TAL (Battula et al., 2011). In further support of this finding this group also demonstrate NKCC2A mRNA expression levels were selectively elevated accompanied by increased NKCC2 activity in TNF-/- mice with no differences in NKCC2B, and F expression levels between WT mice and TNF-α -/- mice (Battula et al., 2011). TNF-α administration has proven to be a potent inhibitor to sodium reabsorption at the TAL causing exaggerated natriuretic responses and blood pressure lowering effects (Evans et al., 1989, Nakatsuji et al., 1990). Interestingly, it has been reported that UMOD facilitates the co-transport of NKCC2 to the apical membrane of TAL cells (Mutig et al., 2011b) and that UMOD exerts its immunosuppressive effects by binding with high affinity to TNF-α (Wu et al., 2008). This data suggests that in the absence of *UMOD* or altered available UMOD at the apical surface of TAL cells will result in enhanced levels of TNF-α production; in turn reducing NKCC2 activity and Na^+ reabsorption.

Given the hypothesis that altered *UMOD* expression regulates arterial pressure by controlling Na^+ reabsorption, this chapter investigated levels of the pro-inflammatory cytokine TNF-α levels in WT and KO mice (± 2% NaCl) and the subsequent effects on renal Na^+ handling transporters. *In vitro* assays were utilised to further test the potential mechanistic role of *UMOD* related Na^+ transport.

5.2 Aims

- To investigate levels of mRNA abundance of the main renal Na^+ channel transporters in whole kidney tissue and outer medulla tissue from WT and KO mice following six weeks ± salt loading with 2% NaCl.

- To investigate levels of protein expression of the main renal Na^+ channel transporters in whole kidney tissue and outer medulla tissue from WT and KO mice following six weeks ± salt loading with 2% NaCl.

- To investigate the potential mechanistic role of *UMOD* to regulate Na^+ levels at the TAL.

- To utilise immunohistochemistry to investigate localisation of UMOD in WT and KO mouse kidney tissue following six weeks ± 2% NaCl.

5.3 Method

5.3.1 Ion transporter and cytokine expression analysis

RNA was extracted and prepared from WT and KO mouse whole kidney and outer medulla tissue ($\pm$2% NaCl) as described in section 2.3.8. The following Na^+ transporters and *TNF-α* were assessed; *UMOD, NKCC2, ENaC, ROMK, Na^+/K^+ -ATPase-a, Na^+/K^+ -ATPase-β*, and *NHe3* using Taqman® gene expression assays described in section 2.4.1. **Table 5-1** details the assays used in this chapter.

Table 5-1 Taqman® assays used to determine expression levels of Ion transporters.

Transporter	Gene name	Taqman® assay	Reference sequence	Exon boundry
UMOD	Uromodulin	Mm00447649_m1	Nm_0094704	2-3
TNF-α	TNF-α	Mm00443260_g1	Nm_0.13693.2	3-4
NKCC2	SLC12A1	Mm01275821_m1	Nm_001079690.1	19-20
ROMK	KCNJ1	Mm01173990_m1	Nm_001168354.1	1-2
ENaC	SCNN1	Mm00803380_m1	Nm_011324.2	2-3
Na^+/K^+ -ATPase α	ATP1A1	Mm00523255_M1	Nm_144900.2	10-11
Na^+/K^+ -ATPase β	ATP1B1	Mm00437612_m1	Nm_009721.5	2-3
NaHe3	SLC9A3	Mm01352473_m1	Nm_001081060.1	14-15

Expression of *UMOD, TNF-α, NKCC2, ROMK, ENaC, Na^+/K^+ - ATPase* (α and β), and *NHe3* was assessed at the mRNA level in WT and KO mouse kidney and outer medulla tissue ($\pm$ 2% NaCl).

QPCR was used to determine accumulation of mRNA for *NKCC2* isoforms (A, B, and F) as per section 3.3.7.7. The primer specific pairs for murine *NKCC2*A, B, and F are as listed below:

	Forward Primer	Reverse Primer
NKCC2A	5' GGTAACCTCTATCACTGGGT 3'	5'GTCATTGGTTGGATCCACCA 3'
NKCC2B	5'GCCGTGACAGTGACAGCCAT 3'	5' GGATCCACCATCATTGAATCG 3'
NKCC2F	5' GTCATCATCATTGGCCTG 3'	5' GAATCCCACCACATACATAG 3'

Following mRNA expression analysis, the protein levels of the ion transporters and TNF-α were quantified in either: whole kidney tissue, outer medulla tissue, or TAL cell cultures. Protein samples were extracted, prepared, and blotted as per section 2.7 then probed using Abcam® primary and secondary antibodies (Abcam®, Cambridge, UK (**Table 5-2**)) with the exception of UMOD which was probed using AbD SeroTec primary and secondary antibodies (Sheep anti-human Tamm Horsfall Protein, (primary polyclonal antibody)) and STAR88P (secondary HRP Donkey anti-sheep polyclonal antibody), AbD SeroTec, Bio-Rad Laboratories Inc, Puchheim, Germany. The secondary antibodies used for Abcam® specific

primary antibodies were rabbit anti-mouse (polyclonal HRP, ab6709) and Mouse anti-rabbit (polyclonal HRP, ab6728), Abcam®, Cambridge, UK). All Abcam® antibodies were used at a concentration of 1 µg/ml in TBST with 1% milk and blocked with 5% milk. AbD SeroTec antibodies were used at 1:500 dilutions in TBST with 1% BSA and blocked with 5% BSA. All blots were stripped (2.8.5) and reprobed with GAPdh (ab8245) mouse monoclonal primary anti body from Abcam® Cambridge, UK.

Table 5-2 Abcam® primary antibodies used to detect levels of renal Na+ transporters and TNF-α.

Transporter	Gene name	Abcam® antibody	Host species	Clonality	Molecular weight
TNF-α	TNF-α	ab52B3	Mouse	Monoclonal	52
NKCC2	SLC12A1	ab95302	Rabbit	Polyclonal	111
ROMK	KCNJ1	ab85479	Rabbit	Monoclonal	45
Na+/K+-ATPase	ATP1A1	ab7671	Mouse	Polyclonal	112
eNac	SCNN1	ab65710	Rabbit	Polyclonal	76

5.3.2 Enzyme Linked ImmunoSorbent Assay (ELISA)

TNF-α levels were measured in urine from KO and WT mice (±2% NaCl) by enzyme linked immunosorbent assay (ELISA), using a commercially available mouse TNF-α ELISA kit (BD Sciences, Oxford, UK) following the manufacturer's instructions. Section 2.15 in the general methods section outlines the procedure. Urine was collected from WT and KO mice as per section 2.11.1.

5.3.3 Isolation of outer medullary thick ascending limb of the loop of Henle cells

5.3.3.1 Cell Isolation procedure

Male WT mice of 5-7 weeks old were used for TAL cell isolation. Isolation of mTAL cells was performed as previously described (Eng et al., 2007). Mice were anesthetised with isofluorane and the kidneys were perfused with sterile 0.9% saline solution via retrograde perfusion of the aorta. Once the kidneys were excised they were cut along the corticopapillary axis, to expose the medulla. The inner strip of the outer medulla was then dissected out and minced with a sterile blade in 0.1% (w/v) collagenase solution (collagen type IV collagenase prepared in Hanks Balanced Saline) (Sigma Aldrich, Poole, UK and Gibco®,

Paisley, UK) that was gassed with 95% oxygen. The pulp was then incubated for ten minutes at 37°C. The cell suspension was sedimented on ice and mixed with Hanks Balanced Saline (HBSS) containing 2% (w/v) BSA, and the crude suspension of tubles was collected. The remaining undigested tissue was collagenase treated a further three times. The combined supernatants were spun at a low speed (1000 RPM) for ten minutes, and resuspended in HBSS. The resuspension was passed over a 52µm nylon mesh membrane (Fisher Scientific, Loughborough, UK). The filtered solution was discarded and the tubules collected on the mesh were washed with HBSS and centrifuged for 5 minutes at a low speed (500 RPM). The supernatant was aspirated and the cells were resuspended with Clonetics™ REGM™ growth media supplemented with the growth factor BulletKit™ (CC-3190): hEGF, 0.5 ml; hydrocortisone, 0.5 ml; epinephrine, 0.5 ml; insulin, 0.5 ml; triiodothyronine 0.5 ml; transferrin, 0.5 ml; GA- 1000, 0.5 ml; FBS, 2.5 ml. The tubule suspension was then aliquoted onto a four wells of a six well plate containing individual cell culture inserts (BD Biosciences, Oxford, UK), to insure polarisation. The cells were grown to approximately 70% confluence prior to any experiment, with fresh media changes every 48 hours.

5.3.3.2 *UMOD* knockdown

Mouse TAL cells were cultured from WT mice only as cells from KO mice did not culture beyond 30 % confluence. As a representation WT TAL cells were treated ±siRNA to knock down *UMOD*. Upon confluence, mouse TAL cells underwent transient siRNAoligo-mediated *UMOD* gene silencing over a 4 hour period. Constituents of the transfection reaction per well are as follows: 500 µl Optimem®, 10 nM siRNA (*UMOD* siRNA, Cy™3 negative control, or *GAPDH* (Ambion, Manchester, UK)), and Lipofectamine®2000 at a 3:1 ratio (Lipofectamine®2000: siRNA). The transfection mix was added to the insert containing the cells and the well under the insert on each plate. Reactions were performed in triplicate and each experiment was repeated 3 times. Following the 4 hour silencing period normal growth media replaced the transfection mix on cell cultures for 4 hours with incubation at 37°C, followed by overnight quiescing with RPMI 1640 media (Gibco, Manchester, UK). The optimum conditions for transient delivery of *UMOD* siRNA into TAL cells was assessed using siRNA that targeted *GAPDH* and Cy™3, as positive and negative controls respectively. Each siRNA was transfected separately into TAL cell cultures as

described above at the following concentrations: 5 nM, 10 nM, 15 nM, 20 nM, 30 nM, 50 nM, and 100 nM. RNA was isolated as per section 2.3.8 and *GAPDH* and *UMOD* measured by qRT-PCR (2.4) with Applied biosystems Taqman® assay probes (NM_0094804, and NM_008084.2; *UMOD* and *GAPDH* respectively). Protein levels of UMOD were assessed (2.7) using antibodies summarised in **Table 5-2**.

5.3.3.3 TNF-α stimulation

Following siRNAoligo-mediated *UMOD* gene silencing, RPMI 1640 media was removed and cell cultures were treated ± with TNF-α (5 nM) (Peprotech New Jersey, USA) for a six hour period in fresh RPMI 1640 media.

5.3.3.4 Cell culture conditions

The knock down of *UMOD* in WT TAL cells and incubations with TNF-α gave rise to the following cell culture conditions; scrambled control (WT cells treated with 10 nM negative control siRNA), scrambled control + TNF-α (WT TAL cells treated with 10 nM negative control siRNA + TNF-α (5 nM)), siRNA treated cells (WT TAL cells treated with *UMOD* siRNA (10 nM)), and siRNA treated cells + TNF-α (WT TAL cells treated with 10 nM *UMOD* siRNA + TNF-α (5 nM)).

5.3.3.5 Immunocytochemistry

For immunocytochemistry cells seeded directly onto two chamber tissue culture treated glass slides (BD Biosciences Oxford, UK). The cells cultures were washed several times with PBS, fixed with freshly prepared 4% paraformaldehyde in PBS for 1 hour, and rinsed several times with fresh PBS. Cells were permeabilized with 0.1% Triton X-100 (v/v) in PBS for 1 hour at room temperature. Primary (Sheep anti-human Tamm Horsfall Protein, primary polyclonal antibody, Ab Sero Tec, Puchheim, Germany) and secondary antibodies (Donkey anti sheep conjugated with Alexa Fluor 488, Invitrogen, Paisley, UK) were diluted with PBS containing 0.1% FBS. Antibodies were diluted at a 1:1000. Primary antibodies were incubated overnight at 4°C, whilst secondary antibodies were incubated at room temperature (protected from light). After each sequence with either a primary or secondary antibody, the slides were washed five times with a high-salt solution containing 1% BSA and 2.3% NaCl in PBS (w/v), followed by a single wash with PBS. Cells were stained with 1 µg/ml 4,6-diamidino-2-phenylindole

(DAPI) (Sigma Aldrich, Poole, UK) for 5 minutes followed by a single wash with PBS. The glass slides were mounted with cover slips and fixed with DPX (Sigma Aldrich, Poole, UK). Slides were examined using a Nikon Microphot FXA microscope equipped for epifluorescence illumination. Nuclear and cytoplasmic fluorescence was measured by laser scanning cytometry (LSC) using UV and 488 nm wavelength argon ion lasers to excite the fluorescence of DAPI and Alexa Fluor 488. Nuclear colouring was based on blue fluorescence for DAPI and green for Alexa Fluor 488. The integrated value of green fluorescence represented *UMOD* immunofluorescence.

5.3.4 Immunohistochemistry

Kidney sections from WT and KO mice following 6 weeks ± 2% NaCl were analysed for expression of Na^+ transporters. A detailed outline of the procedure can be found in section 2.12.5. **Table 5-3** summarises the primary antibodies and dilutions/concentrations used. All antibodies were diluted in 1 % BSA (w/v) in PBS.

Table 5-3 Summary of antibodies, dilutions, and length of incubations used for Immunohistochemistry.

Antibody/Protein	Dilution/Incubation time	Source/Product number
UMOD	1:1000 / Overnight	Santa Cruz / sc-20631
NKCC2	1:500 / Overnight	Abcam / ab60301
TNF-α	1:1000 / 2 hours	Abcam / ab1793
Na^+/K^+ ATPase	1:500 / 2 hours	Abcam / ab7671

5.4 Results

5.4.1 Renal Na⁺ channel mRNA expression analysis

Analysis by qRT-PCR on RNA isolated from whole kidney and outer medulla revealed an increased *UMOD* expression in WT mice upon salt loading (1.00 ± 0.1 vs. 1.62 ± 0.2 and 1.00 ± 0.2 vs. 3.15 ± 2.4; relative expression in whole kidney and outer medulla, WT normal NaCl vs. WT +2% NaCl, *p=0.04, **p<0.001), whereas no expression was detected in renal tissue from KO mice (± 2% NaCl) **(Figure 5-1 A and B)**. Relative expression of *NKCC2* in whole kidney was not different between the strains (±2% NaCl) (1.00 ± 0.6, 1.42 ± 0.1, 1.33 ± 0.3, and 1.14 ± 0.1; WT normal NaCl, WT +2% NaCl, KO normal NaCl, and KO +2% NaCl respectively, p=0.8) **(Figure 5-1 C)**. Whereas, KO mice following 2% NaCl treatment resulted in a significantly reduced *NKCC2* expression in the outer medulla tissue (0.41 ± 0.2 vs. 1.00 ± 0.1, 1.42 ± 0.2, and 1.38 ± 0.1; KO +2% NaCl vs. WT normal NaCl, WT +2% NaCl, and KO normal salt, **p=0.003) **(Figure 5-1 D)**.

Relative expression levels of *NKCC2* isoforms (A, B, and F) were assessed in outer medulla tissue from WT and KO mice (±2% NaCl) **(Figure 5-2)**. *NKCC2*A was significantly increased in WT mice upon salt loading (1.00 ± 0.2 vs. 1.73 ± 0.2; WT normal salt vs. WT +2% NaCl,*p<0.05). Salt loading KO mice (+2% NaCl) resulted in lower *NKCC2*A expression compared to all groups (0.37 ± 0.1 vs. 1.00 ± 0.2 (‡p<0.001), 1.73 ± 0.2 (#p=0.001), and 0.60 ± 0.2 (*p<0.05); KO +2% NaCl vs. WT normal NaCl, WT +2% NaCl, and KO normal NaCl respectively)) **(Figure 5-2 A)**. *NKCC2*F was significantly increased in KO +2% NaCl vs. WT normal NaCl only (1.74 ± 0.2 vs.1.00 ± 0.2, KO +2% NaCl vs. WT normal NaCl, *p<0.05) **(Figure 5-2 B)**. *NKCC2*B mRNA expression levels demonstrated an approximate 4.5 fold increase in WT mice upon salt loading with 2% NaCl (1.00 ± 0.2 vs. 4.85 ± 0.1; WT normal NaCl vs. WT + 2% NaCl, ***p<0.0001). KO mice under normal NaCl conditions revealed attenuated expression of *NKCC2*B compared to the WT mice under normal NaCl conditions (1.00 ± 0.2 vs. 2.15 ± 0.2; WT normal NaCl vs. KO normal NaCl, **p=0.002). KO mice +2% NaCl had significantly reduced *NKCC2*B relative expression compared to the KO normal NaCl group and WT salt loaded mice (2% NaCl) (1.03 ± 0.2 vs. 2.15 ± 0.2, and 4.85 ± 0.1; KO +2% NaCl vs. KO normal NaCl and WT +2% NaCl, ***p<0.0001) **Figure 5-2 C)**.

Salt loading the WT mice with 2% NaCl resulted in an increased *ENaC* expression in whole kidney tissue (1.00 ± 0.06 vs. 1.70 ± 0.07; WT normal NaCl vs. WT +2% NaCl, *p<0.05). In the KO mice, under normal NaCl conditions, *ENac* expression was at similar levels to that of the salt loaded WT mice and was significantly increased compared to the non salt loaded WT mice (1.00 ± 0.06 vs. 1.85 ± 0.1; WT mice vs. KO mice (normal NaCl),*p<0.05). Salt loaded KO mice demonstrated a significant reduction in *ENac* expression in whole kidney tissue compared to all other groups (***p<0.0001) **(Figure 5-3 A)**. Outer medulla tissue from KO mice (+2% NaCl) demonstrated reduced *ENac* expression compared to the non salt loaded KO mice (normal NaCl) (1.93 ± 0.05 vs. 1.01 ± 0.2, KO mice vs. KO mice +2% NaCl, **p=0.001) **(Figure 5-3 B)**. Under normal NaCl conditions, levels of *Na$^+$ /K$^+$ ATPase a* in whole kidney tissue was increased in KO mice compared to the WT mice (2.30 ± 0.1 vs.1.00 ± 0.2, KO vs. WT, ‡p=0.0003). KO mice +2% NaCl had significantly increased expression levels of *Na$^+$ /K$^+$ ATPase a* compared to all groups (***p<0.0001) **(Figure 5-3 C)**. WT mice +2% NaCl had elevated expression of *Na$^+$ /K$^+$ ATPase a* in outer medulla tissue compared to all groups (***p<0.0001). Salt loaded KO mice had significantly reduced *Na$^+$ /K$^+$ ATPase a* expression compared to non salt loaded KO mice (*p<0.05) **(Figure 5-3 D)**. *Na$^+$ /K$^+$ ATPase β* levels in whole kidney tissue was not different between the groups (p=0.24) **(Figure 5-3 E)**. Whereas KO mice +2% NaCl had reduced expression levels of *Na$^+$ /K$^+$ ATPase β* in outer medulla tissue compared to all other groups (*p<0.05) **(Figure 5-3 F)**. Relative expression levels of *NHe3* were not altered in whole kidney tissue between the groups (p=0.26) **(Figure 5-3 G)**. KO mice under normal NaCl conditions had significantly increased *NHe3* expression in outer medulla tissue compared to all groups (***p<0.0001), which was attenuated upon 2% NaCl loading (**p<0.001) **(Figure 5-3 H)**. *ROMK* was undetected by qRT-PCR in whole kidney tissue from WT or KO mice (± 2% NaCl). Outer medulla levels of *ROMK* were reduced in KO mice upon salt loading compared with all groups (*p<0.05) **(Figure 5-3 I)**.
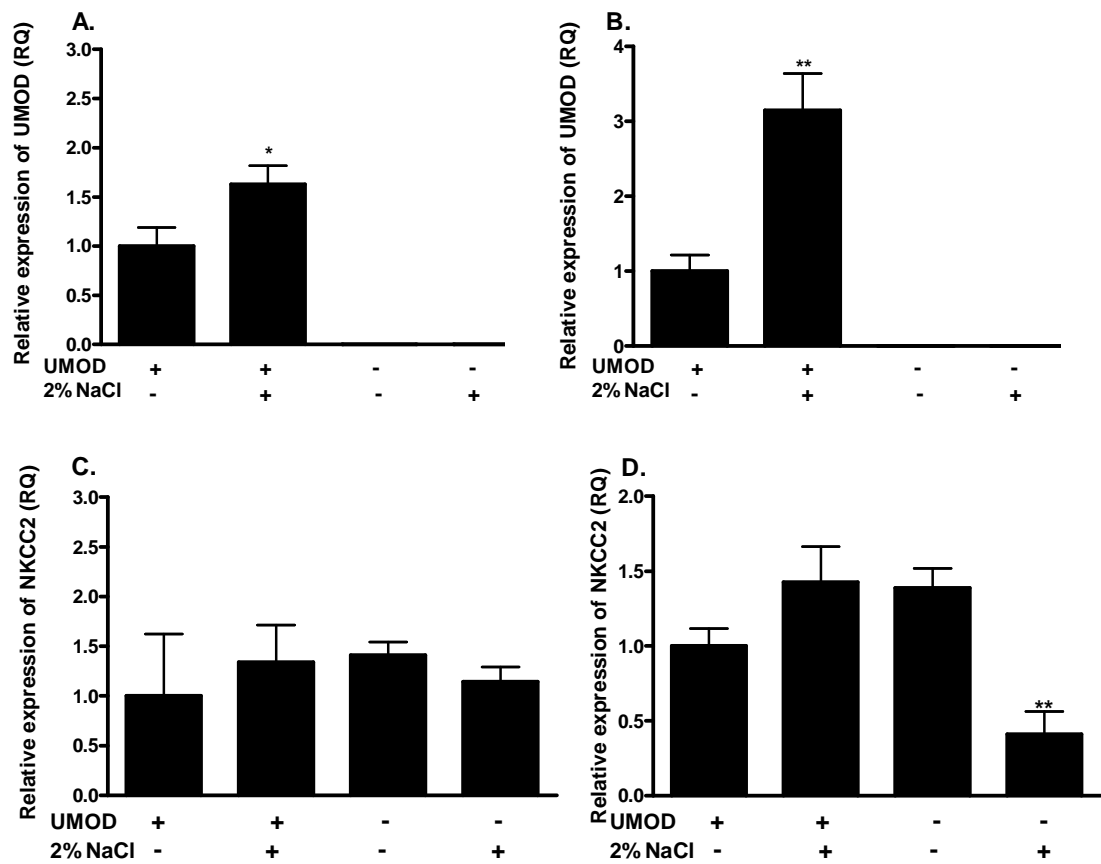
Figure 5-1 qRT-PCR analysis of *UMOD* and *NKCC2* in WT and KO mice (± 2% NaCl) from whole kidney (A and C) and outer medulla tissue (B and D).

RNA was extracted from snap frozen whole kidney and outer medulla tissue of male WT and KO mice (±2% NaCl). *UMOD* and NKCC2 mRNA abundance was by qRT-PCR using gene specific probes. *UMOD* mRNA abundance was is elevated in WT mice upon salt loading with 2% NaCl in both **(A)** whole kidney and **(B)** outer medulla tissue. **(C)** Relative expression of *NKCC2* was not different between the strains or altered by salt loading. **(D)** In the absence of *UMOD* and the addition of 2% NaCl resulted in a significant reduction in *NKCC2* expression. Data are shown as Mean RQ ± SEM (Cycle threshold values were normalised to β-actin mRNA and expressed relative to the WT mice under normal NaCl conditions), n=5 per group, *p=0.04, **p=0.001. Analysed by One way ANOVA followed by Tukey's post Hoc multiple comparison test.
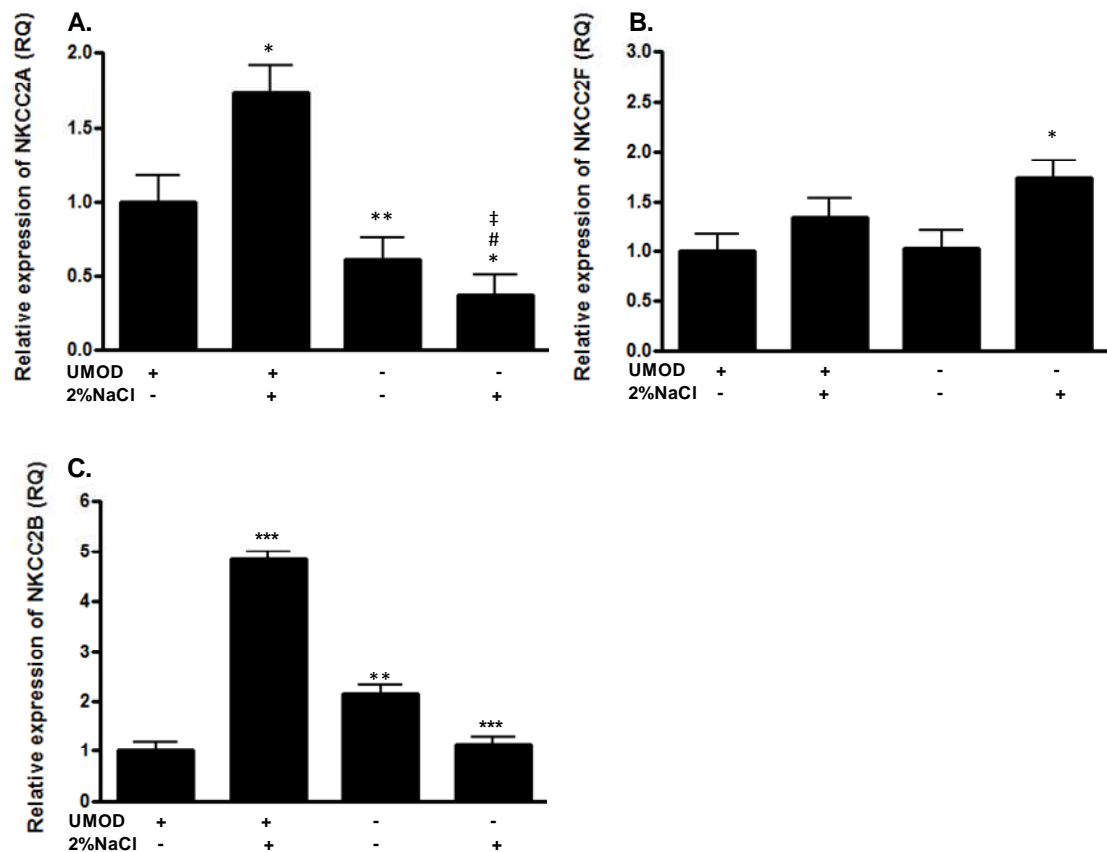
Figure 5-2 qRT-PCR analysis of the three major *NKCC2* isoforms; A, F, and B in WT and KO mice (± 2% NaCl) from outer medulla tissue.

RNA was extracted from snap frozen outer medulla tissue of WT and KO mice (±2% NaCl). NKCC2 A, B, and F mRNA abundance was assessed in outer medulla tissue by QPCR using gene specific primers. Salt loading with 2% NaCl resulted in significantly increased **(A)** *NKCC2*A and **(C)** *NKCC2*B expression in WT mice. In the absence of *UMOD* there was a significantly reduced **(A)** *NKCC2*A and **(C)** *NKCC2*B expression in KO mice, which was further attenuated upon NaCl loading. **(B)** *NKCC2*F was not changed in WT mice ± 2% NaCl, whereas KO mice had increased expression when salt loaded. Data are shown as Mean RQ ± SEM (Cycle threshold values were normalised to β-actin mRNA and expressed relative to the WT mice under normal NaCl conditions) n=5 per group,*p<0.05 (KO normal salt vs. KO salt loaded), **p<0.002 (KO normal salt vs. WT salt loaded), ***p<0.0001 (WT normal salt vs. WT salt loaded and KO salt loaded vs. KO normal salt and WT salt loaded), ‡ p<0.001 (KO salt loaded vs. WT normal salt), and #p<0.0001 (KO salt loaded vs. WT salt loaded). Analysed by One way ANOVA followed by Tukey's post Hoc multiple comparison test.
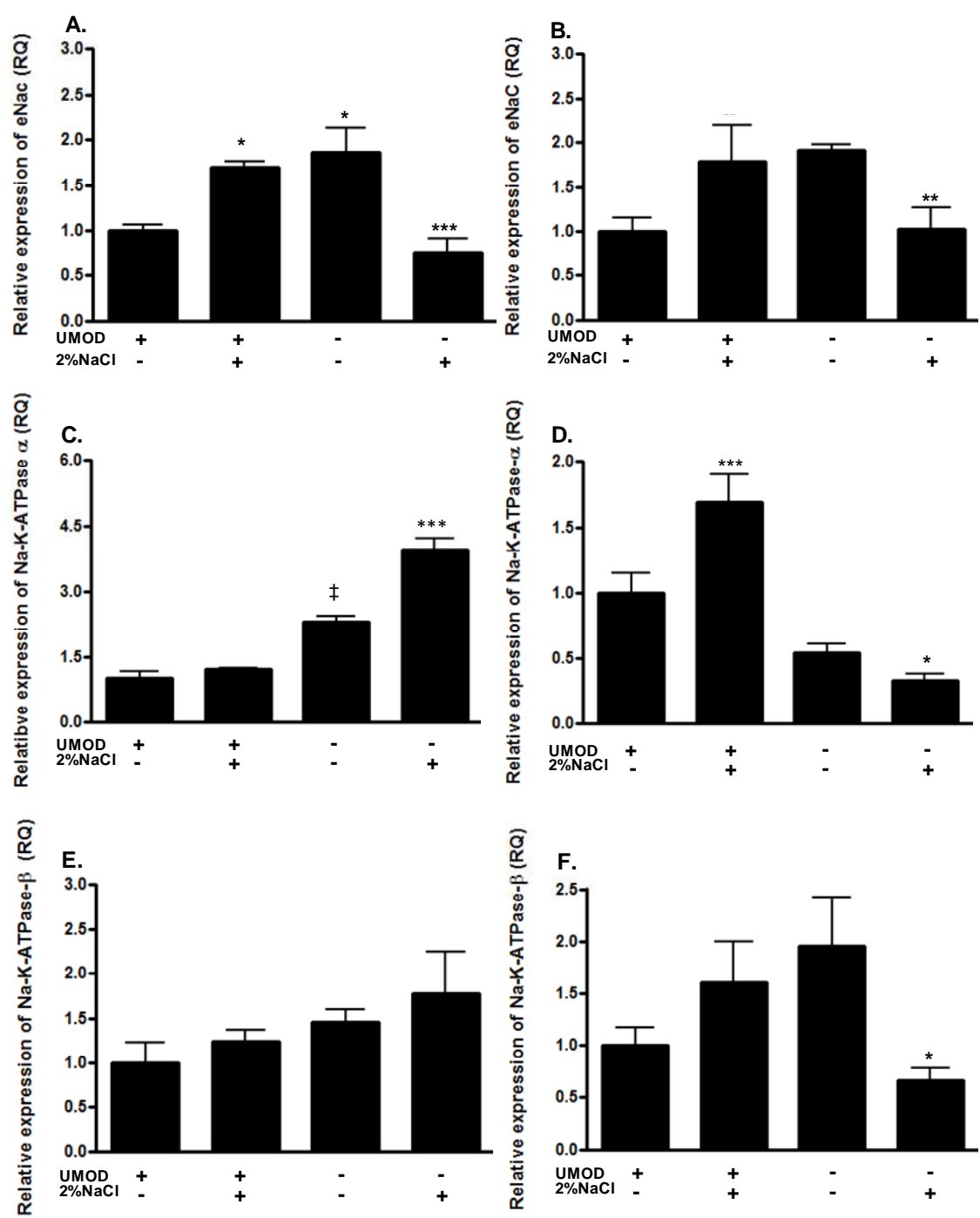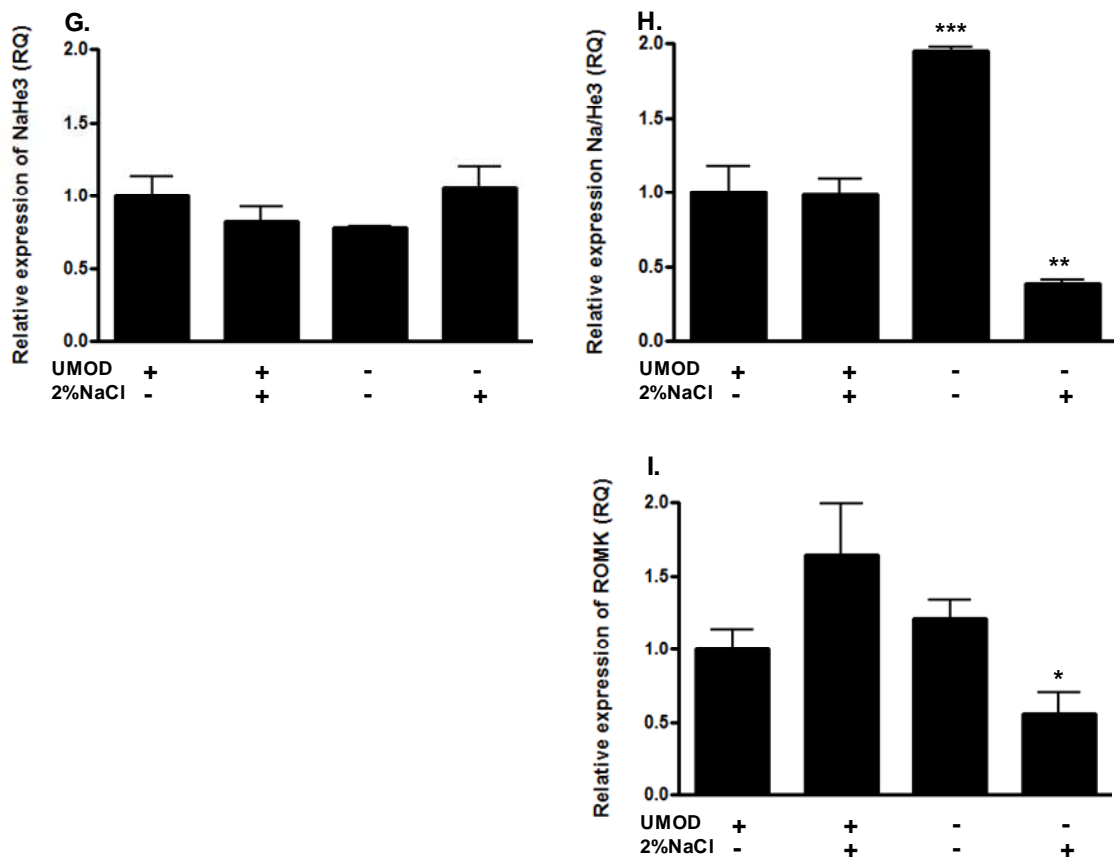
Figure 5-3 qRT-PCR analysis of TAL Na+ channels from whole kidney (A, C, E, and G) and outer medulla tissue (B, D, F, H, and I) in WT and KO mice (± 2% NaCl).

RNA was extracted from snap frozen whole kidney and outer medulla tissue of WT and KO mice (±2% NaCl). The TAL transporter mRNA abundance was assessed by qRT-PCR using gene specific probes. **(A)** WT mice displayed increased *ENac* expression in whole kidney when salt loaded (2% NaCl). KO mice under normal NaCl conditions had increased expression to comparable levels as salt loaded WT mice, which was attenuated with 2% NaCl stimulation. **(B)** In outer medulla tissue the KO mice +2% NaCl had reduced *ENac* expression. **(C)** Na^+ /K^+ ATPase α mRNA abundance in whole kidney was increased in KO mice under normal and 2% NaCl conditions. **(D)** However, was reduced in KO mice when assessed in outer medulla tissue upon salt loading. WT mice upon salt loading displayed increased expression of Na^+ /K^+ ATPase α. **(E)** Na^+ /K^+ ATPase β was not different between the strains or conditions in whole kidney tissue. **(F)** The KO mice +2% NaCl revealed reduced levels of Na^+ /K^+ ATPase β in the outer medulla tissue. **(G)** *NHe3* was not altered between the strains ± 2% NaCl in whole kidney tissue. **(H)** However in outer medulla tissue salt loading increased expression in WT mice but reduced levels in KO mice. **(I)** *ROMK* was only detected in outer medulla tissue revealing reductions in mRNA abundance in KO salt loaded mice. Data are shown as Mean RQ ± SEM (Cycle threshold values were normalised to β-actin mRNA and expressed relative to the WT mice under normal NaCl conditions) n=5 per group,*p<0.05, **p<0.001, ‡ p=0.003, ***p<0.0001. Analysed by One way ANOVA followed by Tukey's post Hoc multiple comparison test.

5.4.2 Renal Na⁺ channel protein expression analysis

Following mRNA expression analysis protein analysis was utilised to assess Na^+ $/K^+$ ATPase, NKCC2, ENaC, and ROMK from whole kidney tissue in WT and KO mice to reveal no difference between the strains under normal NaCl or 2% NaCl conditions **(Figure 5-4).** Representative immunoblots are shown in **(Figure 5-4 A).** Protein expression was determined by densitometry in n=2 for salt loaded animals and n=3 for normal NaCl treated animals; statistical analysis was not performed **(Figure 5-4 B-E).**

5.4.3 Interactions between UMOD, TNF-α and NKCC2 in the TAL.

Under normal NaCl conditions, urinary TNF-α levels were significantly greater in KO mice compared to WT (4.61 ± 0.09 pg/24h vs. 34.95 ± 0.05 pg/24h; WT vs. KO mice, n=5 per group, **p<0.001). Salt intake over a 6 week period increased the levels of urinary TNF-α in both WT and KO mice (4.61 ± 0.09 pg/24h vs. 29.97 ± 0.01 pg/24h and 34.95 ± 0.05 pg/24h vs. 163.13 ± 0.01 pg/24h; WT normal NaCl vs. WT +2% NaCl and KO normal NaCl vs. KO +2% NaCl respectively, n=5 per group, **p<0.001 and ***p<0.0001). This increase was approximately 5-fold in the KO mice upon salt loading (***p<0.0001) **(Figure 5-5 A).**

QRT-PCR on RNA isolated from kidney outer medulla showed an increase in the abundance of *TNF-α* in both WT and KO animals on salt-loading, reaching statistical significance in KO mice (1.39 ± 0.2 vs. 2.51 ± 0.5; KO normal NaCl vs. KO +2% NaCl, n=5 per group,*p=0.01) **(Figure 5-5 B).** The mRNA abundance of the *NKCC2*A was measured in mouse TAL cells ± TNF-α stimulation, ± *UMOD* siRNA. In the presence of *UMOD,* stimulation with TNF-α decreased relative *NKCC2*A mRNA levels (1.00 ± 0.03 vs. 0.51 ± 0.08; WT cells vs. cells + TNF-α stimulation, **p<0.001, n=3). *UMOD* knockdown caused an even greater reduction in *NKCC2*A transcript levels (1.00 ± 0.03 vs. 0.26 ± 0.2, WT cells vs. cells + *UMOD* siRNA treatment, ***p<0.0001, n=3) that could not be further lowered by the addition of exogenous TNF-α **(Figure 5-5 C).** In mTAL cells, stimulation with TNF-α was found to increase the relative levels of *UMOD* mRNA by approximately 3.5-fold (***p<0.0001, n=3) **(Figure 5-5 D).** Immunocytochemistry confirms the knockdown of *UMOD* in WT mTAL cells **(Figure 5-5 E).** Suggesting TNF-α can reduce the levels of NKCC2A mRNA in primary mTAL cells, and that this effect is enhanced in the absence of *UMOD*.

Stimulation with TNF-α was found to increase the relative levels of UMOD mRNA, creating a negative feedback loop in which the TNF-α induced reduction in NKCC2A gene expression is switched off through increasing the production of cell-surface *UMOD*. Ultimately, suggesting that *UMOD* acts as a negative regulator of TNF-α production by the TAL to maintain NaCl homeostasis.

Protein expression levels of the Na^+ transporters were assessed in outer medulla tissue from WT and KO mice ± 2% NaCl **(Figure 5-6)**, representative immunoblots are shown in **Figure 5-6 A**. The addition of 2% NaCl increased UMOD expression in outer medulla tissue of WT mice by approximately 1.34 fold compared to the WT normal NaCl animals (54.63 ± 1.9 % intensity vs. 40.67 ± 1.9 % intensity, n=5 per group, **p<0.001) **(Figure 5-6 B)**. Expression levels of NKKC2 were increased in WT salt loaded mice compared to WT mice under normal NaCl conditions although did not reach statistical significance (58.29 ± 0.8 % intensity vs. 52.36 ± 2.1 % intensity, n=5 per group, *p<0.01). Salt loading the KO mice resulted in reduced NKCC2 expression compared to the normal NaCl treated KO animals (41.39 ± 4.1 % intensity vs. 28.99 ± 1.5 % intensity, n=5 per group, #p<0.05) **(Figure 5-6 C)**. There was an attenuated NKCC2 expression in salt loaded KO mice in comparison to salt loaded WT mice (28.99 ± 1.5 % intensity, n=5 per group, **p<0.01) **(Figure 5-6 C)**. Levels of TNF-α were significantly increased in both mouse strains following salt loading with 2% NaCl (18.25 ± 1.1 % intensity vs. 34.23 ± 7.1 % intensity; WT normal NaCl vs. WT + 2% NaCl and 10.09 ± 1.8 % intensity vs. 54.08 ± 1.9 % intensity; KO normal NaCl vs. KO + 2% NaCl, n=5 per group, *p<0.01, **p<0.001) **(Figure 5-6 D)**.

Protein levels of UMOD, TNF-α, and NKCC2 were determined in TAL cells in which *UMOD* was silenced **(Figure 5-7)**. Representative immunoblots are shown in **Figure 5-7 A**. UMOD protein levels were successfully knocked down in WT mouse TAL cells by addition of *UMOD* siRNA (10 nM) (86.02 ± 1.0 % intensity vs. 5.28 ± 1.1 % intensity and 126.26 ± 1.8% intensity vs. 5.11 ± 3.7 % intensity; scrambled control treated cells vs. scramble + TNF-α treated cells, *UMOD* siRNA treated cells vs. UMOD siRNA treated cells + TNF-α respectively, ‡** p<0.001, n=3). Incubation of TAL cells for 6 hours with TNF-a (5 nM) increased the relative protein levels of UMOD by approximately 1.46 fold than cells treated with

scrambled siRNA only (n=3, **p<0.001) but not in cells in which UMOD mRNA was silenced with UMOD siRNA **(Figure 5-7 B)**. Total NKCC2 protein expression was increased in scramble control treated cells when incubated with TNF-α by approximately 1.4 fold compared to scramble control treated cells (n=3, **p<0.001). NKKC2 protein levels were reduced when *UMOD* expression was knocked down by siRNA (55.10 ± 2.1 % intensity vs. 96.14 ± 0.8 % intensity, n=3, **p<0.001). In the absence of *UMOD* and stimulation with TNF-α further reduced NKCC2 protein expression (21.09 ± 3.2 % intensity vs. 55.10 ± 2.1% intensity, n=3, **p<0.001) which was significantly lower compared to all other conditions (# p<0.001) **(Figure 5-7 C)**. TNF-α protein levels were assessed in cells treated ± *UMOD* siRNA only. TNF-α expression was increased in TAL cells that had *UMOD* knocked down by siRNA compared to scramble control treated cells (93.34 ± 1.7 % intensity vs. 87.73 ± 0.8 % intensity; UMOD siRNA treated cells vs. scramble treated cells, n=3, *p=0.03) **(Figure 5-7 D)**.
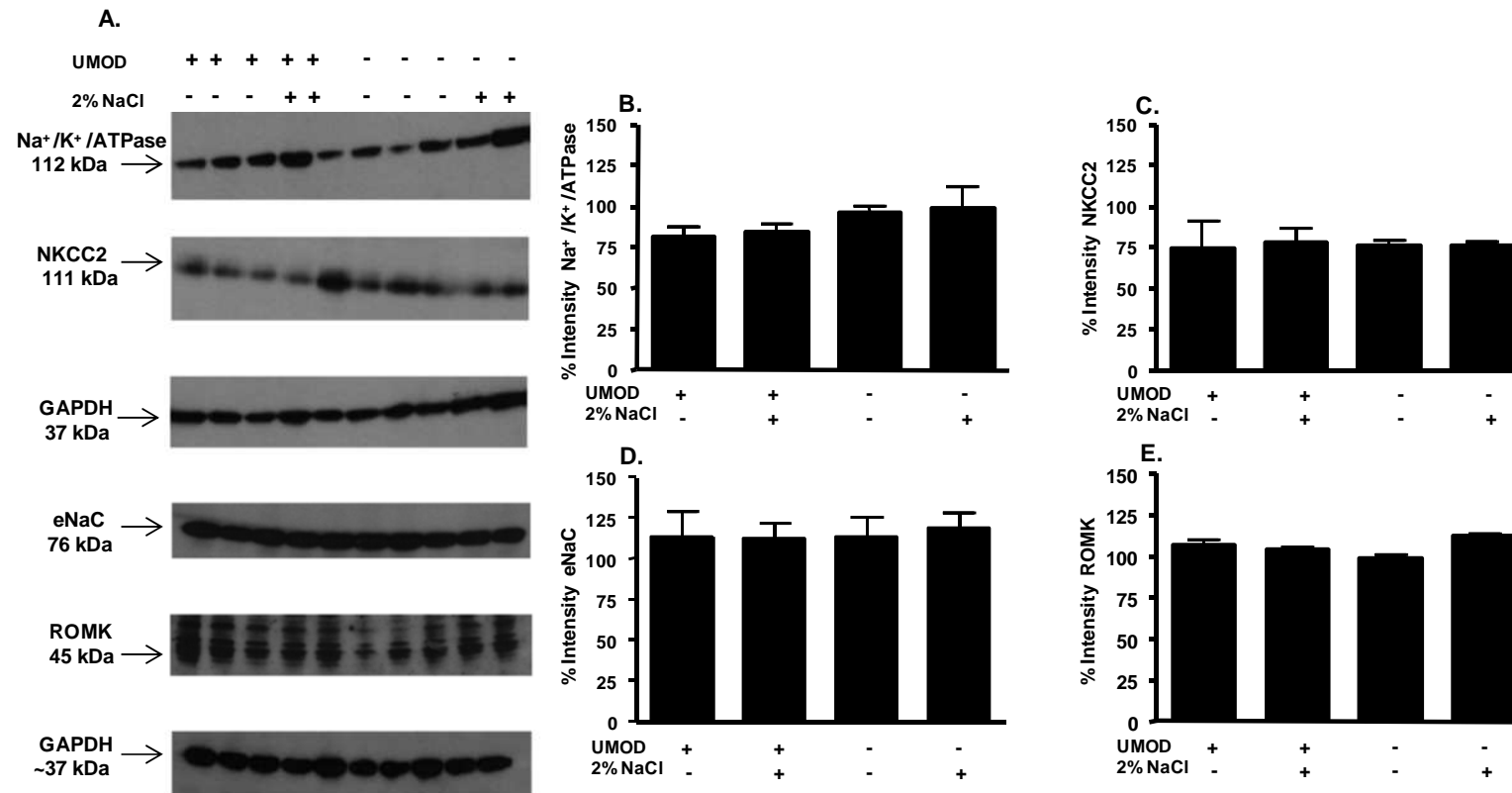
Figure 5-4 Western blot analysis of Na$^+$ transport channels in WT and KO mice (±2% NaCl) from whole kidney tissue.

Protein lysates from snap frozen whole kidney tissue from male WT and KO mice (±2%NaCl) was prepared, quantified, electrophoreses, blotted, and probed for the main TAL Na$^+$ transporters. **(A)** Representative Immunoblots. Densitometry showed no difference in protein expression levels of **(B)** Na$^+$/K$^+$ ATPase, **(C)** NKCC2, **(D)** ENac, or **(E)** ROMK between the WT and KO mice (±2% NaCl). GAPDH demonstrates equivalent sample loading and expression levels are displayed as % intensity normalised to GAPDH (Mean ± SEM). All data sets were measured by densitometry using the global background subtraction method
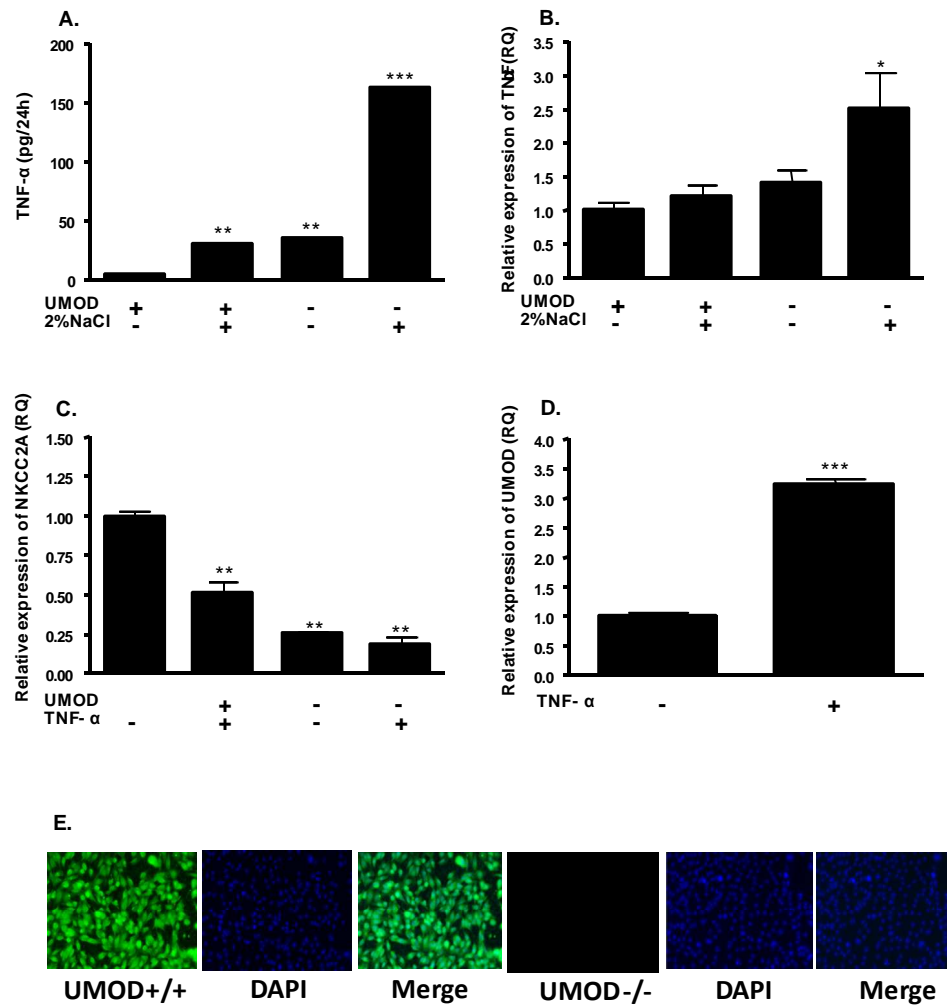
Figure 5-5 Investigation into the relationship between UMOD and TNF-α.

Urine samples collected from male WT and KO mice following 6 weeks ±2% NaCl were assessed for levels of TNF-α by ELISA. **(A)** KO mice have significantly increased urinary TNF-α levels under salt loading conditions (+2% NaCl) compared to all groups, ***p<0.0001. WT mice also have significantly increased urinary TNF-α levels following salt loading, **p<0.001. All data expressed as Mean ± SEM, n=5 per group and analysed by One way ANOVA followed by Tukey's post hoc test. RNA was extracted from outer medulla tissue of WT and KO mice (±2% NaCl). *TNF-α* mRNA abundance was assessed by qRT-PCR using gene specific probes. **(B)** qRT-PCR showed an increase in the abundance of *TNF-α* gene in both WT and KO mice on salt-loading, reaching statistical significance in KO mice (*p=0.01), n=3 per group, data shown as Mean RQ ± SEM, analysed via student T-test. TAL cells from male WT mice were extracted and cultured for 6 days. Cells were then treated ±10nM *UMOD* siRNA for 4 hours, followed by ±5 nM TNF-α for 6 hours. NKCC2 A, and *TNF-α* mRNA abundance were assessed by qRT-PCR using gene specific probes. **(C)** In the presence of *UMOD*, stimulation with TNF-α decreased relative *NKCC2*A mRNA levels (**p<0.001, n=3). *UMOD* knockdown caused a greater reduction in *NKCC2*A transcript levels (***p<0.0001, n=3) that could not be further lowered by the addition of exogenous TNF-α. Data are expressed as Mean RQ ± SEM, n=3 per group and analysed by One way ANOVA followed by Tukey's post hoc test. **(D)** Simulation of mTAL cells with 5 nM TNF-α caused an increase in the relative levels of *UMOD* mRNA by approximately 3.5-fold (***p<0.0001, n=3) data shown as Mean RQ ± SEM, analysed via student's T-test. **(E)** Immunocytochemistry confirms the knock down of *UMOD* in TAL cells (representative images are shown).
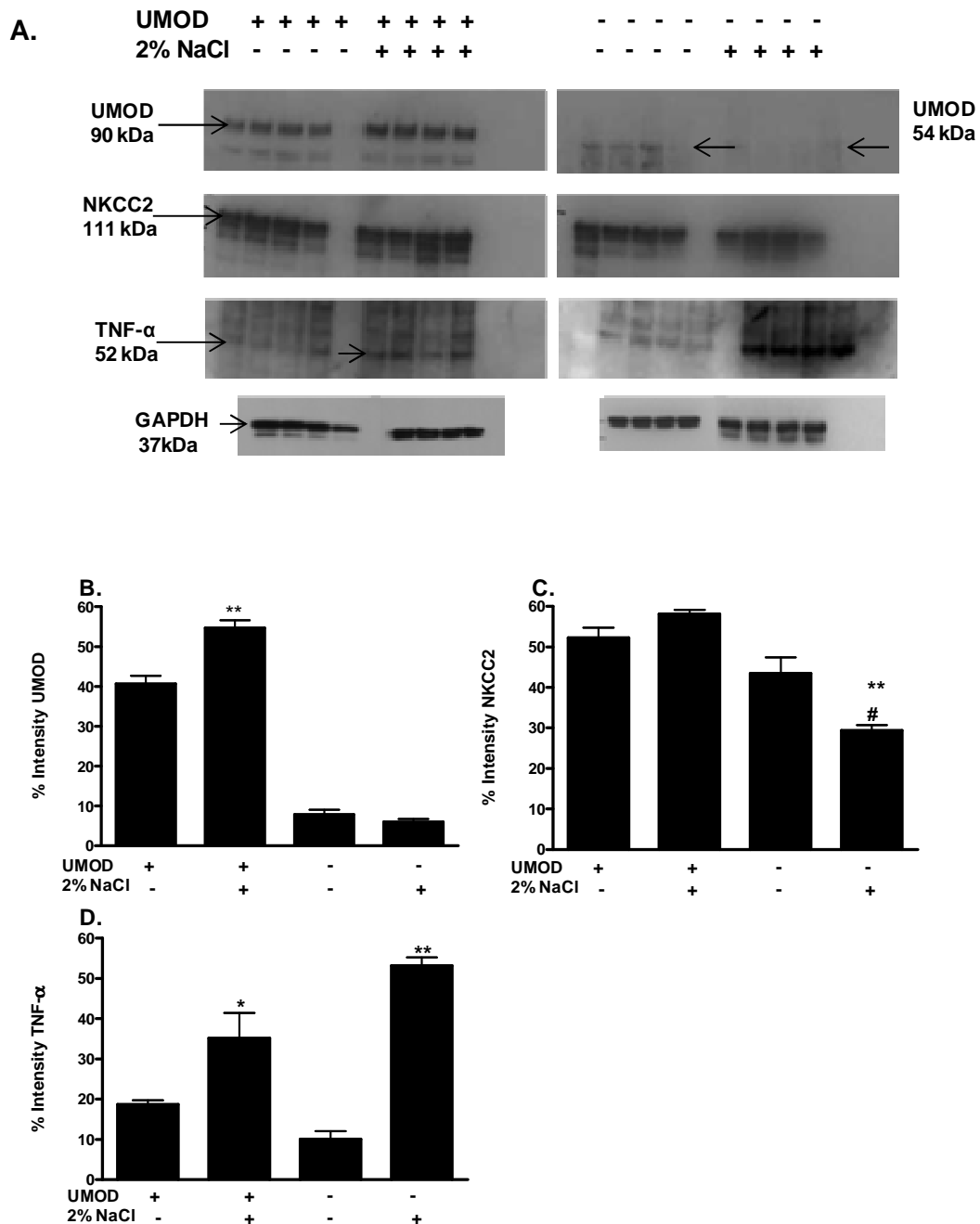
Figure 5-6 Western blot analysis of UMOD, NKCC2, and TNF-α from outer medulla tissue of WT and KO mice (± 2% NaCl).

Protein lysates from snap frozen outer medulla tissue from male WT and KO mice (±2%NaCl) was prepared, quantified, electrophoreses, blotted, and probed for UMOD, NKCC2, and TNF-α. **(A)** Representative Immunoblots. **(B)** Salt loading significantly increase protein expression levels of UMOD in outer medulla tissue of WT mice (n=5 per group, **p<0.001). **(C)** NKCC2 protein levels were attenuated in KO mice upon salt loading (KO normal vs. KO +2%NaCl, n=5 per group, #p<0.05 and WT mice +2%NaCl vs. KO mice +2%NaCl, n=5 per group, **p<0.01). **(D)** TNF-α levels were increased in both mouse strains upon salt loading (n=5 per group, *p<0.05, **p<0.001). GAPDh demonstrates equivalent sample loading and expression levels are displayed as % intensity normalised to GAPDH (Mean ± SEM). All data sets were measured by densitometry using the global background subtraction method for UMOD, NKCC2, and GAPDH however the local background subtraction method was used for measuring TNF-α as the background varied across the blot. Data sets were analysed by One way ANOVA followed by Tukey's post Hoc test.
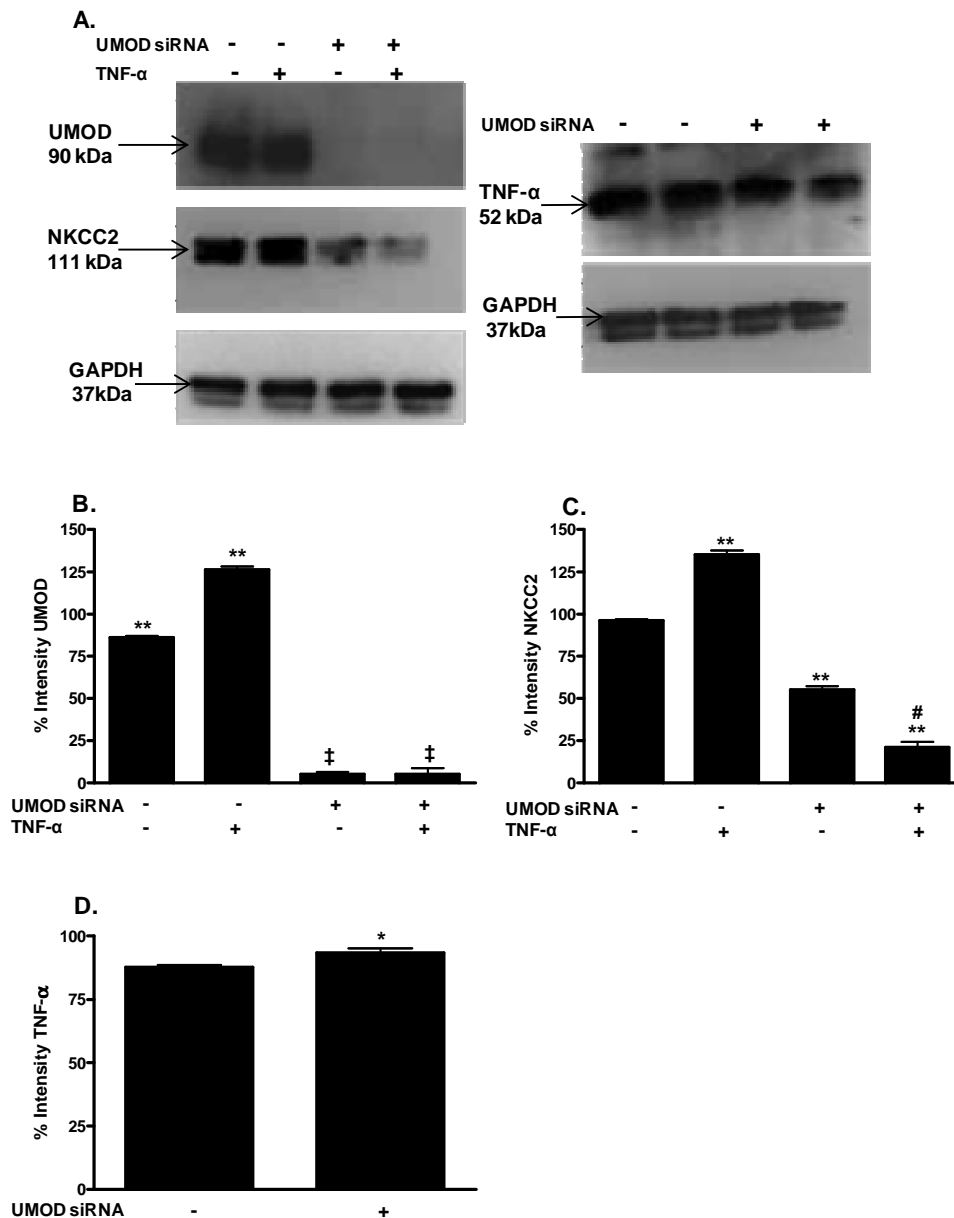
Figure 5-7 Western blot analysis of UMOD, NKCC2, and TNF-α from TAL cells ± *UMOD* siRNA.

Protein lysates from TAL cells from male WT (± *UMOD* siRNA (10nM) and TNF-α (5nM)) were prepared, quantified, electrophoreses, blotted, and probed for UMOD, NKCC2, and TNF-α **(A)** Representative Immunoblots. **(B)** The knock down of *UMOD* was successful in WT mouse TAL cells using siRNA (10 nM) by transient transfection and was not altered with the addition of TNF-α stimulation (5 nM) (‡ $p < 0.001$). WT cells (scrambled control siRNA (10 nM treated)) treated with TNF-α resulted in significantly increased *UMOD* expression levels (**$p < 0.001$). **(C)** Total NKCC2 protein levels were increased in TNF-α stimulated WT cells (**$p < 0.001$). In the absence of *UMOD* total NKCC2 protein expression levels were reduced ($p < 0.001$), which was further attenuated upon TNF-α stimulation compared to all other conditions (#$p < 0.001$). **(D)** TNF-α protein levels are increased in cells treated with siRNA to knock down UMOD compared to the WT cells treated with scrambled control siRNA (*$p = 0.03$). GAPDH demonstrates equivalent sample loading and expression levels are displayed as % intensity normalised to GAPDH (Mean ± SEM). All data sets were measured by densitometry using the global background subtraction method. Cell experiments were represent Mean ± SEM, n=3 independent replicates. Data analysed by One way ANOVA followed by Tukey's post hoc test.

5.4.4 Immunohistochemistry

Immunohistochemistry for UMOD showed strong staining in the WT mice in the outer medulla specifically at the TAL. Weak tubular staining was apparent in the KO mice with distribution in the outer medulla. On a cellular level UMOD staining was positive in the WT mice and accentuated in the apical region. In contrast, cells in knockout animals only showed positivity in the basolateral and middle cellular regions. Salt-loading increased the intensity of UMOD staining in the WT animals but did not affect the staining pattern in the KO strain **(Figure 5-8)**.

NKCC2 staining clearly demonstrates localisation at the apical membrane of the TAL within the inner stripe of the outer medulla in both strains. KO mice illustrate weaker staining intensity than the WT mice under normal NaCl conditions. An increase of NKCC2 stain intensity can be appreciated at the apical membrane of kidney section of salt loaded (2% NaCl) WT mice. In contrast, KO mice +2% NaCl display dramatic reductions in staining intensity **(Figure 5-9)**.

WT and KO mouse kidney sections stained for TNF-α demonstrates increased staining is found highly expressed in the interstitium between the nephron segments. At 20x magnification it can be seen that TNF-α staining is more concentrated in the KO mice under basal conditions. Both mouse strains upon salt loading displayed increase signal intensity, however abundance is more apparent in the KO salt loaded mice **(Figure 5-10)**.
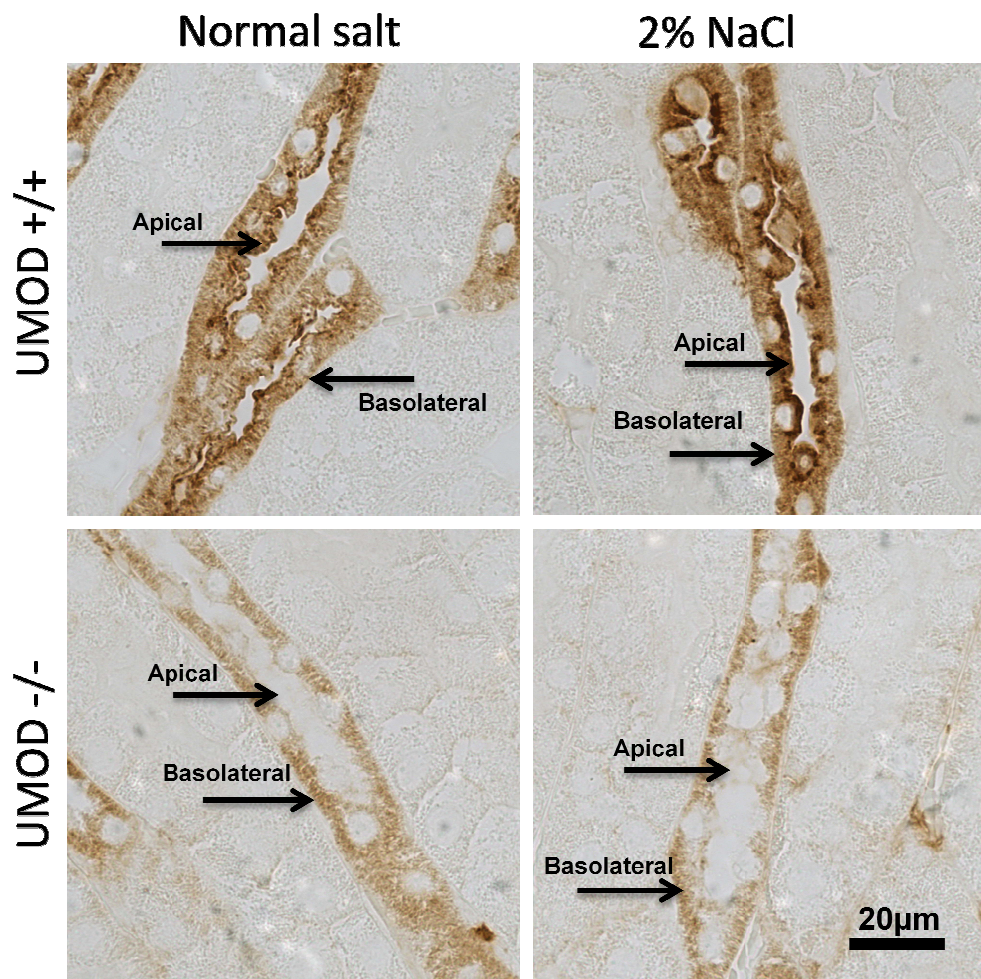
Figure 5-8 Immunohistochemical staining for UMOD in kidney sections of WT and KO mice (± 2% NaCl).

Paraffin embedded kidney tissue from WT and KO mice (±2% NaCl) were sectioned at 3µm thick and stained to investigate the localisation of UMOD. Immunohistochemistry for UMOD in WT (± 2% NaCl) revealed clear staining in the thick ascending limb of the outer medulla. The cellular distribution is different between strains with apical distribution in WT mice. Staining is much weaker in KO mice and only seen in the basolateral membrane and middle regions of the cells. Shown are x 40 magnification fields of representative kidney sections (scale bar 20µm). Staining was not quantified. Black arrows represent the position of the apical and basolateral membranes.
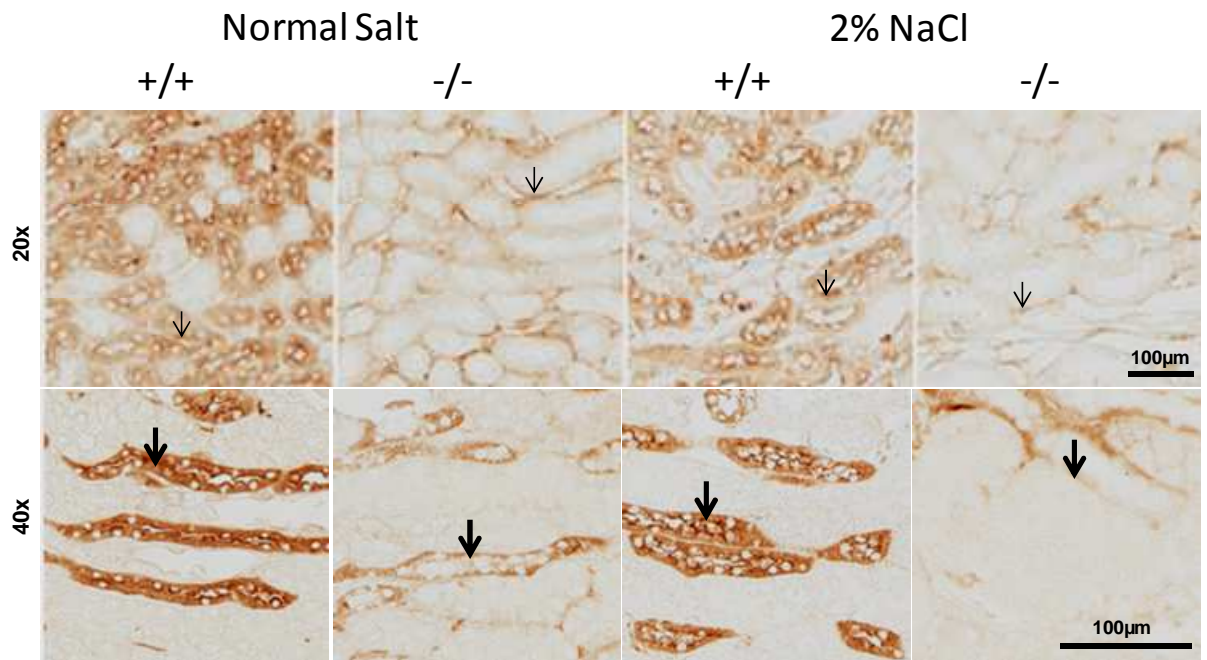
Figure 5-9 Immunohistochemical staining for NKCC2 in kidney section of WT and KO mice (± 2% NaCl).

Paraffin embedded kidney tissue from WT and KO mice (±2% NaCl) were sectioned at 3μm thick and stained to investigate the localisation of NKCC2. Immunohistochemistry for NKCC2 demonstrates staining is localised to the apical membrane at the TAL in both mouse strains under normal NaCl conditions, however weaker staining is apparent in the KO mice. Shown are 20x and 40x magnification fields of representative kidney sections (scale bars represent 100μm).Staining was not quantified. Black arrows indicate the position of the apical membrane.
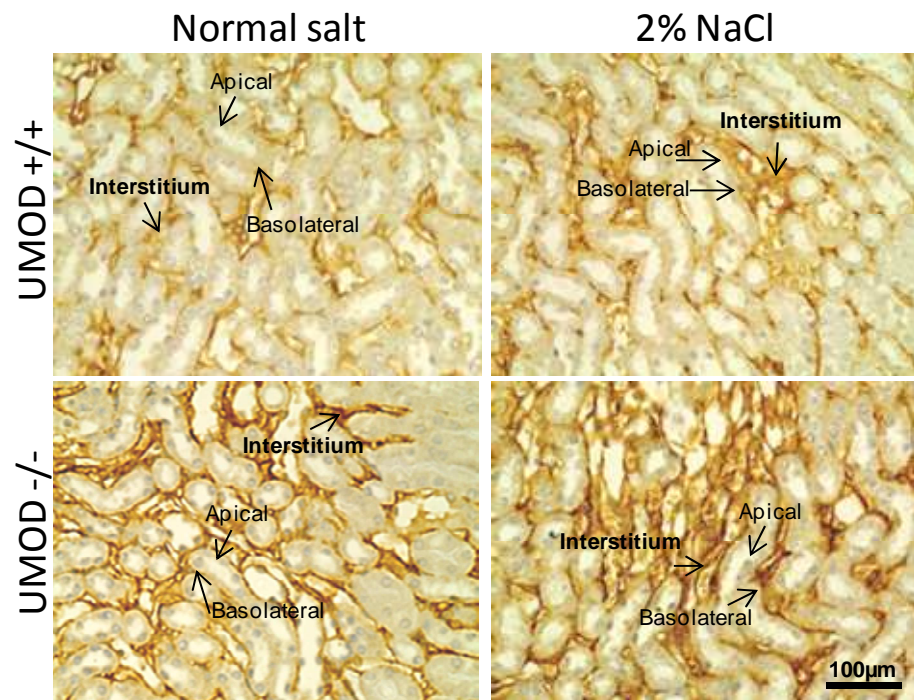
Figure 5-10 Immunohistochemical staining for TNF-α in kidney section of WT and KO mice (± 2% NaCl).

Paraffin embedded kidney tissue from WT and KO mice (±2% NaCl) were sectioned at 3µm thick and stained to investigate the localisation of TNF-α. The distribution of the TNF-α stain can be seen in the interstitium between the nephron segments. Staining patterns are similar between the strains with more intensity in the KO. Staining is more prevalent in both strains upon salt loading, with KO mice displaying increased staining compared to that of the salt loaded WT mice. Shown are 20x magnification fields of representative kidney sections (scale bar represents 100µm). Staining was not quantified. Black arrows indicate the region of the interstitium, apical and basolateral membranes.

5.5 Discussion

Experimental work in this chapter explored differential expression analysis of the major Na$^+$ handling transporters in the kidney of WT and KO mice before and after 6 weeks of salt loading, to determine the role of *UMOD* in sodium homeostasis and blood pressure regulation. Results have demonstrated that *UMOD* plays a direct role in sodium handling by mediating levels of TNF-α at the TAL, maintaining control of Na$^+$ reabsorption via modulation of NKCC2 providing evidence of a novel functional pathway of BP regulation by *UMOD* that impacts renal sodium/volume homeostasis.

Normally, the kidney synthesises large quantities of UMOD and urinary excretion is used as an indicator for renal tubular function (Torffvit et al., 1998). A positive correlation between urinary UMOD and dietary salt intake demonstrates that in subjects with high salt sensitivity, there is a greater excretion of UMOD than in the urine of low salt intake (Torffvit et al., 2004). This implies that reduced synthesis of the protein may cause or reflect renal dysfunction. Indeed, urinary UMOD reductions have been implicated in pathological conditions such as acute tubular necrosis, diabetic nephropathy, hyperprostaglandin E syndrome triggered by inflammatory cytokines, and active lupus nephritis (Bernard et al., 1987, McLaughlin et al., 1993, Schroter et al., 1993, Tsai et al., 2000). In addition, urinary UMOD excretion is said to be reduced in patients with *UMOD* mutations responsible for the 3 autosomal dominant tubulo-interstitial nephropathies; medullary cystic kidney disease type 2, familial juvenile hyperuricemic nephropathy, and glomerulocystic kidney disease which are postulated to cause misfolding and impair trafficking of UMOD inhibiting its actions at the apical membrane (Williams et al., 2009). However, there is a lack of reports in the literature examining renal tissue samples to explore the roles of *UMOD* expression and physiological function in these conditions. Therefore, in the clinic urinary UMOD seems to be an accessible marker to assess renal disease although still does not explain functional roles of the gene.

Accordingly, a lower UMOD excretion (either genetically or acquired) is associated with less sodium reabsorption implicating the role of UMOD in sodium homeostasis. To test this hypothesis the effects of salt loading may elucidate its

function further. Ying *et al* studied dietary salt effects on renal *UMOD* expression in rats and reported that salt loading increased mRNA expression levels, additionally furosemide treatment alongside 8% NaCl loading further augmented *UMOD* expression along with increased luminal NaCl (Ying and Sanders, 1998). These findings suggest that high salt intake may directly promote self aggregation of UMOD at the apical surface, forming a highly negatively charged, hydrophobic, gel like barrier in an attempt to regulate NaCl uptake at the TAL, thus maintaining electrolyte flux. These findings are consistent with the results in this chapter; relative *UMOD* mRNA levels demonstrated a significant increase when measured in whole kidney from WT mice upon salt loading. The augmented expression was further enhanced by approximately 2 fold when assessed in outer medulla tissue, suggesting a dilution effect when assessing whole kidney as UMOD is exclusive to the TAL. Alongside the reported increased *UMOD* mRNA abundance in the outer medulla tissue from WT mice, there was also an increased expression of total NKCC2 with 2% NaCl in this strain.

Previous immunolocalisation experiments revealed that NKCC2 is expressed at the apical cell surface and also in subapical vesicles, where intracellular trafficking regulates NKCC2 membrane expression. Vasopressin has been shown to shuttle the subapical vesicles of NKCC2 to the apical surface, leading to enhanced activity and expression levels (Gimenez and Forbush, 2003). The transporter undergoes constitutive exocytosis at the TAL (Caceres et al., 2009) suggesting NKCC2 trafficking is a continuous dynamic process rather than a triggered event. Ares *et al* studied endocytosis and recycling of NKCC2 in the absence of stimuli and reported that NKCC2 undergoes retrieval from the plasma membrane at a rate that closely matches the reported exocytosis insertion (Ares et al., 2011). These reports suggest that under basal conditions and in the absence of stimuli dynamic trafficking of NKCC2 occurs. NKCC2 demonstrates co-localisation with UMOD and NaCl reabsorption in the TAL has been reported to be impaired in the absence of UMOD (Mutig et al., 2011b). These findings may explain the reduced BP and NKCC2 expression in the KO mice and the opposing effects demonstrated in the WT mice where NKCC2 expression and BP were increased upon salt loading.

In contrast to salt losing syndromes, enhanced NKCC2 activity leads to hypertension caused by augmented NaCl reabsorption and volume expansion. In 2004, Sonalker *et al* illustrated that spontaneously hypertensive rats (SHR) had 4 fold higher expression levels of total NKCC2 (Sonalker et al., 2004). This group later measured membrane bound and total NKCC2 in the outer medulla in these rats by subcellular fractionation and found no difference in the surface to intracellular ratio of NKCC2 (Sonalker et al., 2007). Yet, progression from normotension to hypertension (5 – 8 weeks of age) in SHR was accompanied by a two fold increase in the surface to intracellular ratio of NKCC2 (Gimenez and Forbush, 2003). Additionally, in Dahl salt sensitive rats, NKCC2 dependent TAL transport, phosphorylation, and cell surface NKCC2 were enhanced upon salt loading with increased BP (Haque et al., 2011). Indicating that during salt stimuli in WT mice, increased UMOD expression may modulate NKCC2 trafficking beyond essential requirements altering Na^+ uptake, ECF volume, and increasing arterial pressure, suggesting, that net sodium balance requires synchronised actions between UMOD and apical Na^+ transporters.

In further support of this concept, and consistent with previous studies (Bachmann et al., 2005), the KO mice in our study displayed significantly reduced mRNA expression levels of total NKCC2 in the outer medulla region. When salt loaded the KO mice display further reductions in NKCC2 mRNA abundance, suggesting that high salt intake blunts NKCC2 trafficking in the absence of *UMOD*. This is consistent with findings in rat studies on high salt diets where total NKCC2 expression was augmented however, NKCC2 dependent TAL transport and cell surface NKCC2 were significantly reduced, indicating increased intracellular levels of NKCC2 were responsible for the augmented expression levels of total NKCC2 (Haque et al., 2011). This decreased NKCC2 trafficking to the apical membrane may contribute to the increased sodium excretion in the KO mice. Interestingly, KO mice under normal NaCl conditions showed total NKCC2 expression was increased to a similar level as that reported in the salt loaded WT mice. This is consistent with studies from Bachmann *et al* who found increased total NKCC2 expression in *UMOD* KO mice under normal salt conditions, with a disproportionate accumulation of NKCC2 in the subapical vesicle enriched compartment of the TAL (Mutig et al., 2011b). This accumulation may reflect an altered turnover, possibly via impaired degradation

of NKCC2 or simply an increase intracellular accumulation in the absence of UMOD.

The exact mechanisms of interaction between UMOD and NKCC2 are not clear. GPI anchored proteins have functions in trafficking membrane proteins by mechanisms of lipid rafts, which provide sorting signals to intracellular membrane compartments (Welker et al., 2008, Paladino et al., 2008). Suggesting the co-localisation of UMOD and NKCC2, may share lipid raft localisation as activation of NKCC2 is dependent on the presence of lipid rafts (Wilson et al., 2004). GPI anchored UMOD could, therefore, affect the function of these rafts providing scaffolds to promote interaction with NKCC2 (Rinehart et al., 2005, Delpire and Gagnon, 2008). These possible interactions may serve to explain the failure of NKCC2 activation or localisation at the apical membrane in the absence of UMOD. Implying two considerations that need attention from future studies; is the absence of *UMOD* "switching off" NKCC2 a compensatory mechanism to protect against salt induced essential hypertension, or does *UMOD* protect against salt wasting syndromes and hypotension? To elucidate this further, compartmentalisation studies, phosphorylation studies, and kinetic properties of UMOD in relation to NKCC2 should be studied in TAL cells ± salt stimulation.

In order to investigate this relationship further in the present chapter, the splice variants of NKCC2 were examined in outer medulla tissue from WT and KO mice (±2% NaCl). The three NKCC2 isoforms (NKCC2A, NKCC2B, and NKCC2F) differ in their localisation along the TAL, and their ion transport characteristics. NKCC2A is located in the medullary and cortical TAL and exhibits immediate affinity for Cl$^-$ and accounts for 20% of total NKCC2 abundance. The B isoform shows highest affinity for Cl$^-$ and is primarily located in the macula densa cells and cortical region and represents 10% of transcript abundance. NKCC2F has the lowest affinity for ion transport, however, is mainly located in the medullary TAL, this transcript accounts for 70% of total abundance. The relative distribution of these isoforms and affinity for ion transport matches the luminal concentration of NaCl along the TAL. Mice lacking NKCC2A revealed lower urine osmolality and decreased Cl$^-$ reabsorption with enhanced expression of NKCC2B indicating compensation (Payne et al., 1995). Results here show WT mice under salt

loading conditions display increased expression of NKCC2A in the outer medulla representing increased NaCl reabsorption. Whereas KO mice display lower expression which was further attenuated under salt loading, consistent with previous studies reporting reduced NKCC2A expression and NaCl reabsorption in the presence of increased levels of TNF-α at the TAL (Battula et al., 2011). The previous study described that the increased NKCC2A expression at the TAL was not accompanied by changes in either NKCC2B or F expression. However, results here demonstrate similar trends expression levels of NKCC2A with NKCC2B in that WT mice displayed increased mRNA abundance during salt loading and KO mice had reduced abundance even more so under salt conditions. Schiessl *et al* reported that during times of high salt diet in mice there are significant increases in NKCC2A and NKCC2B mRNA expression levels (Schiessl et al., 2013), suggesting here, the adaptive capacity of the TAL to cope with its reabsorptive needs are altered depending on UMOD expression levels at the TAL. NKCC2F was unchanged in WT mice ± 2% NaCl but increased in KO mice upon salt loading; even though this isoform is the most abundant at the TAL it has the least affinity for Cl^- but as NKCC2A and B were downregulated in KO mice the increased NKCC2F maybe a compensatory mechanism in these mice in an attempt to stabilise ion flux.

It has been demonstrated recently in rabbit TAL cells transfected with UMOD that there was marked reduction in Cl^- concentrations reflecting functional activation of NKCC2. This implies that in the presence of UMOD low Cl^- concentrations may mirror enhanced transport of NaCl triggered by higher NKCC2 phosphorylation. Total NKCC2 expression is reduced in salt loaded KO mice suggesting the transporter is inactivated or intracellular. Increases of NKCC2F expression in KO mice as a result of salt loading may have been a potential compensatory mechanism to regulate sodium uptake in the TAL, however was not efficient enough to do so as the activation of NKCC2 seems to be a chloride sensing mechanism that is not apparent in the KO mice. The results suggest insufficient function of NKCC2 with lower sensitivity of the isoforms to changes in intracellular chloride concentrations in UMOD KO mice.

The sequence of signals and interactions between UMOD and molecular mechanisms that contribute to the dynamics of TAL function still remain elusive. Studies exploring how tubular luminal flow participates in regulation of complex

signals at this region of the nephron may provide information that helps define the relationship between UMOD and mechanisms of TAL NaCl homeostasis. The UMOD KO mice studied here display increased micturition and natriuresis potentially via the inactivation of NKCC2, however, other Na^+ transporters may be involved. Evidence suggests that increased luminal flow of urine, and increased Na^+ excretion may be facilitated by reduced ENaC activity during high salt intake to maintain arterial pressure (Pochynyuk et al., 2010). Studies in mice have shown that if fractional activity of ENaC is closer to zero, capacity to excrete sodium and urine rises. Conversely, as fractional ENaC activity approaches equilibrium, sodium excretion capacity falls. In a corresponding fashion, arterial pressure is expected to be normal in the first instance and elevate in the latter, particularly in the presence of a high sodium diet. These findings support the current results as WT mice display increased ENaC expression upon salt loading when examined in whole kidney and outer medulla tissue, suggesting increased NaCl uptake, volume expansion, and explaining increased BP. Whereas, the opposite effects were demonstrated in the salt loaded KO mice. The TAL encompasses a variety of receptors that enable it to respond to diverse stimuli, purinergic receptors are expressed along the TAL and studies by Cabral *et al* have shown activation of these receptors is achieved by increased release of ATP and contribute essentially to renal function (Unwin et al., 2003). For example in time of high luminal flow and NaCl concentrations, ATP release is increased to activate the P2 purinergic receptors to inactivate Na^+ transport at the TAL (Silva and Garvin, 2009). In P2 receptor knockout mice, ENaC expression and activity was reduced and the animals retain their ability to respond to sodium intake as arterial pressure was not altered (Stockand et al., 2010, Mironova et al., 2011). Therefore the reduced expression of ENaC in KO mice in response to dietary sodium here maybe a compensatory pressure natriuresis response to regulate BP.

An increase in the luminal perfusion rate in mouse proximal tubules to increase Na^+ and $HCO3^-$ reabsorption is associated with direct stimulation of the apical Na^+/H^+ exchanger 3 (NHE3) (Du et al., 2006). Increased luminal flow causes drag force on the brush border microvilli initiating mechanotransduction in the proximal tubule causing the principle cells and the intercalated cells in the collecting duct to respond via central apical transporters. Numerous reports

have described elevated NHE3 mRNA expression before the onset of hypertension in hereditary strains of hypertensive rats (reviewed in (Girardi and Di Sole, 2012)). LaPointe *et al* examined NHE3 function in the renal brush border membrane vesicles of SHR and WKY (Wistar-Kyoto) rats before and during the onset of hypertension, reporting that NHE3 activity was increased in renal proximal tubules in SHR before onset of hypertension and remained high with elevated blood pressure (LaPointe et al., 2002). Opposite to increased activity and expression levels of NHE3 found during hypertension, NHE3 KO mice display chronic volume depletion and hypotension (Schultheis et al., 1998). In the current study, NHE3 was not different between WT and KO mice either before or after salt loading suggesting either the expression analysis is masked by a dilution effect in the whole kidney or UMOD has no strong relationship with this transporter. However, the KO mice did display increased NHE3 expression in outer medulla tissue which is difficult to interpret as the bulk of the proximal tubule (convoluted tubule S1 and S2) is in the cortex region of the kidney with the straight segment (S3) only descending into the medulla region as far as the mid line between the inner and outer medullary strip. The increased expression in KO mice during normal salt may be a mechanism to regulate tubuloglomerular feedback in times of altered luminal NaCl concentrations, involving the macula densa to reduce renal resistance and increase GFR in an attempt to increase NaCl reabsorption (Komlosi et al., 2005). This hypothesis is further supported by reduced expressed NHE3 in outer medulla tissue from KO salt loaded mice, suggesting reduced NaCl reabsorption.

Approximately two thirds of sodium transport along the nephron occurs by active transport. Na+ K+/ATPase at the basolateral membrane of tubular cells is critical in primary active transport across the membrane. Expression is low in the macula densa and thick descending limb of the loop of Henle and minimally expressed at the TAL (Komlosi et al., 2009). Na+ K+/ATPase is composed of α, β, and γ subunits where studies have demonstrated the α subunit participates in the natriuretic response to salt load (Loreaux et al., 2008). Suppression of Na+ K+/ATPase activity markedly increases intracellular sodium (O'Brien et al., 1994). Studies have shown that rodents fed high salt diets display reduced levels of Na+ K+/ATPase in the renal tissues (MacGregor et al., 1981) and pigs administered deoxycorticosterone plus 1% NaCl in the drinking water develop

reduced natriuresis increasing Na+ K+/ATPase inactivity by 30 fold and resulting in augmented arterial pressure (Hamlyn, 1989). In whole kidney tissue only the KO mice displayed increased Na+ K+/ATPase α expression (± 2% NaCl) suggesting increased natriuresis, hence lower ECF volume and lower BP, however, conflicting results were reported in outer medulla tissue where expression levels were reduced. WT mice display increased Na+ K+/ATPase α expression in outer medulla tissue, which would imply increased natriuresis to regulate fluid volume. However, chronic renal function curves assessed natriuresis in these mice demonstrating enhanced fractional sodium in salt loaded KO mice and not the WT mice upon salt loading. Na+ K+/ATPase β revealed no changes in expression pattern between WT and KO mice when assessed in whole kidney tissue, conversely KO mice displayed significant reductions in expression in outer medulla tissue when salt loaded with similar levels to the α subunit. These results demonstrate the importance of activity assays to asses and determine the role UMOD has on these transporters in the co-ordination of Na$^+$ transport. Even though the mechanisms have not been elucidated the results here do show clear difference between the strains in that UMOD does seem to facilitate tubule Na$^+$ reabsorption but during times of salt induced increases in BP may potentially drive excess NaCl reabsorption. The increased diuresis and natriuresis found in the salt loaded KO mice shows a link between increased luminal flow and altered Na$^+$ uptake in the absence of *UMOD*.

Axial flow regulates potassium transport along the nephron facilitating water impermeability at the TAL to maintain high medullary interstitial osmolality for conservation of the renal countercurrent exchange system to produce concentrated or dilute urine. The ATP sensitive potassium channel (ROMK) resides in the apical membrane in the TAL and processes NaCl reabsorption via the recycling of K$^+$ ions into the tubular lumen. It forms a functional unit with NKCC2, the rate limiting transporter. Disrupted ROMK function at the TAL limits NaCl reabsorption resulting in the salt wasting phenotypes observed in Bartter's syndrome. The KO mice in this study displayed significantly reduced ROMK expression in the outer medulla tissue under salt loading conditions, confirming a potential role of *UMOD* in regulating NaCl transport. Renigunta, *et al* identified UMOD as a ROMK interacting protein, regulating ROMK function by increasing its expression at the cell surface of the TAL apical membrane (Renigunta et al.,

2011). Furthermore, this group observed a decrease in ROMK immunoreactivity in the plasma membrane enriched fractions of *UMOD* KO mice kidney compared to WT counterparts. They demonstrated that *UMOD* ablation results in large accumulation of ROMK in the sub apical vesicles resulting in delayed or decreased surface expression leading to salt wasting in the following fashion: fluid enters the TAL at high concentrations of Na^+ and Cl^- with low concentrations of K^+. Therefore, the stochiometric flux of Na^+ and K^+ into the cell via the co-transporter (NKCC2) would rapidly deplete K^+ levels in the luminal fluid, preventing efficient reabsorption of Na^+ and Cl^-. This stimulation is normally avoided by the recycling of K^+ entering the cell back into the lumen. Thus, the absence of K^+ recycling results in markedly impaired NaCl reabsorption. Studies in 2010 by Fang *et al* demonstrated that resistive hypertension results from inhibited ROMK channel function and expression providing evidence into the role of the channel in blood pressure maintenance and further supporting the role of UMOD in Na^+ and BP control (Fang et al., 2010).

Collectively, the expression studies described here alongside previous reports illustrate that UMOD functionally mediates NaCl transport at the TAL. The down regulation of NKCC2 and ROMK in the outer medulla tissue of salt loaded KO mice is of great interest. These channels are co-expressed with UMOD at the apical membrane and are well documented to be linked with salt wasting in times of altered function, suggesting that the reduced arterial pressure and increased natriuresis in the *UMOD* KO mice is driven by altered regulation of these channels. Additionally, it is documented that Na^+ reabsorption at the TAL is adversely affected by increased cytokine production (Ferreri et al., 1997). UMOD has been described as having immunosuppressive effects by binding with high affinity to TNF-α, thereby inhibiting inflammation (Wu et al., 2008).

The KO mice in this study display increased levels of urinary TNF-α, which is further increased upon salt loading. This data is consistent with a recent study reporting that salt loading increased TNF-α production by the kidney (Ferreri et al., 2012), and more specifically the TAL (Hao et al., 2011), an effect that is greatly accentuated in *UMOD* KO mice. Furthermore, salt loaded KO mice here display significantly increased mRNA levels of TNF-α in outer medulla tissue. The

elevated levels of TNF-α observed in KO mice suggests that cell-surface UMOD in the WT mice sequesters TNF-α, limiting the amount of cytokine that is generated. In TAL cells, Na$^+$ uptake, across the apical cell membrane, is primarily mediated by NKCC2. Results here, show that TNF-α can reduce the levels of NKCC2A mRNA in primary mTAL cells, and that this effect is enhanced in the absence of UMOD. Ferreri and colleagues previously reported similar results showing that TNF-α is an endogenous inhibitor of the NKCC2A isoform, (Battula et al., 2011). The effect on NKCC2A mimics the effects of Bartter's syndrome in humans which replicates the effect of thiazide diuretics, is associated with low BP, and patients self-select a high salt diet as an adaptive mechanism to maintain their BP.

In mTAL cells, stimulation with TNF-α was found to increase the relative levels of UMOD mRNA, creating a negative feedback loop in which the TNF-α induced reduction in NKCC2A gene expression is switched off through increasing the production of cell-surface UMOD. Ultimately, suggesting that UMOD acts as a negative regulator of TNF-α production by the TAL to maintain NaCl homeostasis. Protein expression analysis from outer medulla tissue of KO mice +2% NaCl and WT cells ± siRNA to knock down *UMOD* expression, revealed consistent trends of increased TNF-α expression along with reduced NKCC2 expression. Transient transfection of siRNA against UMOD was used to mimic the effects of the *UMOD* KO mouse TAL cells. This finding is not unique to this study, previous studies using KO rodent models have also experienced unsuccessful culture of TAL cells (Battula et al., 2012). The TAL cells extracted from KO mice did not culture beyond 30% confluence, therefore as a substitute WT mouse TAL cells were utilised. Results confirm that UMOD plays a critical role in BP regulation by mediating the effects of TNF-α on NKCC2 to maintain sodium homeostasis. *UMOD* KO mice on high salt have a mild Bartter's phenotype, with reduced BP and reduced Na$^+$ reabsorption compared to WT mice. However, protein analysis did detect UMOD expression in the KO mice tissue but at approximately 54 kDa which does not represent a physiologically active protein. Immunohistochemistry also displayed weak but, not absent staining in thick ascending limb in the knockout animals possibly due to the primary antibody being polyclonal raised against amino acids 291-425 corresponding to exons 4-6 and the KO only covered exons 1-4. Weak staining for uromodulin in the basal and middle cellular regions in the knockout mice indicates that the shortened

protein is produced, but is not processed and transported to the apical cell surface. WT mice display increased intensity of staining at the apical membrane upon salt loading which is consistent with expression studies. In the absence of *UMOD*, NKCC2 staining is substantially weaker than the WT mice under normal NaCl conditions. Clear intense apical staining of NKCC2 was found in the WT mice upon salt loading consistent with expression studies, whereas salt loading reduces NKCC2 staining in the salt loaded KO mice. TNF-α was revealed to be increased in both strains upon salt loading although KO mice have increased interstitial staining. Future immunohistochemistry examination should be quantified and double immunocytochemistry should be utilised to examine co-localisation of UMOD and TNF-α.

Collectively, these data suggest that increased renal production of TNF-α may facilitate reduced Na^+ reabsorption along the TAL, thereby increasing the sensitivity of the pressure natriuretic mechanism. The cardiovascular characterisation in the last chapter illustrated that blood pressure differences in UMOD KO mice were driven by altered Na^+ reabsorption at the TAL causing increased pressure naturesis. Metabolomic and microarray investigation revealed UMOD regulates TNF-α and NaCl transport via NKCC2. The work outlined in this chapter has shown that UMOD may play a direct role in blood pressure regulation by modulating the effect of TNF-α on NKCC2A providing evidence of a novel functional pathway of BP regulation through UMOD and renal sodium/volume homeostasis. To confirm these findings translational studies in human kidney samples from normotensive and hypertensive subjects is assessed in the next chapter.

6 Gene expression analysis in the Silesian Renal Tissue Bank collection (a pilot study)

6.1 Introduction

The findings that the minor G allele of rs13333226; in the *cis-acting* region of the *UMOD* gene was associated with lower risk of hypertension, independent of renal function (Padmanabhan et al., 2010), along with UMODs exclusive synthesis and expression at the TAL suggests a putative functional role of *UMOD* in blood pressure regulation via mechanisms on sodium homeostasis. This hypothesis is supported by findings from the previous chapters demonstrating variants in LD with the index SNP (rs13333226) alter *UMOD* promoter activity in a genotype dependent manner and that absent *UMOD* results in reduced blood pressure phenotypes, increased natriuresis, and altered expression of renal sodium transporters. To date there are lacking studies of functional follow up of rare variants implicated from GWAS in human essential hypertension. Analysis of association between index SNPs and measures of gene expression at the transcriptional and translational level in relevant tissues is one way to verify whether implicated variants are functionally important. Although relatively straightforward in concept the relationship between implicated SNP(s) with mRNA abundance always requires availability of relevant human tissue. This chapter examines whether genotype of the index SNP rs13333226 influences *UMOD* expression in a small cohort of human renal tissue and if so does this impact expression of other sodium transporters. Human kidney tissue samples from a cohort of normotensive and hypertensive subjects were utilised as part of a small pilot study to examine the translational findings from the *UMOD* KO mice to confirm the role of UMOD in BP regulation and sodium homeostasis. Access to the human kidney samples in this chapter was kindly facilitated by Dr Maciej Tomaszewski, at the University of Leicester.

6.2 Aims

- To genotype a human cohort for SNP rs13333226.

- To investigate genotype dependent gene expression levels of *UMOD*, *NKCC2*, *TNF-α*, and *NHE3* in human kidney tissue from normotensive and hypertensive subjects following findings from the *UMOD* KO rodent model.

6.3 Methods

6.3.1 Subjects

6.3.1.1 Silesian Renal Tissue bank (SRTB)

The Silesian Renal Tissue Bank (SRTB) is a collection of human renal tissue from hypertensive and normotensive subjects that was gathered to investigate renal expression of candidate genes in human cardiovascular disease. The SRTB is an on-going recruitment of individuals electing for unilateral nephrectompy due to non-invasive renal cancer. These individuals were classified as hypertensive or normotensive based on criteria used in the SHS study (Tomaszewski et al., 2007a). Tissue samples (approximately 1 cm^3) were collected from the healthy (unaffected by cancer) pole of the kidney and appropriately preserved immediately after surgery in RNAlater (Ambion, Texas, USA) for further analysis.

6.3.1.2 The Silesian Hypertension Study (SHS)

The SHS is a cohort of 207 Polish families with essential hypertension from the Silesian region of Southern Poland (Tomaszewski et al., 2007b). All hypertensive index patients were identified and recruited with available members of their families (parents and/or siblings). Out of the 207 families, 629 subjects with clustering of essential hypertension were recruited following phenotyping using standardised questionnaires, physical examinations, basic anthropometry measurements, and fasting blood biochemistry analysis. Blood pressure was measured in triplicate and in accordance with current guidelines (Whitworth, 2003) using a mercury sphygmomanometer. Subjects were considered hypertensive if their BP readings on 3 different occasions were > 140/90 mm Hg (as SBP/DBP) and/or on enrolment they were taking antihypertensive treatment.

6.3.1.3 Western Poland Kidney Project (WPKP)

The Western Poland Kidney Project (WPKP) is an on-going study collecting human renal tissue from patients electing unilateral nephrectompy due to non-invasive renal cancer. A detailed medical history and anthropometric measurements were recorded alongside BP measurements (using an automatic digital BP monitor after 10 minutes of rest, using a cuff size adjusted to the arm

circumference). Hypertension was defined as SBP and/or DBP >140/90 mmHg on 3 separate occasions and/or remaining on antihypertensive treatment. Renal tissue samples were taken from the unaffected pole of the kidney immediately after surgery and placed in RNAlater (Ambion), before being preserved at -80'C.

All patients were recruited in Silesia Poland and all were of white European ancestry. Averages of three BP measurements (after 10 minutes rest) were recorded. Each patient was classified as hypertensive or normotensive in accordance with the guidelines set out by the international society of hypertension (Whitworth, 2003).

6.3.1.4 Bioethical approval

Written, informed consent was obtained from all subjects, in accordance with the Declaration of Helsinki (WMA Declaration of Helsinki - Ethical Principles for Medical Research Involving Human Subjects). All studies had approval from relevant institutional ethical committees.

6.3.2 RNA extraction, cDNA synthesis, and quantitative Real Time PCR

RNA was extracted, validated, and DNAse treated, as per sections 2.2.4 to 2.2.6 in the general methods chapter. The concentration of the samples was quantified as per section 2.2.7 and qRT-PCR was performed using Taqman® assay systems according to section 2.3.1. **Table 6-1** details the Taqman® assays used in this chapter. In this chapter ß-microglobulin was used as the house keeper control gene (assay number Hs_04233590.91, reference sequence NR_036523.1, and exon boundary 1-1) (Life Technilogies, Paisley, UK).

Table 6-1 Taqman® assays used to determine expression levels of *UMOD, TNF-α, NKCC2, and NHE3*

Transporter	Gene name	Taqman® assay	Reference sequence	Exon boundry
UMOD	Uromodulin	Hs00358451_m1	NM_001008389.1	5-6
TNF-α	TNF-α	Hs9999073_m1	NM_000594.2	1-2
NKCC2	SLC12A1	Hs00165731_m1	NM_000338.2	13-14
NaHe3	SLC9A3	Hs000903842_m1	NM_004174.2	11-12

6.3.3 Genotyping

Genotyping was performed as per section 3.3.2.

6.3.4 Statistical analysis

In this chapter, studies using qRT-PCR Taqman$^{®}$ assays were analysed as per section 2.3.2 in the general methods chapter. Genotyping assays of the Silesian and WPKP cohorts were assessed on the basis of Weinberg equilibrium (HWE) using Pearson x^2 test available in SIB-PAIR software (Tomaszewski et al., 2007a). A non conservative cut off value of $p<0.01$ was used as a threshold of the HWE test. SNPs with HWE x^2 statistics corresponding to the probability value of <0.01 were excluded from the association analysis. For statistical comparisons in data sets with more than two groups, analysis of variance (ANOVA) was applied, followed by the Tukey's post hoc test, comparing all samples groups against a designated control group or for comparisons between the groups.

6.4 Results

6.4.1 Demographics

This study was blinded to which subjects were from which independent Silesian cohort, therefore, hypertensive status was the only variable used to distinguish between subjects in the entire cohort in this chapter. Two subject groups have been used; Normotensive and Hypertensive subjects. The clinical demographics are outlined in **Tables 6-2 and 6-3**. Gender of each group is outlined in **Table 6-4**.There was no significant difference between Age (p=0.48), BMI (p=0.32), SBP (p>0.05), and DBP (p>0.05) between normotensive and hypertensive subjects.

6.4.2 Genotype of subjects

The distribution of rs13333226 in subjects genotyped in this chapter was in concordance with HWE (65 subjects were of AG genotype, 41 being of AA genotype, and 31 being of GG genotype) p=0.86 in x^2 test. Five samples of the cohort were undetermined **(Figure 6-1)**.

Table 6-2 General clinical characteristics of Normotensive subjects from the SHS, SRTB, and WPKP cohorts

Variable	Mean	Std. Dev.	Min	Max	n
Age (years)	56.3	11.1	20	75	49
BMI (kgm^2)	25.6	4.1	17.9	37.7	49
SBP (mmHg)	125.2	7.4	108.3	140	49
DBP (mmHg)	78.2	6.5	60	90	49

Table 6-3 General clinical characteristics of Hypertensive subjects from the SHS, SRTB, and WPKP cohorts

Variable	Mean	Std. Dev.	Min	Max	n
Age (years)	63.8	9.1	43	87	99
BMI (kgm^2)	28.9	4.1	20.4	42.3	99
SBP (mmHg)	143.4	12.3	116.6	173	99
DBP (mmHg)	86.8	7.3	70	103	99

Table 6-4 Gender of Normotensive and Hypertensive subjects

Sex	Normotensive	Hypertensive
Male	22	38
Female	27	61
Total	49	99
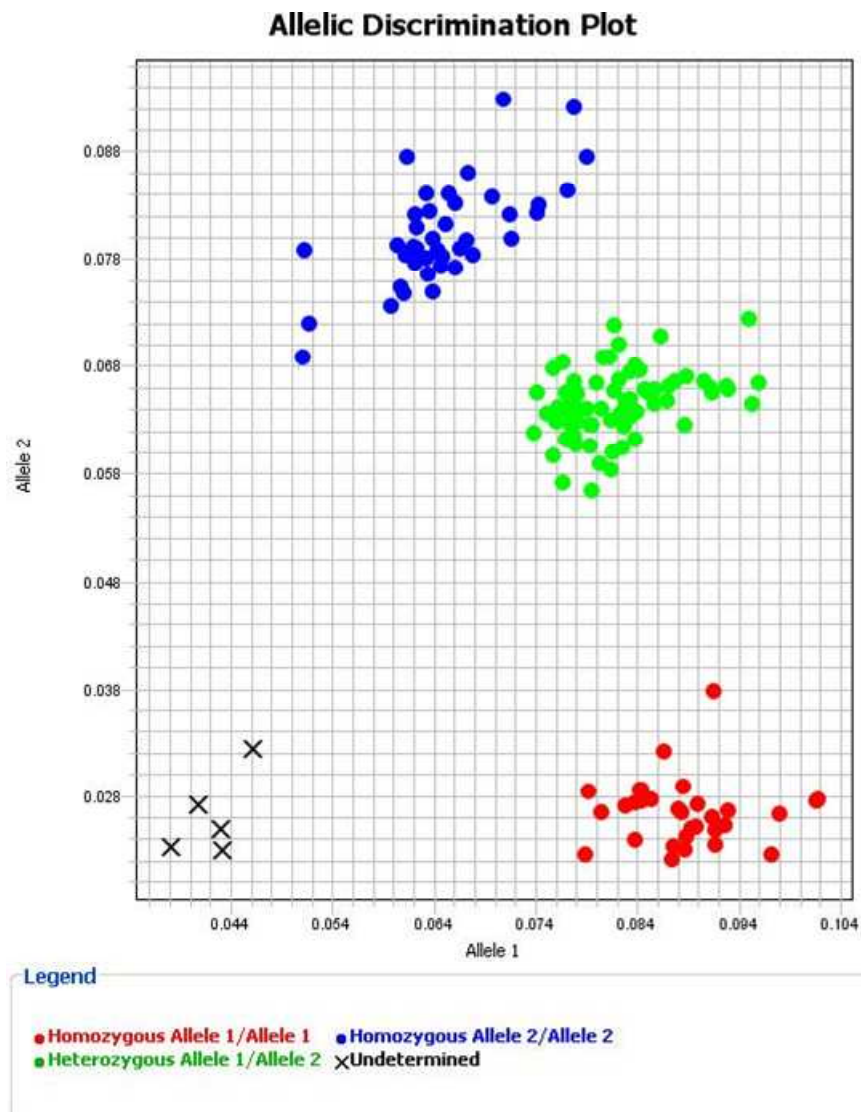
Figure 6-1 Genome cluster plot for rs13333226

Each data point represents an individual subject that was genotyped for rs1333226.The results showed; Green dots are of AG genotype (n=65), blue dots are of AA genotype (n=41), and red dots are of GG genotype (n=31). Black crosses represent undetermined samples (n=5). Genotypes were in accordance of HWE (p=0.86).

6.4.3 Association between rs13333226 polymorphism, gene expression analysis, and hypertension status

In this study rs13333226 was marginally significantly associated with *UMOD* expression and hypertension status (p=0.05), however, when adjusted for centre there was a significant association (p=0.02) **(Table 6-5)**. *UMOD* expression was significantly increased in hypertensive subjects when of AA genotype (***p<0.0001) as was *NKCC2* (**p<0.001) and *NHE3* (**p<0.001) **(Figure 6-3 A)**. There was no difference in *TNF-a* expression levels in subjects of AA genotype (p=0.43) **(Figure 6-3 A)**. Gene expression levels were not different between Hypertensive and Normotensive subjects when of AG genotype for SNP rs13333226 of *UMOD* (p=0.68), *TNF-a* (p=0.60), *NKCC2* (p=0.31), and *NHE3* (p=0.26) **(Figure 6-3 B)**. When rs13333226 was of GG genotype, there was no difference in *UMOD* (p=0.69), *TNF-a* (p=0.79), *NKCC2* (p=0.34), and *NHE3* relative expression levels (p=0.99) between Hypertensive and Normotensive subjects **(Figure 6-3 C)**.

Table 6-5 Association of rs13333226 and hypertension status

Variable	Coefficient	St dev	t	P(<)	95% Conf.	Interval
rs13333226	-0.65	0.34	-1.94	0.05	-1.33	0.17
Centre 3	2.65	1.14	-0.91	0.02	0.37	4.93

Regression analysis reveals SNP rs13333226 was not significantly associated with *UMOD* expression or hypertension in the current cohort (p=0.05). However, when adjusted for centre (place tissues were collected, each place has a centre identification number) there was a significant association (p=0.02).
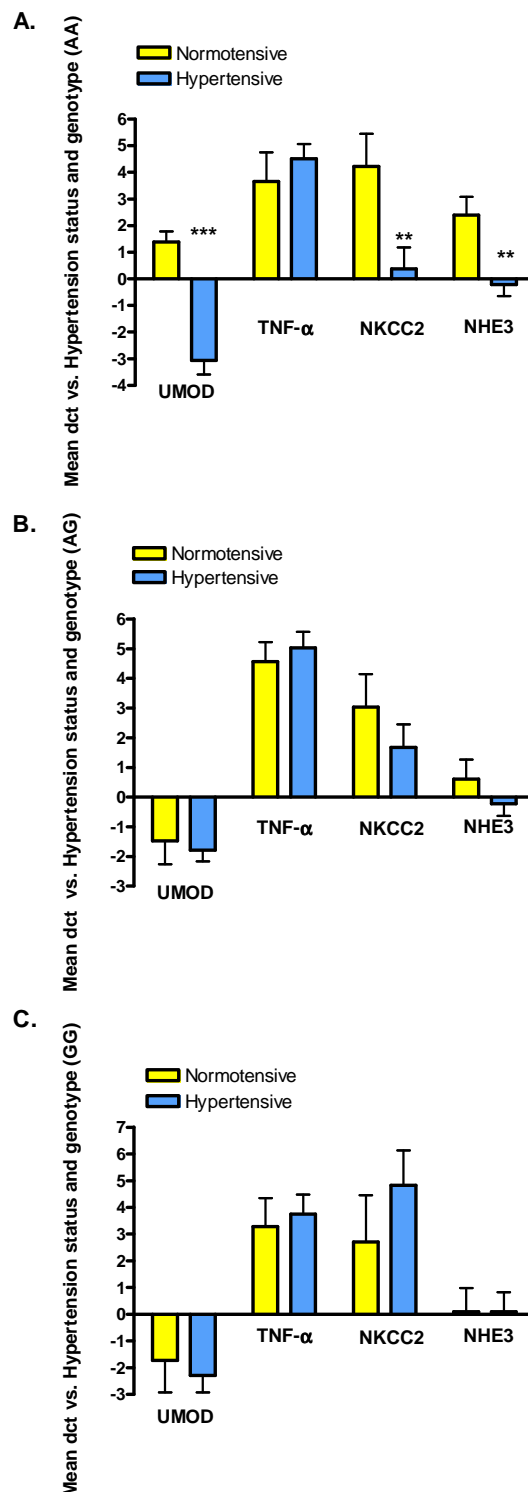
Figure 6-2 Association between Gene expression and rs13333226 vs. hypertension status

(A) *UMOD*, *NKCC2*, and *NHE3* mRNA abundance was increased in Hypertensive subjects when of AA genotype for rs13333226 (**p<0.001, ***p<0.0001, n=41 in total). **(B)** Subjects of AG genotype for rs13333226 show no difference in gene expression levels between Hypertensive vs. Normotensive subjects, n=65 in total. **(C)** Hypertensive and Normotensive subjects of GG genotype for rs13333226 showed no differential gene expression levels, n= 31 in total. Data shown as Mean dct ± SEM. Mean dct derived from ct values of each gene minus ct value of the β-microglobulin house keeper control gene, where increasing dCt represents reduced expression. Analysed by One way ANOVA followed by Tukey's post Hoc multiple comparison test.

6.5 Discussion

Results in this chapter outline the ongoing follow up of the GWAS signal from rs13333226 to elucidate further the functional roles of *UMOD* in blood pressure regulation. This study is the first to investigate *UMOD* expression levels along with other sodium transporters in human renal samples from normotensive and hypertensive individuals. The initial discovery of a significant association between hypertension and rs13333226 genotype by Padmanabhan and colleagues was not replicated in the present study (Padmanabhan et al., 2010) but did reach borderline statistical significance ($p=0.05$). Association only reached statistical significance when adjusted for centre that samples were collected, however the number of normotensive vs. hypertensive subjects within each centre was not divulged in the present study therefore it is difficult to stratify causality in this instance. Nevertheless, results here demonstrate that *UMOD*, *NKCC2*, and *NHE3* expression levels are altered in the absence of the minor G allele of rs13333226. Following segregation by genotype for rs13333226 and hypertensive status, gene expression analysis revealed that hypertensive subjects of AA genotype demonstrated increased expression levels of *UMOD*, *NKCC2*, and *NHE3*. All of which have been implicated in the progression and/or duration of hypertension by means of increased NaCl reabsorption and volume expansion (extensively reviewed in (Ares et al., 2011, Girardi and Di Sole, 2012). The relationship between *UMOD*, and *NKCC2* expression levels are consistent with findings in the previous results chapters. The evidence suggesting that altered *UMOD* expression leads to increased *TNF-α* mRNA abundance, inhibiting *NKCC2* expression at the TAL was not confirmed in the present study. *TNF-α* was not differentially expressed between normotensive and hypertensive individuals of any genotype for rs13333226.

Blood pressure was not significantly different between the groups presumably due to adequate treatment interventions to lower BP in the hypertensive subjects. Pharmacological intervention was unknown in the present study but is a variable used to control sodium transport along the nephron. Diuretics are used as a common treatment to produce natriuresis and diuresis by acting upon Na^+ transporters. Loop diuretics are the most potent class of diuretic therapeutics (Sahay et al., 2007), however, there are limited studies

documenting the direct effects of loop diuretics on *UMOD*. Early studies in the 80's demonstrated that the diuretic action and binding of furosemide and bumetanide did not act via UMOD (Brunisholz et al., 1987) however; conflicting studies report that UMOD binds with furosemide at concentrations close to those required for inhibition of electrolyte transport *in vivo* (Greven, 1983). Furthermore, the same study reported that the sodium concentration necessary for stimulation of active transport in the TAL is also necessary for binding of furosemide to UMOD (Greven, 1983). This hypothesis needs further study but may suggest counter regulatory effects of *UMOD* expression on sodium homeostasis. Interestingly, as gene expression levels were not dissimilar between normotensive and hypertensive individuals when of AG or GG genotype for rs13333226 support the hypothesis that the G allele is associated with lower risk of hypertension by means of altered *UMOD* expression at the TAL impacting sodium homeostasis. This finding should be confirmed by being repeated in a larger cohort and of differing sub-group populations.

Genotyping assays show that allele frequencies of contrasting genotype for rs13333226 were more frequent than the initial GWAS study. The present study demonstrates that approximately 47.4 % of the tested cohorts were of AG genotype for rs13333226, with 29.9 % being of AA genotype, and the remaining 22.6 % being of GG genotype which equates to a MAF of approximately 44%. This is substantially higher than expected when the MAF in the original GWAS study was only 18 %. However, in support, the population distributions seem highly variable, even between like groups, with sub European population between 11 % and 25 %, and global populations between 2 % and 36% **(outlined in Figure 6-4)** (Abecasis et al., 2010). It would have been informative to distinguish which of the 22.6 % of GG genotype individuals which were hypertensive. This may then substantiate gene expression results. The augmented allele frequency from this cohort vs. the original GWAS suggests other variables may be causing enrichment of this SNP. Thus, there are considerations that must be taken into account: the individuals in the cohort were of a selected population suffering renal cancer; the sample size is not sufficient for accurate assessment of allele frequency; or simply rs13333226 maybe associated more with cancer phenotypes.
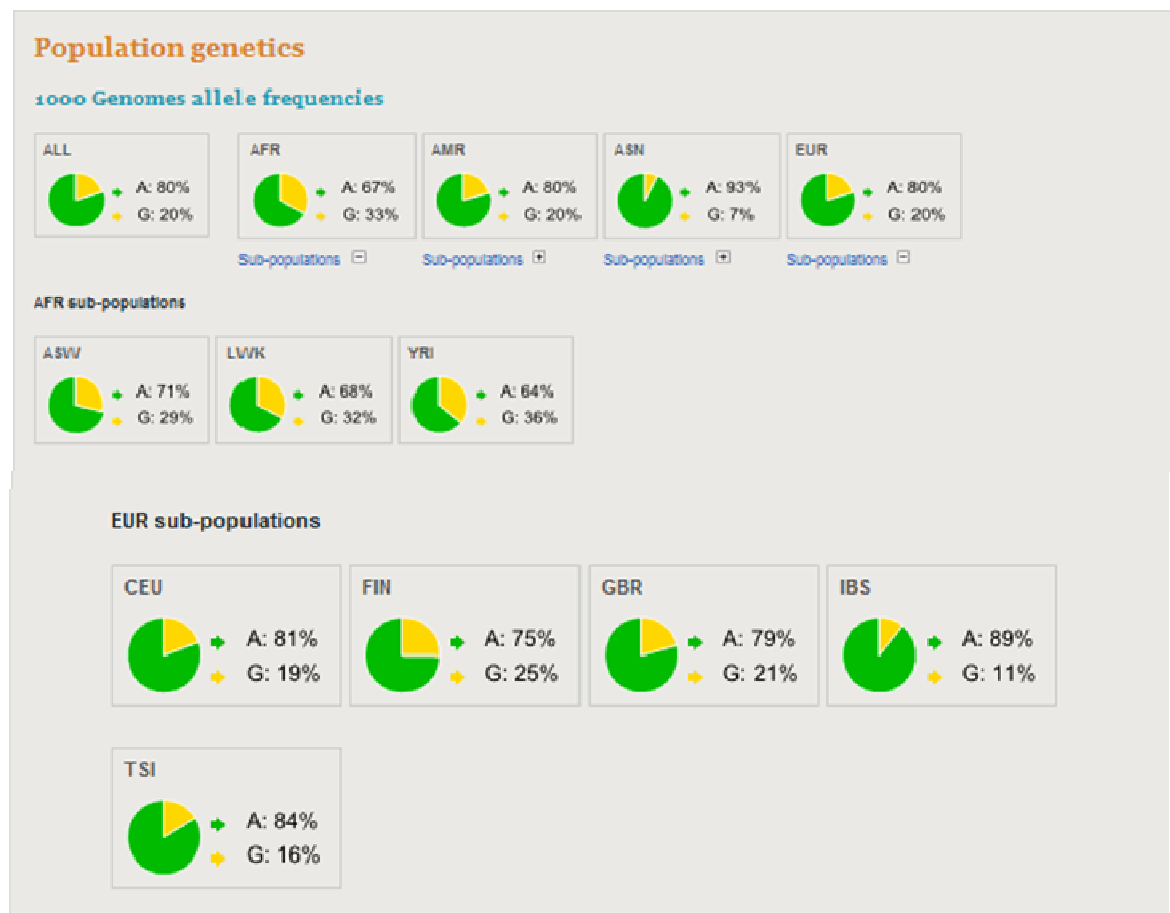
Figure 6-3 Allele frequency of rs13333226 in global populations

Image reproduced from (www.1000genomes.org). ALL represents all assessed populations, AFR = African, AMR = American, ASN = Asian, and EUR = European populations. ASW = African American populations from South West USA, LWK = Luhya Webuye, Kenya, and YRI = Yoruba Inbadan, Nigeria. CEU = Utah residents with Northern and Western ancestry, FIN = Finland, GBR = Great Britain, IBS = Iberian populations in Spain, and TSI = Tuscany in Italy.

To date, there are insufficient biological follow up studies translating GWAS findings into disease mechanisms. Findings must be investigated functionally to validated causality of identified variants and genes for complex traits of essential hypertension. Here we have assessed the functional effects of rs13333226 genotype on *UMOD* expression levels in human renal tissues during hypertension. Demonstrating the G allele of rs13333226 may alter *UMOD* expression at the TAL to regulate sodium homeostasis via mechanisms on other sodium transporters; NKCC2 and NHE3. Although cause and effect are still undetermined, principally, these findings indicate that *UMOD* variants play a role in blood pressure regulation via altered sodium homeostasis. Future work should focus on functional mechanisms of sodium transport in a genotype dependent manner. Such studies are urgently needed, not only to identify variants that may contribute to the complex traits of disease, but perhaps even more importantly, to identify those that mediate differential gene expression resulting from environmental influences.

7 General Discussion

The first successful GWAS for hypertension using an extreme case-control design in which a discovery sample of 1,621 hypertension cases and 1,699 hypercontrols, representing the top 2% and bottom 20% of the BP distribution was conducted (Padmanabhan et al., 2010). Combined with follow-up validation analyses in 19,845 cases and 16,541 controls, a locus upstream of the *UMOD* gene was identified and linked with sodium homeostasis. The ultimate goals of GWAS analysis are to improve patient risk prediction, diagnosis, prevention, and finally to develop treatments that improve quality of life and survival. The reported association between hypertension status and rs13333226 will contribute little without understanding the functional impact of *UMOD* on BP and sodium homeostasis. These findings prompted the present thesis to investigate the mechanisms of altered *UMOD* expression in blood pressure regulation and the development of essential hypertension.

The post GWAS reported analysis here is the first of its kind to include approaches for subsequent functional biological investigation *in vitro, in vivo,* and translational studies in human tissue to explore the role of *UMOD* variants in hypertension and sodium homeostasis. We have identified a SNP, rs4997081, in LD with rs13333226 that altered promoter activity and may be a causal variant altering transcriptional activity of *UMOD*. Furthermore, binding of rs4997081 to *TFAP2A* in a genotype (sequence) dependent manner leads to transcriptional changes of *UMOD* which were associated with altered sodium reabsorption. Cardiovascular characterisation studies revealed significantly lower SBP in the *UMOD* KO mouse which was not sensitive to change by salt loading. Chronic renal function curves demonstrate that the reduced SBP is attained by increased natriuresis via augmented GFR. Expression analysis studied in outer medulla tissue implicated down regulation of the major NaCl transporters in the absence of *UMOD* which were further reduced upon salt loading conditions. In contrast to these findings, WT mice displayed the opposite results with increasing SBP (± 2% NaCl). In particular *NKCC2, ROMK,* and *NHE3* expression levels were reduced in *UMOD* KO mice and more so under salt loading potentially influenced by increased levels of TNF-α at the TAL. These results suggested decreased NaCl reabsorption leading to the reported reduced BP phenotype in the KO mice as *UMOD* acts as a negative regulator of TNF-α production by the TAL to maintain NaCl homeostasis. In human tissue we confirmed that in times of altered *UMOD*

expression there are changes in *NKCC2* and *NHE3* mRNA expression levels but not *TNF-α*. Interestingly we have demonstrated that *UMOD*, *NKCC2*, and *NHE3* expression levels are altered in a genotype dependant manner, suggesting the minor G allele of rs13333226 appears to be associated with altered sodium homeostasis.

Genetic variants collectively identified so far explain only a small fraction of BP variance (< 3%) and often lack replication across studies (Bowden et al., 2010). Phenotypic heterogeneity (Charchar et al., 2008), genetic heterogeneity, differences in allele frequencies or LD patterns (Harrap, 2009), epistasis (Deng, 2007), and gene-environment interactions, may explain the poor replication of implicated genetic variants across studies. The major breakthrough with GWAS has been the identification of robust signals for common diseases and traits and novel pathways of disease. Despite this success, these studies of blood pressure phenotypes have shown that many common variants exert very modest effects, for example the 29 loci identified so far equates to only approximately 0.9 % of the phenotypic variance for systolic and diastolic blood pressure (Ehret et al., 2011). Several explanations for the missing heritability have been proposed, for example on the basis of quantitative genetic variation, causal polymorphisms may be rare (Pritchard, 2001) and in novel pathways. These low frequency, rare variants have larger effects than common variants (Abecasis et al., 2010). However, they have not been fully interrogated for association with BP. Therefore, it is of interest to test whether rare variants, at gene loci contribute to essential hypertension in the general population. Although, the ability of GWAS to detect rare BP influencing variants is hindered by the burden of multiple testing and some studies are simply underpowered to detect the effect sizes that loci exert on blood pressure. The modest findings from individual GWAS for blood pressure quantitative traits led to the progression of large meta-analyses of GWAS. Since 2009 a number of large-scale meta-analyses of GWAS for blood pressure in individuals of European ancestry have identified loci affecting systolic, diastolic, pulse, and mean arterial blood pressure (Newton-Cheh et al., 2009, Levy et al., 2009, Wain et al., 2011).

An important limitation to GWAS is that index SNPs become known as "tag" SNPs and do not offer direct information on the causal variant. To translate these signals to biological function they need to be followed up to evaluate functional

impact. GWAS is based on the principle that a causal variant is located on a haplotype, and therefore a marker allele in LD with the implicated causal variant should show an association with a trait of interest. Observations from sequencing studies of individual loci and large-scale SNP data reveal that alleles of nearby SNPs tend to have stronger correlation with each other across individuals (Nickerson et al., 1998, Daly et al., 2001, Gabriel et al., 2002). That is, they are in strong LD and form limited numbers of haplotypes. These LD SNPs represent a range of complex trait genetic architectures to follow up functionally in the aim to discover polymorphic genes/loci that influence quantitative traits and susceptibility to essential hypertension.

In the present study a 2 Kb region of interest, based on LD around the index SNP was identified to likely harbour the causal variant(s) (Iwai et al., 2006, Zhu et al., 2002). Using promoter activity assays this study was successful in verifying *in vitro* that the minor G allele of rs13333226 identified from the original GWAS was associated with altered transcriptional activity. Furthermore, with site directed mutagenesis we identified a potential causal variant (rs4497081) in LD with rs13333226 that altered promoter activity suggesting that rs13333226 was not a functional variant. It is not an unusual finding that the index SNP is not an implicated functional SNP as GWAS of disease typically result in the identification of genomic susceptibility loci, in which several SNPs showing strong inter-marker LD are equally associated with disease traits (Wang et al., 2011a). Focusing on the tag SNPs only, without systematically capturing the underlying causal variants within a 'tagged' linkage block, limits the functional associations that can be drawn from GWAS. By incorporating the correlation between SNPs in LD a stronger and more consistent association with complex disease traits is expected.

SNPs identified by GWAS often do not map within genes, but upstream in promoter regions therefore, complicating the interpretation of the findings (Hindorff et al., 2009). To narrow the list of plausible causal variants, bioinformatics approaches are often used to prioritise SNPs based on their potential functionality. These tools apply evaluation on for example; potential transcription factor binding sites to specific DNA sequences. Our computational analysis reported one differential transcription factor binding sites associated with rs4997081 on the G allele; *TFAP2A*. One way to investigate the

transcriptional regulation of identified variants is to study the effects of differential transcription factor binding effects on gene expression. These types of analysis add strength and robustness to detected associations with complex disease. In the current study we utilised ChIP to assess whether binding of the TF specifically at the DNA sequence of the G allele causes altered transcriptional activity of *UMOD*. ChIP investigation in this thesis validated the binding of *TFAP2A* to the G allele while suggesting lower affinity of binding to the C allele. Interestingly, when this binding was silenced it reduced promoter activity of the contrasting C allele. This evidence suggests that the repressive activity of *TFAP2A* causes indirect effects on promoter activity on the contrasting C allele. *TFAP2A* activity has been shown to modulate a wide range of interacting proteins (Hilger-Eversheim et al., 2000) thus, it is conceivable that differential binding to variants in the promoter region may account for altered expression of *UMOD* and contribute to functional effects of transcription; however, the exact mechanism remains to be elucidated. Network analysis was performed with IPA to investigate this hypothesis and demonstrated *TFAP2A* signals downstream to TNF-α (Gee et al., 1999, Nyormoi et al., 2001). As increased levels of TNF-α at the TAL have been shown to cause increased natriuresis (Escalante et al., 1994) it could be speculated that the minor G allele binds with *TFAP2A* to regulate levels of the pro-inflammatory cytokine to maintain normal sodium homeostasis. This is in keeping with the initial GWAS findings reported that the minor G allele of rs13333226 was associated with lower risk of hypertension and higher glomerular filtration rate (Padmanabhan et al., 2010). This hypothesis needs further work as at this stage it is not conclusive, investigation into urinary sodium excretion levels and *TFAP2A* expression analysis in these individuals of GG genotype may provide additional information. Importantly, the functional reports here have identified a causal variant (rs4997081) to follow up. Taken together, these studies with the original GWAS findings implicate *UMOD* variants in BP pressure control potentially via sodium homeostasis.

To examine the biological roles of *UMOD* in BP control and sodium homeostasis we performed a number of *in vivo* and *in vitro* experiments. We are the first to demonstrate with cardiovascular characterisation studies in the *UMOD* knockout mice that *UMOD* is directly linked with BP. The absence of *UMOD* resulted in significantly lower blood pressure phenotypes that were not altered upon salt

loading. We have shown using chronic renal function curves novel evidence that differences in arterial pressure are a direct result of enhanced natriuresis and reduced sodium reabsorption in these mice. Extensive *ex vivo* analysis in this thesis has suggested the reduced sodium reabsorption in the absence of *UMOD* may be caused by increased pro-inflammatory cytokines at the TAL. UMOD is said to exert its immunosuppressive affects by binding with high affinity to TNF-α and IL-1 (Sabharanjak et al., 2002, Kirkham et al., 2005). This gives rise to the hypothesis that available UMOD at the apical membrane may play a role in modulating cell surface events, linked with Na^+ reabsorption.

Ferreri *et al* demonstrated TNF-α inhibits ion fluxes in the kidney, particularly Na^+ reabsorption and water movement at the TAL, thus in the absence of UMOD ion transport in the TAL may be modulated by TNF-α release or accumulation which infiltrates the kidney (Escalante et al., 1994). This prompted the histological examination in renal tissue from WT and KO mice (± 2% NaCl). Results revealed the KO mice display enhanced staining for TNF-α and exhibit cellular swelling and oedema in the papillary regions of the kidney under both normal and high salt conditions. These findings are similar to a study performed by El-Achkar *et al* who reported increased acute kidney injury in *UMOD* KO mice caused by increased inflammation in the S3 segment of the kidney. The injured S3 segments were infiltrated with neutrophils and over expression of macrophage inflammatory protein-2 (MIP-2) (El-Achkar et al., 2011). Metabolic analysis from whole kidney homogenates revealed that KO mice have increased levels of metabolites associated with signalling pathways of the pro-inflammatory cytokines TNF-α and IL-1, further supporting the histological findings. Additionally, salt loading the KO mice augmented levels of urinary TNF-α and mRNA expression levels in outer medulla tissue. This data is consistent with a recent study reporting that salt loading increased TNF-α production by the kidney (Ferreri et al., 2012), and more specifically the TAL (Hao et al., 2011). TNF-α administration has proven to be a potent inhibitor to sodium reabsorption at the TAL causing exaggerated natriuretic responses and blood pressure lowering effects (Evans et al., 1989, Nakatsuji et al., 1990) which is consistent with novel results from cardiovascular and renal function studies in this thesis. Interestingly, the Na^+-K^+-$2Cl^-$ cotransporter (NKCC2) expression levels were reduced in the KO salt loaded mice according to microarray analysis.

NKCC2 is selectively expressed in the TAL where it transports the vast majority of NaCl and is said to be modulated by co-localised UMOD (Mutig et al., 2011a). In humans inactivating mutations of the NKCC2 gene (*SLC12A1*) cause a significant reduction in BP, with severe natriuresis developing a severe salt wasting phenotype (Bartter syndrome) (Garcia et al., 1999, Acuna et al., 2010). Re-sequencing of three salt-handling genes (*SLC12A3* (NCC), *SLC12A1* (NKCC2), and *KCNJ1* (ROMK)) in a cohort of over 5000 subjects of the Framingham Heart study showed the large influence rare variants have on BP (Ji et al., 2008). The authors documented 30 mutations in these 3 genes that were inferred to have functional consequences. Carriers of any of the rare variants in the three salt-handling genes (with minor allele frequency ≤ 1 %) had mean reductions of 6.3 mmHg in SBP and 3.4 mm Hg in DBP, compared with the entire cohort. Mutation carriers had mean SBP values 6.6 mm Hg less than their non carrier siblings. These are large effects when compared with those of common variants, for which the effect size is usually 1 mm Hg or less (Ji et al., 2008). Authors conclusively demonstrated that these variants were associated with lower BP (approximately 6-10 mmHg) and were protective against increased risk for hypertension, emphasising the contribution of sodium handling in blood pressure regulation in the general populations.

In contrast to genetic inactivation of NKCC2, enhanced activities of NKCC2 have been linked to salt sensitive hypertension (Ares et al., 2011) consistent with findings here in WT mice. This Indicates the important role NKCC2 plays in blood pressure regulation via sodium homeostasis and ECF volume control. The literature has documented that UMOD modulates NKCC2 at the apical membrane to facilitate NaCl reabsorption (Mutig et al., 2011b). Whilst, TNF-α produced by the TAL acts in an autocrine manner to down regulate NKCC2 expression (Battula et al., 2011), lowering NaCl reabsorption at this site (Bachmann et al., 2005, Sherblom et al., 1988, Mutig et al., 2011b, Hao et al., 2011). These findings combined with promoter assay analysis where TNF-α signalling was implicated with altered *UMOD* expression, prompted the study of expression analysis *in vivo* and *in vitro* of the nephron sodium transporters to examine potential mechanisms that reduced BP and increased natriuresis in *UMOD* KO mice.

A number of the sodium transporters along the nephron were down regulated in the outer medulla tissue in the absence of *UMOD* before and after salt loading. Of particular interest, NKCC2A and ROMK mRNA levels in outer medulla tissue were significantly increased in WT mice upon salt loading which would imply augmented NaCl reabsorption and enhanced volume expansion leading to increased BP reported in these mice. Conversely, KO mice display lower expression which was further attenuated under salt loading, consistent with previous studies reporting reduced NKCC2A expression and NaCl reabsorption in the presence of increased levels of TNF-α at the TAL (Battula et al., 2011). The down regulation of NKCC2 and ROMK in the outer medulla tissue of salt loaded KO mice is of great interest. These channels are co-expressed with UMOD at the apical membrane and are well documented to be linked with salt wasting in times of altered function (Ares et al., 2011, Renigunta et al., 2011), suggesting that the reduced arterial pressure and increased natriuresis in the *UMOD* KO mice is driven by altered regulation of these channels. Collectively, the expression studies described here alongside previous reports illustrate that *UMOD* functionally mediates NaCl transport at the TAL. The elevated levels of TNF-α observed in KO mice suggests that normally cell-surface UMOD acts to sequester TNF-α, limiting the amount of cytokine that is generated.

This hypothesis was confirmed using *in vitro* assays where we demonstrated stimulation with TNF-α increased the relative levels of UMOD mRNA, creating a negative feedback loop in which the TNF-α induced reduction in NKCC2A gene expression is switched off through increasing the production of cell-surface UMOD. Ultimately, this suggests that UMOD acts as a negative regulator of TNF-α production by the TAL to maintain NaCl homeostasis. These data sets suggest that increased renal production of TNF-α may facilitate reduced Na^{+} reabsorption along the TAL, thereby increasing the sensitivity of the pressure natriuretic mechanism. We have demonstrated with the use of promoter activity assays, *in vitro*, and *in vivo* assays that UMOD appear to play a functional role in blood pressure regulation by modulating the effect of TNF-α at the TAL to maintain NKCC2A expression. We have provided evidence of a novel functional pathway of BP regulation through *UMOD* and renal sodium/volume homeostasis.

To investigate this hypothesis the next phase of work was to investigate these findings in human translational studies and to follow up the original GWAS signal of rs13333226. The initial discovery that rs13333226 was significant association with hypertension was not statistically significant in the present study, however the *p* value was 0.05 which shows a trend towards significance which may if repeated with larger numbers transpire to replicate the original reports and will be important to follow up in a larger cohort. This result is particularly interesting as there are no studies to date in complex disease that have followed up GWAS signals in human tissue.

We did confirm that *UMOD* expression was altered in a genotype dependent manner. In the presence of the minor G allele there was no difference in *UMOD* expression between normotensive and hypertensive subjects. Moreover, levels of mRNA abundance of *NKCC2* and *NHE3* were not differentially expressed suggesting sodium reabsorption is maintained confirming our studies that *UMOD* regulates sodium homeostasis. This supports the finding from the GWAS that the minor G allele is associated with lower risk of hypertension and coincides with lower transcriptional activity reported in the promoter activity assays. To further characterise the interdependencies of *UMOD* and *NKCC2* levels and describe potential causal and effect future work should investigate whether knock down of *NKCC2* has an effect on *UMOD* expression. Therefore, if *NKCC2* levels are modulated by therapeutic targets would this impact *UMOD* levels also? The cause and effect hypothesis needs further study but could suggest that *UMOD* signalling is upstream of *NKCC2*.

In support of findings illustrating that levels of *UMOD* regulate *NKCC2* expression to maintain NaCl reabsorption, we reported that hypertensive subjects of AA genotype for rs13333226 did reveal increased mRNA expression levels of *UMOD*, *NKCC2*, and *NHE3*. These findings implicate increased NaCl reabsorption consistent with well documented evidence of these transporters in hypertension. The link between *UMOD*, *NKCC2*, and *TNF-α* however was not replicated, there was no difference in *TNF-α* expression between normotensive and hypertensive individuals of contrasting genotype for rs13333226. Pharmacological treatment for hypertension and cancer was not known in the present study, which may contribute to altered gene expression levels of TNF-α (Balkwill, 2009).

Furthermore, following findings from the first results chapter it would have been interesting to have measured *TFAP2A* expression in this cohort, which may have provided further information on the relationships between *UMOD* expression and *TNF-α* in a genotype dependent manner. In addition cohorts should be genotyped for the functional SNP rs4997081. Nevertheless, a major consideration is that alternative pathways may be altering NKCC2, sodium reabsorption, and BP in times of altered *UMOD* expression.

Many studies have investigated the regulation of NaCl reabsorption at the TAL and have suggested many pathways that enhance the pathophysiological understanding that could be implicated in the study of UMOD. Data from these studies indicate the cascade of events leading to reduced NKCC2 expression involves control of autocoids, hormones, and metabolites as outlined in **Figure 7-1**.

In brief, Ares *et al* reported cyclic guanosine monophosphate (cGMP) inhibits NaCl reabsorption by decreasing translocation of NKCC2 at the apical surface of the TAL (Ares et al., 2008). The effects mediated by cGMP stimulate prostaglandin E2 (PGE2). The diverse biological actions of PGE2 are mediated by activation of receptor subtypes; one of which is expressed in the TAL, prostaglandin E receptor 3 (EP3) (Vio et al., 2012). This receptor is a well characterised G protein coupled receptor that signals mainly via inhibitory G (G_I), diminishing adenylate activity and lowering intracellular cyclic adenosine monophosphate (cAMP) levels (Sugimoto and Narumiya, 2007). Cyclooxygenase-2 (COX2) is a rate limiting enzyme that catalyses the conversion of arachidonic acid to prostanoids, and is expressed in the TAL. It's well established that COX-2 increases the synthesis of PGE2. Ferreri *et al* were the first to demonstrate that PGE2 participates in a negative feedback loop in the TAL via activation of EP3 receptors. They demonstrated that the EP3 signalling increases COX-2 along the TAL (Vio et al., 2012) leading to reduced NKCC2 translocation to the apical membrane. TNF-α production at the TAL also increases COX-2 expression at the TAL leading to the signalling cascade of events already described above (Wang et al., 2002, Ferreri et al., 1999). Systematic studies from these groups have shown that TNF-a mediated induction of COX-2 leads to the decrease in NKCC2 activity. The best studied hormone in the TAL is vasopressin (AVP), which enhances NKCC2 activity via augmented intracellular cAMP (Molony et al., 1987). cAMP

stimulates protein trafficking by activating protein kinase A (PKA) (Caceres et al., 2009) which binds cAMP in response to AVP stimulation (Gapstur et al., 1988) Caceres et al reported that cAMP stimulates the rate of NKCC2 exocytosis via PKA and this trafficking step mediates the increase in steady state surface NKCC2 in the TAL (Caceres et al., 2009). To date we have not assessed downstream signalling events beyond TNF-α will but consider these in future studies.
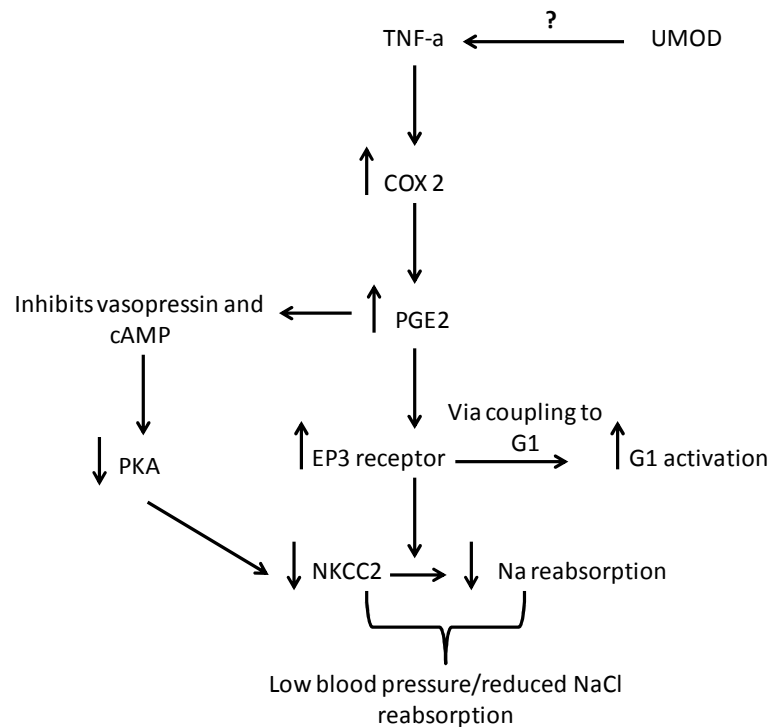
Figure 7-1 Proposed cascade of signalling events contributing to reduced NaCl reabsorption in the absence of *UMOD*.

As we did not perform sodium transport or uptake assays in the present study, our future work will use sodium green and/or rubidium assays initially, to asses sodium transport in the presence or absence of *UMOD*. From here we will start to investigate the serine protease that cleaves UMOD and the role this plays in sodium transport. Some potential experiments to determine the roles in sodium regulation are as follows; **1**- investigate cell adhesion properties between monomeric and polymeric forms of UMOD primary TAL cells, and **2** - determine the relative amounts of polymeric and monomeric forms of UMOD in healthy individuals by *UMOD* promoter SNP genotype. These objectives can be investigated by means of firstly purifying UMOD from urine by salt precipitation (Worcester et al., 1988) in healthy individuals, followed by genotyping for rs13333226 and rs4997081. Precipitated UMOD can then be electrophoresised on

native polyacrylamide gel to estimate proportions of monomer and polymeric UMOD. Cell adhesion assays can be utilised using monomeric and polymeric UMOD protein with a combination of cell lines (e.g. MDCK, Hek293, mIMCD and principal cells of the collecting duct) and primary cells TAL cells where UMOD adhesion will be measured by ELISA. Once cell adhesion has been established these cellular assays can be used to identify inhibitors that block cell adhesion to particular cells. Immunoprecipitation and mass spectrometry can be utilised to identify binding partners of UMOD which may then be tested in cell specific adhesion assays. These analyses will also allow determination of evidence for interactions between ZP domains within UMOD and other proteins containing ZP binding domains. In order to identify the serine protease that cleaves UMOD from the epithelial surface of the TAL a number of protease inhibitors would have to be tested in cells stably expressing UMOD. The media could then be tested for levels of UMOD before and after "cleavage". To date there have been few studies investigating relevant proteases, however Fukuoka, *et al* in 2001 have provided essential information that urinary UMOD is generated by a proteolytic cleavage between F548 and S549, 66 amino acids upstream of a possible GPI-anchor attachment site. These considerations will benefit future studies greatly.

Collectively, results from this thesis and currently known information on *UMOD* variants suggest emerging novel pathways of *UMOD* for BP regulation and hypertension **(Figure 7-2)**. Common variants in the *UMOD* gene have been associated with the risk of CKD, eGFR and hypertension (Kottgen et al., 2010, Padmanabhan et al., 2010, Gudbjartsson et al., 2010). Two SNPs (the T allele rs12917707 and the C allele of rs4293393) within the promoter region of the *UMOD* gene are associated with higher eGFR, decreased risk of CKD and a lower level of urinary UMOD excretion. The minor G allele of rs13333226 (in LD with rs12917707 and rs4293393) is associated with a lower risk of hypertension, reduced urinary UMOD excretion, and increased estimated eGFR in a large GWAS of BP extremes. In line with rs13333226 G allele (low *UMOD* expression), data from KO mice in this thesis, is associated with lower fractional excretion of sodium during conditions of liberal sodium intake, and lower fractional excretion of endogenous lithium, pointing to increased sodium reabsorption at the TAL. Data from this thesis combined with reports from Trudu *et al*, provide further

evidence for the critical role played by *UMOD* in sodium balance and hypertension (Trudu et al., 2013). Our *UMOD* KO mice had significantly lower SBP than the WT mice, they were resistant to salt induced changes of blood pressure and they demonstrated a shift to the left of the pressure-natriuresis curve, Trudu *et al* in contrast showed that *UMOD* over-expression caused a dose dependent increase in *UMOD* expression and excretion associated with an increase in blood pressure, together with reduced natriuresis. This is further supported by evidence from our *UMOD* KO mice where gene expression studies reported *NKCC2* expression was significantly reduced before and after salt loading. Interestingly, TNF-α is also produced by the TAL and acts in an autocrine manner to down regulate *NKCC2* expression, providing a potential link between the intracellular and extracellular roles of *UMOD* in blood pressure control. NKCC2 co-localises with UMOD and cultured TAL cells with low endogenous *UMOD* levels displayed low base-line *NKCC2* expression, which was further reduced upon stimulation with TNF-α indicating *UMOD* plays a permissive role in the modulation of NKCC2-dependent TAL salt reabsorptive function.

The macula densa expresses NKCC2 but not *UMOD*. Luminal chloride sensed by the macula densa via NKCC2 enables modulation of GFR through tubuloglomerular feedback (Briggs and Schnermann, 1987). Detection of elevated luminal chloride levels triggers the release of signalling molecules from the macula densa, causing constriction of the afferent arteriole and a drop in GFR (Briggs and Schnermann, 1987). Two interesting observations may shed some insight into the complex intra and extracellular role of UMOD in salt balance. If NKCC2 activity modulated by intra-cellular UMOD is the cause of BP variation, then in *UMOD* KO mice or humans carrying the low UMOD genetic variant, low BP should be associated with an activation of the renin angiotensin system, but evidence for this is lacking. Furthermore, in humans and salt loaded *UMOD* KO mice, GFR is increased with reduced UMOD, which is unexpected. This is because the increased sodium chloride in the luminal fluid should lead to the macula densa reducing GFR through tubuloglomerular feedback. This raises the possibility that extracellular luminal UMOD may interact with NKCC2 in the macula densa to interfere with tubuloglomerular feedback. Whilst these observations are preliminary, if validated it enlarges the scope of targeting UMOD both intracellularly and within the tubular lumen.

Additionally, mutations in the *UMOD* gene cause MCKD and FJHN that are autosomal dominant diseases characterised by tubulointerstitial nephritis and hyperuricemia. About 58 *UMOD* mutations have been reported so far and most of them occur in exons 3 and 4 encoding for the N-terminal half of the protein, and 3 mutations in exon 5 affecting residues in the ZP domain (Rampoldi et al., 2011, Vyletal et al., 2010, Scolari et al., 2004). The identified mutations in *UMOD* cause protein misfolding, which leads to its aberrant intracellular trafficking, retention in ER, altered formation of supramolecular domains on the apical plasma membrane of TAL cells, abnormal *UMOD* expression in the kidney and decreased urinary UMOD excretion. The decrease in UMOD excretion reflects massive intracellular accumulation of UMOD in tubular cells, leading to tubulointerstitial injury probably facilitated by ER stress, and lead to progressive renal damage.

GWAS discovery followed by functional validation has resulted in a re-focussing of interest in UMOD and its role in BP regulation. These early functional data while promising highlights the importance of further work that needs to be prioritised to elucidate the underpinning molecular mechanisms of UMOD. Some of the crucial questions that need to be investigated include the role of UMOD in maintaining water impermeability in TAL; the effect of UMOD on NKCC2, macula densa, tubuloglomerular feedback, distal sodium transporters, renin-angiotensin-aldosterone system, and whether immune mechanisms play a role in BP regulation by UMOD. More importantly, further insight into these questions will enable development of a therapeutic application, either novel drug or repurposing an existing drug, for targeted treatment. This is crucial, because despite major advances in cardiovascular health, hypertension remains the risk factor contributing most to the overall burden of disease globally and there is a paucity of novel anti-hypertensive drugs in clinical trials or pharmaceutical development pipeline.

This body of work is the first of its kind to perform biological follow up from a GWAS in essential hypertension. We have demonstrated direct links between *UMOD* and sodium reabsorption in every results chapter. Our findings of altered *UMOD* expression in human tissue of GG genotype for SNP rs13333226 functionally support the findings from the original GWAS. Furthermore, absent *UMOD* in KO mice supports findings that decreased urinary uromodulin excretion,

and higher glomerular filtration rate was associated with the G allele (Padmanabhan et al., 2010) as these mice displayed increased natriuresis, increased GFR, resulting in reduced BP that was not affected by salt loading. In the absence of *UMOD* there was altered expression of many sodium transporters along the nephron, most interestingly *NKCC2* which was reproduced in translational in human studies. Collectively our data demonstrates that *UMOD* plays important regulatory roles in sodium homeostasis, fluid volume control, and blood pressure regulation.
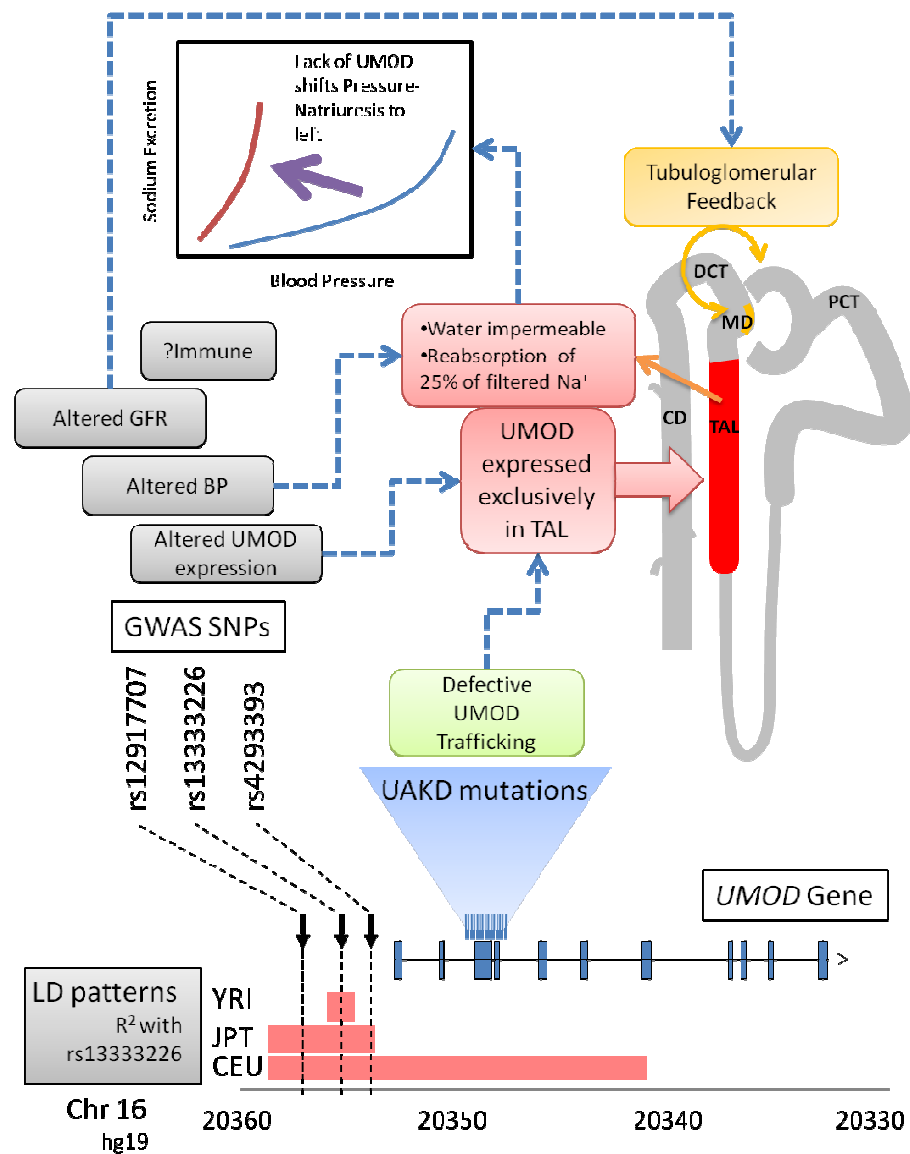
Figure 7-2 The effect of *UMOD* variation on blood pressure regulation and sodium homeostasis.

CEU: European ancestry; CD: Collecting Duct; DCT: Distal Convoluted Tubule; JPT: Japanese ancestry; LD: Linkage Disequilibrium; MD: Macula Densa; PCT: Proximal Convoluted Tubule; TAL: Thick Ascending Limb of Loop of Henle; UAKD: Uromodulin Associated Kidney Disease; YRI: African ancestry.

While genome wide association studies have been very successful in identifying replicated and valid signals for complex traits, the major weakness of GWAS has been that these replicated signals are not causative and in many cases not clearly associated with genes of common disease. The true value of GWAS so far has been in the identification of novel pathways and our study exemplifies this. We have extended the GWAS discovery of rs13333226 in humans, using a *UMOD* KO mouse model, identifying a novel pathway linking uromodulin, sodium homeostasis and hypertension. Further work needs to be prioritised to elucidate the underpinning molecular mechanisms, so that this novel pathway can be translated into new drugs for hypertension.

8 Appendix

Table A1 Differentially expressed genes (n=67) discovered via microarray analysis between WT vs. WT salt loaded mice.

Symbol	Illumina	False Discovery Rate (q-value)	Fold Change	Intensity/RPKM/FPKM	Entrez Gene ID for mouse
ACOX3	ILMN_2949844	0.031	1.30	1033.81	80911
ACVR2B	ILMN_1230145	0.009	1.44	275.74	11481
AHDC1	ILMN_2689187	0.020	-1.39	294.88	230793
ALAS2	ILMN_2675874	0.006	-1.57	194.73	11656
ANGPTL4	ILMN_2759365	0.007	1.51	172.56	57875
AOC3	ILMN_2625920	0.018	1.30	59.79	11754
APOH	ILMN_1243128	0.022	-1.30	106.27	11818
AQP2	ILMN_2794276	0.008	1.57	348.74	11827
AQP3	ILMN_2991272	0.007	1.47	603.08	11828
ARNTL	ILMN_2707510	0.009	-1.40	70.75	11865
BBS2	ILMN_1253752	0.043	-1.34	155.89	67378
BCL6	ILMN_1230353	0.0	-4.97	1249.47	12053
BTC	ILMN_2734097	0.009	1.50	82.42	12223
C1orf51	ILMN_3102736	0.009	1.60	34.53	229599
C4B	ILMN_3049559	0.037	1.36	45.12	625018
C9orf24	ILMN_2617920	0.033	-1.42	34.59	73721
CALR	ILMN_2861176	0.043	-1.35	1229.26	12317
Car15	ILMN_2871660	0.009	1.46	346.05	80733
CCND1	ILMN_2601471	0.035	1.36	1832.80	12443
CISH	ILMN_2718330	0.0	2.74	164.42	12700
CYP2A6	ILMN_2734598	0.0134	1.34	3402.38	13086
DBP	ILMN_2616226	8.3916E-4	1.59	1557.94	13170
Defb42	ILMN_2876755	0.0165	1.45	47.80	619548
EAPP	ILMN_1258998	0.0227	-1.33	40.90	66266
FMO5	ILMN_2620233	7.2727E-4	-1.65	72.59	14263
FTCD	ILMN_1216722	0.002	1.51	224.03	14317

GADD45A	ILMN_2947568	0.007	-1.59	360.38	13197
Gm2016	ILMN_3073818	0.016	1.27	107.25	100039129
GPR112	ILMN_2856383	0.019	1.38	90.25	236798
GSDMC	ILMN_3115255	0.041	1.33	32.28	83492
GTPBP4	ILMN_1216072	0.035	1.31	491.58	69237
HBA1/HBA2	ILMN_1212702	0.006	-1.62	11591.92	110257
HSD3B1	ILMN_1241116	0.012	-1.40	85.96	15493
ID1	ILMN_2672190	0.016	-1.48	216.01	15901
ID4	ILMN_2678714	0.024	-1.35	132.29	15904
IDI1	ILMN_2590923	0.001	-1.63	154.19	319554
IER5L	ILMN_2961005	0.005	-1.45	173.21	72500
IFI27L2	ILMN_2762944	0.006	1.48	162.98	76933
IGFBP3	ILMN_2727503	0.007	-1.27	364.17	16009
IL34	ILMN_2753761	0.020	-1.35	77.08	76527
KIAA1279	ILMN_1255236	0.027	-1.41	180.54	72320
LCN2	ILMN_2712075	7.272E-4	1.80	22.16	16819
LEO1	ILMN_2903351	0.0370	-1.34	86.19	235497
LPAR2	ILMN_2773817	0.035	1.40	18.34	53978
LY6E	ILMN_2984828	0.006	-1.45	616.56	17069
LYPLAL1	ILMN_1254112	0.001	1.52	131.48	226791
MGLL	ILMN_2857957	0.007	1.47	291.22	23945
MID1	ILMN_3159435	0.008	-1.51	83.75	17318
MSMO1	ILMN_2823778	0.041	-1.35	573.30	66234
NR1H4	ILMN_2727013	0.013	1.41	1359.45	20186
NT5E	ILMN_2636285	0.003	-1.49	474.17	23959
PCSK9	ILMN_2756023	0.007	-1.56	99.12	100102
PIGR	ILMN_1225605	0.007	1.38	783.28	18703
PPAP2A	ILMN_1222991	0.022	-1.33	123.16	19012
PROZ	ILMN_2736621	0.040	1.32	59.92	66901
RBP7	ILMN_2733708	0.021	1.34	29.52	63954
SERPINA3	ILMN_1246800	0.013	1.35	26.54	20716
SESN2	ILMN_2948945	0.022	-1.31	104.40	230784
SLC14A2	ILMN_3128363	0.010	1.35	34.62	27411

SLC25A44	ILMN_2734283	0.047	1.34	301.45	229517
SLC5A6	ILMN_1225056	0.024	1.33	327.53	330064
SP5	ILMN_2641201	0.033	-1.32	529.86	64406
STIP1	ILMN_2603953	0.035	-1.31	820.69	20867
TNFAIP2	ILMN_2841289	0.043	-1.39	175.28	21928
TRIB2	ILMN_2432550	0.021	1.47	397.64	217410
UNG	ILMN_3133352	0.040	1.32	33.51	22256
UPP2	ILMN_2462988	0.007	1.45	65.58	76654

Table A2 Differentially expressed genes (n=210) discovered via microarray analysis between KO vs. KO salt loaded mice.

Symbol	Illumina	False Discovery Rate (q-value)	Fold Change	Intensity/RPKM/FPKM	Entrez Gene ID for Mouse
AADAT	ILMN_2594302	0.036	-1.48	922.80	23923
Acnat1	ILMN_2858121	0.009	-1.65	133.74	230161
ACOT4	ILMN_2622613	0.034	-1.33	627.48	171282
ACSL5	ILMN_2892222	0.026	1.37	669.63	433256
ACSM2A	ILMN_2662329	0.002	-1.55	1772.15	233799
ACSM3	ILMN_3111685	0.003	-1.80	4137.37	20216
ACTB	ILMN_2846865	0.003	1.58	730.70	11461
AGPAT2	ILMN_1215901	0.006	1.59	208.04	67512
AHCTF1	ILMN_2717696	0.018	-1.49	371.22	226747
Akr1c14	ILMN_2921215	0.031	-1.55	276.15	105387
ANG	ILMN_2875251	0.022	1.51	107.58	11727
APOA2	ILMN_1247156	1.818E-4	1.75	21.62	11807
APOC1	ILMN_2599794	0.003	1.65	66.37	11812
APRT	ILMN_2630946	0.032	1.35	810.15	11821
AQR	ILMN_2676056	0.045	-1.40	60.68	11834
ARL3	ILMN_1238801	0.035	-1.43	110.04	56350
ASB9	ILMN_2682835	0.034	1.43	290.63	69299
ATG3	ILMN_2651781	0.033	-1.37	415.40	67841
ATXN1	ILMN_1254409	0.038	1.44	286.59	20238
BCAR3	ILMN_2676615	0.038	-1.46	52.08	29815
BCAT1	ILMN_3131478	0.023	1.51	414.96	12035
BCKDHB	ILMN_2660803	0.017	-1.46	335.503	12040
C10orf10	ILMN_2894211	0.001	2.02	78.32	213393
C1qtnf3	ILMN_2760318	0.008	-1.79	432.18	81799
C20orf3	ILMN_2799667	0.032	1.34	996.41	71881
C5orf45	ILMN_1247302	0.002	1.56	185.50	68067
C8A	ILMN_1213805	0.044	-1.43	229.59	230558
CCRN4L	ILMN_2591440	0.032	-1.53	92.60	12457
CD1D	ILMN_2734212	0.043	1.33	28.61	12479

Cd55	ILMN_1248714	0.030	-1.41	82.24	13136
CDC14B	ILMN_2874816	0.029	1.36	178.18	218294
CDKN2C	ILMN_1228366	0.038	1.32	123.91	12580
CHCHD7	ILMN_1240104	0.032	-1.48	1118.33	66433
CHMP5	ILMN_2670352	0.021	-1.63	275.36	76959
CIB2	ILMN_2744587	0.035	1.36	49.70	56506
CIRBP	ILMN_2761594	0.008	1.52	118.06	12696
CLSTN3	ILMN_2827217	0.013	1.50	9.08	232370
Cml3	ILMN_2735046	0.006	-1.57	1472.99	100043497
COL4A4	ILMN_2983387	0.031	-1.47	658.71	12829
COX6C	ILMN_2589039	0.012	-1.54	7900.78	621837
COX7A2	ILMN_2733698	0.044	-1.38	712.90	12866
CRELD2	ILMN_2983948	0.012	-1.63	398.48	76737
CRLS1	ILMN_1231132	0.036	-1.40	507.31	66586
CTAGE5	ILMN_2645138	0.040	-1.44	90.41	217615
CTDSPL	ILMN_2632489	0.024	1.38	415.93	69274
CTGF	ILMN_2909150	0.019	-1.60	1164.44	14219
CYB5A	ILMN_2966632	0.040	-1.28	4517.07	109672
CYFIP2	ILMN_2670713	0.045	-1.38	363.09	76884
CYP24A1	ILMN_2639900	0.0	-3.03	1429.40	13081
CYP2F1	ILMN_2702903	0.003	1.55	33.22	13107
Cyp4a14	ILMN_2691680	8.754E-4	1.76	38.98	13119
CYP4A22	ILMN_1254109	0.029	-1.40	6266.68	13118
Cyp4a31	ILMN_2960044	0.002	1.64	316.21	666168
DAZAP1	ILMN_2860674	0.034	-1.41	166.14	70248
DDC	ILMN_2628647	0.002	1.57	429.18	13195
DGKG	ILMN_1237518	0.007	1.48	81.62	110197
DHRS7	ILMN_1213456	0.032	1.35	320.84	66375
DLD	ILMN_2703657	0.034	-1.39	810.37	13382
DPYD	ILMN_2605329	0.029	-1.38	155.85	99586
EGR1	ILMN_2662926	7.509E-4	1.49	229.31	13653
EHHADH	ILMN_2706120	0.016	-1.55	1295.49	74147
EIF4G2	ILMN_2625167	0.047	-1.33	192.79	13690
ELOVL6	ILMN_2614752	0.003	1.57	233.93	170439

ETHE1	ILMN_2621074	0.001	1.59	736.19	66071
FAAH	ILMN_2766930	0.004	1.55	204.13	14073
FAM69A	ILMN_2842802	0.004	1.56	108.80	67266
FBXO21	ILMN_1244991	0.009	1.42	429.77	231670
FGA	ILMN_2624363	0.012	1.48	194.69	14161
G0S2	ILMN_1257299	0.029	1.38	311.93	14373
GABARAPL1	ILMN_1236958	0.044	1.32	2692.17	57436
GCLC	ILMN_2608016	0.008	-1.68	211.13	14629
GHR	ILMN_3138922	0.041	-1.37	1799.29	14600
Gm13342	ILMN_3163159	3.3492E-4	-2.32	475.19	100041703
Gm4956	ILMN_2911009	0.002	-1.74	211.48	241041
GPD1	ILMN_2808811	0.038	1.36	356.89	14555
GPD2	ILMN_1247257	0.035	1.35	720.51	14571
GPIHBP1	ILMN_1217969	0.048	1.34	36.08	68453
GSTA5	ILMN_1248849	0.001	1.71	894.93	100042314
GZF1	ILMN_3007959	0.007	-1.66	271.69	74533
HBP1	ILMN_3020240	0.034	1.36	927.63	73389
HEXB	ILMN_2829330	0.008	-1.60	2238.59	15212
HIATL1	ILMN_2796878	0.045	-1.47	45.83	66631
HIST1H1C	ILMN_2855315	0.017	1.48	2213.01	50708
HIST1H2BJ	ILMN_2677231	0.011	-1.52	67.05	68024
HK2	ILMN_1239397	0.004	1.816	36.42	15277
HMGCS2	ILMN_1216322	2.673E-4	1.85	101.01	15360
HNRNPA2B1	ILMN_2771074	0.029	-1.47	172.42	53379
HOXD4	ILMN_1219807	0.031	-1.35	205.27	15436
HPRT1	ILMN_2767487	0.036	-1.39	145.58	15452
HRSP12	ILMN_1251300	0.008	-1.67	748.65	15473
HSD11B1	ILMN_3115917	0.001	-1.89	2581.42	15483
HSD17B11	ILMN_2642985	8.264E-5	-2.13	1406.90	114664
HSPE1	ILMN_2960308	0.001	-1.68	1484.44	15528
ID2	ILMN_1228557	0.009	-1.56	1962.45	15902
IFI27	ILMN_3125606	0.004	1.48	1020.93	52668
IFRD2	ILMN_2736762	0.009	-1.52	320.93	15983
IGFBP1	ILMN_1230739	0.031	1.35	9.64	16006

ITGA3	ILMN_2616164	0.035	-1.44	207.78	16400
ITM2B	ILMN_2782082	0.035	-1.36	5389.19	16432
KIF1B	ILMN_1239729	0.011	-1.58	665.34	16561
KTI12	ILMN_2599412	0.040	-1.39	195.68	100087
KYNU	ILMN_1214750	0.00	1.53	76.44	70789
LGALS3BP	ILMN_1258526	0.029	1.36	240.90	19039
LIPA	ILMN_2649291	0.035	-1.37	1062.91	16889
Lipo1	ILMN_2793739	0.032	-1.43	600.52	381236
LPGAT1	ILMN_2720479	0.016	-1.42	147.75	226856
LRRC19	ILMN_1238743	0.016	-1.43	116.53	100061
LSM5	ILMN_2971946	0.038	-1.47	320.93	66373
MAL	ILMN_1248947	0.027	-1.48	956.60	17153
MAP2K1	ILMN_2714534	0.020	-1.56	102.38	26395
MAT2A	ILMN_2593368	0.028	-1.44	999.79	232087
MEMO1	ILMN_2903379	0.030	-1.41	125.60	76890
MGST1	ILMN_2940195	0.018	1.43	487.54	56615
MLEC	ILMN_1222602	0.044	-1.43	433.14	109154
MRPS10	ILMN_2841840	0.038	1.39	151.47	64657
MTMR12	ILMN_2755215	0.037	-1.44	632.10	268783
MXI1	ILMN_2765741	0.042	-1.46	253.45	17859
MYL1	ILMN_2878542	0.042	1.37	10.11	17901
NAA15	ILMN_2848090	0.032	-1.42	177.88	74838
NAMPT	ILMN_2821850	0.002	-1.84	425.40	59027
NDN	ILMN_2622374	0.036	1.33	61.22	17984
NDRG1	ILMN_2646166	0.034	1.43	5554.00	17988
NDUFA5	ILMN_2691460	0.012	-1.55	644.94	68202
NDUFB4	ILMN_1227012	0.004	-1.78	426.18	100041273
NEU1	ILMN_2708906	0.029	1.36	4034.14	18010
NFIB	ILMN_2726585	0.044	-1.34	693.41	18028
NINL	ILMN_2677065	0.046	1.32	143.73	78177
NPHS2	ILMN_2717146	0.001	1.65	261.694	170484
NPM3	ILMN_3093150	0.003	-1.78	104.24	18150
Npm3-ps1	ILMN_2965417	0.031	-1.45	1030.85	108176
NR1D1	ILMN_2749669	4.329E-4	1.87	32.00	217166

NSDHL	ILMN_2594521	0.021	1.45	159.74	18194
NT5C2	ILMN_2630939	0.033	-1.40	109.64	76952
OAT	ILMN_2933112	0.030	1.32	2024.68	18242
ORM1	ILMN_1226935	0.006	1.43	16.96	18405
PAH	ILMN_2731024	0.00	-1.55	3569.18	18478
PCCB	ILMN_2622761	0.00	-1.61	1063.34	66904
PER2	ILMN_2987863	2.277E-4	-2.11	608.11	18627
PGPEP1	ILMN_2846255	0.038	1.37	572.33	66522
PGRMC1	ILMN_2623216	0.0183	-1.44	749.39	53328
PITX2	ILMN_3118071	0.033	-1.44	269.27	18741
PKHD1	ILMN_1223914	0.046	-1.37	116.25	241035
PMPCB	ILMN_2640122	0.021	-1.46	911.17	73078
PPARG	ILMN_1221060	0.031	1.40	26.31	19016
PPP1R3C	ILMN_2667091	0.030	1.38	39.68	53412
PPP6R3	ILMN_1235583	0.034	-1.41	142.22	52036
PRLR	ILMN_2617005	0.002	1.76	47.03	19116
PRPF40A	ILMN_2642806	0.029	-1.46	143.40	56194
PRPSAP2	ILMN_2629446	0.025	-1.57	140.26	212627
PSMD12	ILMN_1216211	0.027	-1.57	187.46	66997
PSMD6	ILMN_1241910	0.032	-1.46	136.54	66413
PTEN	ILMN_2594450	0.002	-1.59	111.36	19211
PTPRB	ILMN_2591731	0.021	-1.45	376.41	19263
PYGL	ILMN_2615015	7.575E-4	1.61	118.64	110095
RAB11FIP5	ILMN_1216781	0.015	1.39	726.18	52055
RGL1	ILMN_2717176	0.029	-1.41	1042.43	19731
RHOB	ILMN_1215212	0.048	-1.45	379.75	11852
RORC	ILMN_2760272	0.007	-1.73	166.12	19885
RPL22L1	ILMN_2678755	0.031	-1.45	96.21	68028
RPS3	ILMN_2637639	0.016	-1.50	1350.70	27050
SCIN	ILMN_1259174	0.029	1.43	553.15	20259
SCOC	ILMN_1216231	0.013	-1.59	373.71	56367
SDHD	ILMN_1239143	0.019	-1.59	1067.94	66925
SEL1L	ILMN_3137920	0.008	-1.69	235.69	20338
SEMA4A	ILMN_1215120	0.011	1.42	1226.18	20351

SEPP1	ILMN_1247553	3.341E-4	-1.82	2763.69	20363
SERPINA1	ILMN_2659680	0.031	1.44	292.95	20703
SERPINB6	ILMN_1250279	0.031	1.37	280.42	20719
SH3TC2	ILMN_1240728	0.016	1.41	434.42	225608
SLC12A1	ILMN_3048630	0.041	-1.31	120.61	20495
SLC16A14	ILMN_1217704	0.016	-1.51	34.45	71781
SLC16A6	ILMN_3152241	0.038	-1.42	54.74	104681
SLC29A3	ILMN_2961091	0.005	1.46	465.38	71279
SLC30A1	ILMN_1224883	0.032	-1.40	235.54	22782
SLC38A2	ILMN_2955671	0.004	-1.88	307.28	67760
SLC38A3	ILMN_2750089	0.037	1.41	82.45	76257
SLC6A19	ILMN_3161159	0.020	1.46	1358.15	74338
Slc7a12	ILMN_2633726	8.7546E-4	1.80	38.44	140918
SLCO1A2	ILMN_1258323	0.020	-1.50	81.39	28250
SLCO3A1	ILMN_1235635	0.001	-1.72	244.47	108116
SLIRP	ILMN_1239860	0.028	-1.53	736.27	380773
SMEK2	ILMN_2683138	0.004	-1.65	426.79	104570
SNX1	ILMN_2605465	0.038	-1.47	422.32	56440
SNX7	ILMN_2760244	0.044	-1.40	689.30	76561
SOCS2	ILMN_2628178	0.003	-1.69	458.40	216233
SPAST	ILMN_1224658	0.036	-1.35	202.46	50850
SQRDL	ILMN_1247947	0.037	-1.47	344.92	59010
SS18	ILMN_1233813	0.012	-1.61	258.08	268996
STX3	ILMN_3162879	0.045	1.33	314.66	20908
TF	ILMN_2485323	0.017	1.57	64.60	22041
THBD	ILMN_1249767	0.028	-1.55	125.87	21824
TIMM8A	ILMN_2896552	0.037	-1.43	1127.97	30058
TKT	ILMN_2607880	0.004	1.58	1191.85	21881
TMEM184C	ILMN_1248892	0.038	-1.45	75.32	234463
TMEM86A	ILMN_2645662	0.016	1.52	478.98	67893
TPRKB	ILMN_2811240	0.027	1.47	136.19	69786
TRPS1	ILMN_2466527	0.010	-1.57	420.58	83925
TSC22D3	ILMN_3150811	0.010	-1.62	1091.63	14605
TSPAN3	ILMN_1251499	0.034	-1.39	58.84	56434

TTC39C	ILMN_1250576	0.034816653934301	-1.33	280.64	72747
TXN	ILMN_3009572	8.76623376623377E-4	-1.87	1184.60	22166
TXNRD1	ILMN_2484465	0.0391042780748663	-1.26	67.36	50493
UCHL3	ILMN_2970879	0.030417439703154	-1.43	293.99	50933
USMG5	ILMN_1219002	0.0048951048951049	-1.71	285.82	66477
USP33	ILMN_3129526	0.0380808080808081	-1.47	680.96	170822
VBP1	ILMN_1243095	0.0253997809419496	-1.47	268.58	22327
YWHAZ	ILMN_2510612	0.00238383838383838	-1.65	118.45	22631
ZBTB38	ILMN_1250618	0.0297416267942584	-1.33	84.93	245007
ZFYVE16	ILMN_1244584	0.029007371007371	-1.48	193.82	218441
ZKSCAN3	ILMN_2491526	0.0117554858934169	-1.60	182.93	72739

Reference List

1988. Sodium, potassium, body mass, alcohol and blood pressure: the INTERSALT Study. The INTERSALT Co-operative Research Group. *J Hypertens Suppl,* 6**,** S584-6.

2007. Genome-wide association study of 14,000 cases of seven common diseases and 3,000 shared controls. *Nature,* 447**,** 661-78.

ABDALLAH, J. G., SCHRIER, R. W., EDELSTEIN, C., JENNINGS, S. D., WYSE, B. & ELLISON, D. H. 2001. Loop diuretic infusion increases thiazide-sensitive Na+/Cl--cotransporter abundance: Role of aldosterone. *Journal of the American Society of Nephrology,* 12**,** 1335-1341.

ABECASIS, G. R., ALTSHULER, D., AUTON, A., BROOKS, L. D., DURBIN, R. M., GIBBS, R. A., HURLES, M. E. & MCVEAN, G. A. 2010. A map of human genome variation from population-scale sequencing. *Nature,* 467**,** 1061-73.

ACUNA, R., MARTINEZ-DE-LA-MAZA, L., PONCE-CORIA, J., VAZQUEZ, N., ORTAL-VITE, P., PACHECO-ALVAREZ, D., BOBADILLA, N. A. & GAMBA, G. 2010. Rare mutations in SLC12A1 and SLC12A3 protect against hypertension by reducing the activity of renal salt cotransporters. *J Hypertens,* 29**,** 475-83.

AGRE, P. & KOZONO, D. 2003. Aquaporin water channels: molecular mechanisms for human diseases. *FEBS Lett,* 555**,** 72-8.

AHLUWALIA, T. S., LINDHOLM, E., GROOP, L. & MELANDER, O. 2011. Uromodulin gene variant is associated with type 2 diabetic nephropathy. *Journal of Hypertension,* 29**,** 1731-1734.

ALLAYEE, H., DE BRUIN, T. W., MICHELLE DOMINGUEZ, K., CHENG, L. S., IPP, E., CANTOR, R. M., KRASS, K. L., KEULEN, E. T., AOUIZERAT, B. E., LUSIS, A. J. & ROTTER, J. I. 2001. Genome scan for blood pressure in Dutch dyslipidemic families reveals linkage to a locus on chromosome 4p. *Hypertension,* 38**,** 773-8.

ALTSHULER, D. & DALY, M. 2007. Guilt beyond a reasonable doubt. *Nat Genet,* 39**,** 813-5.

ALVAREZ-GUERRA, M. & GARAY, R. P. 2002. Renal Na-K-Cl cotransporter NKCC2 in Dahl salt-sensitive rats. *J Hypertens,* 20**,** 721-7.

AMEMIYA, M., LOFFING, J., LOTSCHER, M., KAISSLING, B., ALPERN, R. J. & MOE, O. W. 1995. Expression of NHE-3 in the apical membrane of rat renal proximal tubule and thick ascending limb. *Kidney Int,* 48**,** 1206-15.

AMEUR, A., RADA-IGLESIAS, A., KOMOROWSKI, J. & WADELIUS, C. 2009. Identification of candidate regulatory SNPs by combination of transcription-factor-binding site prediction, SNP genotyping and haploChIP. *Nucleic Acids Res,* 37**,** e85.

ANGIUS, A., PETRETTO, E., MAESTRALE, G. B., FORABOSCO, P., CASU, G., PIRAS, D., FANCIULLI, M., FALCHI, M., MELIS, P. M., PALERMO, M. & PIRASTU, M. 2002. A new essential hypertension susceptibility locus on chromosome 2p24-p25, detected by genomewide search. *Am J Hum Genet,* 71**,** 893-905.

ANNEST, J. L., SING, C. F., BIRON, P. & MONGEAU, J. G. 1979. Familial aggregation of blood pressure and weight in adoptive families. I. Comparisons of blood pressure and weight statistics among families with adopted, natural, or both natural and adopted children. *Am J Epidemiol,* 110**,** 479-91.

ARES, G. R., CACERES, P., ALVAREZ-LEEFMANS, F. J. & ORTIZ, P. A. 2008. cGMP decreases surface NKCC2 levels in the thick ascending limb: role of phosphodiesterase 2 (PDE2). *Am J Physiol Renal Physiol,* 295**,** F877-87.

ARES, G. R., CACERES, P. S. & ORTIZ, P. A. 2011. Molecular regulation of NKCC2 in the thick ascending limb. *Am J Physiol Renal Physiol,* 301**,** F1143-59.

ATWOOD, L. D., SAMOLLOW, P. B., HIXSON, J. E., STERN, M. P. & MACCLUER, J. W. 2001. Genome-wide linkage analysis of blood pressure in Mexican Americans. *Genet Epidemiol,* 20**,** 373-82.

AVIV, A., HOLLENBERG, N. K. & WEDER, A. 2004a. Urinary potassium excretion and sodium sensitivity in blacks. *Hypertension,* 43**,** 707-13.

AVIV, A., HOLLENBERG, N. K. & WEDER, A. B. 2004b. Sodium glomerulopathy: tubuloglomerular feedback and renal injury in African Americans. *Kidney Int,* 65**,** 361-8.

BACHMANN, S., KOEPPEN-HAGEMANN, I. & KRIZ, W. 1985. Ultrastructural localization of Tamm-Horsfall glycoprotein (THP) in rat kidney as revealed by protein A-gold immunocytochemistry. *Histochemistry,* 83**,** 531-8.

BACHMANN, S., MUTIG, K., BATES, J., WELKER, P., GEIST, B., GROSS, V., LUFT, F. C., ALENINA, N., BADER, M., THIELE, B. J., PRASADAN, K., RAFFI, H. S. & KUMAR, S. 2005. Renal effects of Tamm-Horsfall protein (uromodulin) deficiency in mice. *Am J Physiol Renal Physiol,* 288**,** F559-67.

BAILEY-WILSON, J. E. & WILSON, A. F. 2011. Linkage analysis in the next-generation sequencing era. *Hum Hered,* 72**,** 228-36.

BALKWILL, F. 2009. Tumour necrosis factor and cancer. *Nat Rev Cancer,* 9**,** 361-71.

BARBALIC, M., NARANCIC, N. S., SKARIC-JURIC, T., SALIHOVIC, M. P., KLARIC, I. M., LAUC, L. B., JANICIJEVIC, B., FARRALL, M., RUDAN, I., CAMPBELL, H., WRIGHT, A. F., HASTIE, N. D. & RUDAN, P. 2009. A quantitative trait locus for SBP maps near KCNB1 and PTGIS in a population isolate. *Am J Hypertens,* 22**,** 663-8.

BARKER, P. M., NGUYEN, M. S., GATZY, J. T., GRUBB, B., NORMAN, H., HUMMLER, E., ROSSIER, B., BOUCHER, R. C. & KOLLER, B. 1998. Role of gammaENaC subunit in lung liquid clearance and electrolyte balance in newborn mice. Insights into perinatal adaptation and pseudohypoaldosteronism. *J Clin Invest,* 102**,** 1634-40.

BATES, J. M., RAFFI, H. M., PRASADAN, K., MASCARENHAS, R., LASZIK, Z., MAEDA, N., HULTGREN, S. J. & KUMAR, S. 2004. Tamm-Horsfall protein knockout mice are more prone to urinary tract infection: rapid communication. *Kidney Int,* 65**,** 791-7.

BATTULA, S., HAO, S., PEDRAZA, P. L., STIER, C. T. & FERRERI, N. R. 2011. Tumor necrosis factor-alpha is an endogenous inhibitor of Na+-K+-2Cl-cotransporter (NKCC2) isoform A in the thick ascending limb. *Am J Physiol Renal Physiol,* 301**,** F94-100.

BATTULA, S., HAO, S., PEDRAZA, P. L., STIER, C. T. & FERRERI, N. R. 2012. Tumor necrosis factor-alpha induces renal cyclooxygenase-2 expression in response to hypercalcemia. *Prostaglandins Other Lipid Mediat,* 99**,** 45-50.

BAYER, M. E. 1964. An Electron Microscope Examination of Urinary Mucoprotein and Its Interaction with Influenza Virus. *J Cell Biol,* 21**,** 265-74.

BEAUCHAMP, G. K. & FISHER, A. S. 1993. Strain Differences in Consumption of Saline Solutions by Mice. *Physiology & Behavior,* 54**,** 179-184.

BELL, J. T., WALLACE, C., DOBSON, R., WILTSHIRE, S., MEIN, C., PEMBROKE, J., BROWN, M., CLAYTON, D., SAMANI, N., DOMINICZAK, A., WEBSTER, J., LATHROP, G. M., CONNELL, J., MUNROE, P., CAULFIELD, M. & FARRALL,

M. 2006. Two-dimensional genome-scan identifies novel epistatic loci for essential hypertension. *Hum Mol Genet,* 15**,** 1365-74.

BENJAFIELD, A. V., WANG, W. Y., SPEIRS, H. J. & MORRIS, B. J. 2005. Genome-wide scan for hypertension in Sydney Sibships: the GENIHUSS study. *Am J Hypertens,* 18**,** 828-32.

BENTING, J. H., RIETVELD, A. G. & SIMONS, K. 1999. N-Glycans mediate the apical sorting of a GPI-anchored, raft-associated protein in Madin-Darby canine kidney cells. *J Cell Biol,* 146**,** 313-20.

BERENSON, G. S., VOORS, A. W., WEBBER, L. S., DALFERES, E. R., JR. & HARSHA, D. W. 1979. Racial differences of parameters associated with blood pressure levels in children--the Bogalusa heart study. *Metabolism,* 28**,** 1218-28.

BERGLUND, G., ELMSTAHL, S., JANZON, L. & LARSSON, S. A. 1993. The Malmo Diet and Cancer Study. Design and feasibility. *J Intern Med,* 233**,** 45-51.

BERNARD, A. M., OULED, A. A., LAUWERYS, R. R., LAMBERT, A. & VANDELEENE, B. 1987. Pronounced decrease of Tamm-Horsfall proteinuria in diabetics. *Clin Chem,* 33**,** 1264.

BERNASCONE, I., VAVASSORI, S., DI PENTIMA, A., SANTAMBROGIO, S., LAMORTE, G., AMOROSO, A., SCOLARI, F., GHIGGERI, G. M., CASARI, G., POLISHCHUK, R. & RAMPOLDI, L. 2006. Defective intracellular trafficking of uromodulin mutant isoforms. *Traffic,* 7**,** 1567-79.

BETTINELLI, A., BIANCHETTI, M. G., GIRARDIN, E., CARINGELLA, A., CECCONI, M., APPIANI, A. C., PAVANELLO, L., GASTALDI, R., ISIMBALDI, C., LAMA, G. & ET AL. 1992. Use of calcium excretion values to distinguish two forms of primary renal tubular hypokalemic alkalosis: Bartter and Gitelman syndromes. *J Pediatr,* 120**,** 38-43.

BIANCHI, G., FOX, U. & IMBASCIA.E 1974. Development of a New Strain of Spontaneously Hypertensive Rats. *Life Sciences,* 14**,** 339-347.

BINDER, A. 2007. A review of the genetics of essential hypertension. *Curr Opin Cardiol,* 22**,** 176-84.

BIRON, P., MONGEAU, J. G. & BERTRAND, D. 1976. Familial aggregation of blood pressure in 558 adopted children. *Can Med Assoc J,* 115**,** 773-4.

BLEYER, A. J., WOODARD, A. S., SHIHABI, Z., SANDHU, J., ZHU, H., SATKO, S. G., WELLER, N., DETERDING, E., MCBRIDE, D., GORRY, M. C., XU, L., GANIER, D. & HART, T. C. 2003. Clinical characterization of a family with a mutation in the uromodulin (Tamm-Horsfall glycoprotein) gene. *Kidney Int,* 64**,** 36-42.

BOCHUD, M., BOVET, P., VOLLENWEIDER, P., MAILLARD, M., PACCAUD, F., WANDELER, G., GABRIEL, A. & BURNIER, M. 2009. Association between white-coat effect and blunted dipping of nocturnal blood pressure. *Am J Hypertens,* 22**,** 1054-61.

BOWDEN, D. W., AN, S. S., PALMER, N. D., BROWN, W. M., NORRIS, J. M., HAFFNER, S. M., HAWKINS, G. A., GUO, X., ROTTER, J. I., CHEN, Y. D., WAGENKNECHT, L. E. & LANGEFELD, C. D. 2010. Molecular basis of a linkage peak: exome sequencing and family-based analysis identify a rare genetic variant in the ADIPOQ gene in the IRAS Family Study. *Hum Mol Genet,* 19**,** 4112-20.

BREYER, M. D. & BREYER, R. M. 2001. G protein-coupled prostanoid receptors and the kidney. *Annu Rev Physiol,* 63**,** 579-605.

BRIGGS, J. P. & SCHNERMANN, J. 1987. The tubuloglomerular feedback mechanism: functional and biochemical aspects. *Annu Rev Physiol,* 49**,** 251-73.

BROWN, D. A. & ROSE, J. K. 1992. Sorting of GPI-anchored proteins to glycolipid-enriched membrane subdomains during transport to the apical cell surface. *Cell,* 68**,** 533-44.

BRUNEVAL, P., HINGLAIS, N., ALHENC-GELAS, F., TRICOTTET, V., CORVOL, P., MENARD, J., CAMILLERI, J. P. & BARIETY, J. 1986. Angiotensin I converting enzyme in human intestine and kidney. Ultrastructural immunohistochemical localization. *Histochemistry,* 85**,** 73-80.

BRUNISHOLZ, M. C., LYNN, K. L. & HUNT, J. S. 1987. Loop-acting diuretics do not bind to Tamm-Horsfall urinary glycoprotein. *Clin Sci (Lond),* 73**,** 305-10.

BUNAG, R. D. 1983. Facts and Fallacies About Measuring Blood-Pressure in Rats. *Clinical and Experimental Hypertension Part a-Theory and Practice,* 5**,** 1659-1681.

CACERES, P. S., ARES, G. R. & ORTIZ, P. A. 2009. cAMP stimulates apical exocytosis of the renal Na(+)-K(+)-2Cl(-) cotransporter NKCC2 in the thick ascending limb: role of protein kinase A. *J Biol Chem,* 284**,** 24965-71.

CAMPESE, V. M. 1994. Salt sensitivity in hypertension. Renal and cardiovascular implications. *Hypertension,* 23**,** 531-50.

CAMPESE, V. M., PARISE, M., KARUBIAN, F. & BIGAZZI, R. 1991. Abnormal renal hemodynamics in black salt-sensitive patients with hypertension. *Hypertension,* 18**,** 805-12.

CARLSON, S. H. & WYSS, J. M. 2000. Long-term telemetric recording of arterial pressure and heart rate in mice fed basal and high NaCl diets. *Hypertension,* 35**,** E1-5.

CARRETERO, O. A. & OPARIL, S. 2000a. Essential hypertension : part II: treatment. *Circulation,* 101**,** 446-53.

CARRETERO, O. A. & OPARIL, S. 2000b. Essential hypertension. Part I: definition and etiology. *Circulation,* 101**,** 329-35.

CASTROP, H. & SCHNERMANN, J. 2008. Isoforms of renal Na-K-2Cl cotransporter NKCC2: expression and functional significance. *Am J Physiol Renal Physiol,* 295**,** F859-66.

CAULFIELD, M., MUNROE, P., PEMBROKE, J., SAMANI, N., DOMINICZAK, A., BROWN, M., BENJAMIN, N., WEBSTER, J., RATCLIFFE, P., O'SHEA, S., PAPP, J., TAYLOR, E., DOBSON, R., KNIGHT, J., NEWHOUSE, S., HOOPER, J., LEE, W., BRAIN, N., CLAYTON, D., LATHROP, G. M., FARRALL, M. & CONNELL, J. 2003. Genome-wide mapping of human loci for essential hypertension. *Lancet,* 361**,** 2118-23.

CHANG, S. S., GRUNDER, S., HANUKOGLU, A., ROSLER, A., MATHEW, P. M., HANUKOGLU, I., SCHILD, L., LU, Y., SHIMKETS, R. A., NELSON-WILLIAMS, C., ROSSIER, B. C. & LIFTON, R. P. 1996. Mutations in subunits of the epithelial sodium channel cause salt wasting with hyperkalaemic acidosis, pseudohypoaldosteronism type 1. *Nat Genet,* 12**,** 248-53.

CHANG, Y. P., LIU, X., KIM, J. D., IKEDA, M. A., LAYTON, M. R., WEDER, A. B., COOPER, R. S., KARDIA, S. L., RAO, D. C., HUNT, S. C., LUKE, A., BOERWINKLE, E. & CHAKRAVARTI, A. 2007. Multiple genes for essential-hypertension susceptibility on chromosome 1q. *Am J Hum Genet,* 80**,** 253-64.

CHANNICK, B. J., ADLIN, E. V. & MARKS, A. D. 1969. Suppressed plasma renin activity in hypertension. *Arch Intern Med,* 123**,** 131-40.

CHARCHAR, F., ZIMMERLI, L. & TOMASZEWSKI, M. 2008. The pressure of finding human hypertension genes: new tools, old dilemmas. *J Hum Hypertens,* 22**,** 821-8.

CIULLO, M., BELLENGUEZ, C., COLONNA, V., NUTILE, T., CALABRIA, A., PACENTE, R., IOVINO, G., TRIMARCO, B., BOURGAIN, C. & PERSICO, M. G. 2006. New susceptibility locus for hypertension on chromosome 8q by efficient pedigree-breaking in an Italian isolate. *Hum Mol Genet,* 15**,** 1735-43.

CLARKE, C., FLORES-MUNOZ, M., MCKINNEY, C. A., MILLIGAN, G. & NICKLIN, S. A. 2013. Regulation of cardiovascular remodeling by the counter-regulatory axis of the renin-angiotensin system. *Future Cardiol,* 9**,** 23-38.

COLEMAN, T. G., GUYTON, A. C., COWLEY, A. W., JR., BOWER, J. D., NORMAN, R. A., JR. & MANNING, R. D., JR. 1977. Feedback mechanisms of arterial pressure control. *Contrib Nephrol,* 8**,** 5-12.

COLLINS, A., LONJOU, C. & MORTON, N. E. 1999. Genetic epidemiology of single-nucleotide polymorphisms. *Proc Natl Acad Sci U S A,* 96**,** 15173-7.

COOPER, R. S., LUKE, A., ZHU, X., KAN, D., ADEYEMO, A., ROTIMI, C., BOUZEKRI, N. & WARD, R. 2002. Genome scan among Nigerians linking blood pressure to chromosomes 2, 3, and 19. *Hypertension,* 40**,** 629-33.

COWLEY, A. W., JR. 1992. Long-term control of arterial blood pressure. *Physiol Rev,* 72**,** 231-300.

CUI, J., HOPPER, J. L. & HARRAP, S. B. 2002. Genes and family environment explain correlations between blood pressure and body mass index. *Hypertension,* 40**,** 7-12.

CUSHMAN, D. W., CHEUNG, H. S. & PETERSON, A. E. 1971. Properties of the angiotensin-converting enzyme of lung. *Chest,* 59**,** Suppl:10S+.

DAHAN, K., DEVUYST, O., SMAERS, M., VERTOMMEN, D., LOUTE, G., POUX, J. M., VIRON, B., JACQUOT, C., GAGNADOUX, M. F., CHAUVEAU, D., BUCHLER, M., COCHAT, P., COSYNS, J. P., MOUGENOT, B., RIDER, M. H., ANTIGNAC, C., VERELLEN-DUMOULIN, C. & PIRSON, Y. 2003. A cluster of mutations in the UMOD gene causes familial juvenile hyperuricemic nephropathy with abnormal expression of uromodulin. *J Am Soc Nephrol,* 14**,** 2883-93.

DAHAN, K., FUCHSHUBER, A., ADAMIS, S., SMAERS, M., KROISS, S., LOUTE, G., COSYNS, J. P., HILDEBRANDT, F., VERELLEN-DUMOULIN, C. & PIRSON, Y. 2001. Familial juvenile hyperuricemic nephropathy and autosomal dominant medullary cystic kidney disease type 2: two facets of the same disease? *J Am Soc Nephrol,* 12**,** 2348-57.

DALGIN, G. S., DREVER, M., WILLIAMS, T., KING, T., DELISI, C. & LIOU, L. S. 2008. Identification of novel epigenetic markers for clear cell renal cell carcinoma. *J Urol,* 180**,** 1126-30.

DALY, M. J., RIOUX, J. D., SCHAFFNER, S. F., HUDSON, T. J. & LANDER, E. S. 2001. High-resolution haplotype structure in the human genome. *Nat Genet,* 29**,** 229-32.

DE BAAIJ, J. H., GROOT KOERKAMP, M. J., LAVRIJSEN, M., VAN ZEELAND, F., MEIJER, H., HOLSTEGE, F. C., BINDELS, R. J. & HOENDEROP, J. G. 2013. Elucidation of the distal convoluted tubule transcriptome identifies new candidate genes involved in renal Mg(2+) handling. *Am J Physiol Renal Physiol,* 305**,** F1563-73.

DECLUE, J. W., GUYTON, A. C., COWLEY, A. W., COLEMAN, T. G., NORMAN, R. A. & MCCAA, R. E. 1978. Subpressor Angiotensin Infusion, Renal Sodium Handling, and Salt-Induced Hypertension in Dog. *Circulation Research,* 43**,** 503-512.

DELPIRE, E. & GAGNON, K. B. 2008. SPAK and OSR1: STE20 kinases involved in the regulation of ion homoeostasis and volume control in mammalian cells. *Biochem J,* 409**,** 321-31.

DENG, A. Y. 2007. Genetic basis of polygenic hypertension. *Hum Mol Genet*, 16 Spec No. 2**,** R195-202.

DIAMOND, H. S. & PAOLINO, J. S. 1973. Evidence for a postsecretory reabsorptive site for uric acid in man. *J Clin Invest*, 52**,** 1491-9.

DU, Z., YAN, Q., DUAN, Y., WEINBAUM, S., WEINSTEIN, A. M. & WANG, T. 2006. Axial flow modulates proximal tubule NHE3 and H-ATPase activities by changing microvillus bending moments. *Am J Physiol Renal Physiol*, 290**,** F289-96.

EHRET, G. B. 2010. Genome-wide association studies: contribution of genomics to understanding blood pressure and essential hypertension. *Curr Hypertens Rep*, 12**,** 17-25.

EHRET, G. B., MUNROE, P. B., RICE, K. M., BOCHUD, M., JOHNSON, A. D., CHASMAN, D. I., SMITH, A. V., TOBIN, M. D., VERWOERT, G. C., HWANG, S. J., PIHUR, V., VOLLENWEIDER, P., O'REILLY, P. F., AMIN, N., BRAGG-GRESHAM, J. L., TEUMER, A., GLAZER, N. L., LAUNER, L., ZHAO, J. H., AULCHENKO, Y., HEATH, S., SOBER, S., PARSA, A., LUAN, J., ARORA, P., DEHGHAN, A., ZHANG, F., LUCAS, G., HICKS, A. A., JACKSON, A. U., PEDEN, J. F., TANAKA, T., WILD, S. H., RUDAN, I., IGL, W., MILANESCHI, Y., PARKER, A. N., FAVA, C., CHAMBERS, J. C., FOX, E. R., KUMARI, M., GO, M. J., VAN DER HARST, P., KAO, W. H., SJOGREN, M., VINAY, D. G., ALEXANDER, M., TABARA, Y., SHAW-HAWKINS, S., WHINCUP, P. H., LIU, Y., SHI, G., KUUSISTO, J., TAYO, B., SEIELSTAD, M., SIM, X., NGUYEN, K. D., LEHTIMAKI, T., MATULLO, G., WU, Y., GAUNT, T. R., ONLAND-MORET, N. C., COOPER, M. N., PLATOU, C. G., ORG, E., HARDY, R., DAHGAM, S., PALMEN, J., VITART, V., BRAUND, P. S., KUZNETSOVA, T., UITERWAAL, C. S., ADEYEMO, A., PALMAS, W., CAMPBELL, H., LUDWIG, B., TOMASZEWSKI, M., TZOULAKI, I., PALMER, N. D., ASPELUND, T., GARCIA, M., CHANG, Y. P., O'CONNELL, J. R., STEINLE, N. I., GROBBEE, D. E., ARKING, D. E., KARDIA, S. L., MORRISON, A. C., HERNANDEZ, D., NAJJAR, S., MCARDLE, W. L., HADLEY, D., BROWN, M. J., CONNELL, J. M., HINGORANI, A. D., DAY, I. N., LAWLOR, D. A., BEILBY, J. P., LAWRENCE, R. W., CLARKE, R., et al. 2011. Genetic variants in novel pathways influence blood pressure and cardiovascular disease risk. *Nature*, 478**,** 103-9.

EITSUKA, T., NAKAGAWA, K., ONO, Y., TATEWAKI, N., NISHIDA, H., KURATA, T., SHOJI, N. & MIYAZAWA, T. 2012. Amadori-glycated phosphatidylethanolamine up-regulates telomerase activity in PANC-1 human pancreatic carcinoma cells. *Febs Letters*, 586**,** 2542-2547.

EL-ACHKAR, T. M., MCCRACKEN, R., RAUCHMAN, M., HEITMEIER, M. R., AL-ALY, Z., DAGHER, P. C. & WU, X. R. 2011. Tamm-Horsfall protein-deficient thick ascending limbs promote injury to neighboring S3 segments in an MIP-2-dependent mechanism. *Am J Physiol Renal Physiol*, 300**,** F999-1007.

EL-ACHKAR, T. M., WU, X. R., RAUCHMAN, M., MCCRACKEN, R., KIEFER, S. & DAGHER, P. C. 2008. Tamm-Horsfall protein protects the kidney from ischemic injury by decreasing inflammation and altering TLR4 expression. *Am J Physiol Renal Physiol*, 295**,** F534-44.

EL-GHARBAWY, A. H., NADIG, V. S., KOTCHEN, J. M., GRIM, C. E., SAGAR, K. B., KALDUNSKI, M., HAMET, P., PAUSOVA, Z., GAUDET, D., GOSSARD, F. & KOTCHEN, T. A. 2001. Arterial pressure, left ventricular mass, and aldosterone in essential hypertension. *Hypertension*, 37**,** 845-50.

ELLIOTT, P., MARMOT, M., DYER, A., JOOSSENS, J., KESTELOOT, H., STAMLER, R., STAMLER, J. & ROSE, G. 1989. The INTERSALT study: main results, conclusions and some implications. *Clin Exp Hypertens A*, 11**,** 1025-34.

ENG, B., MUKHOPADHYAY, S., VIO, C. P., PEDRAZA, P. L., HAO, S., BATTULA, S., SEHGAL, P. B., MCGIFF, J. C. & FERRERI, N. R. 2007. Characterization of a long-term rat mTAL cell line. *Am J Physiol Renal Physiol,* 293**,** F1413-22.

ENQUOBAHRIE, D. A., WILLIAMS, M. A., QIU, C., MUHIE, S. Y., SLENTZ-KESLER, K., GE, Z. & SORENSON, T. 2009. Early pregnancy peripheral blood gene expression and risk of preterm delivery: a nested case control study. *BMC Pregnancy Childbirth,* 9**,** 56.

ESCALANTE, B. A., FERRERI, N. R., DUNN, C. E. & MCGIFF, J. C. 1994. Cytokines Affect Ion-Transport in Primary Cultured Thick Ascending Limb of Henles Loop Cells. *American Journal of Physiology,* 266**,** C1568-C1576.

EVANS, D. A., JACOBS, D. O., REVHAUG, A. & WILMORE, D. W. 1989. The effects of tumor necrosis factor and their selective inhibition by ibuprofen. *Ann Surg,* 209**,** 312-21.

FAN, J. B., CHEN, X., HALUSHKA, M. K., BERNO, A., HUANG, X., RYDER, T., LIPSHUTZ, R. J., LOCKHART, D. J. & CHAKRAVARTI, A. 2000. Parallel genotyping of human SNPs using generic high-density oligonucleotide tag arrays. *Genome Res,* 10**,** 853-60.

FANG, L., LI, D. & WELLING, P. A. 2010. Hypertension resistance polymorphisms in ROMK (Kir1.1) alter channel function by different mechanisms. *Am J Physiol Renal Physiol,* 299**,** F1359-64.

FELLSTROM, B., DANIELSON, B. G., LJUNGHALL, S. & WIKSTROM, B. 1986. Crystal inhibition: the effects of polyanions on calcium oxalate crystal growth. *Clin Chim Acta,* 158**,** 229-35.

FERRANDI, M., SALARDI, S., PARENTI, P., FERRARI, P., BIANCHI, G., BRAW, R. & KARLISH, S. J. 1990. Na+/K+/Cl(-)-cotransporter mediated Rb+ fluxes in membrane vesicles from kidneys of normotensive and hypertensive rats. *Biochim Biophys Acta,* 1021**,** 13-20.

FERRERI, N. R., AN, S. J. & MCGIFF, J. C. 1999. Cyclooxygenase-2 expression and function in the medullary thick ascending limb. *Am J Physiol,* 277**,** F360-8.

FERRERI, N. R., HAO, S., PEDRAZA, P. L., ESCALANTE, B. & VIO, C. P. 2012. Eicosanoids and tumor necrosis factor-alpha in the kidney. *Prostaglandins Other Lipid Mediat,* 98**,** 101-6.

FERRERI, N. R., ZHAO, Y., TAKIZAWA, H. & MCGIFF, J. C. 1997. Tumor necrosis factor-alpha-angiotensin interactions and regulation of blood pressure. *J Hypertens,* 15**,** 1481-4.

FLETCHER, A. P., NEUBERGER, A. & RATCLIFFE, W. A. 1970a. Tamm-Horsfall urinary glycoprotein. The chemical composition. *Biochem J,* 120**,** 417-24.

FLETCHER, A. P., NEUBERGER, A. & RATCLIFFE, W. A. 1970b. Tamm-Horsfall urinary glycoprotein. The subunit structure. *Biochem J,* 120**,** 425-32.

FRAZER, K. A., BALLINGER, D. G., COX, D. R., HINDS, D. A., STUVE, L. L., GIBBS, R. A., BELMONT, J. W., BOUDREAU, A., HARDENBOL, P., LEAL, S. M., PASTERNAK, S., WHEELER, D. A., WILLIS, T. D., YU, F., YANG, H., ZENG, C., GAO, Y., HU, H., HU, W., LI, C., LIN, W., LIU, S., PAN, H., TANG, X., WANG, J., WANG, W., YU, J., ZHANG, B., ZHANG, Q., ZHAO, H., ZHOU, J., GABRIEL, S. B., BARRY, R., BLUMENSTIEL, B., CAMARGO, A., DEFELICE, M., FAGGART, M., GOYETTE, M., GUPTA, S., MOORE, J., NGUYEN, H., ONOFRIO, R. C., PARKIN, M., ROY, J., STAHL, E., WINCHESTER, E., ZIAUGRA, L., ALTSHULER, D., SHEN, Y., YAO, Z., HUANG, W., CHU, X., HE, Y., JIN, L., LIU, Y., SUN, W., WANG, H., WANG, Y., XIONG, X., XU, L., WAYE, M. M., TSUI, S. K., XUE, H., WONG, J. T., GALVER, L. M., FAN, J. B., GUNDERSON, K., MURRAY, S. S., OLIPHANT, A. R., CHEE, M. S., MONTPETIT, A., CHAGNON, F., FERRETTI, V., LEBOEUF, M., OLIVIER, J. F.,

PHILLIPS, M. S., ROUMY, S., SALLEE, C., VERNER, A., HUDSON, T. J., KWOK, P. Y., CAI, D., KOBOLDT, D. C., MILLER, R. D., PAWLIKOWSKA, L., TAILLON-MILLER, P., XIAO, M., TSUI, L. C., MAK, W., SONG, Y. Q., TAM, P. K., NAKAMURA, Y., KAWAGUCHI, T., KITAMOTO, T., MORIZONO, T., NAGASHIMA, A., OHNISHI, Y., SEKINE, A., TANAKA, T., TSUNODA, T., et al. 2007. A second generation human haplotype map of over 3.1 million SNPs. *Nature,* 449**,** 851-61.

FUJIMOTO, M., NAITO, K. & KUBOTA, T. 1980. Electrochemical profile for ion transport across the membrane of proximal tubular cells. *Membr Biochem,* 3**,** 67-97.

FUJITA, T., HENRY, W. L., BARTTER, F. C., LAKE, C. R. & DELEA, C. S. 1980. Factors influencing blood pressure in salt-sensitive patients with hypertension. *Am J Med,* 69**,** 334-44.

FUKUOKA, S. & KOBAYASHI, K. 2001. Analysis of the C-terminal structure of urinary Tamm-Horsfall protein reveals that the release of the glycosyl phosphatidylinositol-anchored counterpart from the kidney occurs by phenylalanine-specific proteolysis. *Biochem Biophys Res Commun,* 289**,** 1044-8.

GABRIEL, S. B., SCHAFFNER, S. F., NGUYEN, H., MOORE, J. M., ROY, J., BLUMENSTIEL, B., HIGGINS, J., DEFELICE, M., LOCHNER, A., FAGGART, M., LIU-CORDERO, S. N., ROTIMI, C., ADEYEMO, A., COOPER, R., WARD, R., LANDER, E. S., DALY, M. J. & ALTSHULER, D. 2002. The structure of haplotype blocks in the human genome. *Science,* 296**,** 2225-9.

GAPSTUR, S. M., HOMMA, S. & DOUSA, T. P. 1988. cAMP-binding proteins in medullary tubules from rat kidney: effect of ADH. *American Journal of Physiology,* 255**,** F292-300.

GARCIA, N. H., PLATO, C. F., STOOS, B. A. & GARVIN, J. L. 1999. Nitric oxide-induced inhibition of transport by thick ascending limbs from Dahl salt-sensitive rats. *Hypertension,* 34**,** 508-13.

GARTY, H. & PALMER, L. G. 1997. Epithelial sodium channels: function, structure, and regulation. *Physiol Rev,* 77**,** 359-96.

GEE, J. M., ROBERTSON, J. F., ELLIS, I. O., NICHOLSON, R. I. & HURST, H. C. 1999. Immunohistochemical analysis reveals a tumour suppressor-like role for the transcription factor AP-2 in invasive breast cancer. *J Pathol,* 189**,** 514-20.

GELLER, D. S., RODRIGUEZ-SORIANO, J., VALLO BOADO, A., SCHIFTER, S., BAYER, M., CHANG, S. S. & LIFTON, R. P. 1998. Mutations in the mineralocorticoid receptor gene cause autosomal dominant pseudohypoaldosteronism type I. *Nat Genet,* 19**,** 279-81.

GIMENEZ, I. & FORBUSH, B. 2003. Short-term stimulation of the renal Na-K-Cl cotransporter (NKCC2) by vasopressin involves phosphorylation and membrane translocation of the protein. *J Biol Chem,* 278**,** 26946-51.

GIRARDI, A. C. & DI SOLE, F. 2012. Deciphering the mechanisms of the Na+/H+ exchanger-3 regulation in organ dysfunction. *Am J Physiol Cell Physiol,* 302**,** C1569-87.

GO, A. S., CHERTOW, G. M., FAN, D., MCCULLOCH, C. E. & HSU, C. Y. 2004. Chronic kidney disease and the risks of death, cardiovascular events, and hospitalization. *N Engl J Med,* 351**,** 1296-305.

GONG, M., ZHANG, H., SCHULZ, H., LEE, Y. A., SUN, K., BAHRING, S., LUFT, F. C., NURNBERG, P., REIS, A., ROHDE, K., GANTEN, D., HUI, R. & HUBNER, N. 2003. Genome-wide linkage reveals a locus for human essential (primary) hypertension on chromosome 12p. *Hum Mol Genet,* 12**,** 1273-7.

GREEN, D. R. 2000. Apoptosis and sphingomyelin hydrolysis: The flip side. *Journal of Cell Biology,* 150**,** F5-F7.

GREVEN, J. 1983. Studies on the renal receptors of loop diuretics. *Clin Exp Hypertens A,* 5**,** 193-208.

GUAN, Y. F., HAO, C. M., CHA, D. R., RAO, R., LU, W. D., KOHAN, D. E., MAGNUSON, M. A., REDHA, R., ZHANG, Y. H. & BREYER, M. D. 2005. Thiazolidinediones expand body fluid volume through PPAR gamma stimulation of ENaC-mediated renal salt absorption. *Nature Medicine,* 11**,** 861-866.

GUDBJARTSSON, D. F., HOLM, H., INDRIDASON, O. S., THORLEIFSSON, G., EDVARDSSON, V., SULEM, P., DE VEGT, F., D'ANCONA, F. C., DEN HEIJER, M., WETZELS, J. F., FRANZSON, L., RAFNAR, T., KRISTJANSSON, K., BJORNSDOTTIR, U. S., EYJOLFSSON, G. I., KIEMENEY, L. A., KONG, A., PALSSON, R., THORSTEINSDOTTIR, U. & STEFANSSON, K. 2010. Association of variants at UMOD with chronic kidney disease and kidney stones-role of age and comorbid diseases. *PLoS Genet,* 6**,** e1001039.

GUYTON, A. C. 1967. Regulation of cardiac output. *N Engl J Med,* 277**,** 805-12.

GUYTON, A. C. 1987. Renal-Function Curve - a Key to Understanding the Pathogenesis of Hypertension. *Hypertension,* 10**,** 1-6.

GUYTON, A. C. 1991. Blood pressure control--special role of the kidneys and body fluids. *Science,* 252**,** 1813-6.

GUYTON, A. C., COLEMAN, T. G., YOUNG, D. B., LOHMEIER, T. E. & DECLUE, J. W. 1980. Salt balance and long-term blood pressure control. *Annu Rev Med,* 31**,** 15-27.

GUYTON, A. C., RICHARDSON, T. Q. & LANGSTON, J. B. 1964. Regulation of cardiac output and venous return. *Clin Anesth,* 3**,** 1-34.

HAMET, P., MERLO, E., SEDA, O., BROECKEL, U., TREMBLAY, J., KALDUNSKI, M., GAUDET, D., BOUCHARD, G., DESLAURIERS, B., GAGNON, F., ANTONIOL, G., PAUSOVA, Z., LABUDA, M., JOMPHE, M., GOSSARD, F., TREMBLAY, G., KIROVA, R., TONELLATO, P., ORLOV, S. N., PINTOS, J., PLATKO, J., HUDSON, T. J., RIOUX, J. D., KOTCHEN, T. A. & COWLEY, A. W., JR. 2005. Quantitative founder-effect analysis of French Canadian families identifies specific loci contributing to metabolic phenotypes of hypertension. *Am J Hum Genet,* 76**,** 815-32.

HAMLIN, L. M. & FISH, W. W. 1977. Physical properties of Tamm-Horsfall glycoprotein and its glycopolypeptide. *Int J Pept Protein Res,* 10**,** 270-6.

HAMLYN, J. M. 1989. Increased levels of a humoral digitalis-like factor in deoxycorticosterone acetate-induced hypertension in the pig. *J Endocrinol,* 122**,** 409-20.

HANSSON, J. H., NELSON-WILLIAMS, C., SUZUKI, H., SCHILD, L., SHIMKETS, R., LU, Y., CANESSA, C., IWASAKI, T., ROSSIER, B. & LIFTON, R. P. 1995. Hypertension caused by a truncated epithelial sodium channel gamma subunit: genetic heterogeneity of Liddle syndrome. *Nat Genet,* 11**,** 76-82.

HAO, S., ZHAO, H., DARZYNKIEWICZ, Z., BATTULA, S. & FERRERI, N. R. 2011. Differential regulation of NFAT5 by NKCC2 isoforms in medullary thick ascending limb (mTAL) cells. *Am J Physiol Renal Physiol,* 300**,** F966-75.

HAQUE, M. Z., ARES, G. R., CACERES, P. S. & ORTIZ, P. A. 2011. High salt differentially regulates surface NKCC2 expression in thick ascending limbs of Dahl salt-sensitive and salt-resistant rats. *Am J Physiol Renal Physiol,* 300**,** F1096-104.

HARING, M., OFFERMANN, S., DANKER, T., HORST, I., PETERHANSEL, C. & STAM, M. 2007. Chromatin immunoprecipitation: optimization, quantitative analysis and data normalization. *Plant Methods,* 3**,** 11.

HARRAP, S. B. 2003. Where are all the blood-pressure genes? *Lancet,* 361**,** 2149-51.

HARRAP, S. B. 2009. Blood pressure genetics: time to focus. *J Am Soc Hypertens,* 3**,** 231-7.

HARRAP, S. B., STEBBING, M., HOPPER, J. L., HOANG, H. N. & GILES, G. G. 2000. Familial patterns of covariation for cardiovascular risk factors in adults: The Victorian Family Heart Study. *Am J Epidemiol,* 152**,** 704-15.

HART, T. C., GORRY, M. C., HART, P. S., WOODARD, A. S., SHIHABI, Z., SANDHU, J., SHIRTS, B., XU, L., ZHU, H., BARMADA, M. M. & BLEYER, A. J. 2002. Mutations of the UMOD gene are responsible for medullary cystic kidney disease 2 and familial juvenile hyperuricaemic nephropathy. *J Med Genet,* 39**,** 882-92.

HEBERT, S. C. & ANDREOLI, T. E. 1984. Control of NaCl transport in the thick ascending limb. *Am J Physiol,* 246, F745-56.

HEBERT, S. C. & ANDREOLI, T. E. 1986. Ionic conductance pathways in the mouse medullary thick ascending limb of Henle. The paracellular pathway and electrogenic Cl- absorption. *J Gen Physiol,* 87**,** 567-90.

HERRERA, M., HONG, N. J., ORTIZ, P. A. & GARVIN, J. L. 2009. Endothelin-1 inhibits thick ascending limb transport via Akt-stimulated nitric oxide production. *J Biol Chem,* 284**,** 1454-60.

HILGER-EVERSHEIM, K., MOSER, M., SCHORLE, H. & BUETTNER, R. 2000. Regulatory roles of AP-2 transcription factors in vertebrate development, apoptosis and cell-cycle control. *Gene,* 260**,** 1-12.

HINDORFF, L. A., SETHUPATHY, P., JUNKINS, H. A., RAMOS, E. M., MEHTA, J. P., COLLINS, F. S. & MANOLIO, T. A. 2009. Potential etiologic and functional implications of genome-wide association loci for human diseases and traits. *Proc Natl Acad Sci U S A,* 106**,** 9362-7.

HOOVER, R. S., POCH, E., MONROY, A., VAZQUEZ, N., NISHIO, T., GAMBA, G. & HEBERT, S. C. 2003. N-Glycosylation at two sites critically alters thiazide binding and activity of the rat thiazide-sensitive Na(+):Cl(-) cotransporter. *J Am Soc Nephrol,* 14**,** 271-82.

HORTON, J. K., DAVIES, M., TOPLEY, N., THOMAS, D. & WILLIAMS, J. D. 1990. Activation of the inflammatory response of neutrophils by Tamm-Horsfall glycoprotein. *Kidney Int,* 37, 717-26.

HOYER, J. R. & SEILER, M. W. 1979. Pathophysiology of Tamm-Horsfall protein. *Kidney Int,* 16**,** 279-89.

HOYER, J. R., SISSON, S. P. & VERNIER, R. L. 1979. Tamm-Horsfall glycoprotein: ultrastructural immunoperoxidase localization in rat kidney. *Lab Invest,* 41**,** 168-73.

HUANG, P. L., HUANG, Z., MASHIMO, H., BLOCH, K. D., MOSKOWITZ, M. A., BEVAN, J. A. & FISHMAN, M. C. 1995. Hypertension in mice lacking the gene for endothelial nitric oxide synthase. *Nature,* 377**,** 239-42.

HUANG, Y. J., CHRETIEN, N., BILODEAU, A. S., ZHOU, J. F., LAZARIS, A. & KARATZAS, C. N. 2005. Goat uromodulin promoter directs kidney-specific expression of GFP gene in transgenic mice. *BMC Biotechnol,* 5**,** 9.

HUETTEMAN, D. A. & BOGIE, H. 2009. Direct blood pressure monitoring in laboratory rodents via implantable radio telemetry. *Methods Mol Biol,* 573**,** 57-73.

HUMMLER, E., BARKER, P., GATZY, J., BEERMANN, F., VERDUMO, C., SCHMIDT, A., BOUCHER, R. & ROSSIER, B. C. 1996. Early death due to defective neonatal lung liquid clearance in alpha-ENaC-deficient mice. *Nat Genet,* 12**,** 325-8.

HUNT, S. C., ELLISON, R. C., ATWOOD, L. D., PANKOW, J. S., PROVINCE, M. A. & LEPPERT, M. F. 2002. Genome scans for blood pressure and hypertension: the National Heart, Lung, and Blood Institute Family Heart Study. *Hypertension,* 40**,** 1-6.

IKEDA, K., NARA, Y. & YAMORI, Y. 1991. Indirect Systolic and Mean Blood-Pressure Determination by a New Tail Cuff Method in Spontaneously Hypertensive Rats. *Laboratory Animals,* 25**,** 26-29.

IWAI, N., KAJIMOTO, K., KOKUBO, Y. & TOMOIKE, H. 2006. Extensive genetic analysis of 10 candidate genes for hypertension in Japanese. *Hypertension,* 48**,** 901-7.

JAMES, K., WEITZEL, L. R., ENGELMAN, C. D., ZERBE, G. & NORRIS, J. M. 2003. Genome scan linkage results for longitudinal systolic blood pressure phenotypes in subjects from the Framingham Heart Study. *BMC Genet,* 4 Suppl 1**,** S83.

JI, W., FOO, J. N., O'ROAK, B. J., ZHAO, H., LARSON, M. G., SIMON, D. B., NEWTON-CHEH, C., STATE, M. W., LEVY, D. & LIFTON, R. P. 2008. Rare independent mutations in renal salt handling genes contribute to blood pressure variation. *Nat Genet,* 40**,** 592-9.

JORDAN, J., TOKA, H. R., HEUSSER, K., TOKA, O., SHANNON, J. R., TANK, J., DIEDRICH, A., STABROTH, C., STOFFELS, M., NARAGHI, R., OELKERS, W., SCHUSTER, H., SCHOBEL, H. P., HALLER, H. & LUFT, F. C. 2000. Severely impaired baroreflex-buffering in patients with monogenic hypertension and neurovascular contact. *Circulation,* 102**,** 2611-8.

KAHLE, K. T., WILSON, F. H., LENG, Q., LALIOTI, M. D., O'CONNELL, A. D., DONG, K., RAPSON, A. K., MACGREGOR, G. G., GIEBISCH, G., HEBERT, S. C. & LIFTON, R. P. 2003. WNK4 regulates the balance between renal NaCl reabsorption and K+ secretion. *Nat Genet,* 35**,** 372-6.

KAMYNINA, E., DEBONNEVILLE, C., HIRT, R. P. & STAUB, O. 2001. Liddle's syndrome: a novel mouse Nedd4 isoform regulates the activity of the epithelial Na(+) channel. *Kidney Int,* 60**,** 466-71.

KATO, N., MIYATA, T., TABARA, Y., KATSUYA, T., YANAI, K., HANADA, H., KAMIDE, K., NAKURA, J., KOHARA, K., TAKEUCHI, F., MANO, H., YASUNAMI, M., KIMURA, A., KITA, Y., UESHIMA, H., NAKAYAMA, T., SOMA, M., HATA, A., FUJIOKA, A., KAWANO, Y., NAKAO, K., SEKINE, A., YOSHIDA, T., NAKAMURA, Y., SARUTA, T., OGIHARA, T., SUGANO, S., MIKI, T. & TOMOIKE, H. 2008. High-density association study and nomination of susceptibility genes for hypertension in the Japanese National Project. *Hum Mol Genet,* 17**,** 617-27.

KILCOYNE, M. M., THOMSON, G. E., BRANCHE, G., WILLIAMS, M., GARNIER, C., CHILES, B. & SOLAND, T. 1974. Characteristics of hypertension in the black population. *Circulation,* 50**,** 1006-13.

KIM, B. C., KIM, W. Y., PARK, D., CHUNG, W. H., SHIN, K. S. & BHAK, J. 2008. SNP@Promoter: a database of human SNPs (single nucleotide polymorphisms) within the putative promoter regions. *BMC Bioinformatics,* 9 Suppl 1**,** S2.

KIM, H. T., SONG, I. Y. & PIEDRAHITA, J. 2003. Kidney-specific activity of the bovine uromodulin promoter. *Transgenic Res,* 12**,** 191-201.

KIRKHAM, M., FUJITA, A., CHADDA, R., NIXON, S. J., KURZCHALIA, T. V., SHARMA, D. K., PAGANO, R. E., HANCOCK, J. F., MAYOR, S. & PARTON, R. G. 2005. Ultrastructural identification of uncoated caveolin-independent early endocytic vehicles. *J Cell Biol,* 168**,** 465-76.

KITAMURA, M. 2008. Endoplasmic reticulum stress and unfolded protein response in renal pathophysiology: Janus faces. *Am J Physiol Renal Physiol,* 295**,** F323-34.

KOMLOSI, P., BELL, P. D. & ZHANG, Z. R. 2009. Tubuloglomerular feedback mechanisms in nephron segments beyond the macula densa. *Curr Opin Nephrol Hypertens,* 18**,** 57-62.

KOMLOSI, P., FINTHA, A. & BELL, P. D. 2005. Renal cell-to-cell communication via extracellular ATP. *Physiology (Bethesda),* 20**,** 86-90.

KOTTGEN, A., GLAZER, N. L., DEHGHAN, A., HWANG, S. J., KATZ, R., LI, M., YANG, Q., GUDNASON, V., LAUNER, L. J., HARRIS, T. B., SMITH, A. V., ARKING, D. E., ASTOR, B. C., BOERWINKLE, E., EHRET, G. B., RUCZINSKI, I., SCHARPF, R. B., CHEN, Y. D., DE BOER, I. H., HARITUNIANS, T., LUMLEY, T., SARNAK, M., SISCOVICK, D., BENJAMIN, E. J., LEVY, D., UPADHYAY, A., AULCHENKO, Y. S., HOFMAN, A., RIVADENEIRA, F., UITTERLINDEN, A. G., VAN DUIJN, C. M., CHASMAN, D. I., PARE, G., RIDKER, P. M., KAO, W. H., WITTEMAN, J. C., CORESH, J., SHLIPAK, M. G. & FOX, C. S. 2009. Multiple loci associated with indices of renal function and chronic kidney disease. *Nat Genet,* 41**,** 712-7.

KOTTGEN, A., HWANG, S. J., LARSON, M. G., VAN EYK, J. E., FU, Q., BENJAMIN, E. J., DEHGHAN, A., GLAZER, N. L., KAO, W. H., HARRIS, T. B., GUDNASON, V., SHLIPAK, M. G., YANG, Q., CORESH, J., LEVY, D. & FOX, C. S. 2010. Uromodulin levels associate with a common UMOD variant and risk for incident CKD. *J Am Soc Nephrol,* 21**,** 337-44.

KOTTGEN, A., YANG, Q., SHIMMIN, L. C., TIN, A., SCHAEFFER, C., CORESH, J., LIU, X., RAMPOLDI, L., HWANG, S. J., BOERWINKLE, E., HIXSON, J. E., KAO, W. H. & FOX, C. S. 2012. Association of estimated glomerular filtration rate and urinary uromodulin concentrations with rare variants identified by UMOD gene region sequencing. *PLoS One,* 7**,** e38311.

KRISTJANSSON, K., MANOLESCU, A., KRISTINSSON, A., HARDARSON, T., KNUDSEN, H., INGASON, S., THORLEIFSSON, G., FRIGGE, M. L., KONG, A., GULCHER, J. R. & STEFANSSON, K. 2002. Linkage of essential hypertension to chromosome 18q. *Hypertension,* 39**,** 1044-9.

KRUSHKAL, J., FERRELL, R., MOCKRIN, S. C., TURNER, S. T., SING, C. F. & BOERWINKLE, E. 1999. Genome-wide linkage analyses of systolic blood pressure using highly discordant siblings. *Circulation,* 99**,** 1407-10.

KUNEŠ J, Z. J. 2006. Developmental windows and environment as important factors in the expression of genetic information: a cardiovascular physiologist`s view. *Clin Sci (Lond),* 111**,** 295-305.

LANDER, E. S., LINTON, L. M., BIRREN, B., NUSBAUM, C., ZODY, M. C., BALDWIN, J., DEVON, K., DEWAR, K., DOYLE, M., FITZHUGH, W., FUNKE, R., GAGE, D., HARRIS, K., HEAFORD, A., HOWLAND, J., KANN, L., LEHOCZKY, J., LEVINE, R., MCEWAN, P., MCKERNAN, K., MELDRIM, J., MESIROV, J. P., MIRANDA, C., MORRIS, W., NAYLOR, J., RAYMOND, C., ROSETTI, M., SANTOS, R., SHERIDAN, A., SOUGNEZ, C., STANGE-THOMANN, N., STOJANOVIC, N., SUBRAMANIAN, A., WYMAN, D., ROGERS, J., SULSTON, J., AINSCOUGH, R., BECK, S., BENTLEY, D., BURTON, J., CLEE, C., CARTER, N., COULSON, A., DEADMAN, R., DELOUKAS, P., DUNHAM, A., DUNHAM, I., DURBIN, R., FRENCH, L., GRAFHAM, D., GREGORY, S.,

HUBBARD, T., HUMPHRAY, S., HUNT, A., JONES, M., LLOYD, C., MCMURRAY, A., MATTHEWS, L., MERCER, S., MILNE, S., MULLIKIN, J. C., MUNGALL, A., PLUMB, R., ROSS, M., SHOWNKEEN, R., SIMS, S., WATERSTON, R. H., WILSON, R. K., HILLIER, L. W., MCPHERSON, J. D., MARRA, M. A., MARDIS, E. R., FULTON, L. A., CHINWALLA, A. T., PEPIN, K. H., GISH, W. R., CHISSOE, S. L., WENDL, M. C., DELEHAUNTY, K. D., MINER, T. L., DELEHAUNTY, A., KRAMER, J. B., COOK, L. L., FULTON, R. S., JOHNSON, D. L., MINX, P. J., CLIFTON, S. W., HAWKINS, T., BRANSCOMB, E., PREDKI, P., RICHARDSON, P., WENNING, S., SLEZAK, T., DOGGETT, N., CHENG, J. F., OLSEN, A., LUCAS, S., ELKIN, C., UBERBACHER, E., FRAZIER, M., et al. 2001. Initial sequencing and analysis of the human genome. *Nature,* 409**,** 860-921.

LAPOINTE, M. S., SODHI, C., SAHAI, A. & BATLLE, D. 2002. Na+/H+ exchange activity and NHE-3 expression in renal tubules from the spontaneously hypertensive rat. *Kidney Int,* 62**,** 157-65.

LASKER, N., HOPP, L., GROSSMAN, S., BAMFORTH, R. & AVIV, A. 1985. Race and sex differences in erythrocyte Na+, K+, and Na+-K+-adenosine triphosphatase. *J Clin Invest,* 75**,** 1813-20.

LEVEY, A. S. 1990. Measurement of renal function in chronic renal disease. *Kidney Int,* 38**,** 167-84.

LEVY, D., DESTEFANO, A. L., LARSON, M. G., O'DONNELL, C. J., LIFTON, R. P., GAVRAS, H., CUPPLES, L. A. & MYERS, R. H. 2000. Evidence for a gene influencing blood pressure on chromosome 17. Genome scan linkage results for longitudinal blood pressure phenotypes in subjects from the framingham heart study. *Hypertension,* 36**,** 477-83.

LEVY, D., EHRET, G. B., RICE, K., VERWOERT, G. C., LAUNER, L. J., DEHGHAN, A., GLAZER, N. L., MORRISON, A. C., JOHNSON, A. D., ASPELUND, T., AULCHENKO, Y., LUMLEY, T., KOTTGEN, A., VASAN, R. S., RIVADENEIRA, F., EIRIKSDOTTIR, G., GUO, X., ARKING, D. E., MITCHELL, G. F., MATTACE-RASO, F. U., SMITH, A. V., TAYLOR, K., SCHARPF, R. B., HWANG, S. J., SIJBRANDS, E. J., BIS, J., HARRIS, T. B., GANESH, S. K., O'DONNELL, C. J., HOFMAN, A., ROTTER, J. I., CORESH, J., BENJAMIN, E. J., UITTERLINDEN, A. G., HEISS, G., FOX, C. S., WITTEMAN, J. C., BOERWINKLE, E., WANG, T. J., GUDNASON, V., LARSON, M. G., CHAKRAVARTI, A., PSATY, B. M. & VAN DUIJN, C. M. 2009. Genome-wide association study of blood pressure and hypertension. *Nat Genet,* 41**,** 677-87.

LEVY, D., LARSON, M. G., BENJAMIN, E. J., NEWTON-CHEH, C., WANG, T. J., HWANG, S. J., VASAN, R. S. & MITCHELL, G. F. 2007. Framingham Heart Study 100K Project: genome-wide associations for blood pressure and arterial stiffness. *BMC Med Genet,* 8 Suppl 1**,** S3.

LHOTTA, K. 2010. Uromodulin and chronic kidney disease. *Kidney Blood Press Res,* 33**,** 393-8.

LHOTTA, K., GRUBER, J., SGONC, R., FEND, F. & KONIG, P. 1998. Apoptosis of tubular epithelial cells in familial juvenile gouty nephropathy. *Nephron,* 79**,** 340-4.

LICHT, C. M., DE GEUS, E. J., SELDENRIJK, A., VAN HOUT, H. P., ZITMAN, F. G., VAN DYCK, R. & PENNINX, B. W. 2009. Depression is associated with decreased blood pressure, but antidepressant use increases the risk for hypertension. *Hypertension,* 53**,** 631-8.

LIFTON, R. P., DLUHY, R. G., POWERS, M., RICH, G. M., COOK, S., ULICK, S. & LALOUEL, J. M. 1992a. A chimaeric 11 beta-hydroxylase/aldosterone

synthase gene causes glucocorticoid-remediable aldosteronism and human hypertension. *Nature,* 355**,** 262-5.

LIFTON, R. P., DLUHY, R. G., POWERS, M., RICH, G. M., GUTKIN, M., FALLO, F., GILL, J. R., JR., FELD, L., GANGULY, A., LAIDLAW, J. C. & ET AL. 1992b. Hereditary hypertension caused by chimaeric gene duplications and ectopic expression of aldosterone synthase. *Nat Genet,* 2**,** 66-74.

LIFTON, R. P., GHARAVI, A. G. & GELLER, D. S. 2001. Molecular mechanisms of human hypertension. *Cell,* 104, 545-56.

LIU, Y., EL-ACHKAR, T. M. & WU, X. R. 2012. Tamm-Horsfall protein regulates circulating and renal cytokines by affecting glomerular filtration rate and acting as a urinary cytokine trap. *J Biol Chem,* 287**,** 16365-78.

LOFFING, J., PIETRI, L., AREGGER, F., BLOCH-FAURE, M., ZIEGLER, U., MENETON, P., ROSSIER, B. C. & KAISSLING, B. 2000. Differential subcellular localization of ENaC subunits in mouse kidney in response to high- and low-Na diets. *Am J Physiol Renal Physiol,* 279, F252-8.

LOHMEIER, T. E., KASTNER, P. R., SMITH, M. J. & GUYTON, A. C. 1980. Is Aldosteronism Important in the Maintenance of Arterial Blood-Pressure and Electrolyte Balance during Sodium Depletion. *Hypertension,* 2, 497-505.

LOREAUX, E. L., KAUL, B., LORENZ, J. N. & LINGREL, J. B. 2008. Ouabain-Sensitive alpha1 Na,K-ATPase enhances natriuretic response to saline load. *J Am Soc Nephrol,* 19, 1947-54.

LUFT, F. C. 1998. Molecular genetics of human hypertension. *J Hypertens,* 16**,** 1871-8.

LUFT, F. C. 2001. Twins in cardiovascular genetic research. *Hypertension,* 37**,** 350-6.

LUFT, F. C., GRIM, C. E., FINEBERG, N. & WEINBERGER, M. C. 1979a. Effects of volume expansion and contraction in normotensive whites, blacks, and subjects of different ages. *Circulation,* 59**,** 643-50.

LUFT, F. C., MILLER, J. Z., GRIM, C. E., FINEBERG, N. S., CHRISTIAN, J. C., DAUGHERTY, S. A. & WEINBERGER, M. H. 1991. Salt sensitivity and resistance of blood pressure. Age and race as factors in physiological responses. *Hypertension,* 17**,** I102-8.

LUFT, F. C., RANKIN, L. I., BLOCH, R., WEYMAN, A. E., WILLIS, L. R., MURRAY, R. H., GRIM, C. E. & WEINBERGER, M. H. 1979b. Cardiovascular and humoral responses to extremes of sodium intake in normal black and white men. *Circulation,* 60**,** 697-706.

LYNN, K. L., SHENKIN, A. & MARSHALL, R. D. 1982. Factors affecting excretion of human urinary Tamm-Horsfall glycoprotein. *Clin Sci (Lond),* 62**,** 21-6.

MA, L., LIU, Y., EL-ACHKAR, T. M. & WU, X. R. 2012. Molecular and cellular effects of Tamm-Horsfall protein mutations and their rescue by chemical chaperones. *J Biol Chem,* 287**,** 1290-305.

MACGREGOR, G. A., FENTON, S., ALAGHBAND-ZADEH, J., MARKANDU, N. D., ROULSTON, J. E. & DE WARDENER, H. E. 1981. An increase in a circulating inhibitor of Na+,K+-dependent ATPase: a possible link between salt intake and the development of essential hypertension. *Clin Sci (Lond),* 61 Suppl 7**,** 17s-20s.

MACGREGOR, G. A., MARKANDU, N. D., BEST, F. E., ELDER, D. M., CAM, J. M., SAGNELLA, G. A. & SQUIRES, M. 1982. Double-blind randomised crossover trial of moderate sodium restriction in essential hypertension. *Lancet,* 1**,** 351-5.

MALAGOLINI, N., CAVALLONE, D. & SERAFINICESSI, F. 1997. Intracellular transport, cell-surface exposure and release of recombinant Tamm-Horsfall glycoprotein. *Kidney International,* 52, 1340-1350.

MANJUNATH, G., TIGHIOUART, H., CORESH, J., MACLEOD, B., SALEM, D. N., GRIFFITH, J. L., LEVEY, A. S. & SARNAK, M. J. 2003a. Level of kidney function as a risk factor for cardiovascular outcomes in the elderly. *Kidney Int,* 63, 1121-9.

MANJUNATH, G., TIGHIOUART, H., IBRAHIM, H., MACLEOD, B., SALEM, D. N., GRIFFITH, J. L., CORESH, J., LEVEY, A. S. & SARNAK, M. J. 2003b. Level of kidney function as a risk factor for atherosclerotic cardiovascular outcomes in the community. *J Am Coll Cardiol,* 41, 47-55.

MANSFIELD, T. A., SIMON, D. B., FARFEL, Z., BIA, M., TUCCI, J. R., LEBEL, M., GUTKIN, M., VIALETTES, B., CHRISTOFILIS, M. A., KAUPPINEN-MAKELIN, R., MAYAN, H., RISCH, N. & LIFTON, R. P. 1997. Multilocus linkage of familial hyperkalaemia and hypertension, pseudohypoaldosteronism type II, to chromosomes 1q31-42 and 17p11-q21. *Nat Genet,* 16, 202-5.

MCCARTHY, M. I., ABECASIS, G. R., CARDON, L. R., GOLDSTEIN, D. B., LITTLE, J., IOANNIDIS, J. P. & HIRSCHHORN, J. N. 2008. Genome-wide association studies for complex traits: consensus, uncertainty and challenges. *Nat Rev Genet,* 9, 356-69.

MCDUFFIE, J. E., MOTLEY, E. D., LIMBIRD, L. E. & MALEQUE, M. A. 2000. 5-hydroxytryplamine stimulates phosphorylation of p44/p42 mitogen-activated protein kinase activation in bovine aortic endothelial cell cultures. *Journal of Cardiovascular Pharmacology,* 35, 398-402.

MCLAUGHLIN, P. J., AIKAWA, A., DAVIES, H. M., WARD, R. G., BAKRAN, A., SELLS, R. A. & JOHNSON, P. M. 1993. Uromodulin levels are decreased in urine during acute tubular necrosis but not during immune rejection after renal transplantation. *Clin Sci (Lond),* 84, 243-6.

MEHTA, P. K. & GRIENDLING, K. K. 2007. Angiotensin II cell signaling: physiological and pathological effects in the cardiovascular system. *Am J Physiol Cell Physiol,* 292, C82-97.

MENETON, P., I, I., INAGAMI, T. & SCHNERMANN, J. 2000. Renal physiology of the mouse. *American Journal of Physiology-Renal Physiology,* 278, F339-F351.

MENETON, P., JEUNEMAITRE, X., DE WARDENER, H. E. & MACGREGOR, G. A. 2005. Links between dietary salt intake, renal salt handling, blood pressure, and cardiovascular diseases. *Physiol Rev,* 85, 679-715.

MIRONOVA, E., PETI-PETERDI, J., BUGAJ, V. & STOCKAND, J. D. 2011. Diminished paracrine regulation of the epithelial Na+ channel by purinergic signaling in mice lacking connexin 30. *J Biol Chem,* 286, 1054-60.

MO, L., HUANG, H. Y., ZHU, X. H., SHAPIRO, E., HASTY, D. L. & WU, X. R. 2004. Tamm-Horsfall protein is a critical renal defense factor protecting against calcium oxalate crystal formation. *Kidney Int,* 66, 1159-66.

MOLLSTEN, A. & TORFFVIT, O. 2010. Tamm-Horsfall protein gene is associated with distal tubular dysfunction in patients with type 1 diabetes. *Scandinavian Journal of Urology and Nephrology,* 44, 438-444.

MOLONY, D. A., REEVES, W. B., HEBERT, S. C. & ANDREOLI, T. E. 1987. ADH increases apical Na+, K+, 2Cl- entry in mouse medullary thick ascending limbs of Henle. *American Journal of Physiology,* 252, F177-87.

MONGEAU, J. G., BIRON, P. & SING, C. F. 1986. The influence of genetics and household environment upon the variability of normal blood pressure: the Montreal Adoption Survey. *Clin Exp Hypertens A,* 8, 653-60.

MUCHMORE, A. V. & DECKER, J. M. 1985. Uromodulin: a unique 85-kilodalton immunosuppressive glycoprotein isolated from urine of pregnant women. *Science,* 229**,** 479-81.

MUNE, T., ROGERSON, F. M., NIKKILA, H., AGARWAL, A. K. & WHITE, P. C. 1995. Human hypertension caused by mutations in the kidney isozyme of 11 beta-hydroxysteroid dehydrogenase. *Nat Genet,* 10**,** 394-9.

MUNROE, P. B., WALLACE, C., XUE, M. Z., MARCANO, A. C., DOBSON, R. J., ONIPINLA, A. K., BURKE, B., GUNGADOO, J., NEWHOUSE, S. J., PEMBROKE, J., BROWN, M., DOMINICZAK, A. F., SAMANI, N. J., LATHROP, M., CONNELL, J., WEBSTER, J., CLAYTON, D., FARRALL, M., MEIN, C. A. & CAULFIELD, M. 2006. Increased support for linkage of a novel locus on chromosome 5q13 for essential hypertension in the British Genetics of Hypertension Study. *Hypertension,* 48**,** 105-11.

MUTIG, K., KAHL, T., SARITAS, T., GODES, M., PERSSON, P., BATES, J., RAFFI, H., RAMPOLDI, L., UCHIDA, S., HILLE, C., DOSCHE, C., KUMAR, S., CASTANEDA-BUENO, M., GAMBA, G. & BACHMANN, S. 2011a. Activation of the Bumetanide-sensitive Na+, K+,2Cl(-) Cotransporter (NKCC2) Is Facilitated by Tamm-Horsfall Protein in a Chloride-sensitive Manner. *Journal of Biological Chemistry,* 286**,** 30200-30210.

MUTIG, K., KAHL, T., SARITAS, T., GODES, M., PERSSON, P., BATES, J., RAFFI, H., RAMPOLDI, L., UCHIDA, S., HILLE, C., DOSCHE, C., KUMAR, S., CASTANEDA-BUENO, M., GAMBA, G. & BACHMANN, S. 2011b. Activation of the bumetanide-sensitive Na+,K+,2Cl- cotransporter (NKCC2) is facilitated by Tamm-Horsfall protein in a chloride-sensitive manner. *J Biol Chem,* 286**,** 30200-10.

NAKATSUJI, K., KII, Y., FUJITANI, B. & ITO, T. 1990. General pharmacology of recombinant human tumor necrosis factor. 1st communication: effects on cardiovascular, gastrointestinal, renal and blood functions. *Arzneimittelforschung,* 40, 218-25.

NEWTON-CHEH, C., JOHNSON, T., GATEVA, V., TOBIN, M. D., BOCHUD, M., COIN, L., NAJJAR, S. S., ZHAO, J. H., HEATH, S. C., EYHERAMENDY, S., PAPADAKIS, K., VOIGHT, B. F., SCOTT, L. J., ZHANG, F., FARRALL, M., TANAKA, T., WALLACE, C., CHAMBERS, J. C., KHAW, K. T., NILSSON, P., VAN DER HARST, P., POLIDORO, S., GROBBEE, D. E., ONLAND-MORET, N. C., BOTS, M. L., WAIN, L. V., ELLIOTT, K. S., TEUMER, A., LUAN, J., LUCAS, G., KUUSISTO, J., BURTON, P. R., HADLEY, D., MCARDLE, W. L., BROWN, M., DOMINICZAK, A., NEWHOUSE, S. J., SAMANI, N. J., WEBSTER, J., ZEGGINI, E., BECKMANN, J. S., BERGMANN, S., LIM, N., SONG, K., VOLLENWEIDER, P., WAEBER, G., WATERWORTH, D. M., YUAN, X., GROOP, L., ORHO-MELANDER, M., ALLIONE, A., DI GREGORIO, A., GUARRERA, S., PANICO, S., RICCERI, F., ROMANAZZI, V., SACERDOTE, C., VINEIS, P., BARROSO, I., SANDHU, M. S., LUBEN, R. N., CRAWFORD, G. J., JOUSILAHTI, P., PEROLA, M., BOEHNKE, M., BONNYCASTLE, L. L., COLLINS, F. S., JACKSON, A. U., MOHLKE, K. L., STRINGHAM, H. M., VALLE, T. T., WILLER, C. J., BERGMAN, R. N., MORKEN, M. A., DORING, A., GIEGER, C., ILLIG, T., MEITINGER, T., ORG, E., PFEUFER, A., WICHMANN, H. E., KATHIRESAN, S., MARRUGAT, J., O'DONNELL, C. J., SCHWARTZ, S. M., SISCOVICK, D. S., SUBIRANA, I., FREIMER, N. B., HARTIKAINEN, A. L., MCCARTHY, M. I., O'REILLY, P. F., PELTONEN, L., POUTA, A., DE JONG, P. E., SNIEDER, H., VAN GILST, W. H., CLARKE, R., GOEL, A., HAMSTEN, A., PEDEN, J. F., et al. 2009. Genome-wide

association study identifies eight loci associated with blood pressure. *Nat Genet,* 41, 666-76.

NG, K. K. & VANE, J. R. 1967. Conversion of angiotensin I to angiotensin II. *Nature,* 216, 762-6.

NICKERSON, D. A., TAYLOR, S. L., WEISS, K. M., CLARK, A. G., HUTCHINSON, R. G., STENGARD, J., SALOMAA, V., VARTIAINEN, E., BOERWINKLE, E. & SING, C. F. 1998. DNA sequence diversity in a 9.7-kb region of the human lipoprotein lipase gene. *Nat Genet,* 19, 233-40.

NOFZIGER, C. & BLAZER-YOST, B. L. 2009. PPAR gamma Agonists, Modulation of Ion Transporters, and Fluid Retention. *Journal of the American Society of Nephrology,* 20, 2481-2483.

NORREGAARD, R., JENSEN, B. L., LI, C., WANG, W., KNEPPER, M. A., NIELSEN, S. & FROKIAER, J. 2005. COX-2 inhibition prevents downregulation of key renal water and sodium transport proteins in response to bilateral ureteral obstruction. *Am J Physiol Renal Physiol,* 289, F322-33.

NYORMOI, O., WANG, Z., DOAN, D., RUIZ, M., MCCONKEY, D. & BAR-ELI, M. 2001. Transcription factor AP-2alpha is preferentially cleaved by caspase 6 and degraded by proteasome during tumor necrosis factor alpha-induced apoptosis in breast cancer cells. *Mol Cell Biol,* 21, 4856-67.

O'BRIEN, W. J., LINGREL, J. B. & WALLICK, E. T. 1994. Ouabain binding kinetics of the rat alpha two and alpha three isoforms of the sodium-potassium adenosine triphosphate. *Arch Biochem Biophys,* 310, 32-9.

OLDHAM, P. D., PICKERING, G., ROBERTS, J. A. & SOWRY, G. S. 1960. The nature of essential hypertension. *Lancet,* 1, 1085-93.

OLIPHANT, A., BARKER, D. L., STUELPNAGEL, J. R. & CHEE, M. S. 2002. BeadArray technology: enabling an accurate, cost-effective approach to high-throughput genotyping. *Biotechniques,* Suppl, 56-8, 60-1.

OLLIER-HARTMANN, M. P., POUGET-ABADIE, C., BOUILLIE, J. & HARTMANN, L. 1984. Variations of urinary Tamm-Horsfall protein in humans during the first thirty years of life. *Nephron,* 38, 163-6.

ORG, E., EYHERAMENDY, S., JUHANSON, P., GIEGER, C., LICHTNER, P., KLOPP, N., VELDRE, G., DORING, A., VIIGIMAA, M., SOBER, S., TOMBERG, K., ECKSTEIN, G., KELGO, P., REBANE, T., SHAW-HAWKINS, S., HOWARD, P., ONIPINLA, A., DOBSON, R. J., NEWHOUSE, S. J., BROWN, M., DOMINICZAK, A., CONNELL, J., SAMANI, N., FARRALL, M., CAULFIELD, M. J., MUNROE, P. B., ILLIG, T., WICHMANN, H. E., MEITINGER, T. & LAAN, M. 2009. Genome-wide scan identifies CDH13 as a novel susceptibility locus contributing to blood pressure determination in two European populations. *Hum Mol Genet,* 18, 2288-96.

ORSO, F., CORA, D., UBEZIO, B., PROVERO, P., CASELLE, M. & TAVERNA, D. 2010. Identification of functional TFAP2A and SP1 binding sites in new TFAP2A-modulated genes. *BMC Genomics,* 11, 355.

PADMANABHAN, S., MELANDER, O., HASTIE, C., MENNI, C., DELLES, C., CONNELL, J. M. & DOMINICZAK, A. F. 2008. Hypertension and genome-wide association studies: combining high fidelity phenotyping and hypercontrols. *J Hypertens,* 26, 1275-81.

PADMANABHAN, S., MELANDER, O., JOHNSON, T., DI BLASIO, A. M., LEE, W. K., GENTILINI, D., HASTIE, C. E., MENNI, C., MONTI, M. C., DELLES, C., LAING, S., CORSO, B., NAVIS, G., KWAKERNAAK, A. J., VAN DER HARST, P., BOCHUD, M., MAILLARD, M., BURNIER, M., HEDNER, T., KJELDSEN, S., WAHLSTRAND, B., SJOGREN, M., FAVA, C., MONTAGNANA, M., DANESE, E., TORFFVIT, O., HEDBLAD, B., SNIEDER, H., CONNELL, J. M., BROWN, M.,

SAMANI, N. J., FARRALL, M., CESANA, G., MANCIA, G., SIGNORINI, S., GRASSI, G., EYHERAMENDY, S., WICHMANN, H. E., LAAN, M., STRACHAN, D. P., SEVER, P., SHIELDS, D. C., STANTON, A., VOLLENWEIDER, P., TEUMER, A., VOLZKE, H., RETTIG, R., NEWTON-CHEH, C., ARORA, P., ZHANG, F., SORANZO, N., SPECTOR, T. D., LUCAS, G., KATHIRESAN, S., SISCOVICK, D. S., LUAN, J., LOOS, R. J., WAREHAM, N. J., PENNINX, B. W., NOLTE, I. M., MCBRIDE, M., MILLER, W. H., NICKLIN, S. A., BAKER, A. H., GRAHAM, D., MCDONALD, R. A., PELL, J. P., SATTAR, N., WELSH, P., MUNROE, P., CAULFIELD, M. J., ZANCHETTI, A. & DOMINICZAK, A. F. 2010. Genome-wide association study of blood pressure extremes identifies variant near UMOD associated with hypertension. *PLoS Genet,* 6**,** e1001177.

PADMANABHAN, S., NEWTON-CHEH, C. & DOMINICZAK, A. F. 2012. Genetic basis of blood pressure and hypertension. *Trends Genet,* 28**,** 397-408.

PAK, J., PU, Y., ZHANG, Z. T., HASTY, D. L. & WU, X. R. 2001. Tamm-Horsfall protein binds to type 1 fimbriated Escherichia coli and prevents E. coli from binding to uroplakin Ia and Ib receptors. *J Biol Chem,* 276**,** 9924-30.

PALADINO, S., LEBRETON, S., TIVODAR, S., CAMPANA, V., TEMPRE, R. & ZURZOLO, C. 2008. Different GPI-attachment signals affect the oligomerisation of GPI-anchored proteins and their apical sorting. *J Cell Sci,* 121**,** 4001-7.

PALMER, L. J. & CARDON, L. R. 2005. Shaking the tree: mapping complex disease genes with linkage disequilibrium. *Lancet,* 366**,** 1223-34.

PAMPLONA, A., FERREIRA, A., BALLA, J., JENEY, V., BALLA, G., EPIPHANIO, S., CHORA, A., RODRIGUES, C. D., GREGOIRE, I. P., CUNHA-RODRIGUES, M., PORTUGAL, S., SOARES, M. P. & MOTA, M. M. 2007. Heme oxygenase-1 and carbon monoxide suppress the pathogenesis of experimental cerebral malaria. *Nature Medicine,* 13**,** 703-710.

PANKOW, J. S., ROSE, K. M., OBERMAN, A., HUNT, S. C., ATWOOD, L. D., DJOUSSE, L., PROVINCE, M. A. & RAO, D. C. 2000. Possible locus on chromosome 18q influencing postural systolic blood pressure changes. *Hypertension,* 36**,** 471-6.

PASCOE, L., CURNOW, K. M., SLUTSKER, L., ROSLER, A. & WHITE, P. C. 1992. Mutations in the human CYP11B2 (aldosterone synthase) gene causing corticosterone methyloxidase II deficiency. *Proc Natl Acad Sci U S A,* 89**,** 4996-5000.

PAUSOVA, Z., GAUDET, D., GOSSARD, F., BERNARD, M., KALDUNSKI, M. L., JOMPHE, M., TREMBLAY, J., HUDSON, T. J., BOUCHARD, G., KOTCHEN, T. A., COWLEY, A. W. & HAMET, P. 2005. Genome-wide scan for linkage to obesity-associated hypertension in French Canadians. *Hypertension,* 46**,** 1280-5.

PAYNE, J. A., XU, J. C., HAAS, M., LYTLE, C. Y., WARD, D. & FORBUSH, B., 3RD 1995. Primary structure, functional expression, and chromosomal localization of the bumetanide-sensitive Na-K-Cl cotransporter in human colon. *J Biol Chem,* 270**,** 17977-85.

PECH, V., THUMOVA, M., DIKALOV, S. I., HUMMLER, E., ROSSIER, B. C., HARRISON, D. G. & WALL, S. M. 2013. Nitric oxide reduces Cl(-) absorption in the mouse cortical collecting duct through an ENaC-dependent mechanism. *Am J Physiol Renal Physiol,* 304**,** F1390-7.

PENNICA, D., KOHR, W. J., KUANG, W. J., GLAISTER, D., AGGARWAL, B. B., CHEN, E. Y. & GOEDDEL, D. V. 1987. Identification of human uromodulin as the Tamm-Horsfall urinary glycoprotein. *Science,* 236**,** 83-8.

PEROLA, M., KAINULAINEN, K., PAJUKANTA, P., TERWILLIGER, J. D., HIEKKALINNA, T., ELLONEN, P., KAPRIO, J., KOSKENVUO, M., KONTULA, K. & PELTONEN, L. 2000. Genome-wide scan of predisposing loci for increased diastolic blood pressure in Finnish siblings. *J Hypertens,* 18**,** 1579-85.

PLATT, R. 1959. The nature of essential hypertension. *Lancet,* 2**,** 55-7.

PLUSKAL, T., CASTILLO, S., VILLAR-BRIONES, A. & ORESIC, M. 2010. MZmine 2: modular framework for processing, visualizing, and analyzing mass spectrometry-based molecular profile data. *BMC Bioinformatics,* 11**,** 395.

POCHYNYUK, O., RIEG, T., BUGAJ, V., SCHROTH, J., FRIDMAN, A., BOSS, G. R., INSEL, P. A., STOCKAND, J. D. & VALLON, V. 2010. Dietary Na+ inhibits the open probability of the epithelial sodium channel in the kidney by enhancing apical P2Y2-receptor tone. *FASEB J,* 24**,** 2056-65.

PRAJCZER, S., HEIDENREICH, U., PFALLER, W., KOTANKO, P., LHOTTA, K. & JENNINGS, P. 2010. Evidence for a role of uromodulin in chronic kidney disease progression. *Nephrol Dial Transplant,* 25**,** 1896-903.

PRESSLER, C. A., HEINZINGER, J., JECK, N., WALDEGGER, P., PECHMANN, U., REINALTER, S., KONRAD, M., BEETZ, R., SEYBERTH, H. W. & WALDEGGER, S. 2006. Late-onset manifestation of antenatal Bartter syndrome as a result of residual function of the mutated renal Na+-K+-2Cl- co-transporter. *J Am Soc Nephrol,* 17, 2136-42.

PRICE, D. A., FISHER, N. D., LANSANG, M. C., STEVANOVIC, R., WILLIAMS, G. H. & HOLLENBERG, N. K. 2002. Renal perfusion in blacks: alterations caused by insuppressibility of intrarenal renin with salt. *Hypertension,* 40**,** 186-9.

PRITCHARD, J. K. 2001. Are rare variants responsible for susceptibility to complex diseases? *Am J Hum Genet,* 69**,** 124-37.

PUPPALA, S., COLETTA, D. K., SCHNEIDER, J., HU, S. L., FAROOK, V. S., DYER, T. D., ARYA, R., BLANGERO, J., DUGGIRALA, R., DEFRONZO, R. A. & JENKINSON, C. P. 2011. Genome-wide linkage screen for systolic blood pressure in the Veterans Administration Genetic Epidemiology Study (VAGES) of Mexican-Americans and confirmation of a major susceptibility locus on chromosome 6q14.1. *Hum Hered,* 71**,** 1-10.

RAFFI, H. S., BATES, J. M., JR., LASZIK, Z. & KUMAR, S. 2005. Tamm-Horsfall protein acts as a general host-defense factor against bacterial cystitis. *Am J Nephrol,* 25**,** 570-8.

RAFFI, H. S., BATES, J. M., JR., LASZIK, Z. & KUMAR, S. 2009. Tamm-horsfall protein protects against urinary tract infection by proteus mirabilis. *J Urol,* 181**,** 2332-8.

RAJENDRAN, L. & SIMONS, K. 2005. Lipid rafts and membrane dynamics. *J Cell Sci,* 118**,** 1099-102.

RAMPOLDI, L., CARIDI, G., SANTON, D., BOARETTO, F., BERNASCONE, I., LAMORTE, G., TARDANICO, R., DAGNINO, M., COLUSSI, G., SCOLARI, F., GHIGGERI, G. M., AMOROSO, A. & CASARI, G. 2003. Allelism of MCKD, FJHN and GCKD caused by impairment of uromodulin export dynamics. *Hum Mol Genet,* 12**,** 3369-84.

RAMPOLDI, L., SCOLARI, F., AMOROSO, A., GHIGGERI, G. & DEVUYST, O. 2011. The rediscovery of uromodulin (Tamm-Horsfall protein): from tubulointerstitial nephropathy to chronic kidney disease. *Kidney Int,* 80**,** 338-47.

RAO, D. C., PROVINCE, M. A., LEPPERT, M. F., OBERMAN, A., HEISS, G., ELLISON, R. C., ARNETT, D. K., ECKFELDT, J. H., SCHWANDER, K., MOCKRIN, S. C. &

HUNT, S. C. 2003. A genome-wide affected sibpair linkage analysis of hypertension: the HyperGEN network. *Am J Hypertens,* 16**,** 148-50.

REEVES, W. B. & MOLONY, D. A. 1988. The physiology of loop diuretic action. *Semin Nephrol,* 8**,** 225-33.

REICH, D. E. & LANDER, E. S. 2001. On the allelic spectrum of human disease. *Trends Genet,* 17**,** 502-10.

RENIGUNTA, A., RENIGUNTA, V., SARITAS, T., DECHER, N., MUTIG, K. & WALDEGGER, S. 2011. Tamm-Horsfall glycoprotein interacts with renal outer medullary potassium channel ROMK2 and regulates its function. *J Biol Chem,* 286**,** 2224-35.

RICE, T., RANKINEN, T., CHAGNON, Y. C., PROVINCE, M. A., PERUSSE, L., LEON, A. S., SKINNER, J. S., WILMORE, J. H., BOUCHARD, C. & RAO, D. C. 2002. Genomewide linkage scan of resting blood pressure: HERITAGE Family Study. Health, Risk Factors, Exercise Training, and Genetics. *Hypertension,* 39**,** 1037-43.

RICE, T., RANKINEN, T., PROVINCE, M. A., CHAGNON, Y. C., PERUSSE, L., BORECKI, I. B., BOUCHARD, C. & RAO, D. C. 2000. Genome-wide linkage analysis of systolic and diastolic blood pressure: the Quebec Family Study. *Circulation,* 102**,** 1956-63.

RICH, G. M., ULICK, S., COOK, S., WANG, J. Z., LIFTON, R. P. & DLUHY, R. G. 1992. Glucocorticoid-remediable aldosteronism in a large kindred: clinical spectrum and diagnosis using a characteristic biochemical phenotype. *Ann Intern Med,* 116**,** 813-20.

RINDLER, M. J., NAIK, S. S., LI, N., HOOPS, T. C. & PERALDI, M. N. 1990. Uromodulin (Tamm-Horsfall glycoprotein/uromucoid) is a phosphatidylinositol-linked membrane protein. *J Biol Chem,* 265**,** 20784-9.

RINEHART, J., KAHLE, K. T., DE LOS HEROS, P., VAZQUEZ, N., MEADE, P., WILSON, F. H., HEBERT, S. C., GIMENEZ, I., GAMBA, G. & LIFTON, R. P. 2005. WNK3 kinase is a positive regulator of NKCC2 and NCC, renal cation-Cl- cotransporters required for normal blood pressure homeostasis. *Proc Natl Acad Sci U S A,* 102**,** 16777-82.

RING, A. M., LENG, Q., RINEHART, J., WILSON, F. H., KAHLE, K. T., HEBERT, S. C. & LIFTON, R. P. 2007. An SGK1 site in WNK4 regulates Na+ channel and K+ channel activity and has implications for aldosterone signaling and K+ homeostasis. *Proc Natl Acad Sci U S A,* 104**,** 4025-9.

SABATTI, C., SERVICE, S. K., HARTIKAINEN, A. L., POUTA, A., RIPATTI, S., BRODSKY, J., JONES, C. G., ZAITLEN, N. A., VARILO, T., KAAKINEN, M., SOVIO, U., RUOKONEN, A., LAITINEN, J., JAKKULA, E., COIN, L., HOGGART, C., COLLINS, A., TURUNEN, H., GABRIEL, S., ELLIOT, P., MCCARTHY, M. I., DALY, M. J., JARVELIN, M. R., FREIMER, N. B. & PELTONEN, L. 2009. Genome-wide association analysis of metabolic traits in a birth cohort from a founder population. *Nat Genet,* 41**,** 35-46.

SABHARANJAK, S., SHARMA, P., PARTON, R. G. & MAYOR, S. 2002. GPI-anchored proteins are delivered to recycling endosomes via a distinct cdc42-regulated, clathrin-independent pinocytic pathway. *Dev Cell,* 2**,** 411-23.

SAHAY, M., NARAYEN, G. & ANURADHA 2007. Sodium transporters in kidney role in health and disease. *J Assoc Physicians India,* 55**,** 135-9.

SALANGA, C. L., O'HAYRE, M. & HANDEL, T. 2009. Modulation of chemokine receptor activity through dimerization and crosstalk. *Cell Mol Life Sci,* 66**,** 1370-86.

SANSOM, S. C., WEINMAN, E. J. & O'NEIL, R. G. 1984. Microelectrode assessment of chloride-conductive properties of cortical collecting duct. *Am J Physiol,* 247**,** F291-302.

SANTAMBROGIO, S., CATTANEO, A., BERNASCONE, I., SCHWEND, T., JOVINE, L., BACHI, A. & RAMPOLDI, L. 2008. Urinary uromodulin carries an intact ZP domain generated by a conserved C-terminal proteolytic cleavage. *Biochem Biophys Res Commun,* 370**,** 410-3.

SARNAK, M. J., LEVEY, A. S., SCHOOLWERTH, A. C., CORESH, J., CULLETON, B., HAMM, L. L., MCCULLOUGH, P. A., KASISKE, B. L., KELEPOURIS, E., KLAG, M. J., PARFREY, P., PFEFFER, M., RAIJ, L., SPINOSA, D. J. & WILSON, P. W. 2003. Kidney disease as a risk factor for development of cardiovascular disease: a statement from the American Heart Association Councils on Kidney in Cardiovascular Disease, High Blood Pressure Research, Clinical Cardiology, and Epidemiology and Prevention. *Circulation,* 108**,** 2154-69.

SCHIESSL, I. M., ROSENAUER, A., KATTLER, V., MINUTH, W. W., OPPERMANN, M. & CASTROP, H. 2013. Dietary Salt Intake Modulates Differential Splicing of the Na/K/2Cl Cotransporter NKCC2. *Am J Physiol Renal Physiol.*

SCHROTER, J., TIMMERMANS, G., SEYBERTH, H. W., GREVEN, J. & BACHMANN, S. 1993. Marked Reduction of Tamm-Horsfall Protein-Synthesis in Hyperprostaglandin E-Syndrome. *Kidney International,* 44**,** 401-410.

SCHULTHEIS, P. J., CLARKE, L. L., MENETON, P., MILLER, M. L., SOLEIMANI, M., GAWENIS, L. R., RIDDLE, T. M., DUFFY, J. J., DOETSCHMAN, T., WANG, T., GIEBISCH, G., ARONSON, P. S., LORENZ, J. N. & SHULL, G. E. 1998. Renal and intestinal absorptive defects in mice lacking the NHE3 Na+/H+ exchanger. *Nat Genet,* 19**,** 282-5.

SCHUSTER, H., WIENKER, T. E., BAHRING, S., BILGINTURAN, N., TOKA, H. R., NEITZEL, H., JESCHKE, E., TOKA, O., GILBERT, D., LOWE, A., OTT, J., HALLER, H. & LUFT, F. C. 1996. Severe autosomal dominant hypertension and brachydactyly in a unique Turkish kindred maps to human chromosome 12. *Nat Genet,* 13**,** 98-100.

SCOLARI, F., CARIDI, G., RAMPOLDI, L., TARDANICO, R., IZZI, C., PIRULLI, D., AMOROSO, A., CASARI, G. & GHIGGERI, G. M. 2004. Uromodulin storage diseases: clinical aspects and mechanisms. *Am J Kidney Dis,* 44**,** 987-99.

SERAFINI-CESSI, F., MALAGOLINI, N. & CAVALLONE, D. 2003. Tamm-Horsfall glycoprotein: biology and clinical relevance. *Am J Kidney Dis,* 42**,** 658-76.

SEVER, P. S. & POULTER, N. R. 1989. A hypothesis for the pathogenesis of essential hypertension: the initiating factors. *J Hypertens Suppl,* 7**,** S9-12.

SHAHID, M., FRANCIS, J. & MAJID, D. S. 2008a. Tumor necrosis factor-alpha induces renal vasoconstriction as well as natriuresis in mice. *Am J Physiol Renal Physiol,* 295**,** F1836-44.

SHAHID, M., FRANCIS, J. & MAJID, D. S. A. 2008b. Tumor necrosis factor-alpha induces renal vasoconstriction as well as natriuresis in mice. *American Journal of Physiology-Renal Physiology,* 295**,** F1836-F1844.

SHERBLOM, A. P., DECKER, J. M. & MUCHMORE, A. V. 1988. The Lectin-Like Interaction between Recombinant Tumor Necrosis Factor and Uromodulin. *Journal of Biological Chemistry,* 263**,** 5418-5424.

SHIMAMOTO, H. & SHIMAMOTO, Y. 1990. Time course of hemodynamic responses to sodium in elderly hypertensive patients. *Hypertension,* 16**,** 387-97.

SICA, D. A. & DOUGLAS, J. G. 2001. The African American Study of Kidney Disease and Hypertension (AASK): new findings. *J Clin Hypertens (Greenwich),* 3**,** 244-51.

SIKRI, K. L., FOSTER, C. L., ALEXANDER, D. P. & MARSHALL, R. D. 1981. Localization of Tamm-Horsfall glycoprotein in the fetal and neonatal hamster kidney as demonstrated by immunofluorescence and immunoelectron microscopical techniques. *Biol Neonate,* 39, 305-12.

SILVA, G. B. & GARVIN, J. L. 2009. Extracellular ATP inhibits transport in medullary thick ascending limbs: role of P2X receptors. *Am J Physiol Renal Physiol,* 297, F1168-73.

SIMCHON, S., MANGER, W. M. & BROWN, T. W. 1991. Dual hemodynamic mechanisms for salt-induced hypertension in Dahl salt-sensitive rats. *Hypertension,* 17, 1063-71.

SIMINO, J., RAO, D. C. & FREEDMAN, B. I. 2012. Novel findings and future directions on the genetics of hypertension. *Curr Opin Nephrol Hypertens,* 21, 500-7.

SIMINO, J., SHI, G., KUME, R., SCHWANDER, K., PROVINCE, M. A., GU, C. C., KARDIA, S., CHAKRAVARTI, A., EHRET, G., OLSHEN, R. A., TURNER, S. T., HO, L. T., ZHU, X., JAQUISH, C., PALTOO, D., COOPER, R. S., WEDER, A., CURB, J. D., BOERWINKLE, E., HUNT, S. C. & RAO, D. C. 2011. Five blood pressure loci identified by an updated genome-wide linkage scan: meta-analysis of the Family Blood Pressure Program. *Am J Hypertens,* 24, 347-54.

SIMON, D. B., BINDRA, R. S., MANSFIELD, T. A., NELSON-WILLIAMS, C., MENDONCA, E., STONE, R., SCHURMAN, S., NAYIR, A., ALPAY, H., BAKKALOGLU, A., RODRIGUEZ-SORIANO, J., MORALES, J. M., SANJAD, S. A., TAYLOR, C. M., PILZ, D., BREM, A., TRACHTMAN, H., GRISWOLD, W., RICHARD, G. A., JOHN, E. & LIFTON, R. P. 1997. Mutations in the chloride channel gene, CLCNKB, cause Bartter's syndrome type III. *Nat Genet,* 17, 171-8.

SIMON, D. B., KARET, F. E., HAMDAN, J. M., DIPIETRO, A., SANJAD, S. A. & LIFTON, R. P. 1996a. Bartter's syndrome, hypokalaemic alkalosis with hypercalciuria, is caused by mutations in the Na-K-2Cl cotransporter NKCC2. *Nat Genet,* 13, 183-8.

SIMON, D. B., NELSON-WILLIAMS, C., BIA, M. J., ELLISON, D., KARET, F. E., MOLINA, A. M., VAARA, I., IWATA, F., CUSHNER, H. M., KOOLEN, M., GAINZA, F. J., GITLEMAN, H. J. & LIFTON, R. P. 1996b. Gitelman's variant of Bartter's syndrome, inherited hypokalaemic alkalosis, is caused by mutations in the thiazide-sensitive Na-Cl cotransporter. *Nat Genet,* 12, 24-30.

SMAGULA, R. M., VAN HALBEEK, H., DECKER, J. M., MUCHMORE, A. V., MOODY, C. E. & SHERBLOM, A. P. 1990. Pregnancy-associated changes in oligomannose oligosaccharides of human and bovine uromodulin (Tamm-Horsfall glycoprotein). *Glycoconj J,* 7, 609-24.

SOBEL, J. D. & KAYE, D. 1985. Reduced uromucoid excretion in the elderly. *J Infect Dis,* 152, 653.

SONALKER, P. A., TOFOVIC, S. P. & JACKSON, E. K. 2004. Increased expression of the sodium transporter BSC-1 in spontaneously hypertensive rats. *J Pharmacol Exp Ther,* 311, 1052-61.

SONALKER, P. A., TOFOVIC, S. P. & JACKSON, E. K. 2007. Cellular distribution of the renal bumetanide-sensitive Na-K-2Cl cotransporter BSC-1 in the inner stripe of the outer medulla during the development of hypertension in the spontaneously hypertensive rat. *Clin Exp Pharmacol Physiol,* 34, 1307-12.

STARREMANS, P. G., KERSTEN, F. F., KNOERS, N. V., VAN DEN HEUVEL, L. P. & BINDELS, R. J. 2003. Mutations in the human Na-K-2Cl cotransporter

(NKCC2) identified in Bartter syndrome type I consistently result in nonfunctional transporters. *J Am Soc Nephrol,* 14, 1419-26.

STAUB, O., DHO, S., HENRY, P., CORREA, J., ISHIKAWA, T., MCGLADE, J. & ROTIN, D. 1996. WW domains of Nedd4 bind to the proline-rich PY motifs in the epithelial Na+ channel deleted in Liddle's syndrome. *EMBO J,* 15, 2371-80.

STECHMAN, M. J., AHMAD, B. N., LOH, N. Y., REED, A. A. C., STEWART, M., WELLS, S., HOUGH, T., BENTLEY, L., COX, R. D., BROWN, S. D. M. & THAKKER, R. V. 2010. Establishing normal plasma and 24-hour urinary biochemistry ranges in C3H, BALB/c and C57BL/6J mice following acclimatization in metabolic cages. *Laboratory Animals,* 44, 218-225.

STEVENS, L. A., CORESH, J., GREENE, T. & LEVEY, A. S. 2006. Assessing kidney function--measured and estimated glomerular filtration rate. *N Engl J Med,* 354, 2473-83.

STEVENS, L. A. & LEVEY, A. S. 2005. Measurement of kidney function. *Med Clin North Am,* 89, 457-73.

STEVENSON, F. K., CLEAVE, A. J. & KENT, P. W. 1971. The effect of ions on the viscometric and ultracentrifugal behaviour of Tamm-Horsfall glycoprotein. *Biochim Biophys Acta,* 236, 59-66.

STIBURKOVA, B., MAJEWSKI, J., SEBESTA, I., ZHANG, W., OTT, J. & KMOCH, S. 2000. Familial juvenile hyperuricemic nephropathy: localization of the gene on chromosome 16p11.2-and evidence for genetic heterogeneity. *Am J Hum Genet,* 66, 1989-94.

STOCKAND, J. D., MIRONOVA, E., BUGAJ, V., RIEG, T., INSEL, P. A., VALLON, V., PETI-PETERDI, J. & POCHYNYUK, O. 2010. Purinergic inhibition of ENaC produces aldosterone escape. *J Am Soc Nephrol,* 21, 1903-11.

SU, S. J. & YEH, T. M. 1999. The dynamic responses of pro-inflammatory and anti-inflammatory cytokines of human mononuclear cells induced by uromodulin. *Life Sci,* 65, 2581-90.

SUGIMOTO, Y. & NARUMIYA, S. 2007. Prostaglandin E receptors. *J Biol Chem,* 282, 11613-7.

SUTHERLAND, D. J., RUSE, J. L. & LAIDLAW, J. C. 1966. Hypertension, increased aldosterone secretion and low plasma renin activity relieved by dexamethasone. *Can Med Assoc J,* 95, 1109-19.

TAMM, I. & HORSFALL, F. L., JR. 1950. Characterization and separation of an inhibitor of viral hemagglutination present in urine. *Proc Soc Exp Biol Med,* 74, 106-8.

TAMM, I. & HORSFALL, F. L., JR. 1952. A mucoprotein derived from human urine which reacts with influenza, mumps, and Newcastle disease viruses. *J Exp Med,* 95, 71-97.

TANDAI-HIRUMA, M., ENDO, T. & KOBATA, A. 1999. Detection of novel carbohydrate binding activity of interleukin-1. *J Biol Chem,* 274, 4459-66.

THOMAS, D. B., DAVIES, M. & WILLIAMS, J. D. 1993. Release of gelatinase and superoxide from human mononuclear phagocytes in response to particulate Tamm Horsfall protein. *Am J Pathol,* 142, 249-60.

TOMA, G., BATES, J. M., JR. & KUMAR, S. 1994. Uromodulin (Tamm-Horsfall protein) is a leukocyte adhesion molecule. *Biochem Biophys Res Commun,* 200, 275-82.

TOMASZEWSKI, M., CHARCHAR, F. J., LYNCH, M. D., PADMANABHAN, S., WANG, W. Y., MILLER, W. H., GRZESZCZAK, W., MARIC, C., ZUKOWSKA-SZCZECHOWSKA, E. & DOMINICZAK, A. F. 2007a. Fibroblast growth factor

1 gene and hypertension: from the quantitative trait locus to positional analysis. *Circulation,* 116**,** 1915-24.

TOMASZEWSKI, M., CHARCHAR, F. J. & SAMANI, N. J. 2007b. Association studies in current cardiovascular genetics - functional variants, tags or both? *J Hum Hypertens,* 21**,** 425-6.

TORFFVIT, O., JORGENSEN, P. E., KAMPER, A. L., HOLSTEIN-RATHLOU, N. H., LEYSSAC, P. P., POULSEN, S. S. & STRANDGAARD, S. 1998. Urinary excretion of Tamm-Horsfall protein and epidermal growth factor in chronic nephropathy. *Nephron,* 79**,** 167-172.

TORFFVIT, O., MELANDER, O. & HULTEN, U. L. 2004. Urinary excretion rate of Tamm-Horsfall protein is related to salt intake in humans. *Nephron Physiol,* 97**,** p31-6.

TRUDU, M., JANAS, S., LANZANI, C., DEBAIX, H., SCHAEFFER, C., IKEHATA, M., CITTERIO, L., DEMARETZ, S., TREVISANI, F., RISTAGNO, G., GLAUDEMANS, B., LAGHMANI, K., DELL'ANTONIO, G., LOFFING, J., RASTALDI, M. P., MANUNTA, P., DEVUYST, O. & RAMPOLDI, L. 2013. Common noncoding UMOD gene variants induce salt-sensitive hypertension and kidney damage by increasing uromodulin expression. *Nat Med,* 19**,** 1655-60.

TSAI, C. Y., WU, T. H., YU, C. L., LU, J. Y. & TSAI, Y. Y. 2000. Increased excretions of beta2-microglobulin, IL-6, and IL-8 and decreased excretion of Tamm-Horsfall glycoprotein in urine of patients with active lupus nephritis. *Nephron,* 85**,** 207-14.

TURNER, J. J., STACEY, J. M., HARDING, B., KOTANKO, P., LHOTTA, K., PUIG, J. G., ROBERTS, I., TORRES, R. J. & THAKKER, R. V. 2003. UROMODULIN mutations cause familial juvenile hyperuricemic nephropathy. *J Clin Endocrinol Metab,* 88**,** 1398-401.

UNWIN, R. J., BAILEY, M. A. & BURNSTOCK, G. 2003. Purinergic signaling along the renal tubule: the current state of play. *News Physiol Sci,* 18**,** 237-41.

VAN ROOIJEN, J. J., KAMERLING, J. P. & VLIEGENTHART, J. F. 1998. Sulfated di-, tri- and tetraantennary N-glycans in human Tamm-Horsfall glycoprotein. *Eur J Biochem,* 256**,** 471-87.

VARGAS-POUSSOU, R., FELDMANN, D., VOLLMER, M., KONRAD, M., KELLY, L., VAN DEN HEUVEL, L. P., TEBOURBI, L., BRANDIS, M., KAROLYI, L., HEBERT, S. C., LEMMINK, H. H., DESCHENES, G., HILDEBRANDT, F., SEYBERTH, H. W., GUAY-WOODFORD, L. M., KNOERS, N. V. & ANTIGNAC, C. 1998. Novel molecular variants of the Na-K-2Cl cotransporter gene are responsible for antenatal Bartter syndrome. *Am J Hum Genet,* 62**,** 1332-40.

VIO, C. P., QUIROZ-MUNOZ, M., CUEVAS, C. A., CESPEDES, C. & FERRERI, N. R. 2012. Prostaglandin E2 EP3 receptor regulates cyclooxygenase-2 expression in the kidney. *Am J Physiol Renal Physiol,* 303**,** F449-57.

VISSER, F. W., MUNTINGA, J. H., DIERCKX, R. A. & NAVIS, G. 2008. Feasibility and impact of the measurement of extracellular fluid volume simultaneous with GFR by 125I-iothalamate. *Clin J Am Soc Nephrol,* 3**,** 1308-15.

VYLET'AL, P., KUBLOVA, M., KALBACOVA, M., HODANOVA, K., BARESOVA, V., STIBURKOVA, B., SIKORA, J., HULKOVA, H., ZIVNY, J., MAJEWSKI, J., SIMMONDS, A., FRYNS, J. P., VENKAT-RAMAN, G., ELLEDER, M. & KMOCH, S. 2006. Alterations of uromodulin biology: a common denominator of the genetically heterogeneous FJHN/MCKD syndrome. *Kidney Int,* 70**,** 1155-69.

VYLETAL, P., BLEYER, A. J. & KMOCH, S. 2010. Uromodulin biology and pathophysiology--an update. *Kidney Blood Press Res,* 33**,** 456-75.

WADE, J. B., FANG, L., LIU, J., LI, D., YANG, C. L., SUBRAMANYA, A. R., MAOUYO, D., MASON, A., ELLISON, D. H. & WELLING, P. A. 2006. WNK1 kinase isoform switch regulates renal potassium excretion. *Proc Natl Acad Sci U S A,* 103, 8558-63.

WAGNER, C. A., LOFFING-CUENI, D., YAN, Q. S., SCHULZ, N., FAKITSAS, P., CARREL, M., WANG, T., VERREY, F., GEIBEL, J. P., GIEBISCH, G., HEBERT, S. C. & LOFFING, J. 2008. Mouse model of type II Bartter's syndrome. II. Altered expression of renal sodium- and water-transporting proteins. *American Journal of Physiology-Renal Physiology,* 294**,** F1373-F1380.

WAIN, L. V., VERWOERT, G. C., O'REILLY, P. F., SHI, G., JOHNSON, T., JOHNSON, A. D., BOCHUD, M., RICE, K. M., HENNEMAN, P., SMITH, A. V., EHRET, G. B., AMIN, N., LARSON, M. G., MOOSER, V., HADLEY, D., DORR, M., BIS, J. C., ASPELUND, T., ESKO, T., JANSSENS, A. C., ZHAO, J. H., HEATH, S., LAAN, M., FU, J., PISTIS, G., LUAN, J., ARORA, P., LUCAS, G., PIRASTU, N., PICHLER, I., JACKSON, A. U., WEBSTER, R. J., ZHANG, F., PEDEN, J. F., SCHMIDT, H., TANAKA, T., CAMPBELL, H., IGL, W., MILANESCHI, Y., HOTTENGA, J. J., VITART, V., CHASMAN, D. I., TROMPET, S., BRAGG-GRESHAM, J. L., ALIZADEH, B. Z., CHAMBERS, J. C., GUO, X., LEHTIMAKI, T., KUHNEL, B., LOPEZ, L. M., POLASEK, O., BOBAN, M., NELSON, C. P., MORRISON, A. C., PIHUR, V., GANESH, S. K., HOFMAN, A., KUNDU, S., MATTACE-RASO, F. U., RIVADENEIRA, F., SIJBRANDS, E. J., UITTERLINDEN, A. G., HWANG, S. J., VASAN, R. S., WANG, T. J., BERGMANN, S., VOLLENWEIDER, P., WAEBER, G., LAITINEN, J., POUTA, A., ZITTING, P., MCARDLE, W. L., KROEMER, H. K., VOLKER, U., VOLZKE, H., GLAZER, N. L., TAYLOR, K. D., HARRIS, T. B., ALAVERE, H., HALLER, T., KEIS, A., TAMMESOO, M. L., AULCHENKO, Y., BARROSO, I., KHAW, K. T., GALAN, P., HERCBERG, S., LATHROP, M., EYHERAMENDY, S., ORG, E., SOBER, S., LU, X., NOLTE, I. M., PENNINX, B. W., CORRE, T., MASCIULLO, C., SALA, C., GROOP, L., VOIGHT, B. F., MELANDER, O., et al. 2011. Genome-wide association study identifies six new loci influencing pulse pressure and mean arterial pressure. *Nat Genet,* 43**,** 1005-11.

WANG, D., PEDRAZA, P. L., ABDULLAH, H. I., MCGIFF, J. C. & FERRERI, N. R. 2002. Calcium-sensing receptor-mediated TNF production in medullary thick ascending limb cells. *Am J Physiol Renal Physiol,* 283**,** F963-70.

WANG, N. N., SYMONS, J. D., ZHANG, H., YANG, G. R., JIA, Z. J., GONZALEZ, F. J., LITWIN, S. E., SOODVILAI, S. & YANG, T. X. 2008. Distinct Functions of Vascular Endothelial and Smooth Muscle PPAR gamma in Regulation of Blood Pressure and Vascular Tone. *Faseb Journal,* 22.

WANG, X., PRINS, B. P., SOBER, S., LAAN, M. & SNIEDER, H. 2011a. Beyond genome-wide association studies: new strategies for identifying genetic determinants of hypertension. *Curr Hypertens Rep,* 13**,** 442-51.

WANG, X., ZHU, H., DONG, Y., TREIBER, F. A. & SNIEDER, H. 2006. Effects of angiotensinogen and angiotensin II type I receptor genes on blood pressure and left ventricular mass trajectories in multiethnic youth. *Twin Res Hum Genet,* 9**,** 393-402.

WANG, Y., O'CONNELL, J. R., MCARDLE, P. F., WADE, J. B., DORFF, S. E., SHAH, S. J., SHI, X., PAN, L., RAMPERSAUD, E., SHEN, H., KIM, J. D., SUBRAMANYA, A. R., STEINLE, N. I., PARSA, A., OBER, C. C., WELLING, P. A., CHAKRAVARTI, A., WEDER, A. B., COOPER, R. S., MITCHELL, B. D., SHULDINER, A. R. & CHANG, Y. P. 2009. From the Cover: Whole-genome association study identifies STK39 as a hypertension susceptibility gene. *Proc Natl Acad Sci U S A,* 106**,** 226-31.

WANG, Z. N., KLIPFELL, E., BENNETT, B. J., KOETH, R., LEVISON, B. S., DUGAR, B., FELDSTEIN, A. E., BRITT, E. B., FU, X. M., CHUNG, Y. M., WU, Y. P., SCHAUER, P., SMITH, J. D., ALLAYEE, H., TANG, W. H. W., DIDONATO, J. A., LUSIS, A. J. & HAZEN, S. L. 2011b. Gut flora metabolism of phosphatidylcholine promotes cardiovascular disease. *Nature,* 472**,** 57-U82.

WARDEN, D. H., SCHUSTER, V. L. & STOKES, J. B. 1988. Characteristics of the paracellular pathway of rabbit cortical collecting duct. *American Journal of Physiology,* 255**,** F720-7.

WEINBERGER, M. H. 1996. Salt sensitivity of blood pressure in humans. *Hypertension,* 27**,** 481-90.

WEISS, K. M. & CLARK, A. G. 2002. Linkage disequilibrium and the mapping of complex human traits. *Trends Genet,* 18**,** 19-24.

WELKER, P., BOHLICK, A., MUTIG, K., SALANOVA, M., KAHL, T., SCHLUTER, H., BLOTTNER, D., PONCE-CORIA, J., GAMBA, G. & BACHMANN, S. 2008. Renal Na+-K+-Cl- cotransporter activity and vasopressin-induced trafficking are lipid raft-dependent. *Am J Physiol Renal Physiol,* 295**,** F789-802.

WHITWORTH, J. A. 2003. 2003 World Health Organization (WHO)/International Society of Hypertension (ISH) statement on management of hypertension. *J Hypertens,* 21**,** 1983-92.

WILLIAMS, S. E., REED, A. A., GALVANOVSKIS, J., ANTIGNAC, C., GOODSHIP, T., KARET, F. E., KOTANKO, P., LHOTTA, K., MORINIERE, V., WILLIAMS, P., WONG, W., RORSMAN, P. & THAKKER, R. V. 2009. Uromodulin mutations causing familial juvenile hyperuricaemic nephropathy lead to protein maturation defects and retention in the endoplasmic reticulum. *Hum Mol Genet,* 18**,** 2963-74.

WILLIAMS, S. M., RITCHIE, M. D., PHILLIPS, J. A., 3RD, DAWSON, E., PRINCE, M., DZHURA, E., WILLIS, A., SEMENYA, A., SUMMAR, M., WHITE, B. C., ADDY, J. H., KPODONU, J., WONG, L. J., FELDER, R. A., JOSE, P. A. & MOORE, J. H. 2004. Multilocus analysis of hypertension: a hierarchical approach. *Hum Hered,* 57**,** 28-38.

WILSON, B. S., STEINBERG, S. L., LIEDERMAN, K., PFEIFFER, J. R., SURVILADZE, Z., ZHANG, J., SAMELSON, L. E., YANG, L. H., KOTULA, P. G. & OLIVER, J. M. 2004. Markers for detergent-resistant lipid rafts occupy distinct and dynamic domains in native membranes. *Mol Biol Cell,* 15**,** 2580-92.

WILSON, F. H., DISSE-NICODEME, S., CHOATE, K. A., ISHIKAWA, K., NELSON-WILLIAMS, C., DESITTER, I., GUNEL, M., MILFORD, D. V., LIPKIN, G. W., ACHARD, J. M., FEELY, M. P., DUSSOL, B., BERLAND, Y., UNWIN, R. J., MAYAN, H., SIMON, D. B., FARFEL, Z., JEUNEMAITRE, X. & LIFTON, R. P. 2001. Human hypertension caused by mutations in WNK kinases. *Science,* 293**,** 1107-12.

WOLF, M. T., BECK, B. B., ZAUCKE, F., KUNZE, A., MISSELWITZ, J., RULEY, J., RONDA, T., FISCHER, A., EIFINGER, F., LICHT, C., OTTO, E., HOPPE, B. & HILDEBRANDT, F. 2007. The Uromodulin C744G mutation causes MCKD2 and FJHN in children and adults and may be due to a possible founder effect. *Kidney Int,* 71**,** 574-81.

WOLF, M. T., WU, X. R. & HUANG, C. L. 2013. Uromodulin upregulates TRPV5 by impairing caveolin-mediated endocytosis. *Kidney Int,* 84**,** 130-7.

WORCESTER, E. M., NAKAGAWA, Y., WABNER, C. L., KUMAR, S. & COE, F. L. 1988. Crystal adsorption and growth slowing by nephrocalcin, albumin, and Tamm-Horsfall protein. *Am J Physiol,* 255**,** F1197-205.

WRIGHT, A., CHARLESWORTH, B., RUDAN, I., CAROTHERS, A. & CAMPBELL, H. 2003. A polygenic basis for late-onset disease. *Trends Genet,* 19**,** 97-106.

WRIGHT, J. T., JR., BAKRIS, G., GREENE, T., AGODOA, L. Y., APPEL, L. J., CHARLESTON, J., CHEEK, D., DOUGLAS-BALTIMORE, J. G., GASSMAN, J., GLASSOCK, R., HEBERT, L., JAMERSON, K., LEWIS, J., PHILLIPS, R. A., TOTO, R. D., MIDDLETON, J. P. & ROSTAND, S. G. 2002. Effect of blood pressure lowering and antihypertensive drug class on progression of hypertensive kidney disease: results from the AASK trial. *JAMA,* 288**,** 2421-31.

WU, T. H., HSIEH, S. C., YU, C. Y., LEE, Y. F., TSAI, C. Y. & YU, C. L. 2008. Intact protein core structure is essential for protein-binding, mononuclear cell proliferating, and neutrophil phagocytosis-enhancing activities of normal human urinary Tamm-Horsfall glycoprotein. *Int Immunopharmacol,* 8**,** 90-9.

WWW.WHO.INT, W. H. O. C. D. 2012. *http://www.euro.who.int/en/what-we-do/health-topics/noncommunicable-diseases/cardiovascular-diseases/news/news/2012/5/world-health-statistics-2012-report-increase-of-hypertension-and-diabetes* [Online]. [Accessed].

XU, X., ROGUS, J. J., TERWEDOW, H. A., YANG, J., WANG, Z., CHEN, C., NIU, T., WANG, B., XU, H., WEISS, S., SCHORK, N. J. & FANG, Z. 1999. An extreme-sib-pair genome scan for genes regulating blood pressure. *Am J Hum Genet,* 64**,** 1694-701.

YANG, C. L., ANGELL, J., MITCHELL, R. & ELLISON, D. H. 2003. WNK kinases regulate thiazide-sensitive Na-Cl cotransport. *J Clin Invest,* 111**,** 1039-45.

YANG, H., WU, C., ZHAO, S. & GUO, J. 2004. Identification and characterization of D8C, a novel domain present in liver-specific LZP, uromodulin and glycoprotein 2, mutated in familial juvenile hyperuricaemic nephropathy. *FEBS Lett,* 578**,** 236-8.

YANG, H. C., LIANG, Y. J., WU, Y. L., CHUNG, C. M., CHIANG, K. M., HO, H. Y., TING, C. T., LIN, T. H., SHEU, S. H., TSAI, W. C., CHEN, J. H., LEU, H. B., YIN, W. H., CHIU, T. Y., CHEN, C. I., FANN, C. S., WU, J. Y., LIN, T. N., LIN, S. J., CHEN, Y. T., CHEN, J. W. & PAN, W. H. 2009. Genome-wide association study of young-onset hypertension in the Han Chinese population of Taiwan. *PLoS One,* 4**,** e5459.

YING, W. Z. & SANDERS, P. W. 1998. Dietary salt regulates expression of Tamm-Horsfall glycoprotein in rats. *Kidney Int,* 54**,** 1150-6.

YU, C. L., LIN, W. M., LIAO, T. S., TSAI, C. Y., SUN, K. H. & CHEN, K. H. 1992. Tamm-Horsfall glycoprotein (THG) purified from normal human pregnancy urine increases phagocytosis, complement receptor expressions and arachidonic acid metabolism of polymorphonuclear neutrophils. *Immunopharmacology,* 24**,** 181-90.

YU, C. L., TSAI, C. Y., LIN, W. M., LIAO, T. S., CHEN, H. L., SUN, K. H. & CHEN, K. H. 1993. Tamm-Horsfall urinary glycoprotein enhances monokine release and augments lymphocyte proliferation. *Immunopharmacology,* 26**,** 249-58.

ZAUCKE, F., BOEHNLEIN, J. M., STEFFENS, S., POLISHCHUK, R. S., RAMPOLDI, L., FISCHER, A., PASCH, A., BOEHM, C. W., BAASNER, A., ATTANASIO, M., HOPPE, B., HOPFER, H., BECK, B. B., SAYER, J. A., HILDEBRANDT, F. & WOLF, M. T. 2010. Uromodulin is expressed in renal primary cilia and UMOD mutations result in decreased ciliary uromodulin expression. *Hum Mol Genet,* 19**,** 1985-97.

ZBIKOWSKA, H. M., SOUKHAREVA, N., BEHNAM, R., CHANG, R., DREWS, R., LUBON, H., HAMMOND, D. & SOUKHAREV, S. 2002. The use of the uromodulin promoter to target production of recombinant proteins into urine of transgenic animals. *Transgenic Res,* 11**,** 425-35.

ZHANG, H., ZHANG, A. H., KOHAN, D. E., NELSON, R. D., GONZALEZ, F. J. & YANG, T. X. 2005. Collecting duct-specific deletion of peroxisome proliferator-activated receptor gamma blocks thiazolidinedione-induced fluid retention. *Proceedings of the National Academy of Sciences of the United States of America,* 102**,** 9406-9411.

ZHAO, X., HO, D., GAO, S., HONG, C., VATNER, D. E. & VATNER, S. F. 2011. Arterial Pressure Monitoring in Mice. *Curr Protoc Mouse Biol,* 1**,** 105-122.

ZHU, D. L., WANG, H. Y., XIONG, M. M., HE, X., CHU, S. L., JIN, L., WANG, G. L., YUAN, W. T., ZHAO, G. S., BOERWINKLE, E. & HUANG, W. 2001. Linkage of hypertension to chromosome 2q14-q23 in Chinese families. *J Hypertens,* 19**,** 55-61.

ZHU, X., CHENG, J., GAO, J., LEPOR, H., ZHANG, Z. T., PAK, J. & WU, X. R. 2002. Isolation of mouse THP gene promoter and demonstration of its kidney-specific activity in transgenic mice. *Am J Physiol Renal Physiol,* 282**,** F608-17.